THEORETICAL MECHANISMS OF INTRINSIC ACTIVITY IN MOLLUSCAN PACEMAKER NEURONS

WILLIAM D. PHILLIPS

Ph. D.

University of Edinburgh

1975.

DECLARATION

This thesis, 'Theoretical Mechanisms of Intrinsic Activity in Molluscan Pacemaker Neurons', submitted for the degree of Ph. D., Edinburgh University, 1975, is an original composition and does not include work submitted for any other degree or professional qualification.

W. D. Phillips.

Dr. D. J. Cosens (Supervisor).

ACKNOWLEDGEMENTS

I am especially grateful to my supervisor, Dr. D. J. Cosens, for much helpful discussion and criticism throughout the course of the project, and for his comments on the draft manuscript. I am indebted to Professor M. S. Laverack and the University of St. Andrews for the use of computing facilities during 1974 and to Peter Balch for advice on computing techniques. Special thanks to my wife, Vivien, for typing the manuscript.

CONTENTS

SUMMARY;

1) There is pronounced variation in the shape, duration, amplitude and frequency of action potentials recorded from spontaneously active cells in the suboesophageal ganglia of the snail, Helix aspersa. A statistically significant negative correlation is demonstrated between the amplitude and frequency of spontaneous action potentials.

2) It is suggested that variations in action potential amplitude and frequency may be dependent on differences in the magnitude of transmembrane ionic equilibrium potentials or conductances, at least in the case of intrinsic 'pacemaker' neurons. However, the observed negative correlation between amplitude and frequency cannot be explained in simple terms.

3) The Hodgkin-Huxley equations as originally formulated imply that repetitive activity can be produced only as a result of sustained depolarization and the equations cannot be used to predict the effects of changes in ionic equilibrium potential or conductance. An equivalent system of absolute potential equations is derived to overcome this difficulty and the system is expanded to include an additional (transient outward current) membrane conductance channel not included in the Hodgkin-Huxley formulation.

4) A method is developed for the production of theoretical current-voltage curves. This method is applied to generate predictions of the changes in membrane properties expected on the basis of the absolute potential equations when the equilibrium potentials and membrane conductances for the main ions contributing to action potential production are altered. These predictions are evaluated in relation to available experimental results and it is concluded

that the absolute potential equations when cautiously applied can provide a valid description of membrane properties under altered ionic conditions.

5) The theoretical current-voltage curves change with the potassium equilibrium potential (E_K) in a manner which clearly predicts the occurrence of intrinsic pacemaker activity when E_K is more depolarized than about -57 mV.

6) Action potential simulation with the absolute potential equations confirms that intrinsic activity should occur for moderately depolarized values of E_K and the 'spontaneous' frequency of simulated action potentials increases as E_K is further depolarized. The relationship between simulated action potential amplitude and frequency strongly resembles that determined in the experimental case, and the range of simulated spontaneous frequencies available is also comparable.

7) Other methods of producing theoretical pacemaker current-voltage curves are examined but prove to be inconsistent with available experimental results. It is concluded that the occurrence and frequency of intrinsic activity in neurons in the suboesophageal ganglia of Helix aspersa is most probably determined in the first instance by intracellular potassium concentration, although other factors could have a modulating effect.

8) The characteristics of burst generation are described for an identifiable bursting neuron ('Big-D cell') of Helix aspersa. The bursting rhythm of this cell is inhibited by cooling and by treatment with ouabain (10^{-4} M). These observations and the modifications in bursting rhythm associated with changes in extracellular potassium

concentration suggest that the electrogenic sodium pump may contribute significantly to the interburst hyperpolarization.

9) A model for the process of burst generation is proposed. It is suggested that extracellular potassium ion accumulation in membrane invaginations stimulates electrogenic sodium pump activity after a short delay and that the subsequent hyperpolarization determines the time course of the interburst hyperpolarization in non-invaginated membrane regions.

10) An electronic analogue of the proposed model mimics bursting activity with sufficient accuracy to justify an attempt at computer simulation using an absolute potential system of equations. Arbitrary equations describing extracellular potassium accumulation and sodium pump activity are derived. The simulation achieved is less than satisfactory and possible reasons for this discrepancy are discussed.

Chapter 1

INTRODUCTION

The term 'pacemaker' is often used rather loosely to describe neurons which show a spontaneous (i.e. unstimulated) cycle of action potential discharge. Cyclic activity may be either monotonic, when the duration of the interval between consecutive action potentials is more or less constant, or less commonly, bimodal, when 'bursts' of action potentials alternate with relatively long periods of inactivity. It is important to distinguish between spontaneous activity which is synaptically driven and that which depends directly on membrane properties and is therefore endogenous (intrinsic). Results obtained with isolated neuron somata show clearly that regular activity can arise intrinsically (ALVING, 1968; CHEN, VON BAUMGARTEN & TAKEDA, 1971) but, in the normal experimental situation, it may be difficult to determine whether a particular activity pattern is intrinsic or whether it depends on remote synaptic input. Because of this, it is impossible to estimate with any accuracy the relative importance of intrinsic and synaptic influences in determining the behaviour of the nervous system as a whole.

This problem is especially intractable because the mechanisms which control the occurrence and frequency of intrinsic activity are barely, if at all, understood. On the other hand, the properties of the membrane mechanisms which determine action production are known in some detail and can be adequately described

in terms of a relatively complex mathematical model (HODGKIN & HUXLEY, 1952d). More recently, the mathematical model has been expanded to include additional membrane mechanisms such that the frequency of repetitive (i.e. artificially stimulated) activity in molluscan neurons can be predicted with some accuracy (CONNOR & STEVENS, 1971c).

While the range of application of the Hodgkin-Huxley equations is considerable (NOBLE, 1966), the original formulation implies that repetitive activity can occur only as a result of sustained artificial depolarization. Nevertheless, it seems reasonable to suppose that a satisfactory theoretical explanation of intrinsic activity will incorporate the equations, possibly in a modified form. In view of this, it is surprising that attempts to explain intrinsic activity using the mathematical model have been made in only two rather specific instances. In the squid giant axon, calcium ions are reported to have a stabilizing effect on membrane structure and large reductions in extracellular calcium concentration can cause intrinsic activity (FRANKENHAEUSER & HODGKIN, 1957). This effect of decalcification can be mimicked using a modified system of the equations (HUXLEY, 1959). Cardiac muscle Purkinje fibre intrinsic pacemaker potentials can also be simulated using the Hodgkin-Huxley system of equations modified in an entirely different and essentially arbitrary manner (NOBLE, 1962). Unfortunately, neither of these explanations of intrinsic activity is in any way applicable in the general case and neither provides a definite indication of how intrinsic activity could arise in nerve membrane under normal conditions.

This thesis represents an attempt to develop a general theoretical explanation for intrinsic activity. As the simpler case,

monotonic pacemakers are considered first, then an attempt is made to extend the theory developed to account for intrinsic activity in bursting neurons. Where appropriate, the theory has been related to experimental observations obtained from cells in the suboesophageal ganglia of the snail, Helix aspersa. This preparation shows a considerable range of spontaneous activity (WALKER et al, 1970) and an individual bursting neuron ('Big-D cell') can be identified in a majority of cases (KERKUT, FRENCH & WALKER, 1970).

It was found convenient to introduce references to published experimental results where relevant in development of the theoretical argument and consequently an extensive literature review is not presented at this point. The material covered by the thesis has been organized into chapters as follows;

Chapter 2, 'Materials & Methods', gives an account only of the experimental techniques used; theoretical and computing methods are discussed where appropriate in subsequent chapters. With the exception of oscilloscopes, all the electronic apparatus required was specially constructed and circuit diagrams are given in each case. The design criteria necessary for accurate intracellular and extracellular recording amplifiers are discussed in relation to the circuits used. The stimulator constructed was relatively little used in obtaining results included in the thesis but is of a rather unorthodox and interesting design and a description of its method of operation has therefore been given.

Chapter 3, 'Preliminary Observations', includes a description of the anatomy of the suboesophageal ganglia of Helix aspersa. The relationship between the anatomy of the ganglia and

spontaneous activity recorded intracellularly from ganglion cells and extracellularly from associated nerves is discussed and possible ways of identifying individual cells from preparation to preparation are considered. The 'Big-D' cell is located in the right parietal ganglion and its identification can be achieved with simultaneous intracellular and extracellular recording. Spontaneous action potentials were found to vary widely in frequency, amplitude and duration and simple experiments demonstrate a distinct negative relationship between amplitude and spontaneous frequency.

The Hodgkin-Huxley equations are described in Chapter 4, 'Theoretical Development', and an equivalent system of absolute potential equations is derived. This system is expanded to include equations describing an additional membrane conductance channel. Both the absolute potential Hodgkin-Huxley equations and the expanded system are used to develop computer programmes for theoretical current-voltage curve production and action potential simulation.

Predictions generated by the computer programmes are described in Chapter 5, 'Theoretical Evaluation', and compare favourably with available experimental results. The alterations in the theoretical current-voltage curves when the potassium equilibrium potential (E_K) is progressively depolarized suggest a plausible general explanation of intrinsic activity. The relationship of the theory to the experimentally observed negative correlation between the amplitude and frequency of spontaneous action potentials is discussed.

The properties of the Big-D cell of Helix aspersa are examined in Chapter 6, 'Bursting Pacemakers'. The experimental

results obtained are discussed together with those available for other identifiable bursting neurons and a model for the process of burst generation is developed. An electronic analogue of the model provides results which are sufficiently encouraging to justify an attempt at computer simulation using an absolute potential system of equations. Such simulation also depends on the arbitrary derivation of a number of equations describing extracellular potassium ion accumulation and electrogenic sodium pump activity. The best simulation available does not mimic real bursting activity with sufficient accuracy and a number of possible reasons for this shortcoming are discussed.

In Chapter 7, 'Conclusions', some general implications of the absolute potential approach are considered and a number of possibilities for further research are suggested.

Many of the Figures given, especially those in theoretical sections, can be understood only with reference to the accompanying text. To assist in interpretation, each Figure has been cross-referenced to the page on which it is first mentioned. This cross-referencing system was felt preferable to the extensive use of lengthy figure legends.

Chapter 2

MATERIALS & METHODS

A) Preparation;

Specimens of Helix aspersa, the common snail, were obtained from Gerard & Haig Ltd, Newdigate, Surrey and were kept in a large glass trough in a cool place until required. The base of the trough was covered with damp paper towelling and water was added at intervals to maintain humidity. Snails kept in this way tend to remain in an active condition. Aestivation can be identified by the presence of a dry whitish membrane covering the mouth of the shell. Activity was restored in snails obtained in this condition by removing the membrane prior to a brief immersion in warm water.

The neurons of active Helix aspersa appear to have higher resting potentials and higher intracellular potassium concentrations than those of inactive (aestivating) snails (KERKUT & WALKER, 1961). Typical resting potentials recorded were -15 to -25 mV for active and -10 to -15 mV for inactive snails. The validity of these results is uncertain since the value for active snails is somewhat lower than those more recently reported e.g. -43 to -63 mV (KERKUT & MEECH, 1967), -40.8 ± 1.1 mV (MORETON, 1968), -42 to -68 mV (WALKER et al, 1970). Nevertheless, as a precaution, active snails were used for all experiments.

Experiments were carried out on the isolated 'brain' consisting of the supraoesophageal (cerebral) and suboesophageal ganglia and associated nerves. These are located as indicated in Figure 1. The dissection procedure was as follows; after most of the shell had been cut away, a posterior portion of the animal was removed and the remaining, anterior, portion (including part of the mantle) was pinned out on a wax block. A pair of pins passing

Anatomy of Helix;

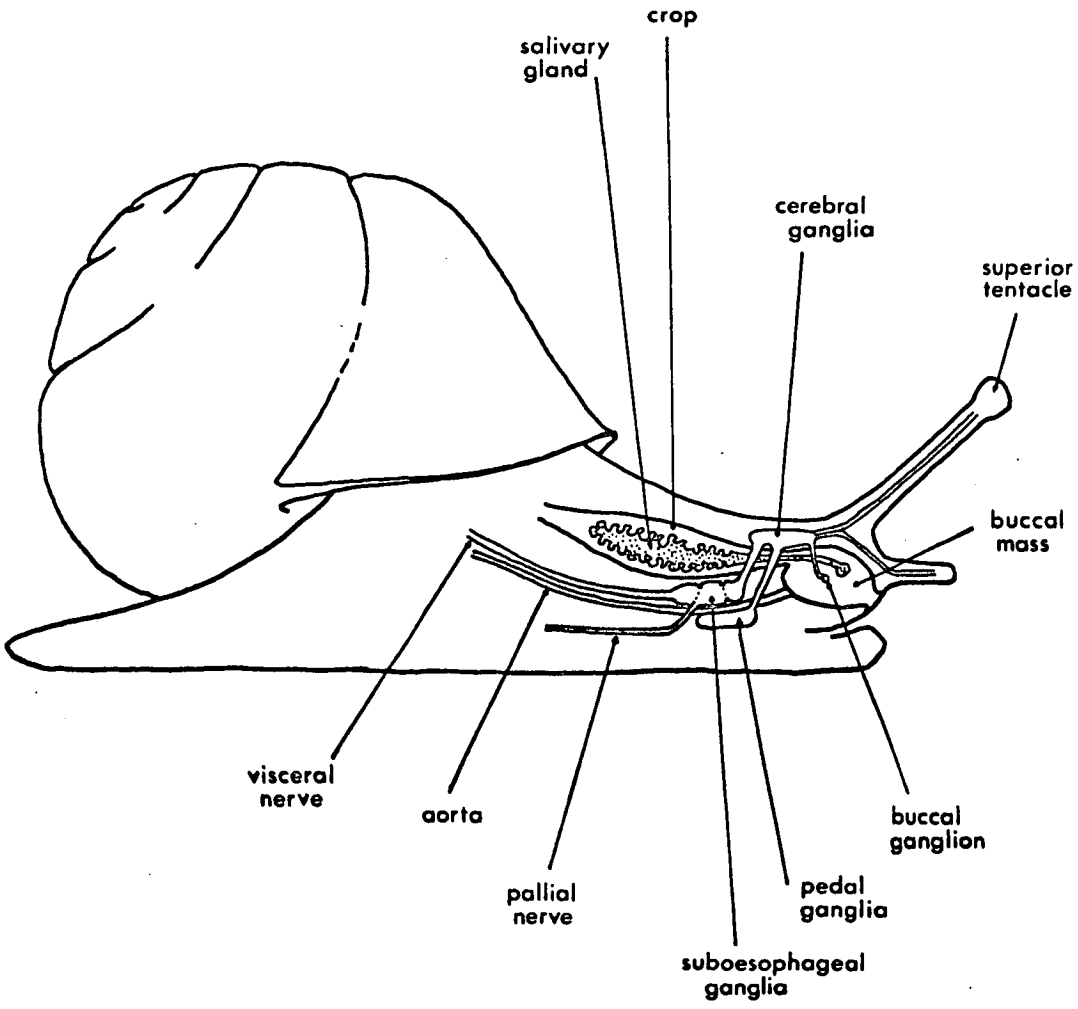

A;

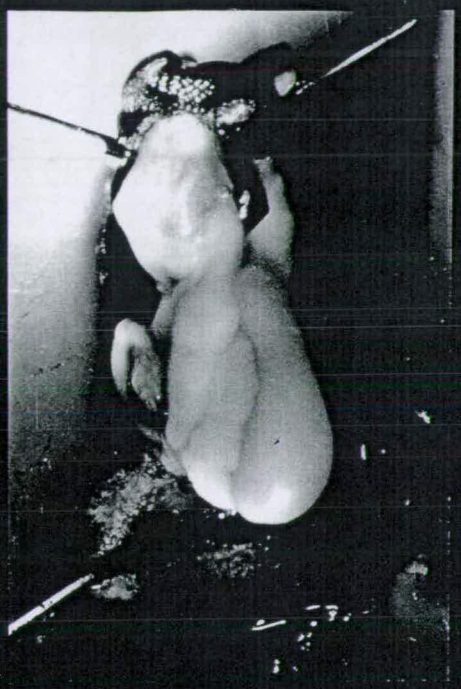

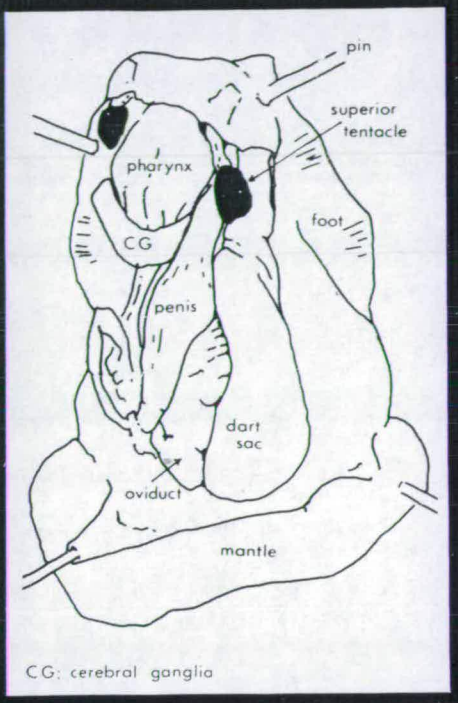

CG: cerebral ganglia

B;

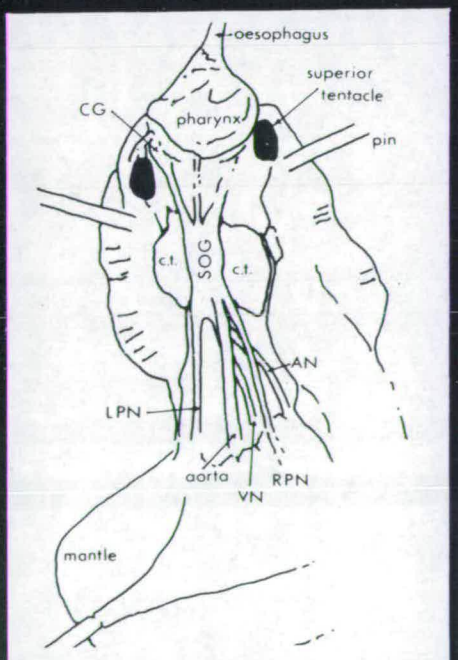

SOG: suboesophageal ganglia
c.t. connective tissue
LPN: left pallial nerve. VN: visceral nerve.
RPN: right pallial nerve. AN: anal nerve.

Excised brain;

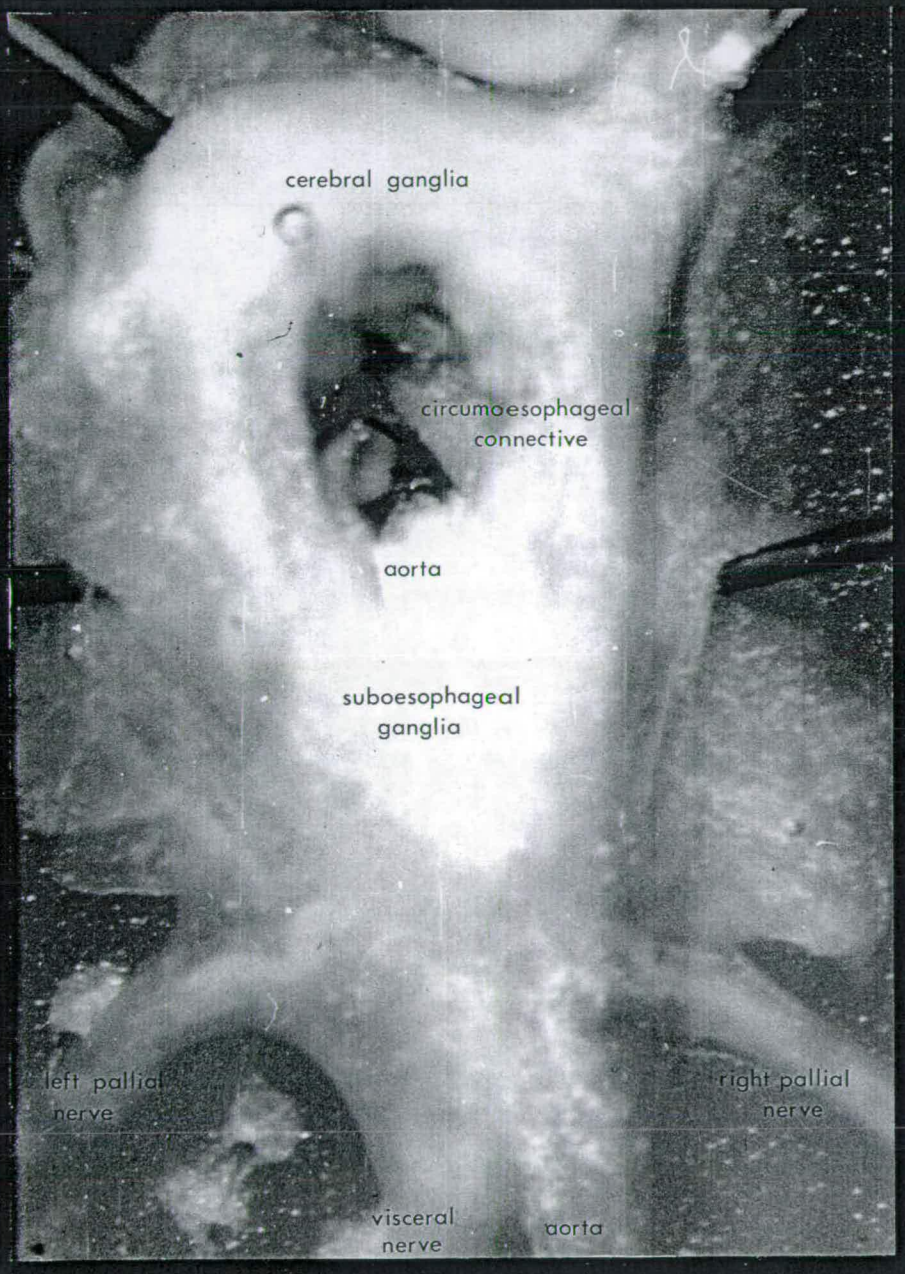

Dissected ganglia (stained);

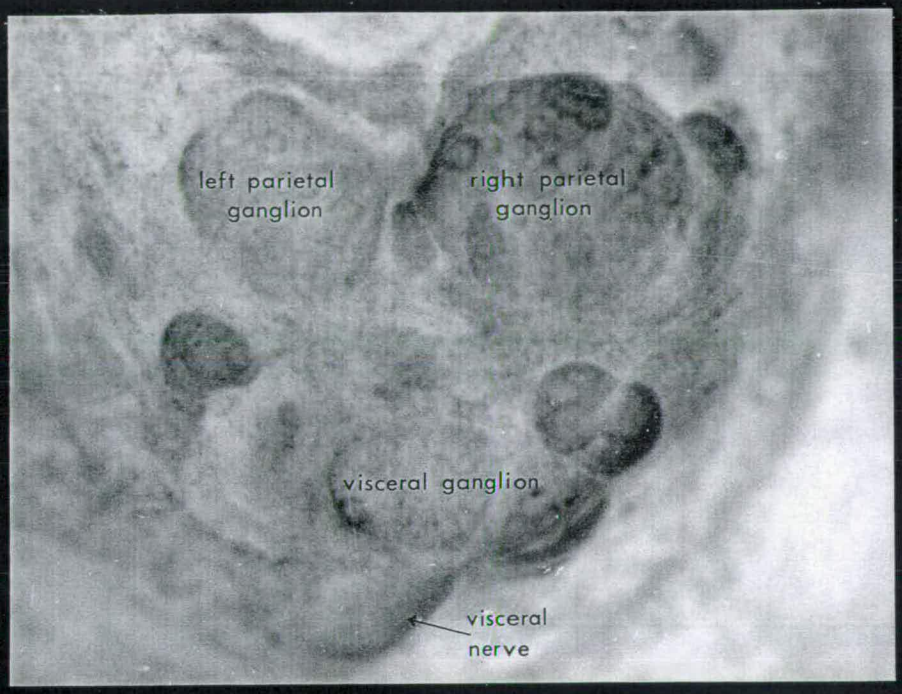

through the foot musculature secured the head anteriorly; a second pair placed just anterior to the margin of the mantle kept the animal in an extended position. Viewing under a binocular microscope, a longitudinal slit was made along the mid-line of the dorsal surface and the opening extended laterally to expose the body contents (Figure 2(A)). The dart sac and associated reproductive organs were removed since these obstruct further dissection. The supra-oesophageal ganglia are clearly visible at this stage and, if the oesophagus and pharyngeal retractor muscle are cut and pulled forward, the suboesophageal ganglionic mass can also be seen (Figure 2(B)). The pharynx is removed by pulling upwards on the oesophagus and cutting around the pharynx at its base. This exposes the whole of the brain which is isolated by cutting the various nerves and the aorta by means of which the brain is gently lifted to facilitate complete removal. The excised brain was placed, dorsal surface uppermost, under saline in a small perspex preparation chamber. The preparation was then pinned out using small insect pins (0.010x10mm) as far as possible with these passing only through connective tissue. The main nerves were stretched slightly to tension the preparation (Figure 3).

The ganglia are invested with two layers of connective tissue. The first of these is thick and separated from the ganglia by a blood sinus. The area overlying the suboesophageal ganglia was carefully removed using watchmakers forceps (No. 5) and miniature springbow scissors (Weiss No. 81053). It was found convenient to start this operation at the anterior right hand corner of the ganglia adjacent to the circumoesophageal commissures and to work downwards and to the left. At this stage individual cells of

the various suboesophageal ganglia are visible. Illumination tends to be rather critical for good visibility and was found to be most effective from behind and at a shallow angle. A photograph of the ganglia, lightly stained with cresyl violet, is given in Figure 4.

The second layer of connective tissue is thin, transparent and very closely applied to the cells in the ganglia. In early experiments this layer was ruptured using a fine tungsten hook mounted on a glass rod after the method described by Walker (1968). When a small slit had been made, slight pressure on the edges of the preparation was usually sufficient to expose a number of individual cells. Although this was done as carefully as possible it was found difficult to avoid cell damage. The method also has the disadvantage that exposed cells lose their original positions in the ganglion and any cell identification thereby becomes less certain. In later experiments it was found possible to penetrate cells directly without removing the inner sheath. The microelectrode was positioned above the cell to be impaled and moved downwards until a small dimple was produced in the overlying tissue. Gentle tapping of the micromanipulator base was generally sufficient to obtain penetration.

B) Preparation chamber;

The preparation chamber used was similar to that described by Moreton (1968) and is illustrated in Figure 5. The compartment in which the preparation is mounted was filled with wax almost to the level of the overflow edge so that a volume of about 2 ml remained. This was filled with saline and the preparation was continuously perfused. Excess saline drained away at a small nick in the overflow edge, at the opposite end of the preparation compartment from the inflow, and was removed from the overflow compartment by suction. Moderate suction was maintained by a water driven vacuum pump connected to the mains water supply. Potentially, 50 Hz interference on the recording trace may result if fluid contact between the saline in the preparation chamber and that in the suction line, external to the cage containing the preparation and recording amplifiers, can be established. This was prevented by the inclusion of an air-lock in the suction line inside the cage. A second possible source of (transient) interference is the vibration produced as fluid is sucked away. This is largely offset by the separate overflow compartment and can be reduced to a minimum by keeping the preparation chamber and the proximal end of the suction line rigid.

The saline inflow line consisted of a length of polythene tubing terminating in a Pasteur pipette which could be clamped in a suitable position above the preparation chamber. Saline was siphoned off from a storage vessel placed above the preparation. Flow rate was regulated by means of a 3-way tap. The arm of the tap at right angles to the inflow line led to a syringe which was used initially to establish siphoning and, at the conclusion of an experiment to clear the inflow line. A saline change was effected

Preparation chamber;

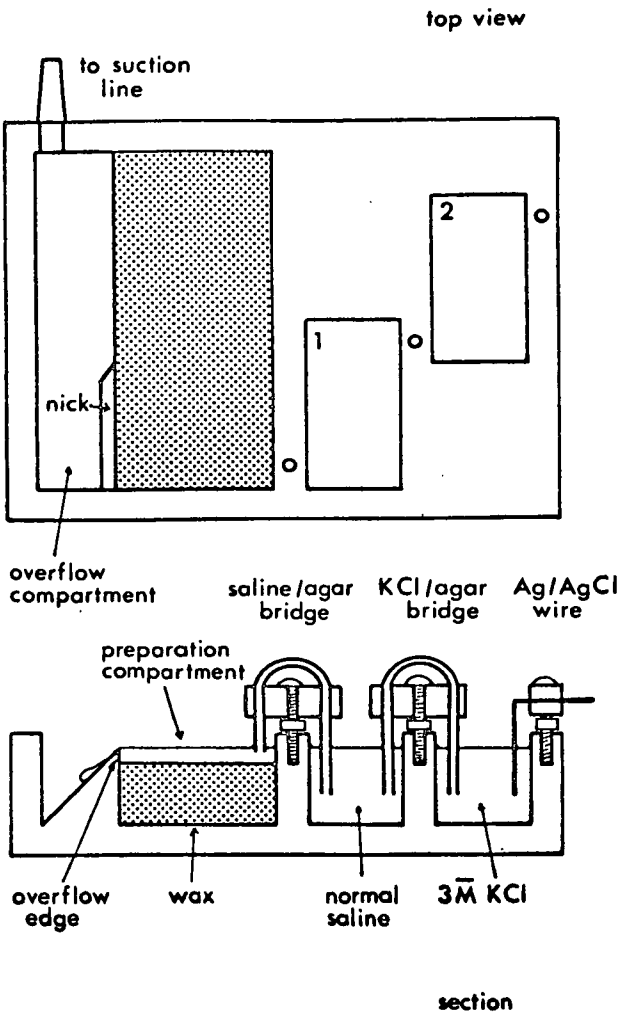

see text for further explanation

Standing potentials in recording circuit;

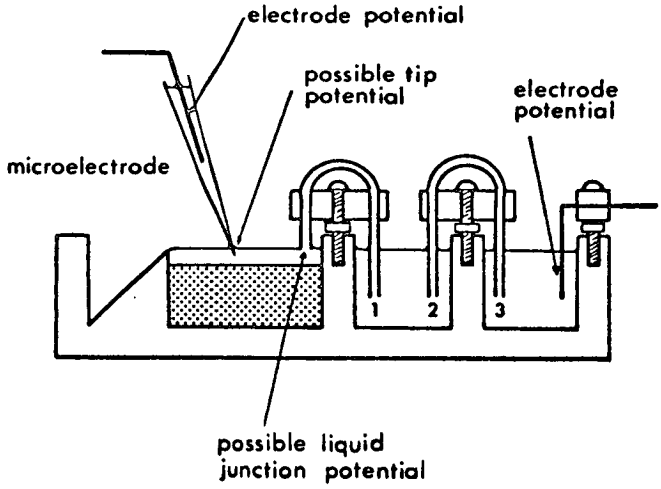

Junction potentials should not occur at the points numbered 1, 2 and 3; see text.

simply by transferring the siphon tube to an adjacent storage vessel containing the new saline. An air bubble was formed in the tube during this process and the progress of the bubble down the inflow line could be followed to the Pasteur pipette. Flow rate was increased at this stage to flush out the bath and to produce a rapid change of the saline bathing the preparation.

The first small compartment is filled with normal saline and is adjacent to the preparation compartment to which it is connected by means of a normal saline/agar bridge. The agar bridge is contained in a short length of polythene tube and is held in position by a small perspex holder. The second small compartment is filled with 3 $\bar{M}$ KCl solution and is connected to the first by a 3 $\bar{M}$ KCl/agar bridge. This arrangement was adopted to facilitate accurate d.c. potential measurements from the preparation when several salines of differing composition were used.

In any practical recording circuit three types of standing potential may interfere with accurate d.c. measurement. These are electrode (metal/liquid) potentials, liquid junction (diffusion) potentials and microelectrode tip potentials. Figure 6 illustrates the occurrence of these potentials in the recording circuit used with the preparation chamber described above.

Electrode potentials occur at the boundary between the non-polarizable silver chloride coated silver wire and the surrounding solution both at the recording and reference electrodes. While these are smaller and more stable than those associated with blank (polarizable) silver wires they are nevertheless sensitive to alteration in temperature and in the composition of the surrounding

solution (KATZ, 1966) and the electrodes must therefore be kept in a constant environment. The potentials at the recording and reference electrodes will, however, be in opposite directions and ideally should cancel out if the two bathing solutions are of identical composition.

Liquid junction potentials arise from the unequal mobilities of electrolyte solutions of differing concentration. These may be overcome by using concentrated KCl solution. This procedure is based on the fact that potassium ions and chloride ions have nearly identical mobilities. Provided their concentrations are much higher than those of other ions in the adjoining medium, diffusion of K^+ and Cl^- ions will short circuit any potential that movement of other ions would tend to produce. Thus a 3 M KCl/agar bridge connecting the reference electrode compartment directly to the preparation compartment would eliminate liquid junction potentials from the recording circuit. However, there is a risk of the solution in the preparation compartment becoming contaminated by diffusion from the bridge and for this reason the first small compartment containing normal saline and connected to the preparation compartment by a normal saline/agar bridge was interposed. This leaves a very small liquid junction potential which will appear when the solution bathing the preparation differs from normal. Errors from this source will be insignificant and can be ignored.

The origin of microelectrode tip potentials is not fully understood but appears to be related to an alteration in the relative mobilities of K^+ ions and Cl^- ions. This could occur either as a result of the adhesion of charged particles to the glass of the microelectrode tip or because of a potential generated

directly at the glass/electrolyte interface. In any event, the microelectrode tip potential can be assumed to make a constant contribution to the recorded potential. The accuracy of measurements of intracellular potential will be unaffected provided they are made with respect to the potential recorded extracellularly in the bathing solution, rather than with respect to zero (earth) potential.

C) Salines;

Normal saline was prepared according to the concentration of electrolytes found in the blood of Helix aspersa (BURTON, 1967). The concentrations used were as follows;

sodium chloride NaCl	60 mM (3.51g/l)
potassium chloride KCl	3 mM (0.22g/l)
calcium chloride $CaCl_2 2H_2O$	6 mM (0.88g/l)
magnesium chloride $MgCl_2 6H_2O$	4 mM (0.81g/l)
sodium bicarbonate $NaHCO_3$	5 mM (0.42g/l)

A 1 M stock solution of each salt was prepared. If the saline solution is made up initially with the salts in relatively high concentration a white precipitate of calcium carbonate may be formed. This will persist even when the solution is diluted to its correct volume with de-ionized water. Precipitation was avoided if the sodium bicarbonate stock solution was diluted to slightly less than half its final volume before being added to a mixture of the other salts also diluted to slightly less than half final volume. Only a small addition of de-ionized water was needed after this to give the correct concentration of salts in the saline solution. Normal saline had a pH of 8.2.

A series of salines of differing potassium concentration was made up simply by adding or omitting potassium chloride, the resulting differences in osmotic pressure being small in potassium deficient solutions. In potassium enriched solutions larger osmotic pressure differences could have been reduced by altering the concentration of other ions. However, such alterations could have an independent effect on membrane properties; other ions were therefore kept at constant concentrations and the resulting changes

in osmotic pressure were tolerated. The compositions of all the salines are given in Table 1.

Table 1.

Composition of salines;

Potassium series

	0mM K^+	1mM K^+	2mM K^+	3mM K^+ (normal)	4mM K^+	5mM K^+
NaCl	60	60	60	60	60	60
KCl	-	1	2	3	4	5
$CaCl_2 \cdot 2H_2O$	6	6	6	6	6	6
$MgCl_2 \cdot 6H_2O$	4	4	4	4	4	4
$NaHCO_3$	5	5	5	5	5	5

	7.5mM K^+	10mM K^+	20mM K^+	30mM K^+	50mM K^+
NaCl	60	60	60	60	60
KCl	7.5	10	20	30	50
$CaCl_2 \cdot 2H_2O$	6	6	6	6	6
$MgCl_2 \cdot 6H_2O$	4	4	4	4	4
$NaHCO_3$	5	5	5	5	5

All concentrations given in mM; all salines made up from 1 mM stock solutions as explained in text.

D) Agar bridges;

Agar bridges were made by preparing a 3% w/v solution of agar in normal saline or 3 $\bar{M}$ KCl as appropriate. The solution was stirred continuously and gently heated to about 60°C. on a hot plate before being boiled under reduced pressure to dissolve the agar completely and to remove air bubbles. The hot agar solution was sucked up into 5 inch lengths of polythene tubing using a syringe. When the agar had set the lengths of tubing were placed under the appropriate solution to avoid dessication and stored in a cold room. When required, suitable lengths ($1\frac{1}{2}$–2ins) were cut from the stored tubing, inserted in small perspex holders and used as bridges in the preparation chamber previously described. Bridges were discarded after a single use.

E) Electrodes;

1) Microelectrodes;

Glass microelectrodes were made from Pyrex glass capillary tubing using a horizontal solenoid (Palmer) electrode puller. An 'initial pull' setting of 6 and a 'furnace' setting of 7 were found to be satisfactory. The electrodes produced had relatively long shafts and, typically, resistances in the range 5-20 megohms when filled with 3 M KCl.

Microelectrodes were filled in two ways. The first method involved filling with methyl alcohol by boiling under reduced pressure, taking care to ensure that no air bubbles remained trapped in the tips. The electrodes were then placed in distilled water for at least 30 mins before being transferred to 3 M KCl (or more usually an alternative filling solution q.v.) for several hours, usually overnight. Electrodes prepared by this method are best used within 48 hours of filling since their condition deteriorates progressively and large tip potentials may develop after this period.

The second method of filling depends on the use of glass fibre. If a few strands of fibre are placed in the electrode glass prior to pulling, the electrode tip is filled directly, by capillary action, when dipped in the filling solution. The electrode barrel can then be filled using a fine hyperdomic needle and a syringe. While air bubbles remain trapped in the tips of some electrodes prepared in this way, the method involves less risk of mechanical damage than filling with alcohol under reduced pressure and the overall yield of satisfactory electrodes is comparable. In addition, the electrodes can be stored dry and only filled immediately before

use, eliminating the possibility of large tip potentials through deterioration.

Microelectrodes filled with 3 M KCl are not altogether satisfactory for recording the activity of Helix neurons. This is because the intracellular chloride concentration is rather low in some cells and can be significantly altered by diffusion of ions from the recording electrode. This can result in an alteration in membrane polarization and in spontaneous activity (see KERKUT & MEECH, 1966; 1967). Under these circumstances potassium acetate or potassium sulphate is often used as an alternative to potassium chloride. These substances are somewhat less soluble than potassium chloride and are generally used at 1 M rather than 3 M concentrations. A slight difficulty arises through the use of silver-silver chloride wire connecting the microelectrode to the recording amplifier input; free chloride ions in the surrounding solution are essential if the silver chloride-liquid interface is to be non-polarizable. Because silver chloride is barely soluble it is some time before this condition can be established if the electrode is filled with an acetate or sulphate salt solution. During this time the electrode will be unstable giving 'noisy' and erratic results. However, if a small amount of potassium chloride is added to the filling solution, stability is ensured while neuronal activity should be unaffected. Microelectrodes were therefore usually filled with a solution containing potassium acetate or potassium sulphate at a concentration of 1 M and potassium chloride at a concentration of 0.1 M and gave consistent results without obvious long term effects on spontaneous activity. The membrane of Helix aspersa neurons seems to be impermeable to both acetate and sulphate ions (KERKUT & THOMAS, 1964)

and membrane potential will therefore be unaffected by diffusion of these ions from the microelectrode tip.

When required, double-barrelled microelectrodes were made using an expoxy resin/hardener mixture ('Araldite') to cement two 2 inch lengths of electrode glass together over a distance of about $1\frac{1}{2}$ inches, leaving about $\frac{1}{2}$ inch of single glass projecting at either end. Once the resin had set, the centre of the electrode assembly was heated over a miniature bunsen flame and twisted through 180^{o} to align the projecting ends. After this the electrodes can be pulled and filled in the normal way.

2) Suction electrodes;

Suction electrodes were made from fine (1 mm outside diameter) polythene tubing. A 3 inch length of tubing was gently heated over a miniature bunsen flame at a point just behind one of its ends. Carefully done, this produced a constriction in the tube and a terminal collar of melted polythene. The internal diameter was least at the base of the collar and increased towards the tip of the electrode. This 'inverse taper' helped to ensure a tight seal when the cut end of a nerve was sucked up into the electrode. Electrodes with minimum internal diameters in the range 100-200 μ were found suitable for recording spontaneous activity in the main nerves associated with the suboesophageal ganglia.

Electrical connection to the interior of the electrode was made by means of a fine silver wire passing down the centre of the electrode tube for most of its length. The tube was mounted on a suitable hypodermic needle and the concentric silver wire was wrapped

Suction electrode system;

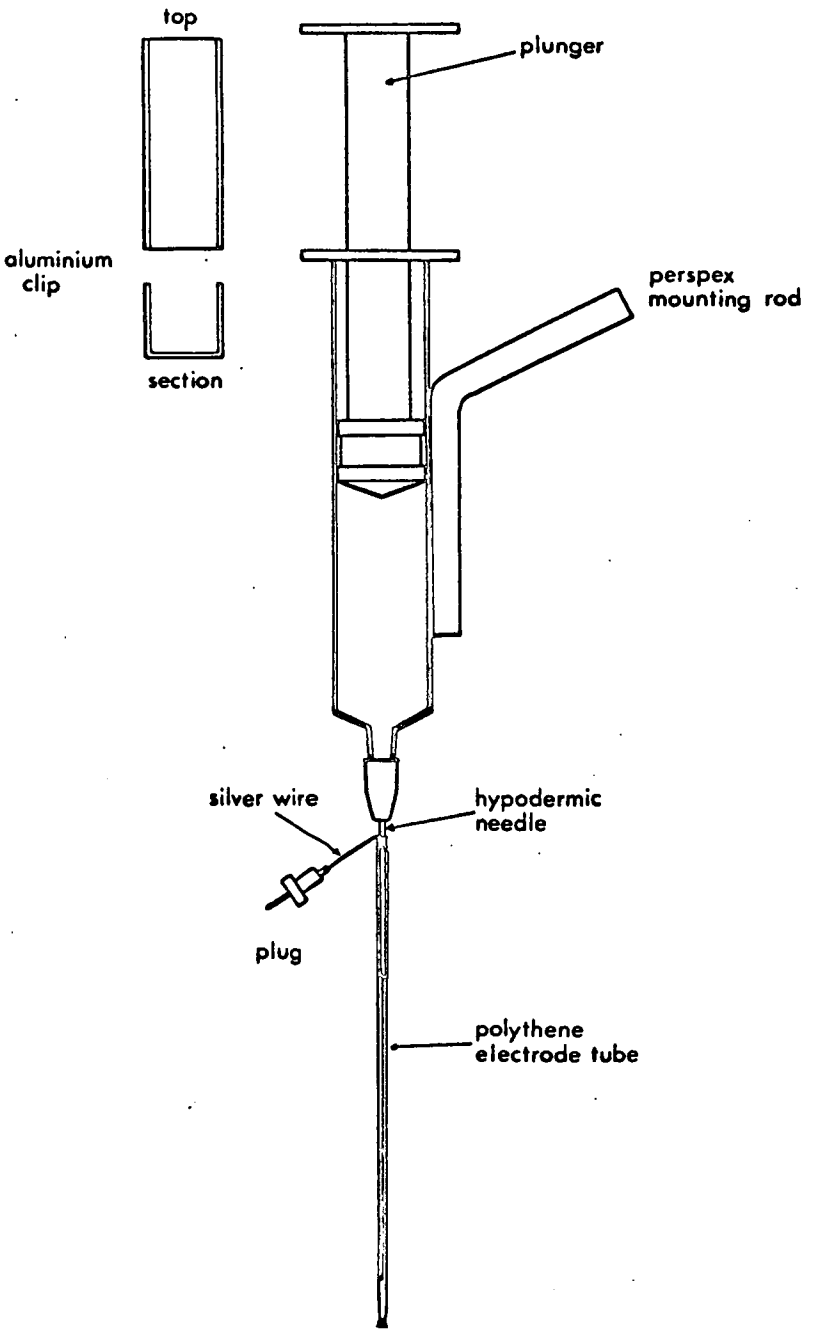

around the base of the needle several times before the joint was sealed with polystyrene cement. A 1 mm plug was soldered to the end of the silver wire to facilitate connection to the recording amplifier input.

The hypodermic needle electrode assembly was mounted directly on a 5 ml syringe. This in turn was glued to a perspex rod which could be rigidly fixed to a micromanipulator. The complete suction electrode system is illustrated in Figure 7. Suction was applied via the syringe and when the cut end of a nerve had been sucked up, suction was increased until a small aluminium clip could be accomodated between the top of the syringe tube and the two flanges on its plunger. In this way a tight seal between the end of the nerve and the electrode could be maintained throughout the recording period.

F) Histology;

Stained sections of the suboesophageal ganglia were prepared according to the following schedule;

1) Dissection, ganglia pinned out on wax.
2) Fixation in 5% glutaraldehyde in phosphate buffer (pH 7.5); 2h.
3) Wash in phosphate buffer; ½h.
4) Dehydration in graded alcohol series (30, 50, 70, 90, absolute); 24h. each.
5) Clear in xylene; 4h.
6) Embed in paraffin wax at 56°C; 3h.
7) Block out in paraffin wax.
8) Sections cut at 15 microns on rotary (Cambridge) microtome.
9) Sections placed on slides previously coated with egg albumen, allowed to dry thoroughly overnight above a hot plate.
10) Staining schedule;

a) Dewax in xylene; 10 min.
b) Hydrate to water through a graded alcohol series (absolute, 90, 70, 50, 30 water); 5 min. each.
c) Stain in cresyl violet (0.5% solution); 5 min.
d) Wash in running water; 2 min.
e) Dehydrate and differentiate in a graded alcohol series (50, 70, 90, absolute); 1 min. each.
f) Clear in xylene; 5 min.
g) Mount under coverslip with DPX mountant.

Sections were photographed on Ilford FP4 35mm film using a Tessovar (low power) or a Zeiss (higher power) photomicroscope system. Prints were made on Ilfobrom (No.2 or No.3) photographic paper.

G) Electronics;

1) Recording amplifiers;

a; Recording membrane potential intracellularly;

The main difficulty in recording intracellularly from individual nerve cells lies in the fact that nerve cells have a substantial source resistance; resting nerve cell membrane resistance is characteristically as high as 5 megohms for individual cells in the visceral ganglion of Helix aspersa (CHAMBERLAIN & KERKUT, 1969). In addition to this, glass microelectrodes sufficiently fine to penetrate individual cells and filled with concentrated potassium chloride will have resistances of 10-20 megohms, giving a combined cell-plus-electrode resistance of 15-25 megohms. The recording situation is shown in Figure 8(A), in which the nerve membrane is represented by its electrical analogue. Clearly, a potential divider is formed between the cell-plus-electrode resistance and R_{in}, the input impedance (resistance) of the recording amplifier. In order to offset attenuation of the input signal across the cell-plus-electrode resistance, the recording amplifier must have an extremely high input impedance. A value of 1,000 megohms, giving a recording error of 1-2% may be taken as the minimum acceptable input impedance.

A second difficulty is associated with the high cell-plus-electrode resistance; if the recording amplifier has even a relatively small input capacity the input signal may be seriously distorted. Figure 8(B) illustrates this situation; if the amplifier input impedance is sufficiently high, the circuit has a time constant given by $(R_m + R_{el}).C_{in}$ (KATZ, 1966). If $(R_m + R_{el})$ is taken as 20

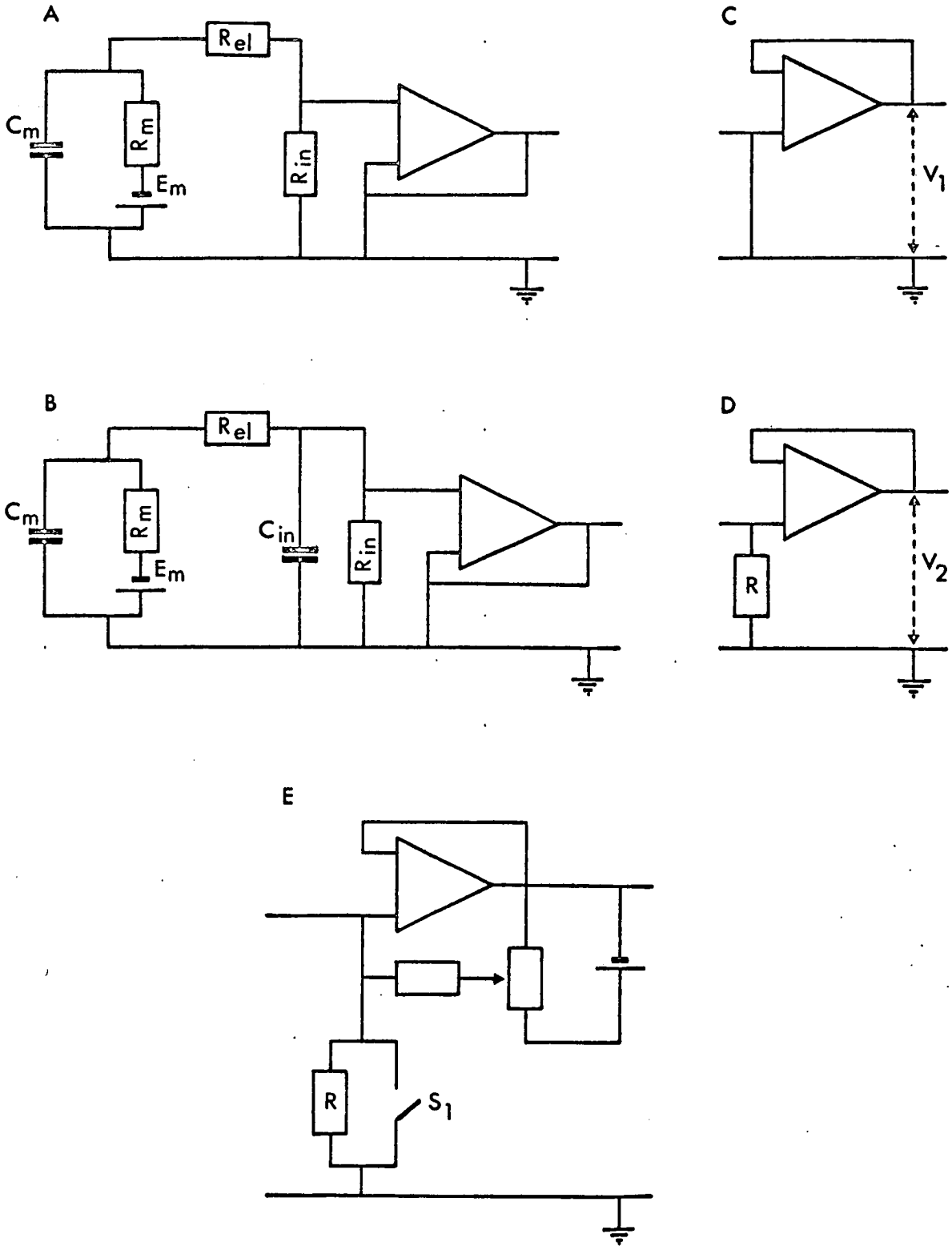

for explanation see text

megohms and C_{in} as 100 picofarads (pF), the time constant has a value of 2 milliseconds, corresponding to an upper limiting frequency of 80 Hz. Clearly, some way must be found of reducing the effect of any input impedance.

The conventional recording amplifier is a valve cathode follower which, properly constructed (BURES, PETRAN & ZACHAR, 1962, p.109), can give an input impedance of 10^{12} ohms or more. Cathodal screening of the input lead reduces the effective input capacity by a factor equivalent to the voltage amplification characteristic (μ) of the valve. However, satisfactory semiconductor designs are now possible which have the advantages of small size and low power consumption, and particularly important, an inherent input capacity which is, generally, substantially lower than that of valves. It was therefore decided to develop a semiconductor circuit as a replacement for the conventional valve cathode follower.

Input impedance of the appropriate magnitude can be obtained in D.C. amplifiers using field effect transistors (F.E.T's) (TOWERS, 1968; WEBB, 1965). However, only a limited number of junction gate F.E.T's are suitable while insulated gate F.E.T's can be damaged through the build-up of electrostatic charges when the input (gate) goes open circuit. As an alternative, integrated circuit voltage follower operational amplifiers are now available with dynamic input impedances of 1,000 megohms or more. This input impedance is achieved through negative feedback and since the input device is a bipolar transistor, there is no possibility of electrostatic damage when the input goes open circuit.

The term dynamic input impedance should not be misinter-

preted. Operational amplifiers in the voltage-follower configuration draw a finite current when the input is earthed directly (Figure 8(C)). This input current gives rise to a voltage at the input called the offset voltage (CLAYTON, 1972). Since the circuit is a unity gain configuration the offset voltage can be measured at the output (V_1). If the input is earthed through a resistance the input current drawn produces a voltage drop across this resistance (R) and there is an alteration in the output voltage (V_2) (Figure 8(D)). The magnitude of the input current is given by $\frac{V_2 - V_1}{R}$. If a signal (δV) is applied at the input there will be a corresponding change (δI) in the input current. The resistance given by $\frac{\delta V}{\delta I}$ is the dynamic input impedance. The important point is that while the dynamic input impedance may be extremely high, the magnitude of the input current can still be sufficient to introduce significant recording errors. In recording intracellularly from nerve cells an input current of 2 nA and a membrane resistance of 5 megohms will give an error of 10 mV in the recorded resting potential. That is, the input current drawn will substantially depolarize the cell. Action potentials produced by such a cell can, however, be recorded accurately if the dynamic input impedance of the voltage-follower is sufficiently high.

If, as an alternative to the input current being drawn through the preparation, this current can be supplied from elsewhere, without substantially reducing the dynamic input impedance, then depolarization is eliminated and a voltage-follower operational amplifier can be used as a basis for a satisfactory recording amplifier. Such a circuit is given in Figure 8(E). The input current is supplied from a battery and potential divider connected

to the output; correct adjustment of the potentiometer is obtained when the output voltage is unaltered by closing the switch (S_1). The reduction in dynamic input impedance is very slight.

The LM 302 voltage-follower operational amplifier was selected as the basis of the recording amplifier. This integrated circuit has typical characteristics as follows; a dynamic input impedance of 10^{12} ohms, an input capacity of 3 pF and a voltage gain of 0.9995, corresponding to an open loop gain of 2,000 (NATIONAL SEMICONDUCTOR CORPORATION, 1971). These characteristics represent an improvement on those of the cathode follower; the input capacity is lower and the voltage gain higher.

Several simple circuit configurations were tested. The circuit finally adopted is given in Figure 9(A) and incorporates two LM 302 integrated circuits. The first of these is a unity gain voltage-follower; the second acts as a low pass active filter having a cut-off frequency of 10 KHz. This gives a bandwidth acceptable for most electrophysiological work and reduces the source noise (WHITFIELD, 1960, p.118) and any high frequency interference. This reduction in bandwidth is also advantageous since the inherent noise level of operational amplifiers is slightly higher than that of discrete devices. The input lead is screened by the output; this reduces the effect of the already small input capacity in the same way as cathodal screening reduces the input capacity in the conventional valve circuit. Figure 9(B) gives a 'Veroboard' layout for the circuit. To reduce any stray capacity all the unused copper strip was removed. Sockets were used for the integrated circuits to prevent heat damage during soldering. The circuit was screened by mounting it in a small earthed aluminium box. In the experimental

A; Voltage-follower amplifier

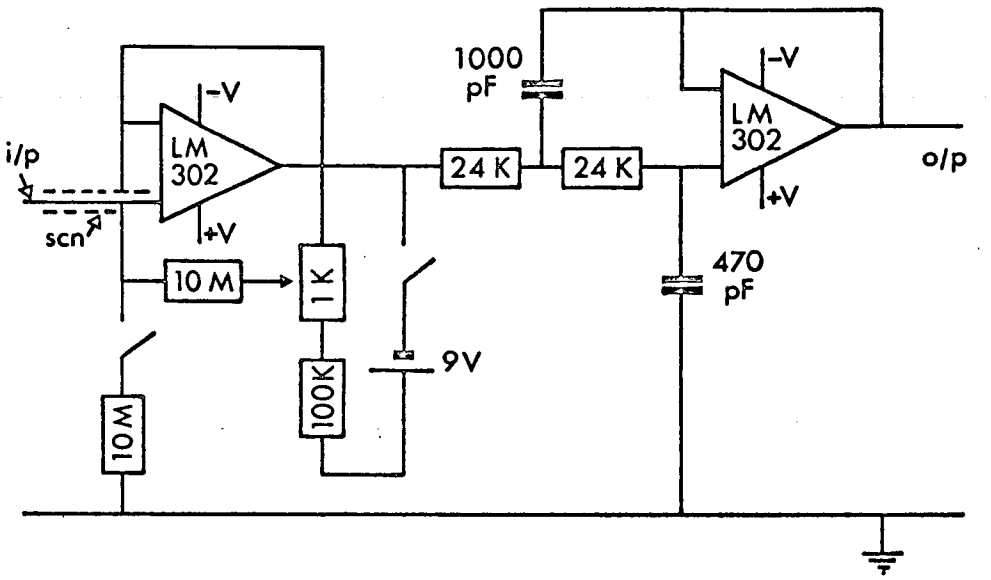

B; Veroboard layout (underside)

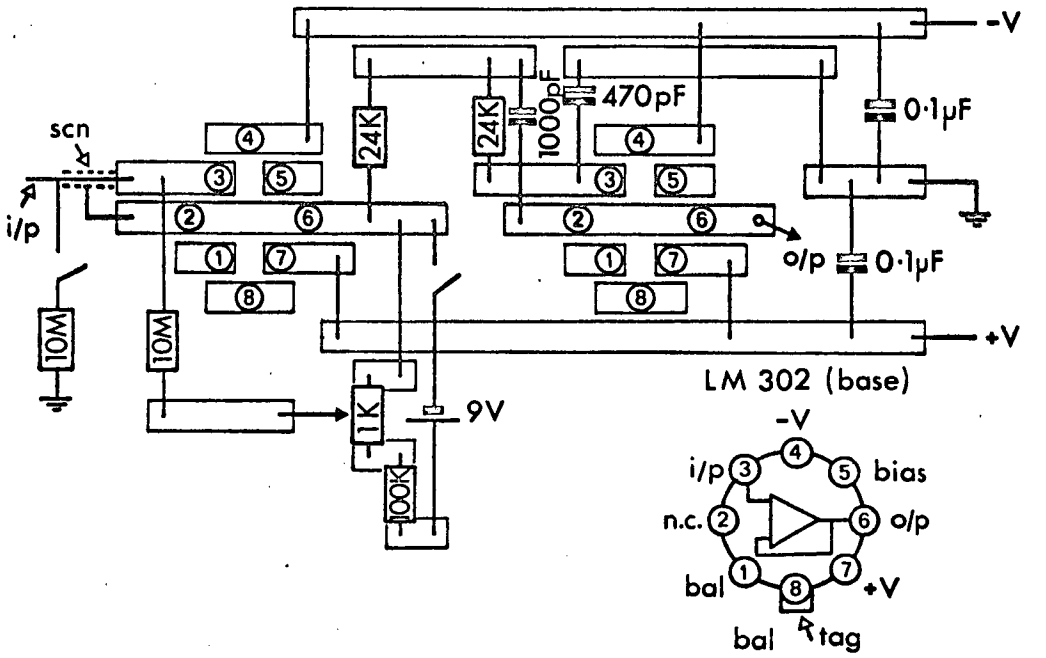

C; Frequency response (10 M in series with input)

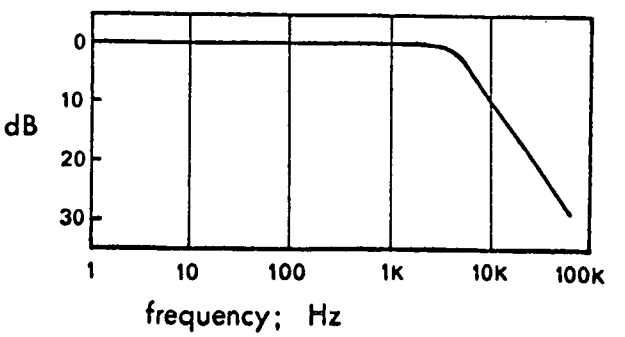

Power supplies;

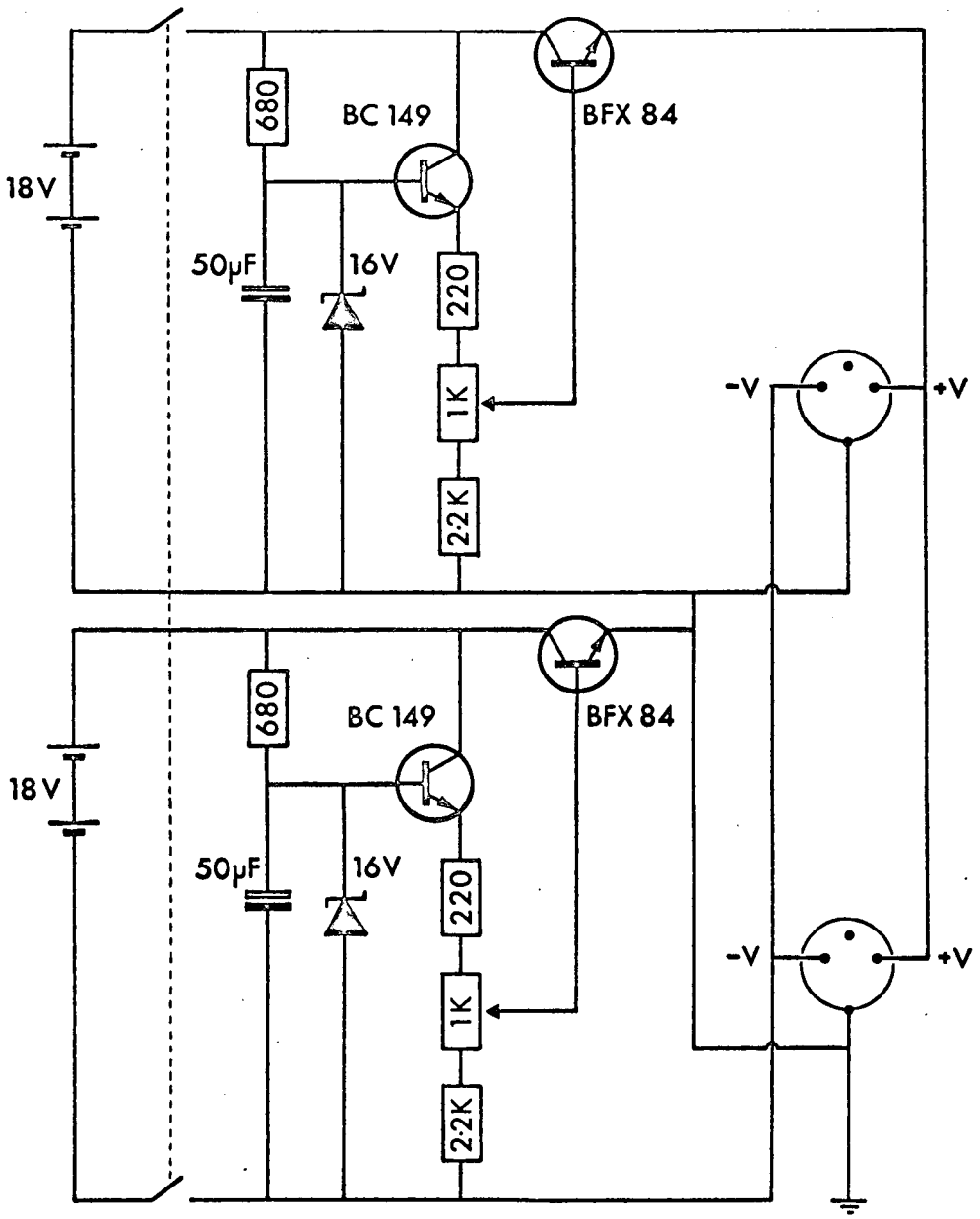

positive and negative output voltages variable in the range 10-14 volts

Recording circuit;

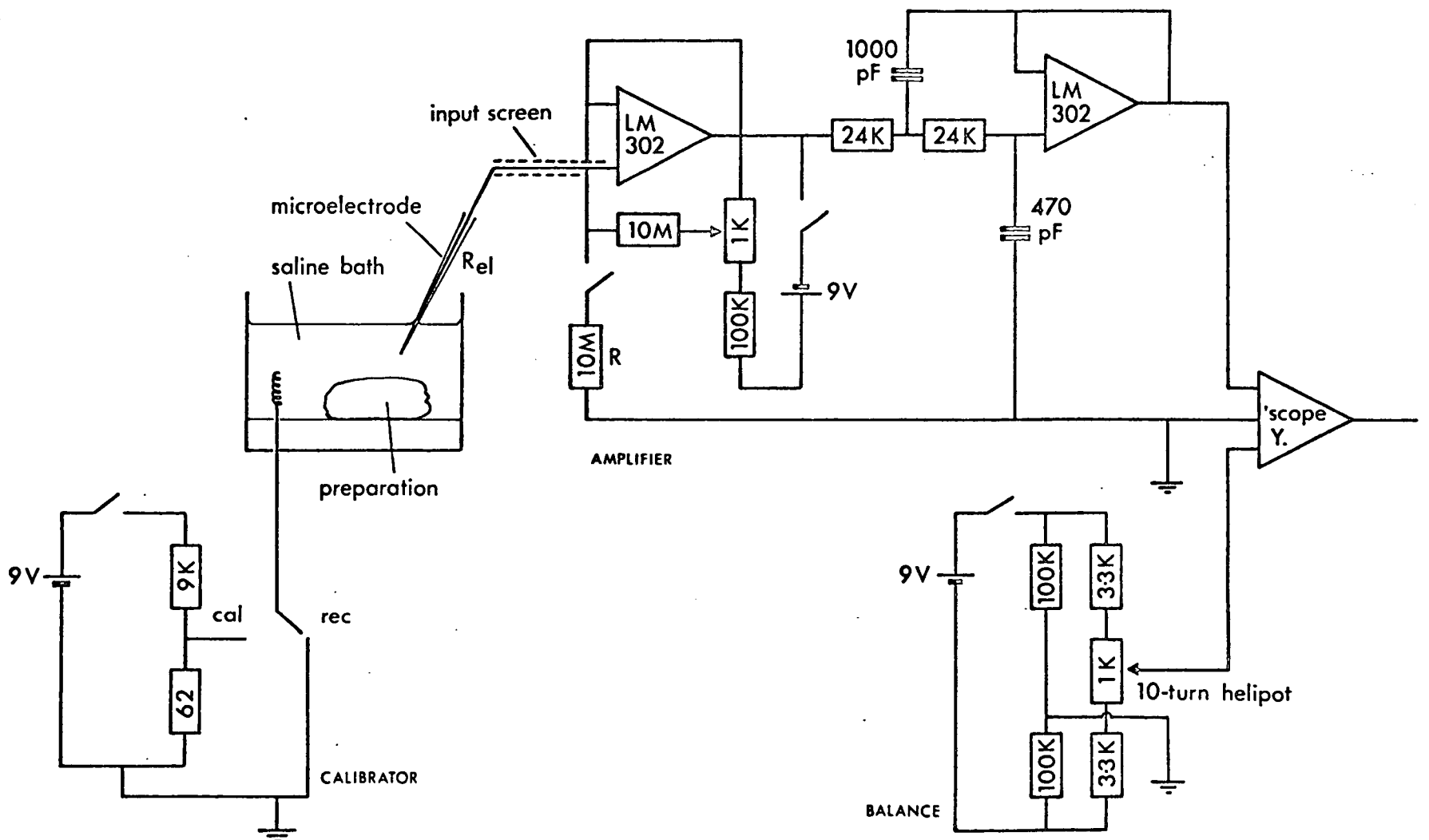

situation this could be placed close to the recording microelectrode and the input connection made with a short (8 cms.) piece of screened lead. (Long input leads are not desirable since they can substantially increase the input capacity.) With a 10 megohm resistance in series with the input, the circuit has the frequency response given in Figure 9(C).

The circuit can conveniently be operated from battery-driven stabilized power supplies since its current consumption is low (10 mA). The circuit for the power supplies used is given in Figure 10. Stabilization is desirable for D.C. amplifiers since alterations in output level ('drift') can occur as a result of variations in power supply voltages. Mains interference is absent from battery driven supplies. Connections between the power supply and the voltage-follower amplifier were made with 2 core shielded lead and 3 pin DIN plugs and sockets and two 0.1 μF capacitors provided decoupling at the power supply input to the amplifier.

The complete recording circuit is given in Figure 11. Any standing output voltage from the amplifier, including electrode tip potentials, can be offset using the balance control which, by virtue of a 10-turn potentiometer, also provides a fine control of recording trace position on the oscilloscope screen. Input offset adjustment controls output voltage directly and involves varying the gains of the input pair of transistors of the LM 302 also using a multi-turn potentiometer. This method was found to be less satisfactory leading to an increased noise level.

In conjunction with the switched 10 megohm resistor (R) on the amplifier input the calibrator is used to measure electrode

resistance (R_{el}). The calibrator supplies a standard 60 mV D.C. signal. Provided the amplifier input impedance is sufficiently high, this is recorded unattenuated unless the 10 megohm resistor is switched in, when there is a reduction in the recorded voltage. The difference in recorded voltages is proportional to electrode resistance which is given by; $R_{el} = R.\frac{60 - V_{(R)}}{V_{(R)}}$ where $V_{(R)}$ is the voltage recorded with the switch closed. Suitable electrodes, those with resistances in the range 10-20 megohms when filled with 3 $\bar{M}$ KCl, can be readily identified.

In later experiments a second type of amplifier was also used for intracellular recording. This had the circuit given in Figure 12 and incorporates a Teledyne Philbrick model TP 1421 operational amplifier. Junction gate field effect transistors are used as the input stages within this device. The input current drawn is extremely small (15 pA) and for practical purposes can be neglected. Input impedance is kept constant by the use of a 10^9 ohm input resistor (R1). Extremely high value resistors suitable for this purpose have become available only recently.

The first 741 operational amplifier buffers the TP 1421 and the proportion of negative feedback can be adjusted (VR1) to obtain exact unity gain at the output. The second 741 provides a negative capacitance facility i.e. any input capacity can be neutralized by positive feedback at higher frequencies and the overall response of the amplifier is consistent with negligible input capacity. 'Backing-off' in this case was supplied by way of a 1 megohm potentiometer connected across the power supply rails. As in the first intracellular amplifier the input was screened by the output.

Intracellular amplifier;

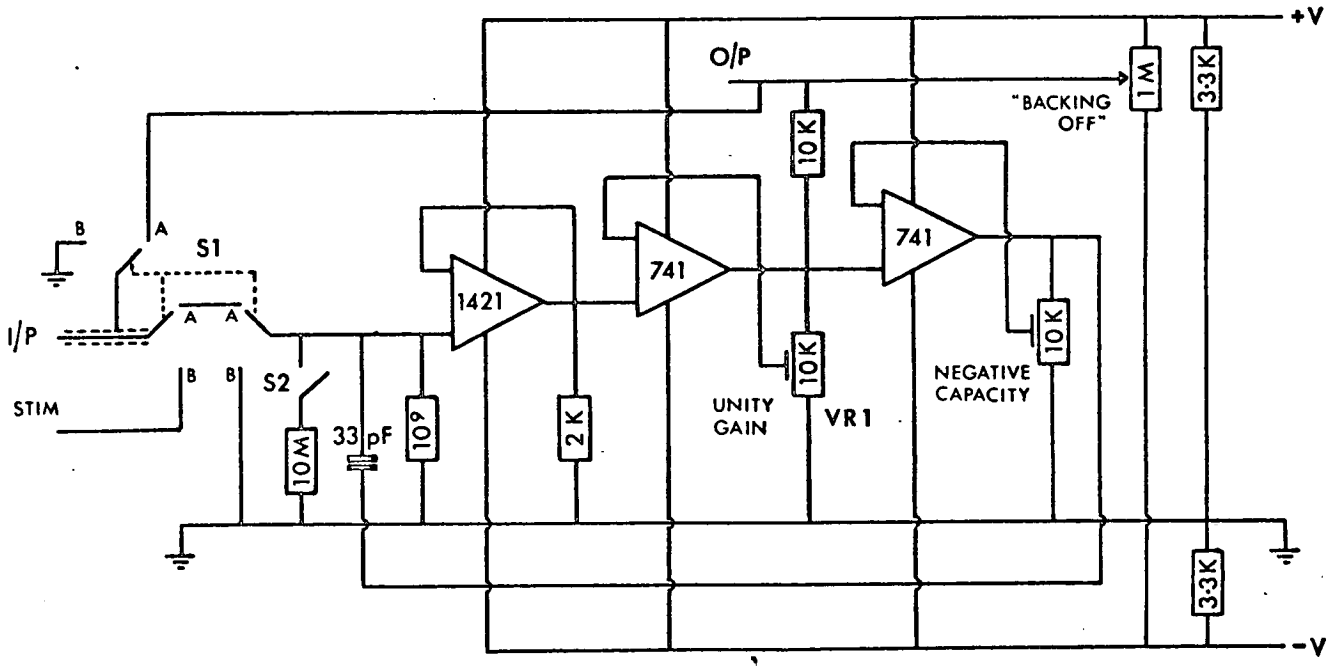

Intracellular amplifier ; veroboard layout (underside) ;

741 ; underside

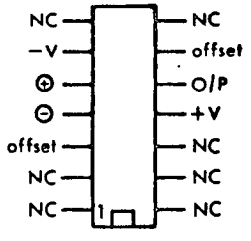

1421; underside

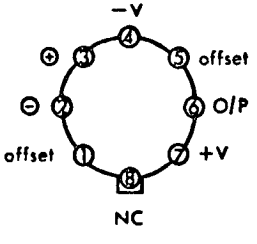

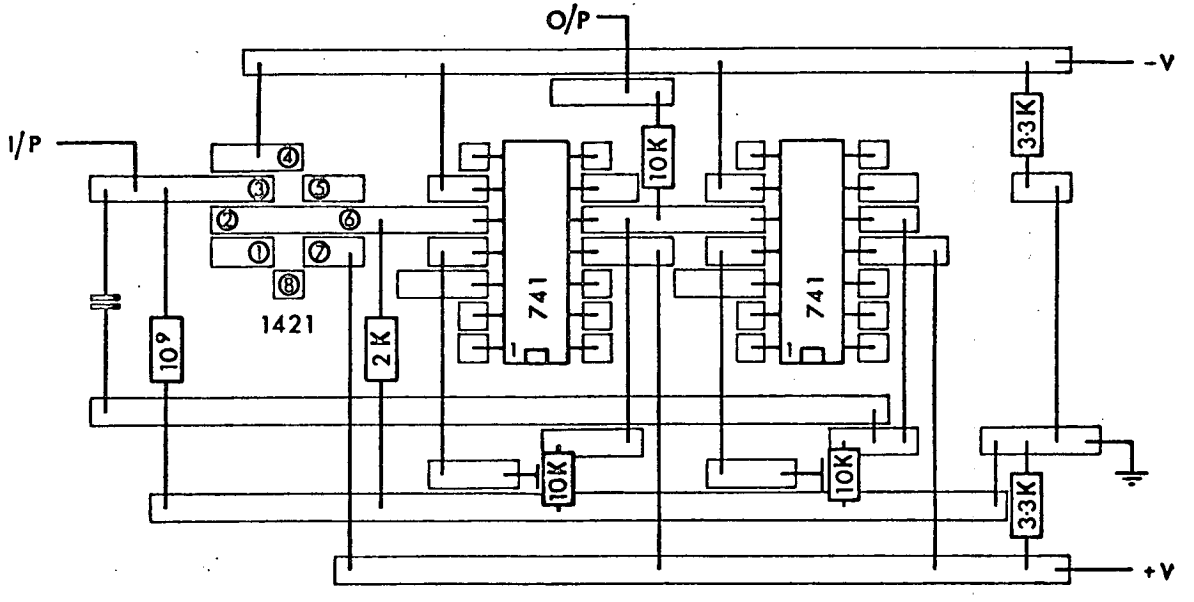

The imput switch S1 allows the intracellular recording microelectrode to be used for stimulation; at the same time the amplifier input and the input screen are earthed to prevent damage to the input stages of the TP 1421 through capacitative coupling to the stimulus leads. The amplifier was constructed according to the veroboard layout shown in Figure 13 and was mounted in an earthed aluminium box. A small aluminium cover was used to screen S1 from the rest of the circuit within the box. Power supply connections were made via 2 core shielded lead and 3 pin DIN plugs and sockets from the stabilized power supply already described.

b; Extracellular recording;

The specifications of an amplifier suitable for extracellular recording are less stringent than those of an amplifier for intracellular recording. Essentially, nerve activity is recorded as the potential produced across the tissue resistance between the recording electrodes. Successful recording depends on increasing this resistance as far as possible. If hook electrodes are used, this is achieved by lifting the nerve out of the saline bath into a layer of oil or directly into the air. With suction electrodes it is sufficient to ensure a tight seal between the nerve and the end of the electrode. In either case, the signal source resistance will be small compared to that of individual nerve cells. In addition, electrode resistance will not be substantial. The combined source-plus-electrode resistance would not be expected to exceed 100 K or so, and could in fact be very much lower. An amplifier input impedance in the range 10-100 megohms should be adequate to ensure a signal loss of less than 1%.

Differential extracellular amplifier;

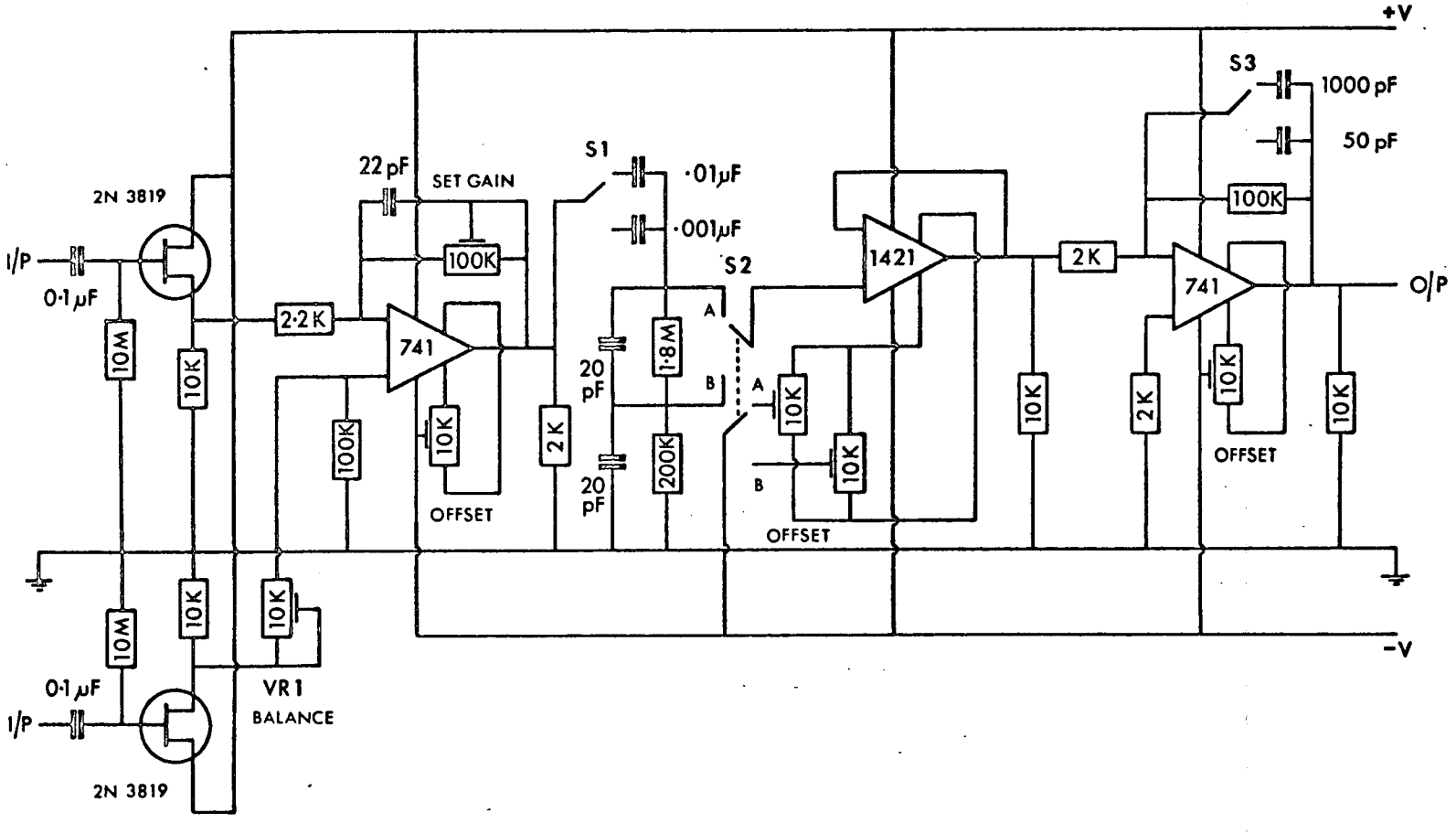

A component of the tissue resistance to earth will shunt the tissue resistance between the recording electrodes and may lead to substantial signal loss especially when recordings are made from large nerve bundles. In view of this inherent signal attenuation a unity gain amplifier is not appropriate although, depending on the oscilloscope available, the gain required may not be substantial.

Since extracellular D.C. levels are of little interest in the present context the amplifier may be A.C. coupled although a reasonable low frequency response is desirable so that fairly slow action potentials do not become further attenuated. The high frequency response of the amplifier should be restricted since this effects a reduction in source noise as in the case of the intracellular amplifier. Bandwidth reduction is especially important in an extracellular amplifier since only small amplitude input signals may be available.

The amplifier circuit used is given in Figure 14. Differential inputs are provided so that nerve activity need not be recorded with respect to earth. However, either input may be earthed to obtain single-sided operation. The gains of the two inputs can be matched by means of the balance control (VR1). S1 provides low frequency cut-off options of 10 or 100 Hz and S3 high frequency cut-off options of 1000 Hz or 20 KHz; S2 provides gain options of 2000X (A) or 200X (B). The offset potentiometers are adjusted in each case for zero D.C. output from the corresponding operational amplifier. The amplifier was constructed in an earthed aluminium box and power supply connections were made via 2 core shielded lead and 3 pin DIN plugs and sockets from a $\pm$ 9V battery supply.

Differential amplifier;

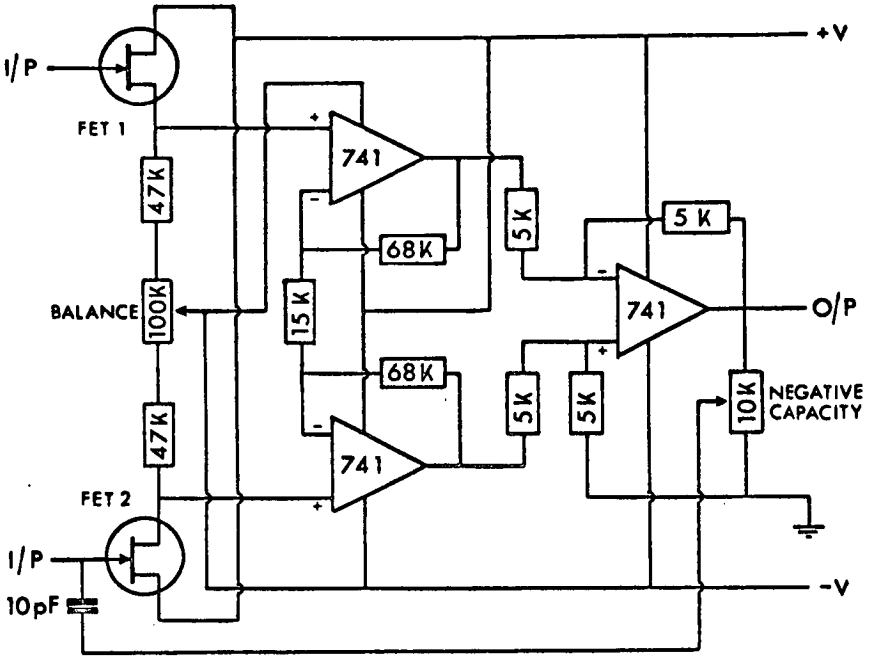

FET 1&2; U250A

c; Differential high input impedance amplifier;

For some experiments it was desirable to monitor stimulus current delivered to the preparation. This involves recording the potential produced across a fixed resistance in series with the stimulating microelectrode. High impedance differential inputs are required if the recording amplifier is not to shunt the microelectrode resistance and thereby reduce the effective stimulus current.

The circuit used is given in Figure 15. Differential inputs are provided by a low noise dual junction gate F.E.T., type U250A. The input current drawn at each input is very small (1 pA) and input impedance is correspondingly high. The overall voltage gain of the amplifier is 10X. Maximum common mode rejection is obtained by adjustment of the balance control and a negative capacitance facility is available for the non-inverting input. Either input may be earthed.

This amplifier was occasionally used for intracellular and also for extracellular recording since its low noise characteristics proved to be useful.

2) Stimulator;

The stimulator used was constructed very much along the lines of that described by Bannister & Kay (1965) and consists of a number of units which, by appropriate interconnection, provide a comprehensive range of stimulating facilities. Some modifications were necessary due to the use of substitute transistors. Circuit diagrams incorporating these and other slight alterations are given below along with brief circuit descriptions for each unit. Power supply circuits are also given.

a; Time-base unit;

The circuit of the time-base unit is given in Figure 16. The time-base waveform of the final oscilloscope display provides the input for the unit which consists of a potential divider and a triple emitter-follower and serves merely as an impedance converter and to attenuate the time-base waveform from its original amplitude of 150 volts or so, to a level suitable for triggering the next unit of the stimulator.

b; Delay unit;

The delay unit (Figure 17) provides one trigger pulse per time-base sweep. The attenuated time-base waveform with an excursion of about 9 volts is fed, via an emitter-follower (TR5) to a complementary bistable circuit (TR6, TR7). The D.C. level of the time-base waveform can be adjusted by means of a stepped 10 position switch (S1) and the emitter-follower TR4, a smooth control (VR1) spanning each step. Spatial position of the trigger pulse along

the oscilloscope x-axis is thereby controlled. Changes in time-base velocity have no effect on spatial position.

The output of the unit is a short positive-going pulse corresponding to the leading edge of the complementary bistable pulse.

c; Tetanus unit;

The tetanus unit (Figure 18) generates a train of trigger pulses of controlled frequency. This can be varied between 1/sec. and 1,000/sec. and the overall duration of the train from 10 msec to 10 sec. The pulses superimpose on the display from sweep to sweep whatever their frequency.

The monostable TR9, TR10 can be activated either by a delay unit trigger pulse or manually (sw1, PB1) and determines train duration via the emitter-follower TR11 and the 'gating' transistor TR12. The pulse repetition frequency (p.r.f.) is derived from the multivibrator (astable) TR13, TR14. Train duration is altered by means of S2 (coarse) and S3 (fine) and p.r.f. by means of S4 (coarse) and S5 (intermediate); VR2 providing continuously variable fine control. Continuous operation is obtained either switched (sw2) or manually (PB2).

The multivibrator output is fed via the emitter-follower TR15 to a differentiating and clipping network such that the output of the unit is a series of short positive-going trigger pulses.

The use of Zener diodes in the two switching circuits should be noted. This substantially increases the permissible variation in the value of the timing resistors for given values of

Time-base unit ;

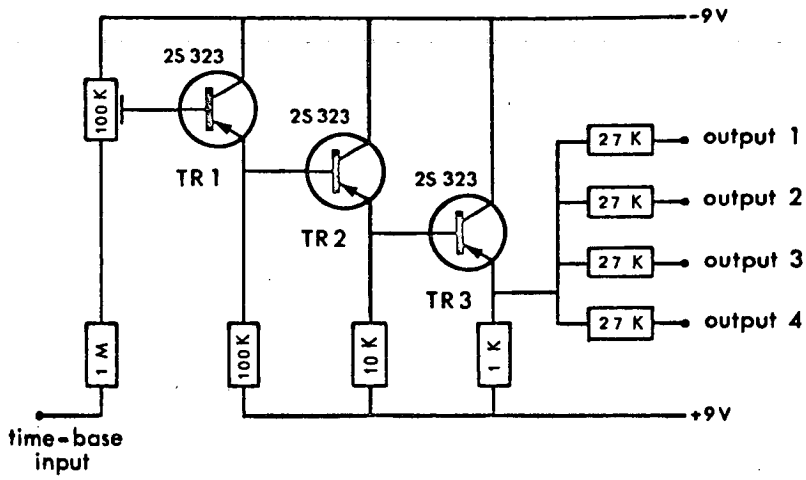

Delay unit;

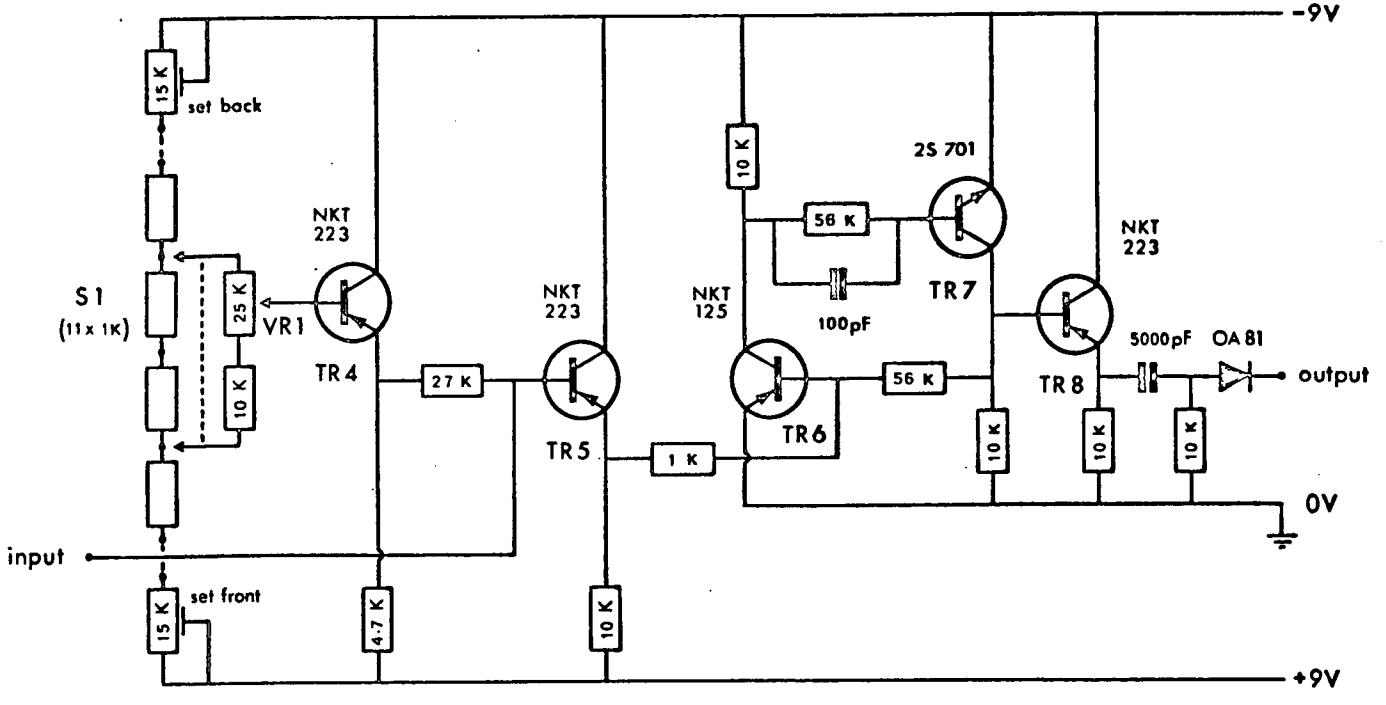
-9V
15 K
set back
NKT
223
S1
(11 x 1K)
25 K
VR1
10 K
TR4
27 K
NKT
223
TR5
1 K
10 K
58 K
2S 701
100pF
TR7
NKT
125
TR6
56 K
NKT
223
TR8
5000pF
OA 81
output
10 K
10 K
10 K
0V
input
15 K
set front
4.7 K
10 K
+9V

Tetanus unit;

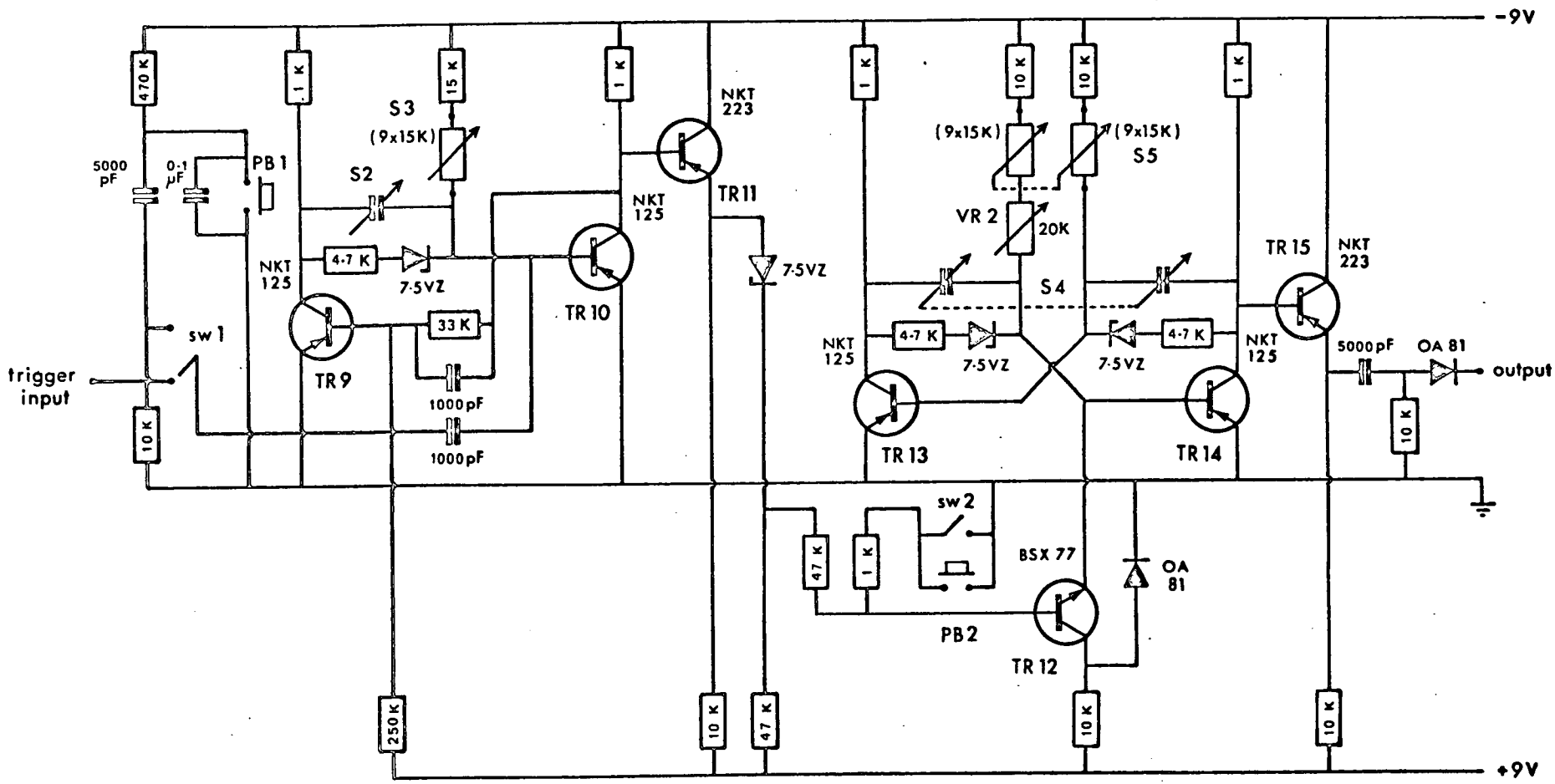

Stimulator unit;

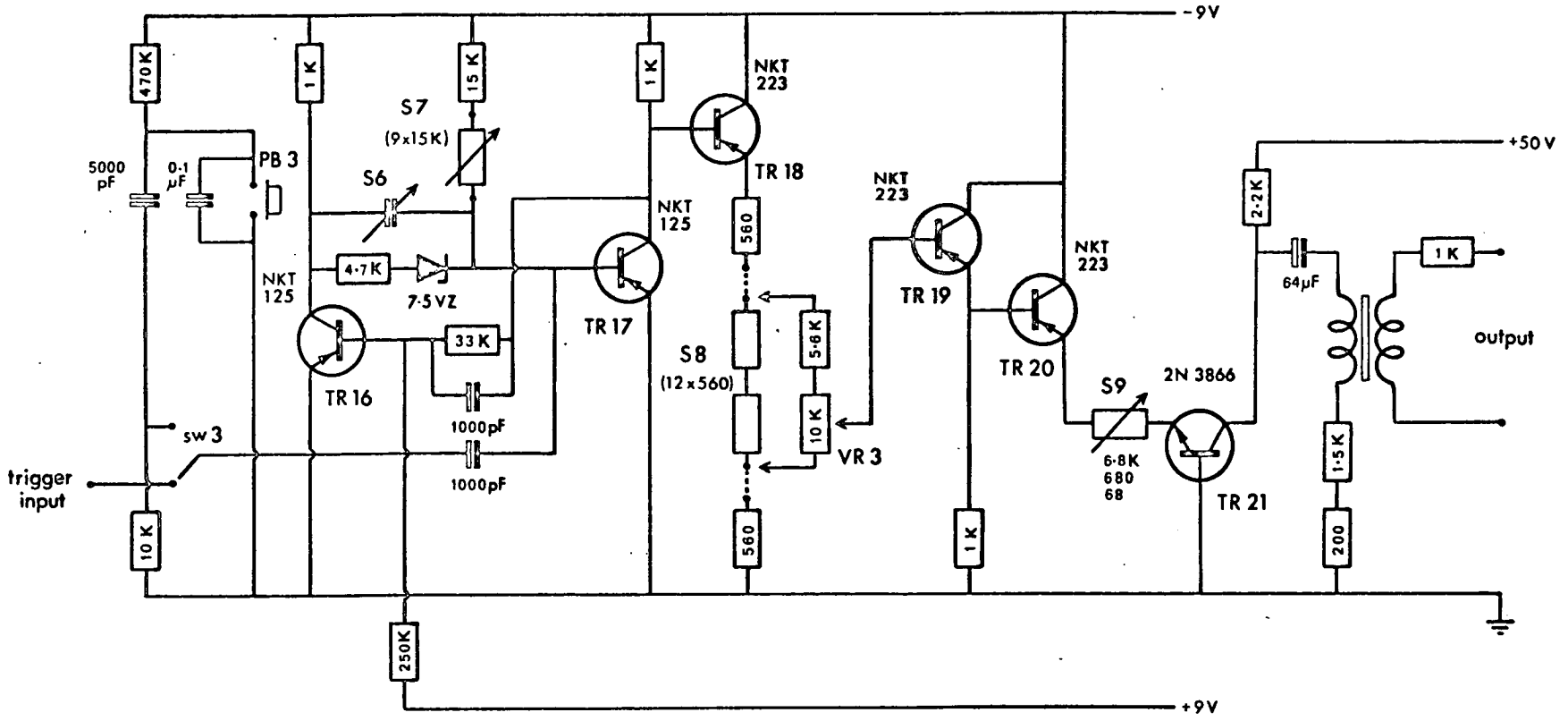

Direct output unit;

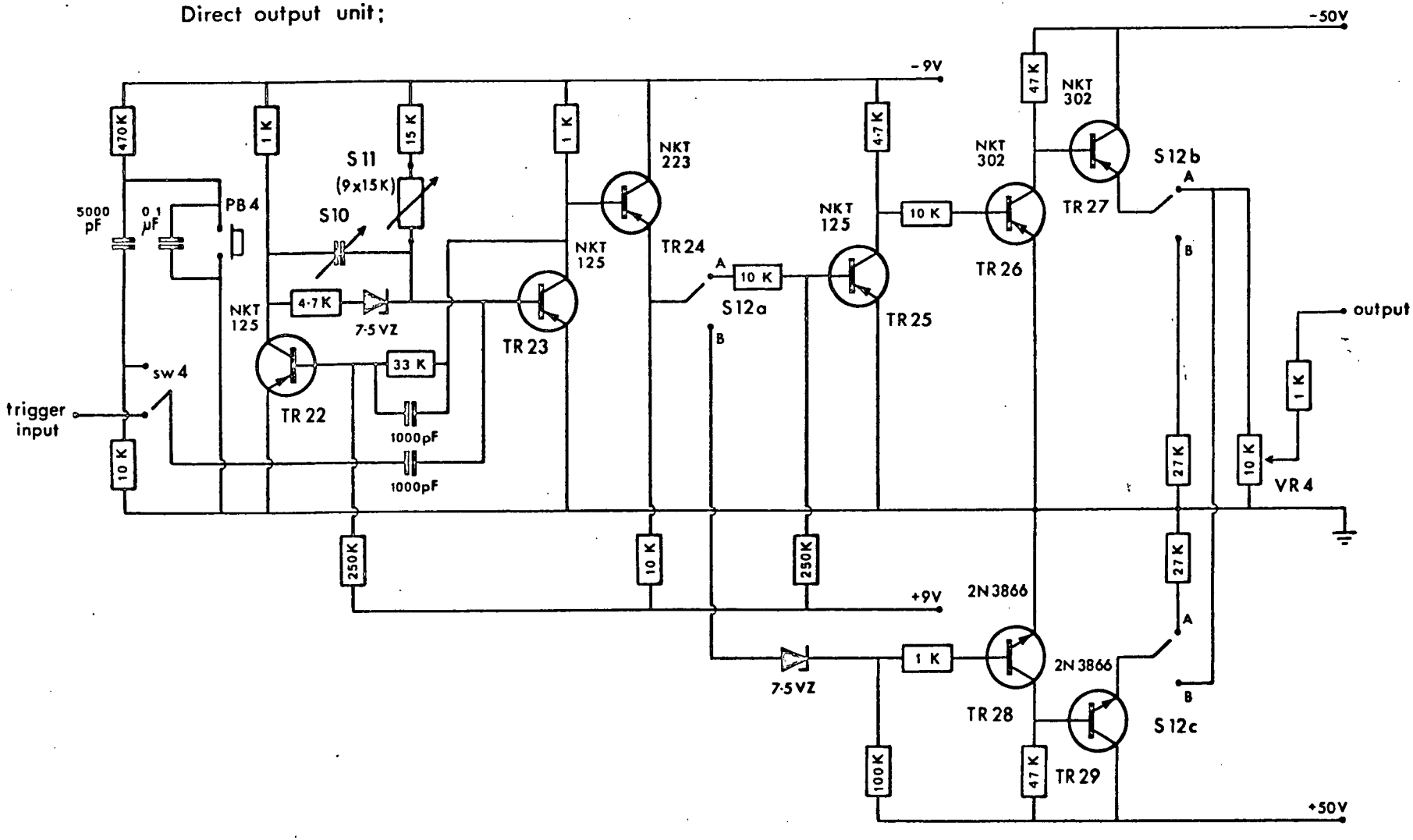

Power supply unit (±9V);

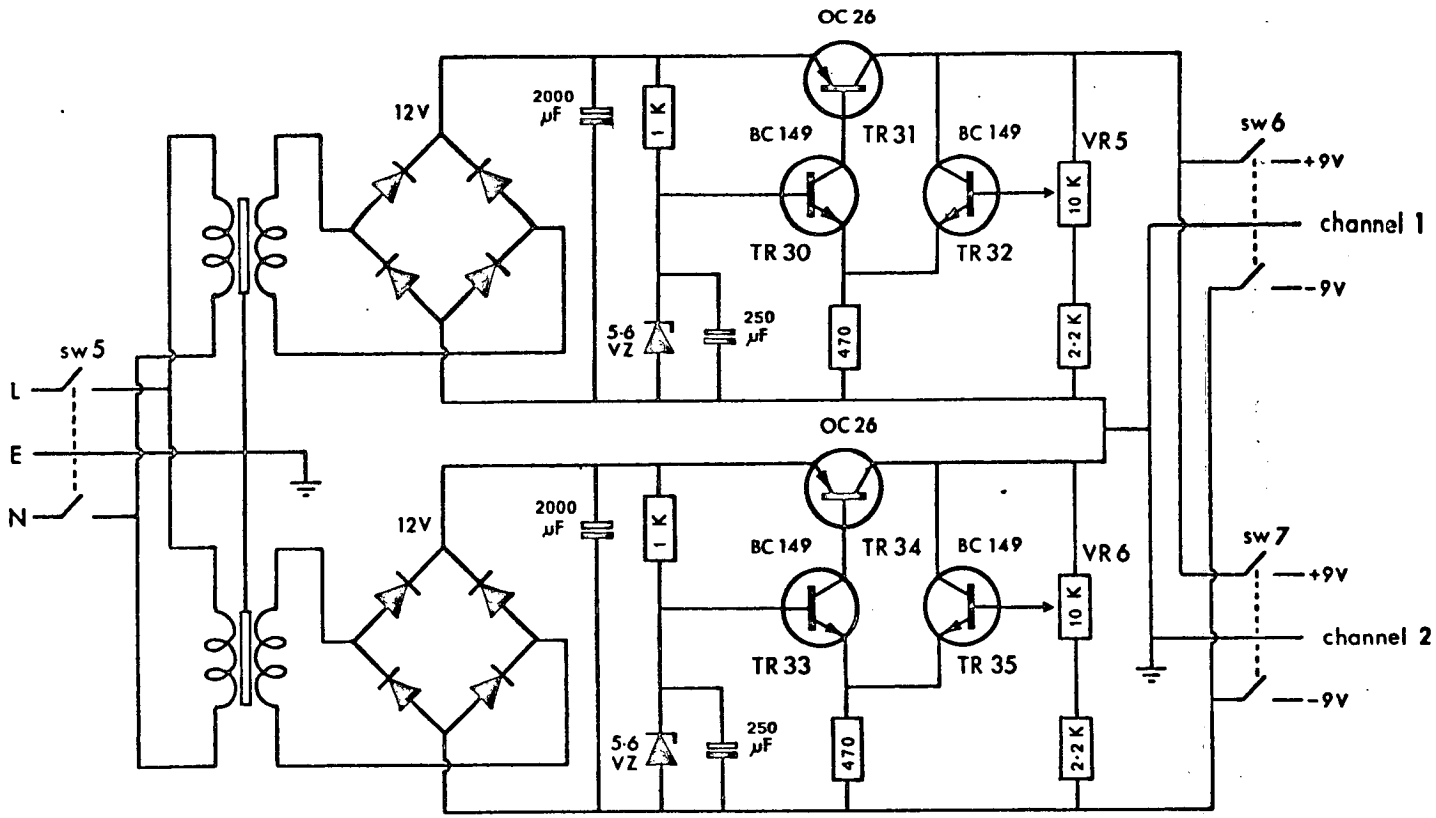

Power supply unit (±50V);

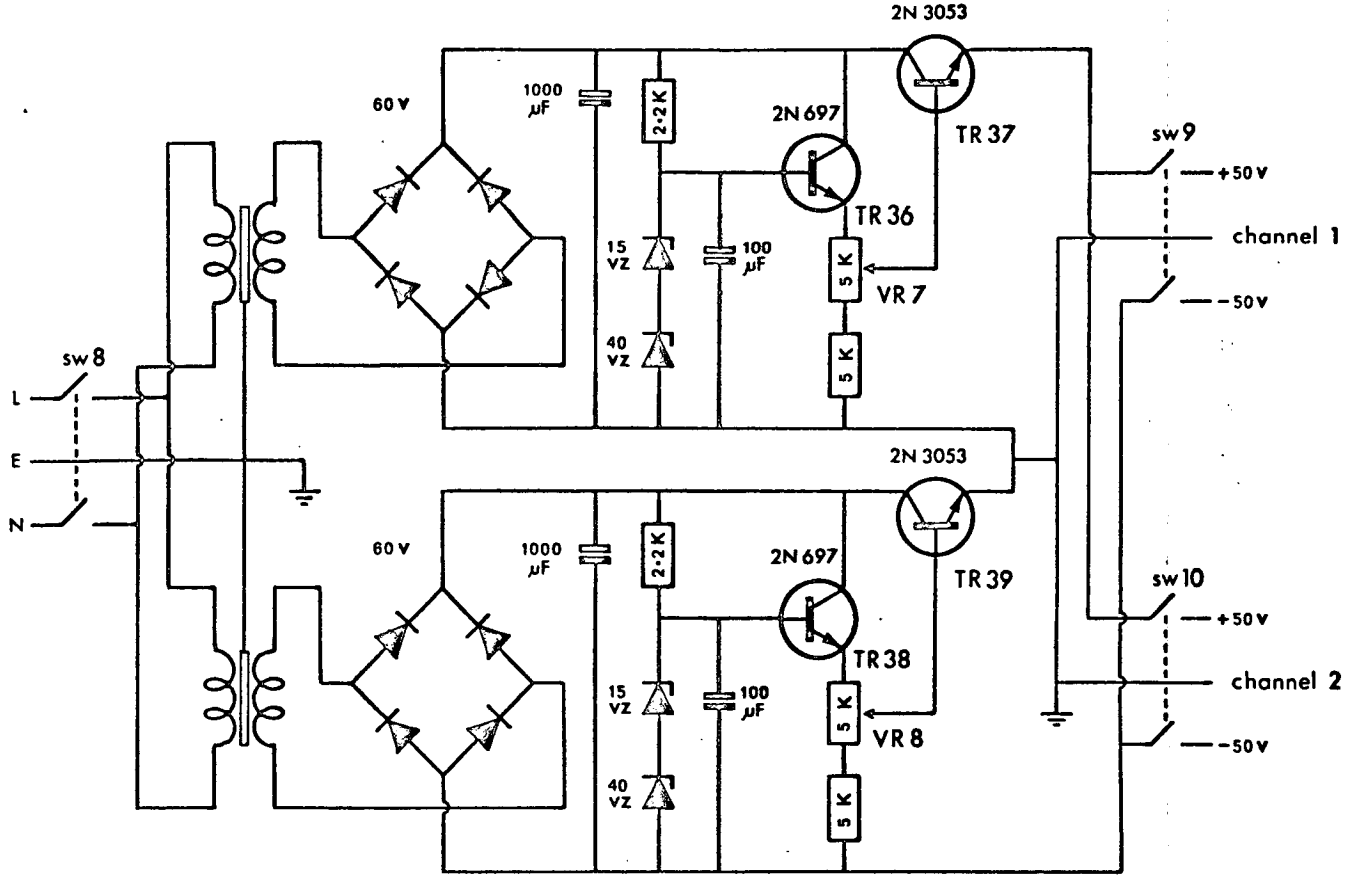

the timing capacitors (BANNISTER, 1963). A wide range of train durations and pulse repetition frequencies can therefore be obtained through resistive rather than capacitative switching giving greater accuracy and simplifying switching requirements.

In the monostable (train duration) circuit, TR9 is normally off and TR10 saturated, its base being fed via 1 kilohm and 4.7 kilohm resistances in series with the Zener diode. A variable resistance controlled by S3 is in parallel. The Zener voltage is arranged to be about 20% less than the supply voltage. When the circuit is triggered, in this case by a positive pulse applied to the base of TR10, TR10 is driven off and TR9 is driven on. The potential at TR9 collector is now about 0 V and the base potential of TR10 (connected to TR9 collector via a capacitor) is about +9 V. TR10 base potential will decay as the capacitor discharges through the Zener diode and serial resistances and through the variable resistance. However, when the base potential decays to the Zener voltage the Zener diode will cut off and the time course of further decay will be determined by the value of the variable resistance.

d; Stimulator unit;

An isolated stimulus pulse of variable duration (100 μsec - 100 msec) and amplitude and suitable for extracellular stimulation is produced by the stimulator unit (Figure 19). The unit can be triggered automatically, by delay unit or tetanus unit pulses, or manually (sw3, PB3).

The pulse duration circuit operates in the same way as the train duration circuit of the tetanus unit. TR21 in the constant

current (grounded base) configuration, delivers the output pulse. Output pulses are available in three current ranges 0–100 μA, 0–1 mA and 0–10 mA and the switched coarse and intermediate current amplitude controls are S9 and S8, VR3 giving continuous fine control.

The output transformer, type 5K 9445/3 by Jorgen Schou of Copenhagen, is doubly screened and is especially suitable for stimulus isolation (GULD, 1959). Output pulses remain tolerably rectangular, and of more or less constant amplitude, for durations of up to 10 msec.

e; Direct output unit;

The direct output unit (Figure 20) provides positive or negative rectangular pulses suitable for intracellular stimulation. Triggering is either automatic or manual as in the case of the stimulator unit.

Pulse duration, variable from 100 μsec – 10sec., is controlled by S10 and S11, and pulse amplitude, variable from 0–50 volts, by VR4. Pulse polarity can be changed by means of S12 which also switches the appropriate output to the final amplitude potentiometer.

f; Power supply units;

A two channel stimulator, consisting of 1 time-base unit, 4 delay units, 2 tetanus units, 2 stimulator units and 2 direct output units, has the following power supply requirements; +9 V at 150 mA, –9 V at 500 mA, +50 V at 150 mA, –50 V at 100 mA. These requirements were met by two stabilized power supply units of fairly

orthodox series regulator design.

Two pairs of transistors in the long tail pair configuration formed the basis of regulation in the ± 9 V supply circuit (Figure 21). Output voltages, variable between VZ, the Zener voltage, and the input voltage are adjusted by means of VR5 (+9 V) and VR6 (-9 V).

In the ± 50 V supply unit (Figure 22) stabilization depends on emitter-followers (TR36, TR38). Output voltages in this case are variable up to VZ and adjusted by VR7 (+50 V) and VR8 (-50 V).

Power supply components were chosen well within their ratings to ensure satisfactory performance even for long periods of continuous operation.

The various units of the stimulator, each constructed in an aluminium chassis (9" x 4" x 6") were mounted on metal shelves along with the power supply units (9" x 6" x 6"). The power to each unit was delivered via a series of 4 mm plugs and sockets and decoupling at each supply point was provided by a low value resistor and a capacitor.

3) Digital time-source, divider, trigger and counter;

For accurate time calibration of continuous photographic records precise timing pulses at a number of fixed frequencies are essential. The circuit developed for this purpose uses the 50 Hz from the mains supply as a convenient reference frequency. A 6.3 volt r.m.s. sine wave from a transformer was converted to a 5 volt D.C. pulse train by the arrangement shown in Figure 23(A). The Zener diode (D1) limits the amplitude of the sine wave and the crude square wave produced is passed to an SN 7400 TTL (transistor-transistor logic) integrated circuit connected to form a Schmitt trigger. This provides D.C. pulses sufficiently square to drive subsequent TTL integrated circuits. The mains derived pulse train passes to an SN 7490 (decade counter) integrated circuit connected in the divide-by-ten configuration and a pulse output at 10 Hz is produced. A series of four subsequent 7490's connected in the divide-by-ten configuration provide pulse outputs at 1 Hz, 0.1 Hz, 0.01 Hz, and 0.001 Hz.

For time calibration a suitable pulse output was displayed on the oscilloscope along with the recording trace. The inter-pulse intervals on the timing trace provide a convenient D.C. reference level and if the oscilloscope is properly adjusted pulse height can be used for amplitude calibration of the photographic record. When both traces were required for recording purposes the timing signal was displayed in the form of a brief differentiated and attenuated positive pulse via the differential inputs of one trace.

Although this circuit was designed primarily as a time-

A; Digital divider;

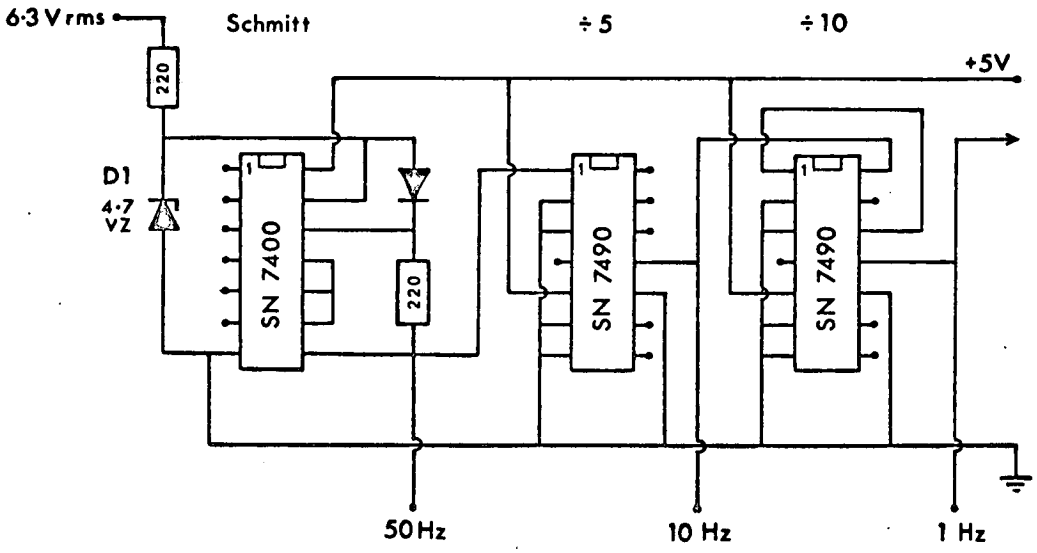

B; Decade counter;

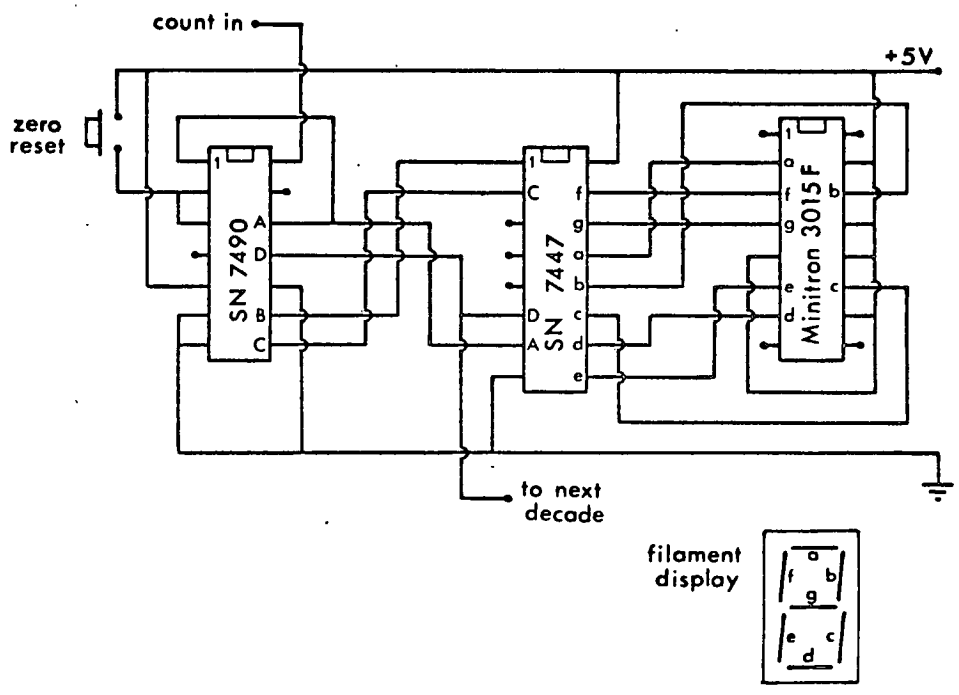

Power supply; digital divider, counter;

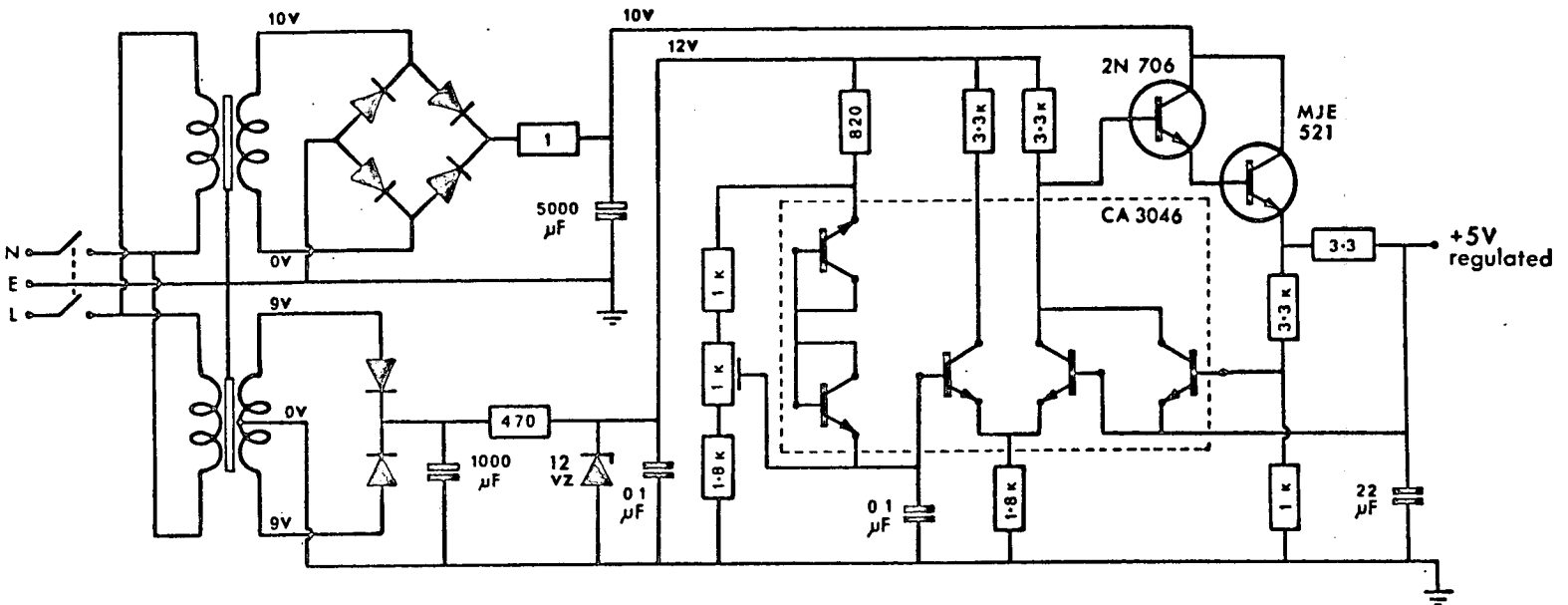

source, the output pulses available are suitable for triggering the oscilloscope. In combination with the stimulator described above the unit may be used to produce superimposed records, at fast sweep speeds, of responses to well spaced stimuli at fixed time intervals. The 1 Hz and 0.1 Hz outputs were especially useful in this context. With the stimulator alone such superimposed records can be obtained only manually from the oscilloscope since stimulus repetition rate and sweep speed are directly related.

A three digit electronic counter was incorporated in the time-source unit. This could be reset to zero at any time and was used in several ways. When stimulating at 0.1 Hz the 1 Hz output was connected to the counter input; the count displayed gave an indication of the number of stimuli previously delivered and of when the next stimulus was imminent allowing the camera shutter to be opened at the appropriate time. Alternatively the duration of a continuous photographic record could be measured. In experiments where salines were changed the total time in each solution was monitored and changes could be made at regular intervals.

Figure 23(B) shows the circuit of a single decade of the counter. This consists of an SN 7490 decade counter, an SN 7447 7-segment decoder-driver and a Minitron 3015F 7-segment alpha-numeric filament indicator.

The circuit of the 5 V power supply used for the time source unit is given in Figure 24. Since the current is high (~1A) and good stability is essential for TTL integrated circuits this is of a relatively sophisticated design and features fold-back current limiting. A good heat sink for the power transistor (MJE 521) is

essential.

The completed time-source unit proved to be a useful and versatile addition to the normal range of electrophysiological equipment.

H) Miscellaneous;

To minimize mains interference the preparation chamber, recording amplifiers and power supplies, micromanipulators and binocular microscope were all enclosed within a Faraday cage. This consisted of $\frac{1}{4}$" mesh wire netting covering the top and sides of a metal framework. The floor of the cage was screened by a thin (18 SWG) sheet of aluminium mounted on a chipboard and softwood box containing sand to increase its weight. The whole cage assembly was mounted on four rubber 'Barrymounts'. These effectively damp all extraneous mechanical vibrations above a frequency of about 20 Hz and thereby reduce the possibility of vibrational interference at the recording microelectrode. It was not found necessary to screen the front of the cage.

Two Prior micromanipulators were used and the bases of these were rigidly fixed to the floor of the cage, one on either side of the preparation chamber.

All electrical connections to equipment inside the cage were made with coaxial (screened) cable and the recording trace(s) displayed on a Tektronix 502A or Tektronix 545 oscilloscope. Photographic records were taken using a Cossor model 1428 oscillograph camera (Kodak Linagraph paper, RP30), or preferably using a Nihon Kohden model PC-2A camera (Kodak Linagraph paper, 553) when this was available. Photographic papers were developed in Ilford Contrast FF developer (1:9, 3 mins) and rinsed off before being fixed in Ilford Hypam (1:4, 3 mins), washed (30 mins) and dried. Occasionally a Polaroid oscilloscope camera was used.

Chapter 3

PRELIMINARY OBSERVATIONS

A) Anatomy;

1) Introduction;

It is appropriate when studying nervous activity in any particular preparation, to consider this activity in relation to the morphology and phyllogenetic significance of the CNS. The genus Helix belong to the suborder Stylommatophera of the Pulmonata and the 200 or so species are among the most highly advanced of the gastropod molluscs, showing a degree of cephalization not present in lower orders.

The most prominent feature of the gross anatomy of the CNS in gastropods is chiastoneury, that is the crossing of pleural-visceral connectives through torsion (BULLOCK & HORRIDGE, 1965). This is especially clear in the primitive Prosobranchiata in which the connectives form a figure-of-eight with the visceral ganglion. The morphologically right intestinal ganglion lies to the left in a supraintestinal position; conversely the morphologically left intestinal ganglion lies to the right in a subintestinal position (Figure 25(A)).

In groups considered to be derivative and more advanced, chiastoneury is replaced to varying degrees by euthyneury in which there is no crossing or only slight crossing of peripheral nerves. In Opisthobranchiata (including the genus Aplysia) euthyneury may be associated with a detorsion process, but of several explanations advanced for euthyneury in the Pulmonata the most attractive is the zygosis theory (KRULL, 1934). This is illustrated in Figure 25 and assumes that the supraintestinal ganglion is lost and that the visceral loop has come to incorporate a secondary connection

Zygosis theory;

A; primitive prosobranch

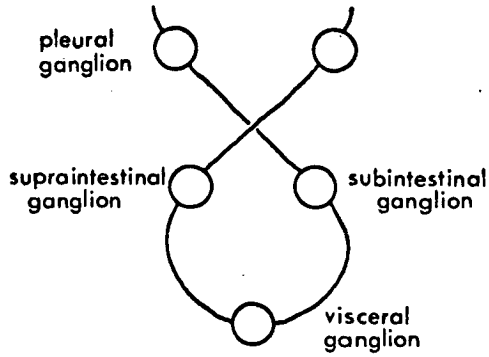

B; prosobranch with right zygoneury

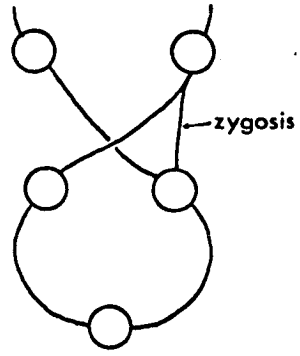

C; Helcinid prosobranch

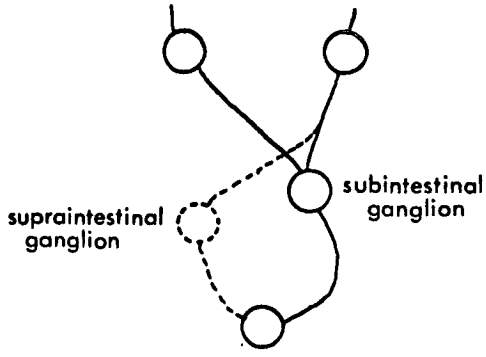

D; primitive pulmonate

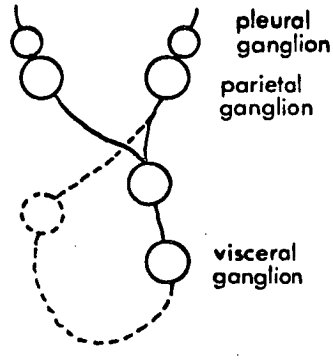

E; advanced pulmonate

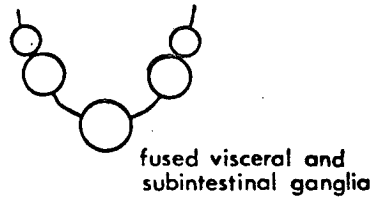

After Krull (1934)

(zygosis) between the subintestinal and right parietal ganglia.

The visceral ganglion is almost always unpaired and supposedly median though it may represent an originally paired structure. With increasing cephalization the visceral ganglion is the last to fuse with others. In advanced pulmonates, fusion with the subintestinal ganglion has taken place (Figure 25(E)).

The parietal ganglia are not present primitively and probably originated by division of the pleural ganglia (BULLOCK & HORRIDGE, 1965). In their presence, the pleural ganglia are reduced and usually lack associated nerves, the parietal nerves innervating homologous areas.

2) Anatomy of suboesophageal ganglia of Helix aspersa;

The dorsal surface of the suboesophageal ganglia of Helix aspersa is illustrated in Figure 26. The ganglia are highly condensed forming a solid mass. The pleural and parietal ganglia are barely distinct and in mature snails it is difficult to separate the left parietal from the visceral ganglion especially in the anterior part of the brain (KERKUT, FRENCH & WALKER, 1970). The fissure separating the right parietal and the visceral ganglia however is always clear.

Serial sections of the suboesophageal ganglionic mass were prepared according to the schedule previously given. Two brains were sectioned in the vertical (dorsal-ventral) plane and two in the horizontal (anterior-posterior) plane. A number of the vertical sections were chosen to illustrate the morphology of the ganglionic mass and photographs of these are given in Figure 27 (A)-(F). The

approximate location of each section is indicated by the corresponding line in Figure 26. Two representative horizontal sections are shown in Figure 28; (A) is a more superficial section than (B). Figure 29 shows vertical sections of the posterior (A) and anterior (B) regions of the right parietal ganglion at higher magnification.

The whole of the suboesophageal ganglion complex including the pedal ganglia is enclosed in connective tissue. The aorta passes through the centre of this mass and can be easily identified in all the vertical sections. A pair of lateral plates of connective tissue are also present (Figure 27(B), (C), (D)). These presumably have a protective function in the intact animal.

The organization of the individual ganglia is of a typically molluscan nature. Each has a central core of fibrous matter or neuropile surrounded by an outer covering (rind) of cell bodies. This is clear in sections of the visceral ganglion (Figure 27(D)). In addition the ganglion contents are retained by an inner sheath of connective tissue separated from the outer sheath by a blood sinus as previously mentioned. The inner sheath is closely applied to the ganglion cell bodies (Figure 29). These higher magnification photographs also show that the interneuronal space is loosely occupied by glial cells, identifiable by their nuclei. These may be condensed to some extent around the larger neural somata as in the case of the giant cell of Figure 29(A). Individual axons are clearly seen in Figure 29(B) and indicate the characteristically monopolar nature of molluscan nerve cells (TAUC, 1966). Where the neuronal nucleus can be identified it is frequently large and may occupy about 50% of the available space.

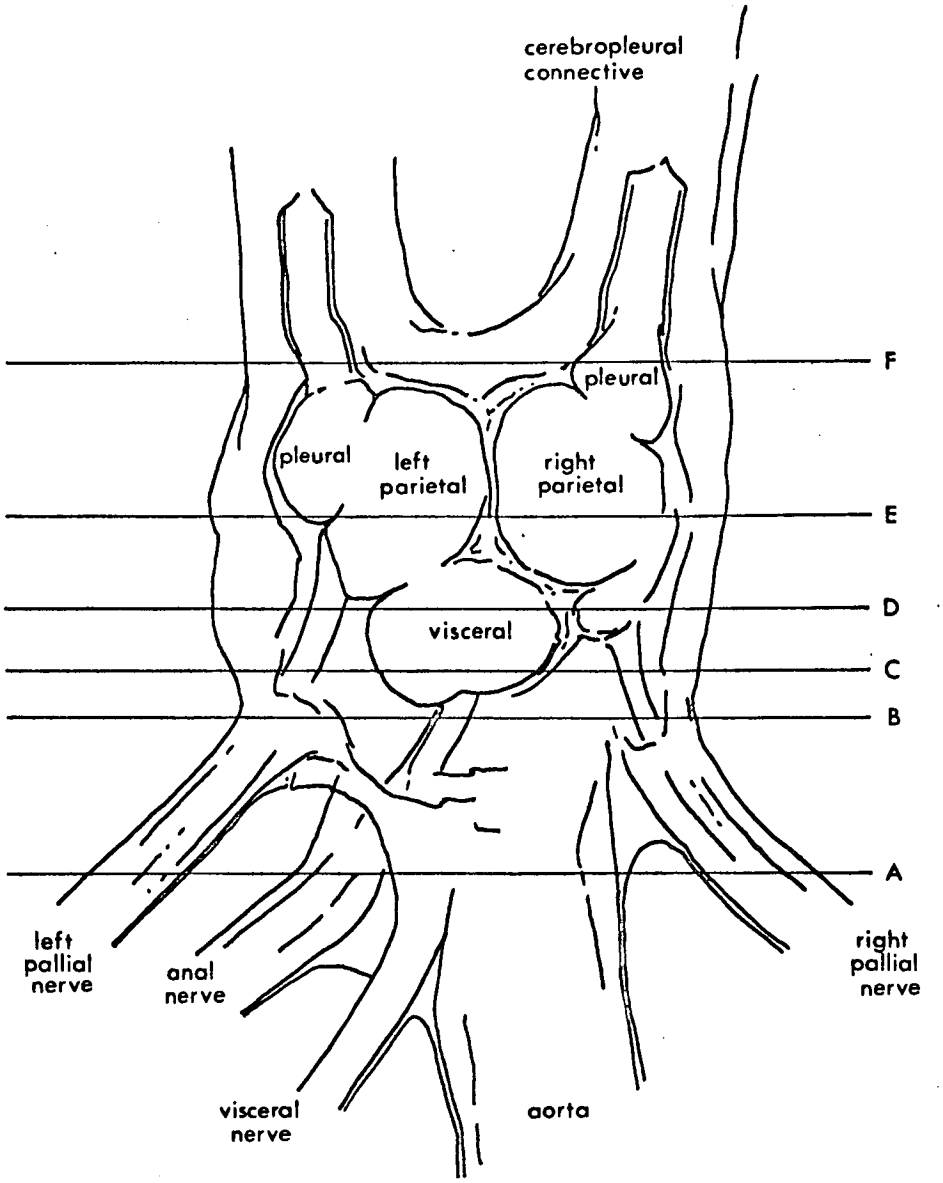

Suboesophageal ganglia of Helix aspersa, dorsal surface;

Horizontal lines indicate approximate locations of vertical sections illustrated in Figure 27(A)-(F);

Vertical sections;

A

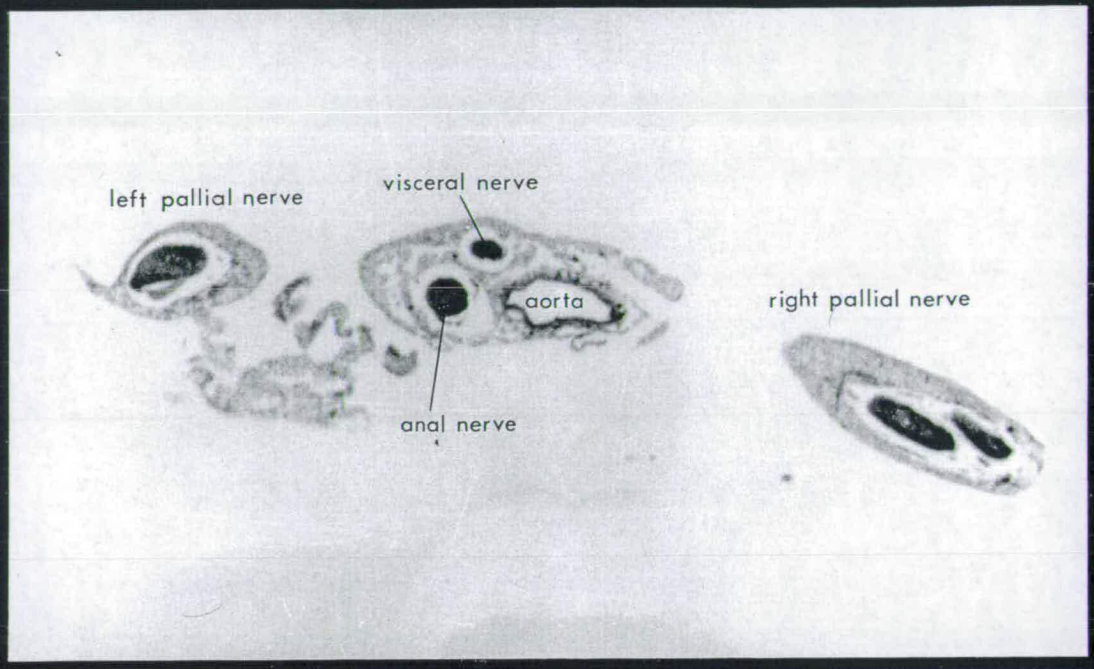

B

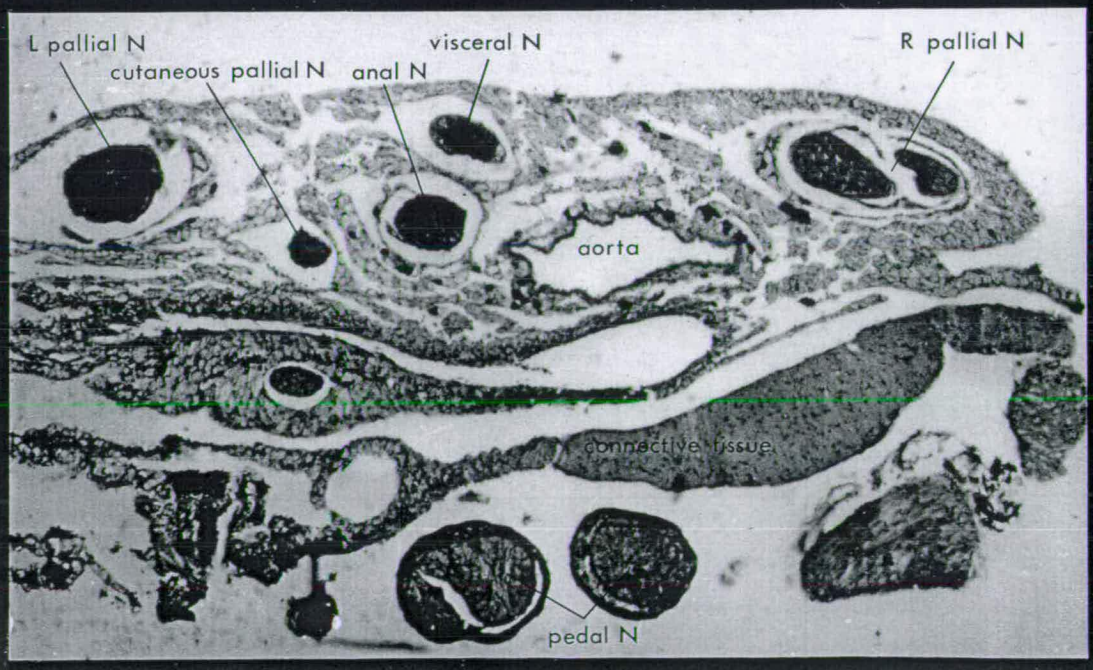

FIGURE 27 continued;

Vertical sections;

C

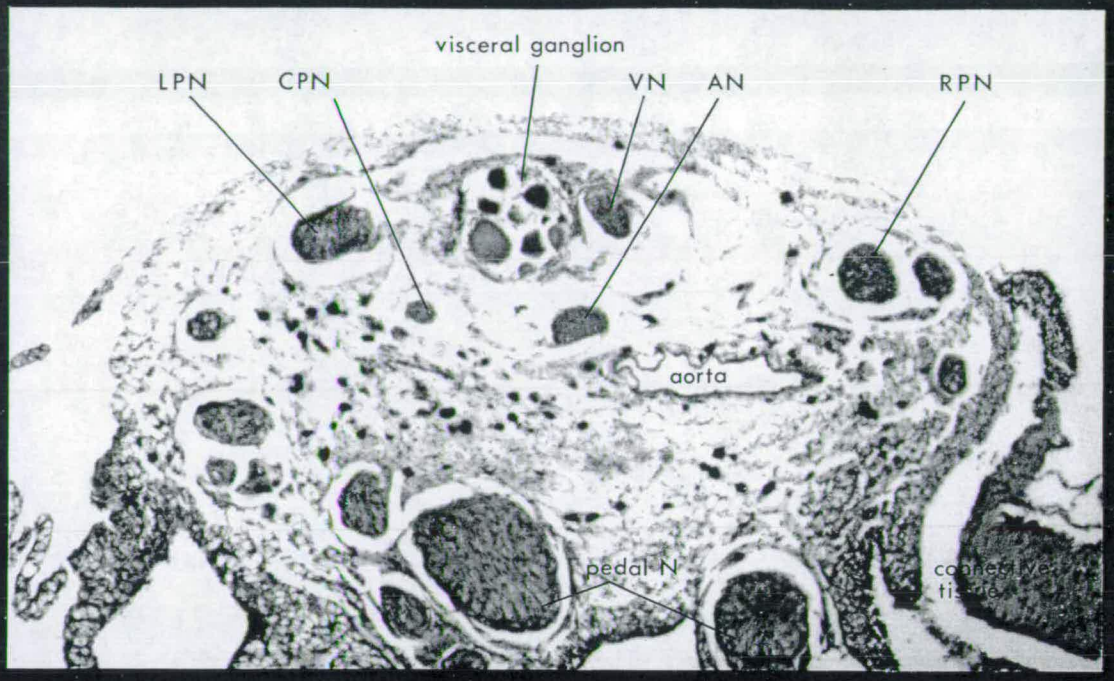

D

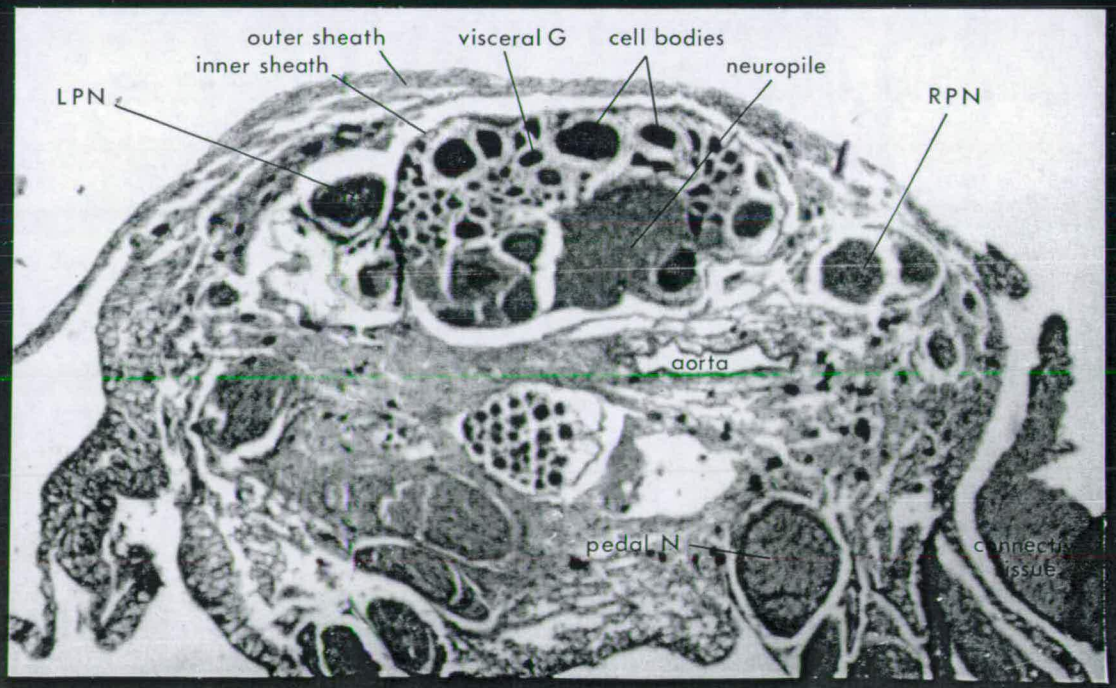

FIGURE 27 continued;

Vertical sections;

E

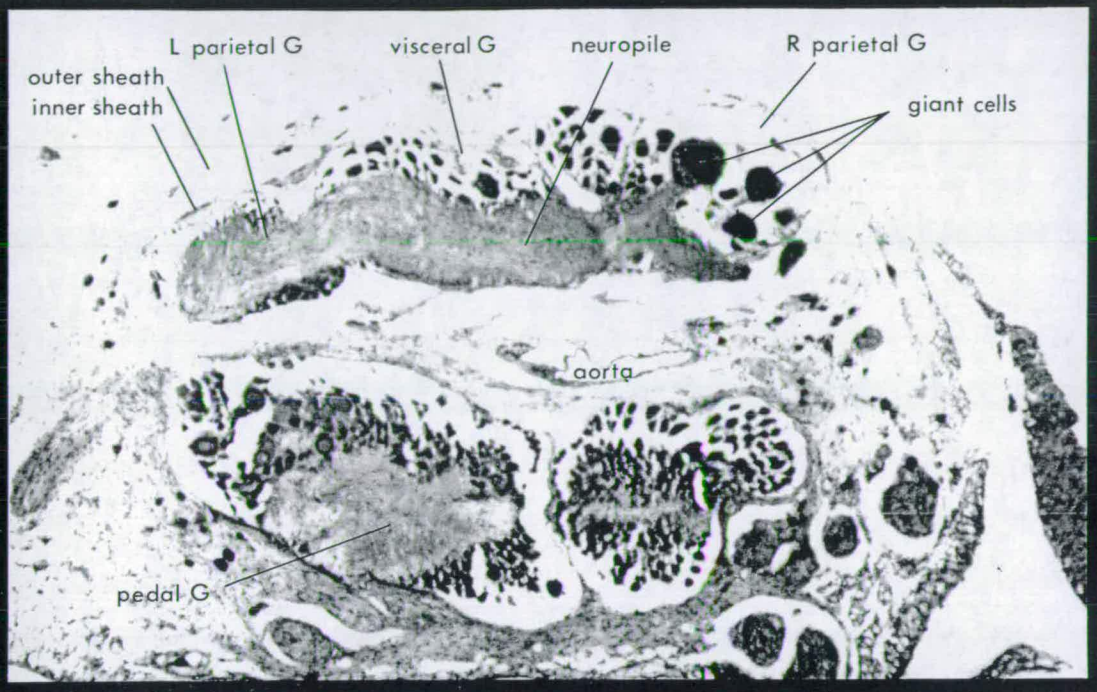

F

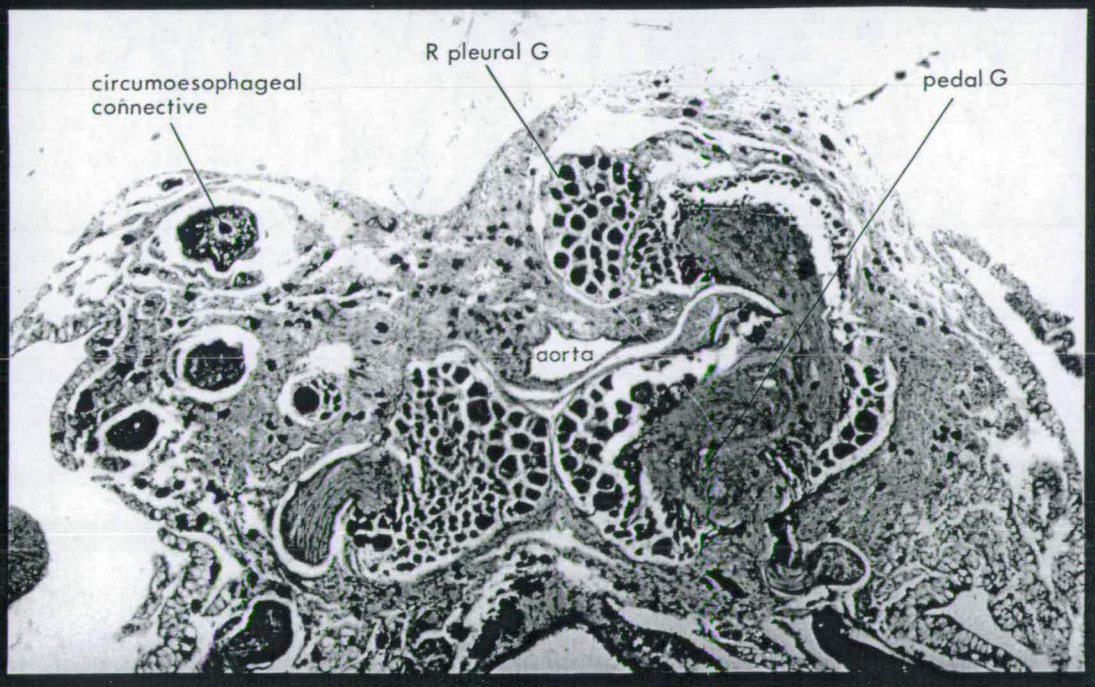

Horizontal sections;

A

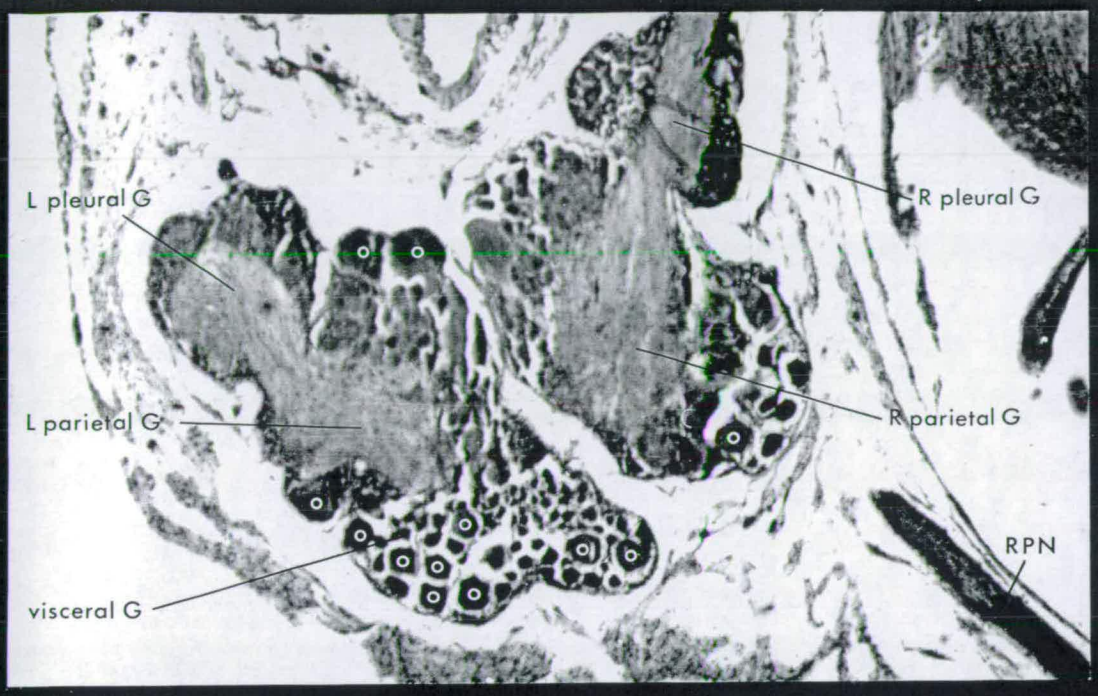

B

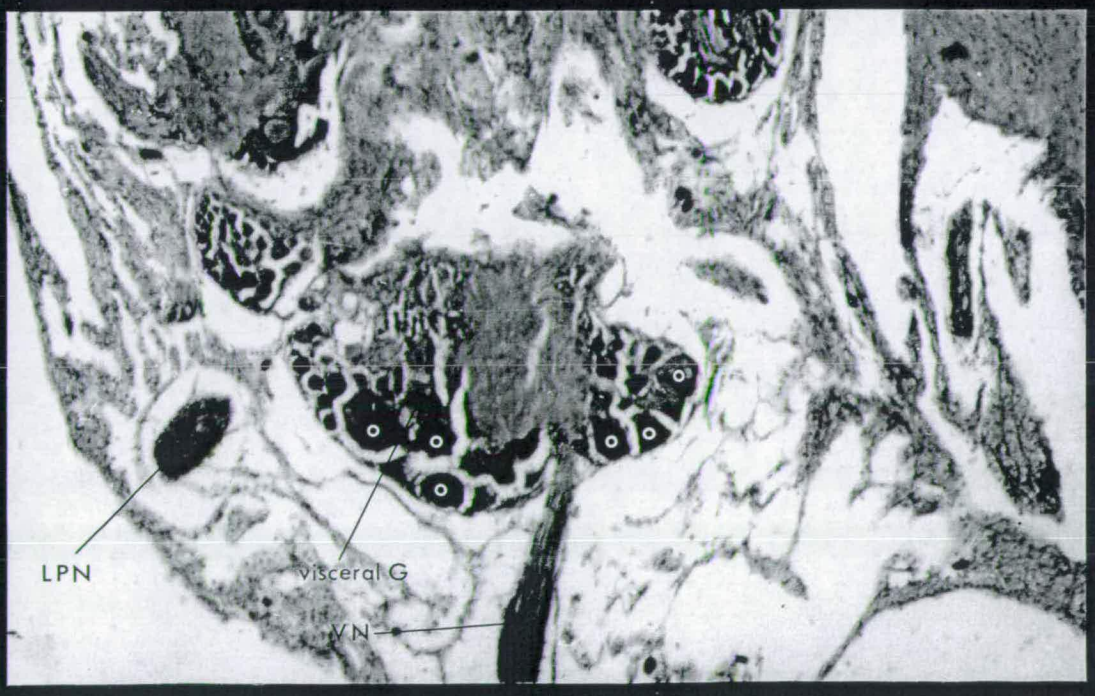

o giant cells

In sections of more anterior regions of the suboesophageal mass (Figure 27(E)) the neuropile of the various ganglia becomes more or less continuous ventrally and the ganglion cells occupy a dorsal position.

Individual axons cannot be identified in sections of the main nerves even at high magnification; electron microscopy seems to be required for this purpose (BULLOCK & HORRIDGE, 1965). However, the abundance of glial cell nuclei in the main nerves and in the neuropile is apparent. The glial cells form a perineurium around the nerve trunk and a complex endoneurium consisting of a series of septa arranged in a willow-tree pattern projecting inwards from the perineurium (SCHLOTE, 1957). Electron microscope studies show that the larger fibres may be deeply invaginated and that glial cell processes penetrate into the invaginations. The somata of the ganglion cells are also subject to glial invagination (BULLOCK & HORRIDGE, 1965).

From the electrophysiological point of view the most important of the ganglion cells are the so called giant cells since these will be most easily visible under experimental conditions. While no definite discontinuity in the frequency distribution of cell size has been established, cells classified as giants appear to be more or less constant in number and in position within the ganglion; 9 or 10 occur in each parietal ganglion and about 20 in the visceral ganglion (BULLOCK & HORRIDGE, 1965). A number of these, accessible through their superficial location, can be identified as unique individuals physiologically (KERKUT & WALKER, 1962; WALKER et al, 1970) and by Procion yellow injection (KERKUT, FRENCH & WALKER, 1970). Several giant cells are indicated in the horizontal sections

of Figure 28 (white circles). Three, located in the right parietal ganglion, are clearly visible in the section of Figure 27(E), from its location and size the largest of these can be identified as the Big-D cell (KERKUT & HORN, 1968). This cell is often the largest in the Helix aspersa brain and is so called because it is depolarized by acetylcholine (KERKUT & WALKER, 1962; KERKUT & MEECH, 1966). The giant cell of Figure 29(A) has been identified as the Big-D cell.

B) Spontaneous activity;

1) Introduction;

Individual cells, identifiable from preparation to preparation are clearly useful in any electrophysiological study of invertebrate material. In the suboesophageal ganglionic mass of Helix aspersa, the axonal pathways of 10 identifiable giant cells have been mapped using the fluorescent dye Procion yellow M-4R (KERKUT, FRENCH & WALKER, 1970). Action potential shape and frequency have also been used as criteria for neuron identification but without reference to peripheral pathways (WALKER et al, 1970). Very substantial variation in the shape of action potentials and their spontaneous frequency was found. Action potential duration varied between 3 and 20 msec in different cells and positive afterpotential ('undershoot') values between 2 and 30 mV. In general the action potentials of spontaneously active cells had smaller positive afterpotentials than those of silent cells. Spontaneous action potential frequency varied from zero in silent cells to a regular rate of 3-4 per second.

2) Intracellular recording;

In order to illustrate this range of spontaneous activity and if possible to locate a number of identifiable cells for subsequent experiments, a series of preparations was carried out in which the exposed ganglia were carefully sketched from life and the locations of visible large cells indicated. (Photographs of the unstained ganglia show little detail). As many of these cells as possible were impaled using 3 $\overline{M}$ KCl-filled recording micro-

electrodes with resistances in the range 10-20 MΩ. A continuous record of spontaneous activity was obtained from one oscilloscope (Cossor 1428 camera) and where possible single frames illustrating action potential shape were taken using a Polaroid camera and a second (triggered) oscilloscope. The positions of silent cells penetrated were noted. Typical results are given in Figures 30 and 31. These illustrate a considerable variation in the amplitude, frequency and shape of spontaneous action potentials.

It became clear from these preliminary preparations (and subsequent preparations have tended to confirm) that conclusive cell identification on the basis of position and the characteristics of spontaneous action potentials for a proportion of the cells listed by Walker et al (1970) is by no means easy. Several factors contribute to this difficulty. Firstly, since the neurons of Helix aspersa are not heavily pigmented, cell visibility is limited even under the best lighting conditions. Visibility could be improved by the application of a vital dye such as methylene blue. However, the effect on metabolism of such dyes is uncertain and could presumably alter spontaneous activity. Secondly, the general morphology of the suboesophageal ganglionic mass is somewhat variable from preparation to preparation. The parietal ganglia, for example, usually meet towards the anterior (Figure 30) but sometimes they do not (Figure 31). In addition, the inner connective tissue sheath does not bind the ganglion contents so tightly that their appearance cannot be altered according to the way in which the preparation has been tensioned. This flexibility is presumably necessary in the intact animal to enable the entire head and foot to be withdrawn into the shell. In the condensed nervous system of

Suboesophageal ganglia; Location and spontaneous activity of visible large cells in a single preparation;

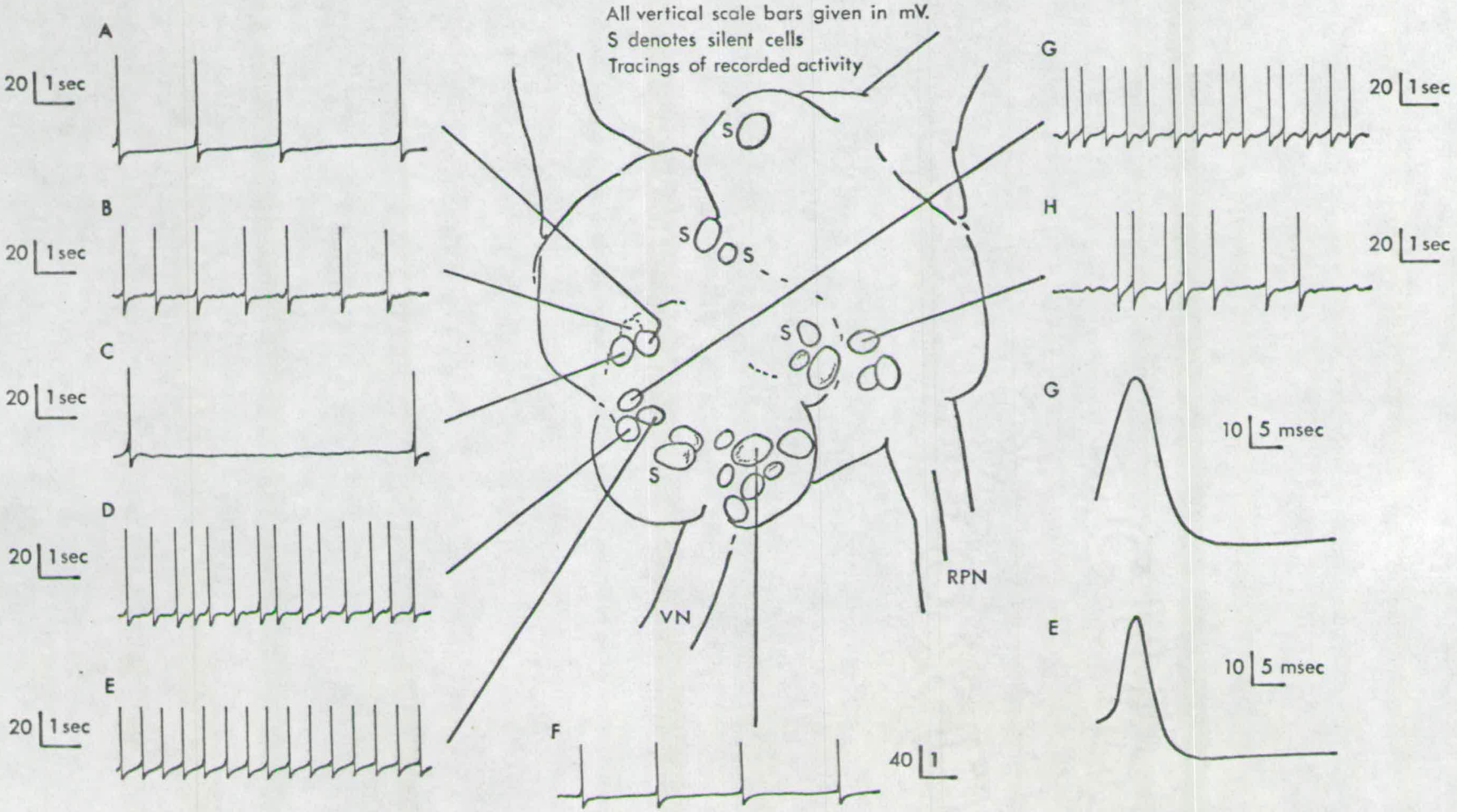

Suboesophageal ganglia; Location and spontaneous activity of visible large cells in a single preparation;

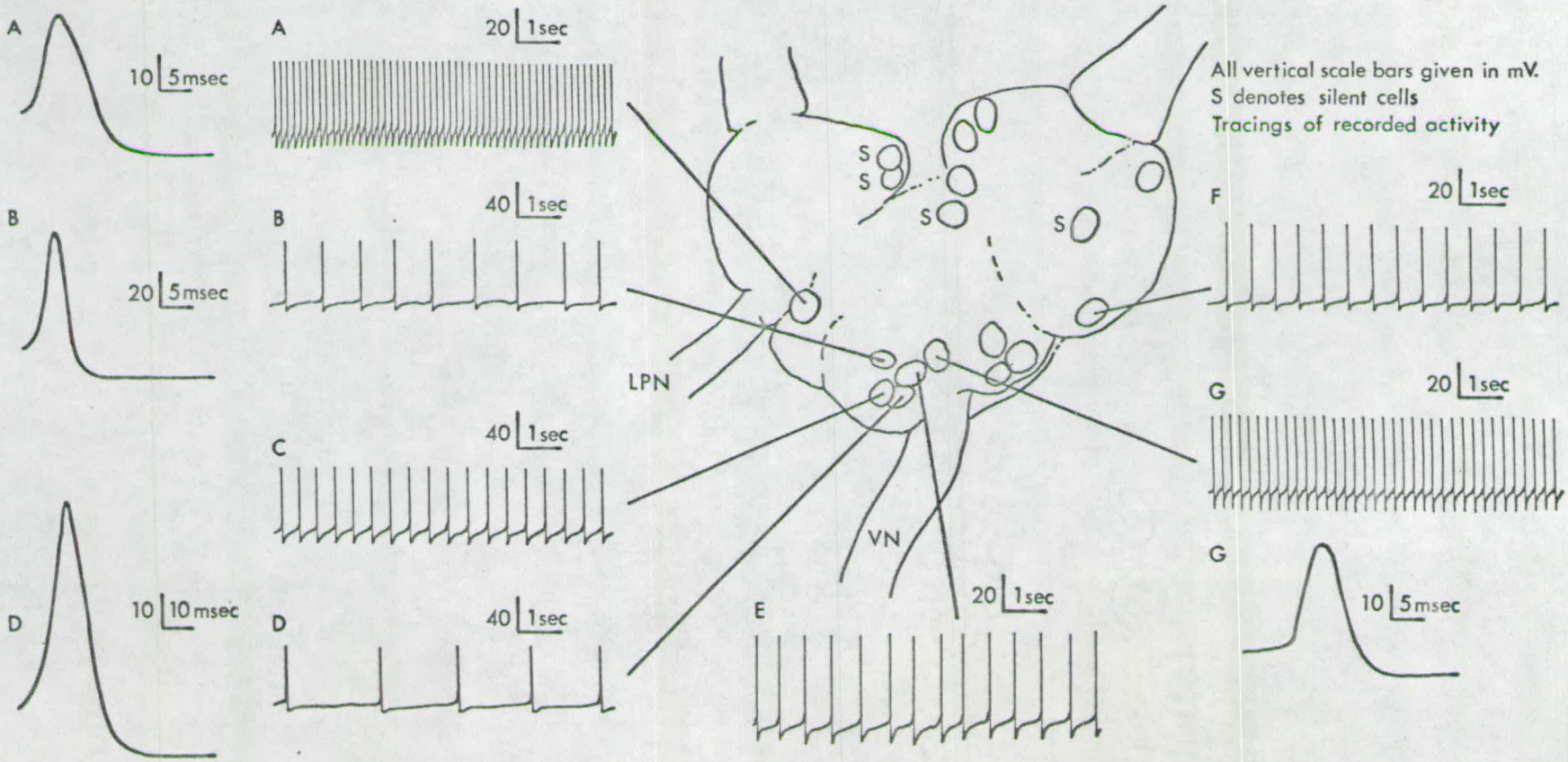

Helix greater flexibility may be required than in the case of Planorbis or Lymnea with more diffuse nervous systems.

It is thus difficult to interpret a generalized diagram of cell position in relation to a specific preparation.

These difficulties could be overcome through the adequate identification of cells in histological section, marking cells, after recording their spontaneous activity, with a suitable dye (Procion yellow or cobalt chloride) and mapping their peripheral pathways by this means and also by extracellular recording and stimulation. Except in the case of cells with very characteristic action potential shapes or a characteristic pattern of activity, cell identification based solely on position and action potential characteristics must be regarded as statistical. That such identification is possible is significant but does not provide a convenient means of locating particular cells from preparation to preparation.

An exhaustive study of this nature was outwith the scope of the present project and therefore, in attempting to identify cells, attention was restricted to those giant cells for which axon pathways have already been established (KERKUT, FRENCH & WALKER, 1970). Of these ten, five are spontaneously active and two display characteristic types of activity. The axon pathways of these two are illustrated in Figure 32. The cell located in the right parietal ganglion has a diameter of 170 μ, exhibits a characteristic 'bursting' pattern of activity and is the Big-D cell previously referred to. (Figures 30 and 31 were chosen to illustrate a range of spontaneous activity and the Big-D cell was not among those penetrated.) The second cell, with a diameter of 150 μ, is located towards the left

Cell locations;

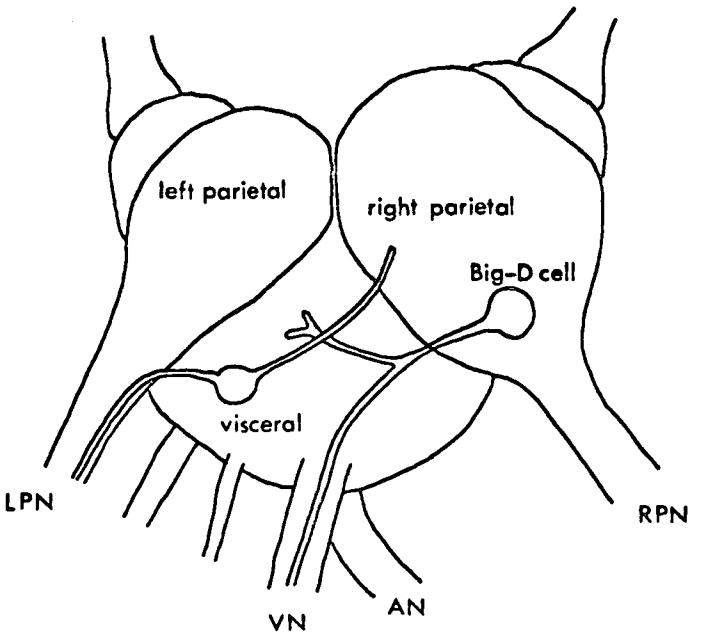

After Kerkut, French & Walker (1970); for explanation see text

of the visceral ganglion and fires spontaneously at a frequency of 3/sec which is relatively high for Helix neurons. It is unusual in that two axons arise directly from the soma. Each of the cells sends an axon down a main nerve of the suboesophageal ganglionic mass and the possibility exists for confirming cell identification through extracellular recording.

3) Extracellular recording;

Since many of the spontaneously active giant cells present in the suboesophageal ganglionic mass appear to have relatively constant firing patterns some reflection of this constancy would be expected in extracellular recordings from the main peripheral nerves, especially if the larger ganglion cells are represented by correspondingly large peripheral axons. To examine this possibility and to assist in cell identification, suction electrode recordings were made from each of the main nerves in a series of preparations. A selection of these results is given in Figures 33 to 36. The 1 Hz time calibration trace given in record A of each of these figures applies to subsequent records except where otherwise indicated. In Figure 33 record D, Figure 35 record E and Figure 36 record D the small deflections of the time calibration trace indicate the occurrence of larger amplitude action potentials. These small pulses were delivered from the stimulator previously described, activated by a second (triggered) oscilloscope.

Although care was taken to ensure a tight seal between the suction electrode and the cut end of a nerve it was sometimes found difficult to obtain satisfactory recordings. When a sufficient length of nerve was present, lifting the end of the suction electrode

FIGURE 33; p 52

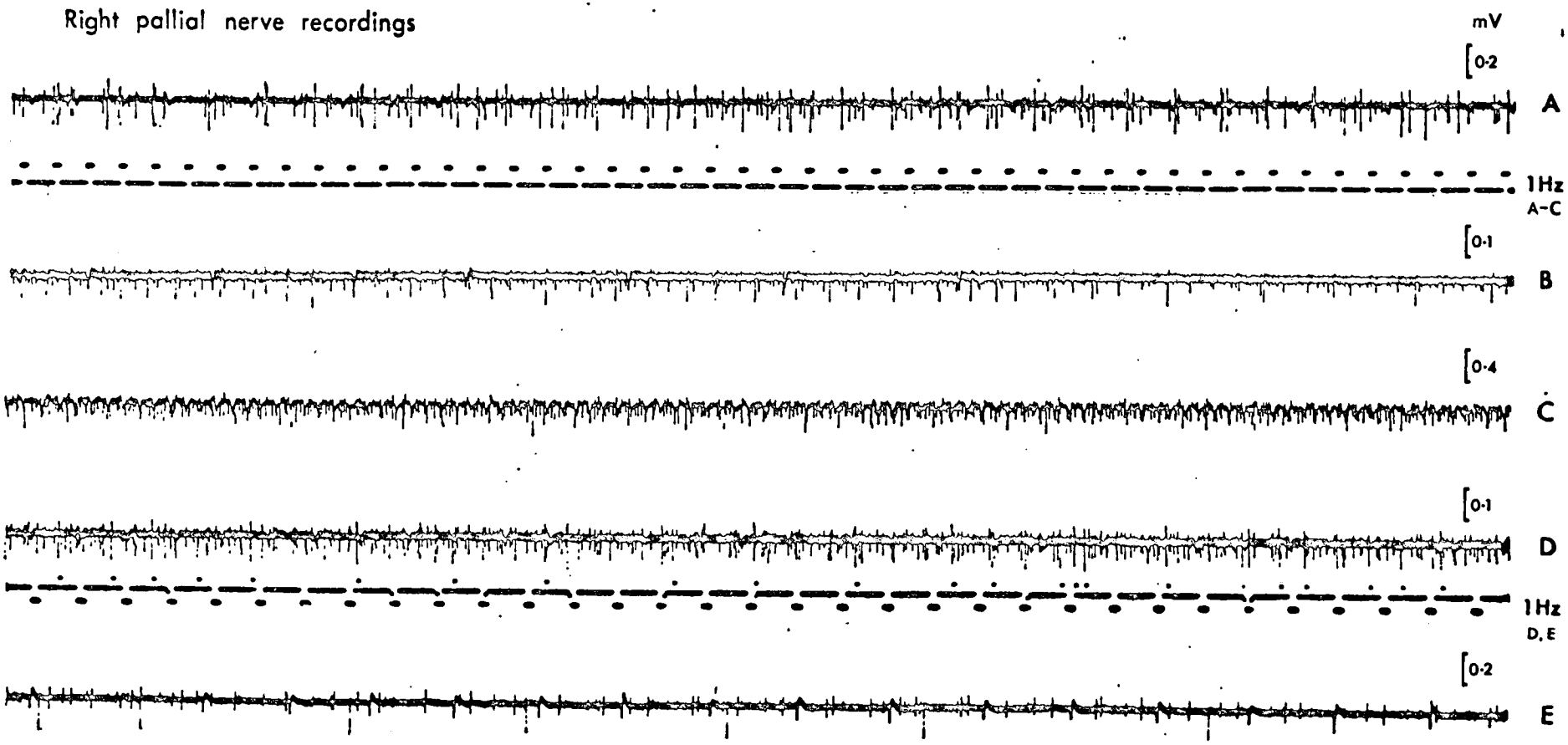

Visceral nerve recordings

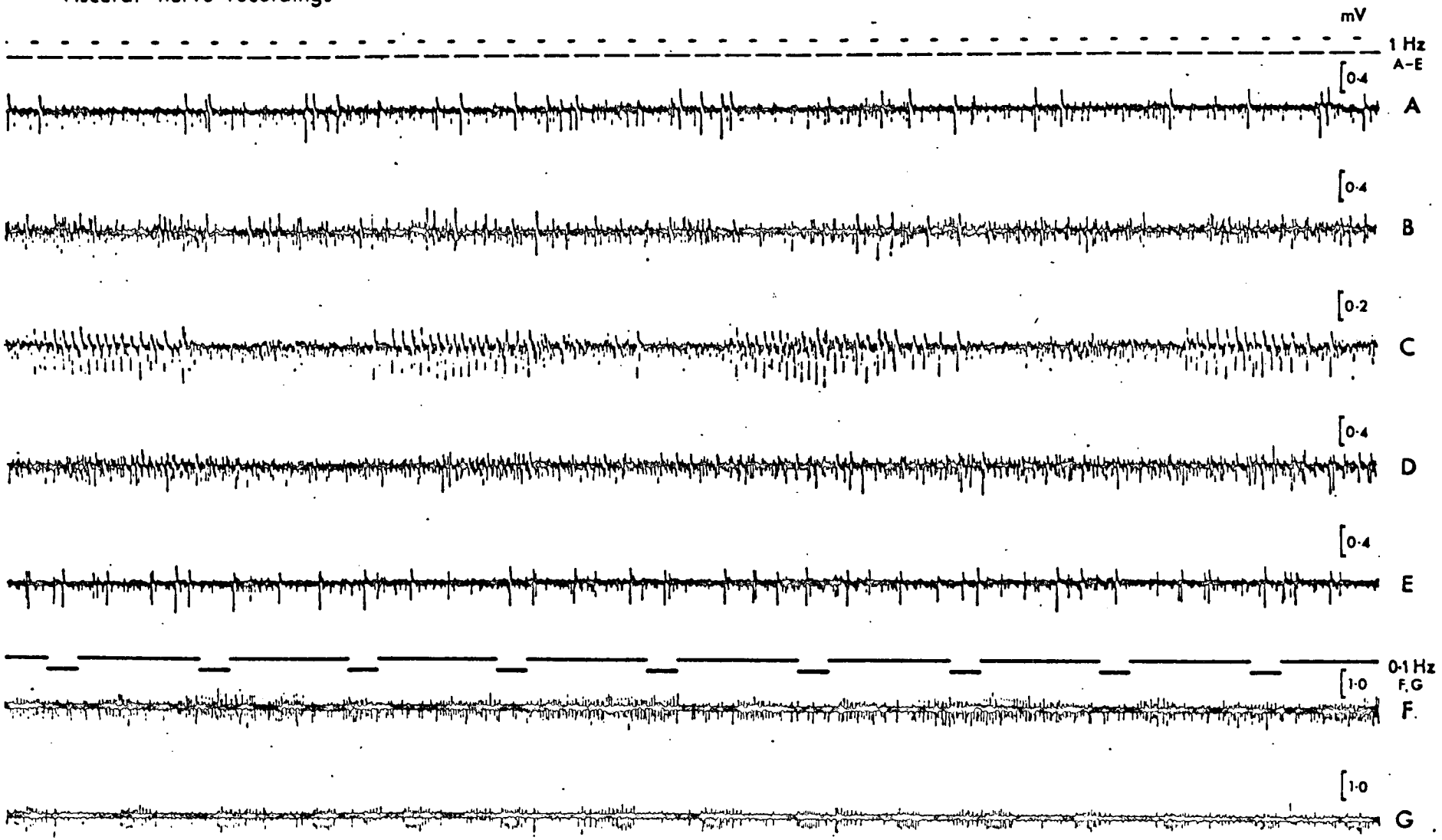

FIGURE 35; p 52

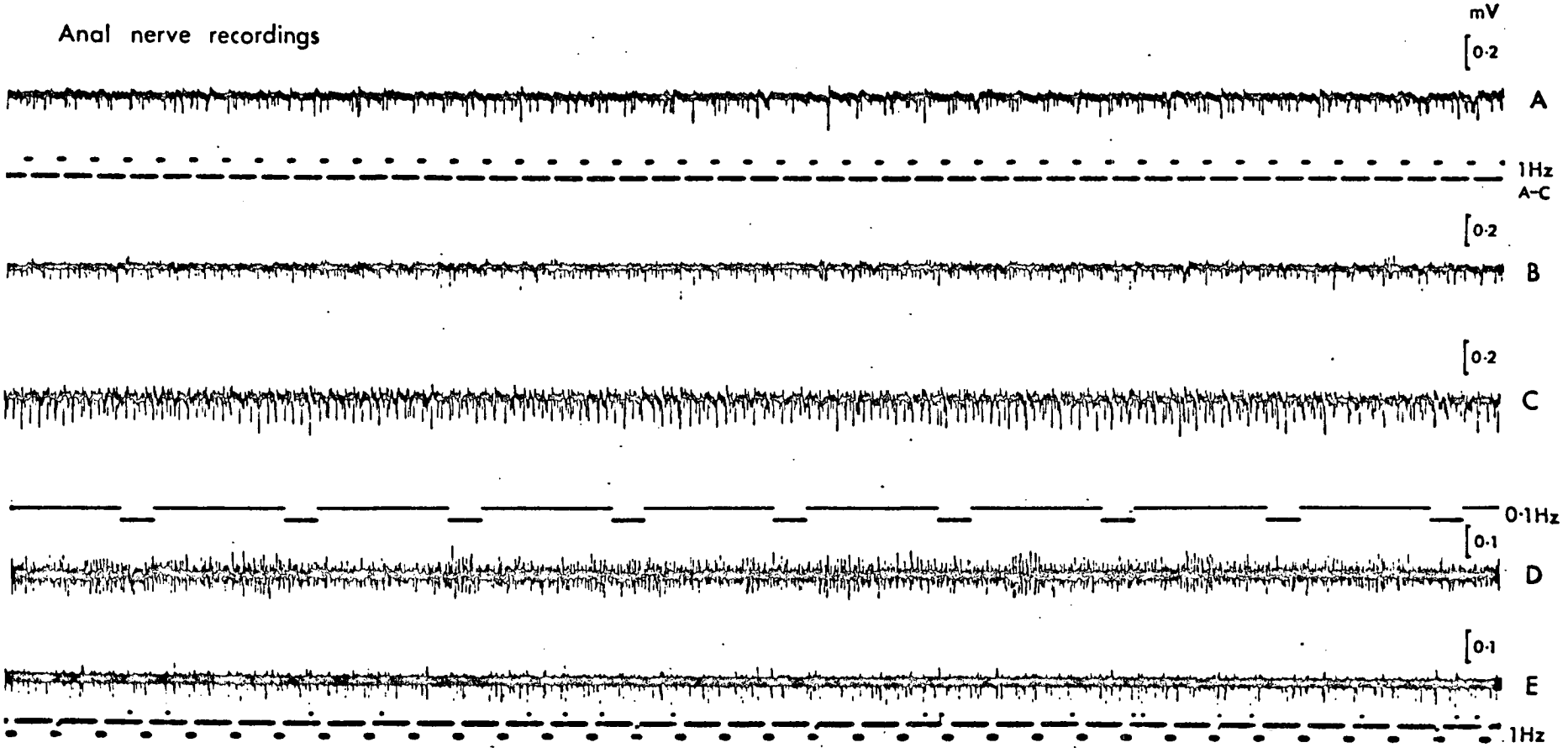

FIGURE 36; p 52

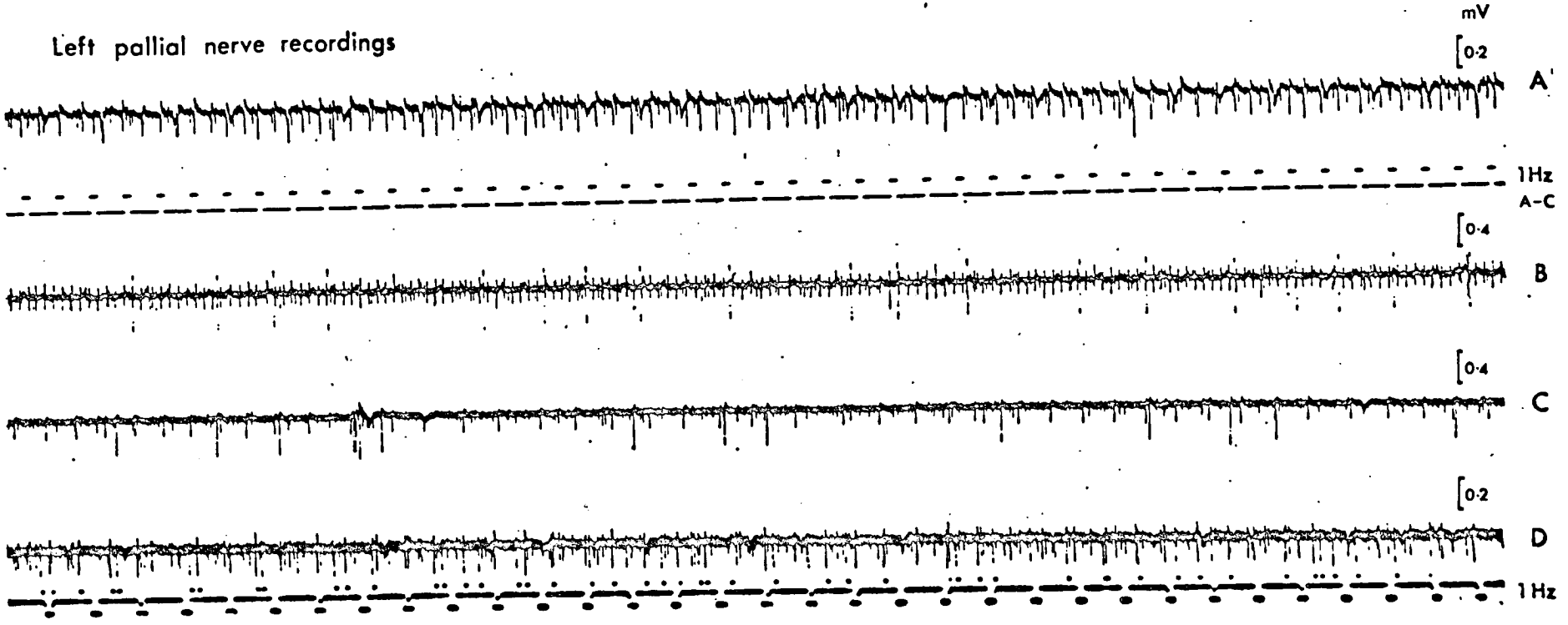

out of the saline bath made little or no difference to the quality of the recording. This suggests that the seal was adequate and that signal attenuation is the result of tissue resistances. A high resistance in series with the recording resistance or, as is more probable a low resistance in parallel, would have this effect. In this context the abundance of glial cells in the nerve trunks may be significant.

The overall picture presented by these extracellular recordings is rather complex. While most records show regularly occurring action potentials of the same amplitude and presumably from a common source, in the case of the right pallial nerve (Figure 33), anal nerve (Figure 35) and left pallial nerve (Figure 36) no consistent pattern of activity can be identified. The left pallial nerve recordings all show regular activity but only in record B does the frequency of obvious action potentials approach that expected for the visceral ganglion cell of Figure 32.

Satisfactory recordings were most easily obtained from the visceral nerve (Figure 34). This is the smallest of the main nerves in cross section (Figure 27(A)) and the 'shunting' tissue resistance during recording may be highest. The activity recorded was somewhat variable but much less so than that of other nerves. In several records particularly C, F and G a definite bursting pattern of discharge can be identified. This suggest that Big-D cell identification can be confirmed by visceral nerve recording. Simultaneous intracellular and extracellular recordings are shown in Figure 37. A provisional visual identification of the Big-D cell was made in each case. After impalement the intracellular record was compared to the extracellular and only when the definite

Visceral nerve, intracellular recordings;

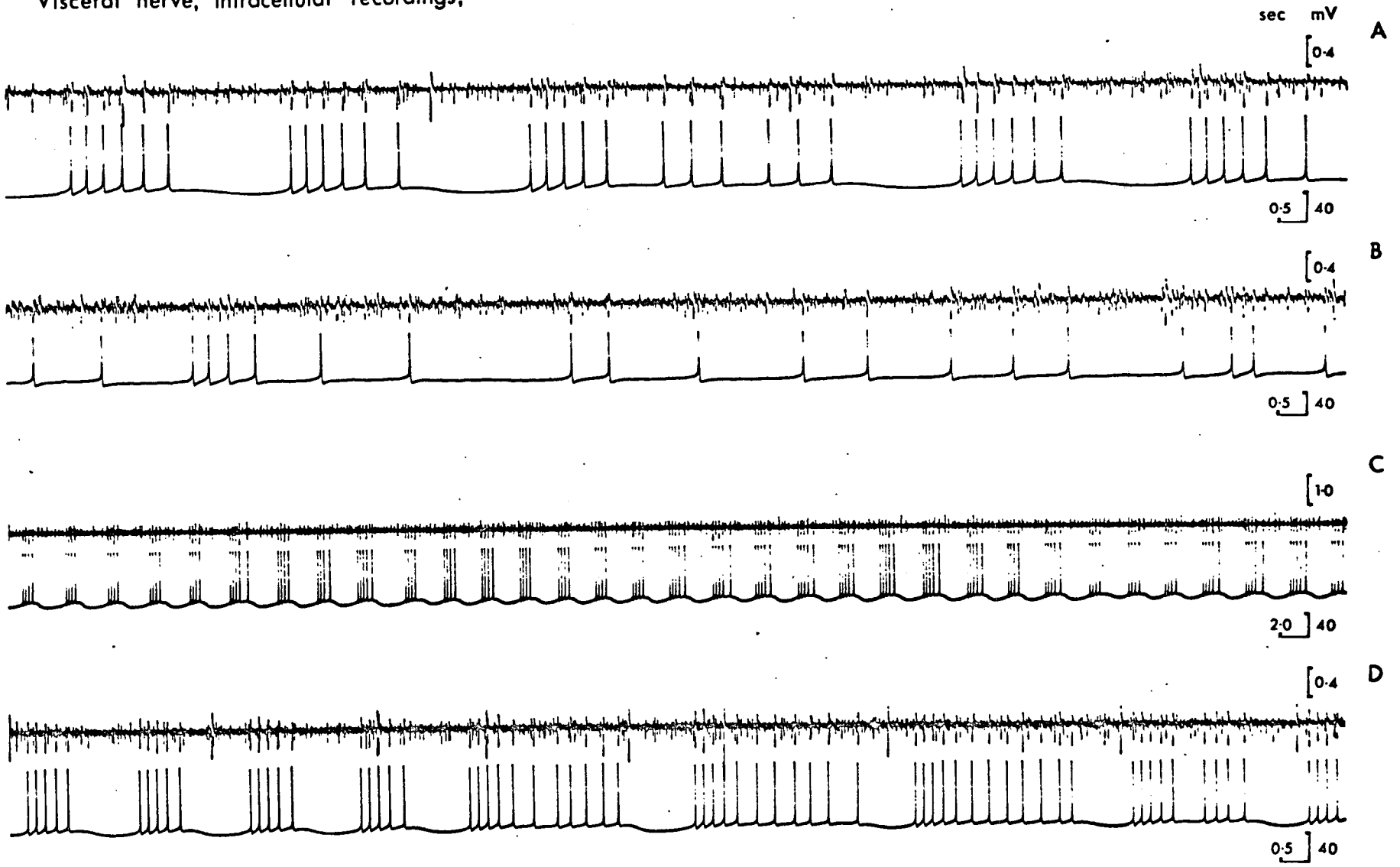

correlation illustrated in records A, C and D was present was the cell identification accepted as valid. In record B the correlation is less clear and cannot be regarded as conclusive. With practice visual identification of the Big-D cell became easier. While its position in the ganglion is not constant, the cell is often whitish in appearance and usually larger than adjacent cells. With concurrent extracellular recording it was found possible to identify the Big-D cell with confidence in approximately 80% of preparations.

The activity of bursting neurons represents a more specialized type of intrinsic activity than that of monotonic pacemakers. It is therefore appropriate that monotonic activity should be considered before the properties of the Big-D cell are examined experimentally. A statistical study of the (predominantly monotonic) spontaneous activity of cells in the suboesophageal ganglia of Helix aspersa is described in the next section and the results of experiments using the Big-D cell are given in Chapter 6, 'Bursting Pacemakers'.

C) Frequency and amplitude of spontaneous action potentials;

1) Introduction;

The occurrence of wide variations in the frequency and amplitude of spontaneous action potentials poses the question of whether these two easily measured parameters are related in any way or whether their variation is independent. This problem has been examined experimentally. Since intrinsic 'pacemakers' in which a relationship might be expected cannot necessarily be distinguished from synaptically driven 'pacemakers' in which the parameters might be independent, a statistical approach was adopted.

Some activity is associated with microelectrode penetration of nerve cells; 'silent' cells produce a short burst of action potentials on penetration, while in spontaneously active cells, the initial frequency is higher. In order to obtain a representative sample of spontaneous action potential frequencies, results were recorded only after a 3-4 minute period from electrode penetration and the presence of spontaneous activity 3-4 minutes after successful penetration was the only criterion used in cell selection. 3 $\overline{M}$ KCl electrodes with resistances in the range 10-20 megohms were used and care was taken not to record twice from the same cell in any one preparation.

A series of at least 30 action potentials from each of 20 cells was recorded from the oscilloscope onto photographic paper. A time calibration signal (1 Hz) was simultaneously recorded. The base level of the calibration trace was aligned with the recording trace on the oscilloscope screen prior to electrode penetration and the calibration trace therefore provided an estimate of the

extracellular (zero) potential level throughout the recording. After a series of action potentials the electrode was removed and any discrepancy between the calibration trace and the zero potential level was measured.

2) Results;

From each series of recorded action potentials 31 were selected, these were numbered 0-30. The spontaneous frequency was calculated from the interval between action potentials 0 and 30; that is the total interval was taken as the sum of the preceding individual intervals for action potentials 1-30. Two measurements were made on each action potential using vernier calipers (Mitutoyo No. 532). In addition to the overall amplitude, the maximum negative potential reached by the action potential undershoot was measured with respect to the calibration trace. This latter amplitude has been termed the negative component and the magnitude of the positive component, or overshoot, of the action potential was obtained from the overall amplitude by subtraction. If the calibration trace and the extracellular zero potential level were not identical at the end of the recording, appropriate corrections were made to the positive and negative component amplitudes. These corrected amplitudes and the overall amplitudes were converted into mV and the mean and standard deviation calculated in each case. Table 2 gives these results along with corresponding spontaneous action potential frequencies for each of 20 cells and Figure 38 shows tracings of the activity recorded from each of the cells ranked in order of action potential amplitude.

Figure 39 shows the mean action potential amplitude values

Table 2

Cell	Amplitude (mV)	Frequency (Hz)	Negative component (mV)	Positive component (mV)	Positive component (%)
1	81.89 (0.88)	2.60	59.65 (0.79)	22.24 (1.14)	27.16
2	79.22 (1.78)	0.36	52.37 (2.10)	26.85 (1.37)	33.89
3	75.84 (1.30)	3.37	55.52 (0.89)	20.32 (1.16)	26.80
4	88.56 (0.73)	0.74	50.88 (0.89)	37.68 (1.06)	42.55
5	91.79 (0.71)	0.31	65.12 (0.90)	26.67 (1.06)	29.05
6	86.29 (0.54)	2.48	58.85 (1.16)	27.44 (1.34)	31.79
7	92.00 (1.01)	0.31	55.79 (0.83)	36.21 (1.26)	39.35
8	79.84 (0.64)	0.95	58.45 (0.58)	21.39 (0.72)	26.79
9	99.04 (0.96)	0.21	68.37 (1.01)	30.67 (1.59)	30.96
10	92.83 (2.99)	0.30	53.17 (3.30)	39.66 (1.09)	42.73
11	76.91 (2.14)	0.54	43.04 (1.59)	33.87 (1.06)	44.04
12	86.37 (0.77)	0.81	56.08 (0.77)	30.29 (0.91)	35.07
13	93.41 (0.79)	0.22	61.71 (1.17)	31.70 (1.48)	33.94
14	75.87 (0.73)	2.70	55.28 (0.77)	20.59 (0.93)	27.14
15	97.65 (0.92)	0.25	54.85 (1.00)	42.80 (1.17)	43.83
16	85.39 (0.82)	1.89	69.04 (0.75)	16.35 (1.00)	19.15
17	94.08 (0.78)	0.68	58.83 (0.81)	35.25 (1.15)	37.47
18	103.84 (1.27)	0.10	66.96 (1.27)	36.88 (1.14)	35.52
19	97.57 (0.65)	0.45	61.20 (0.92)	36.37 (1.00)	37.28
20	89.63 (0.87)	1.44	53.63 (0.89)	36.00 (0.84)	40.17

The figure given in brackets after each mean amplitude value is equal to two standard deviations.

Tracings of spontaneous activity;

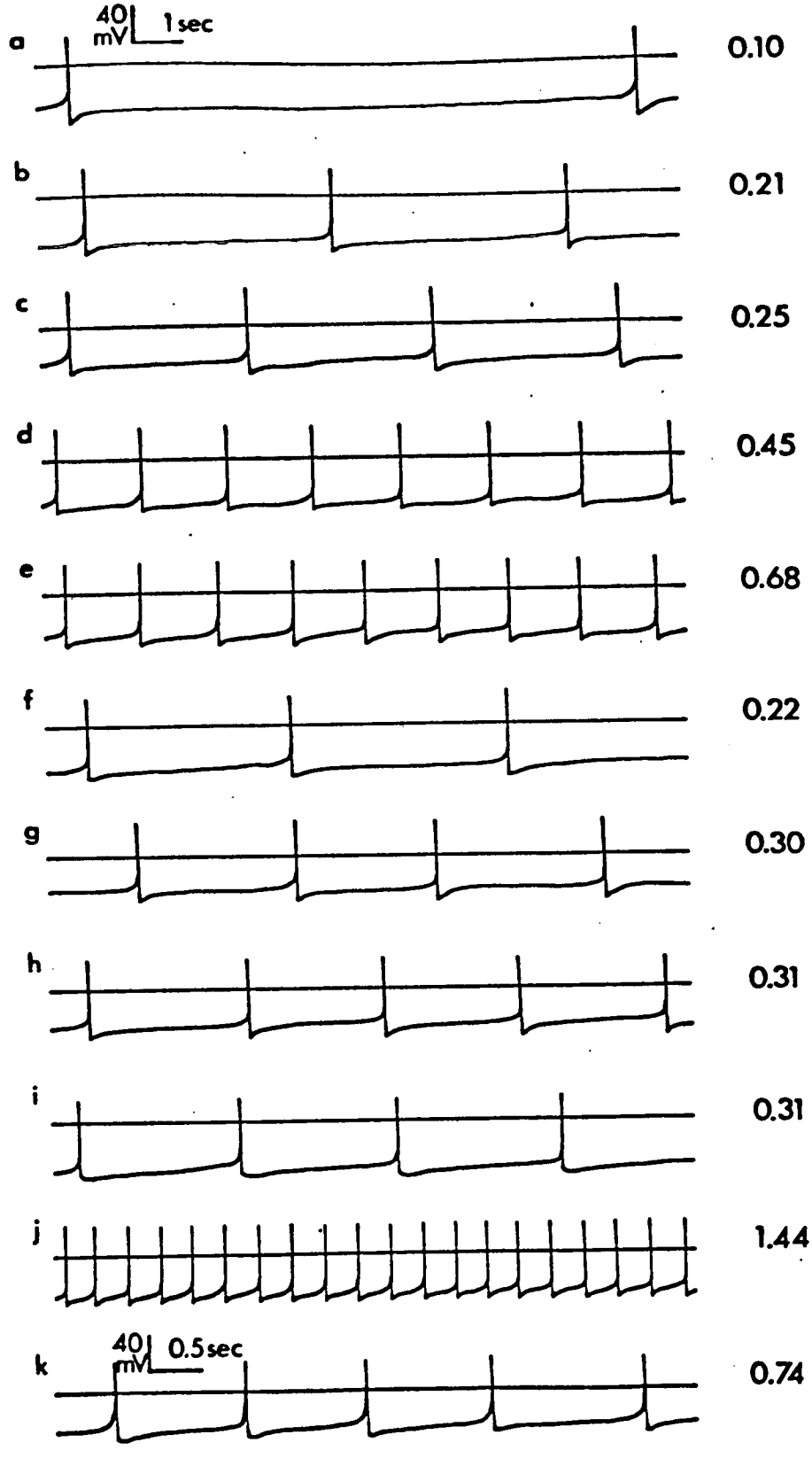

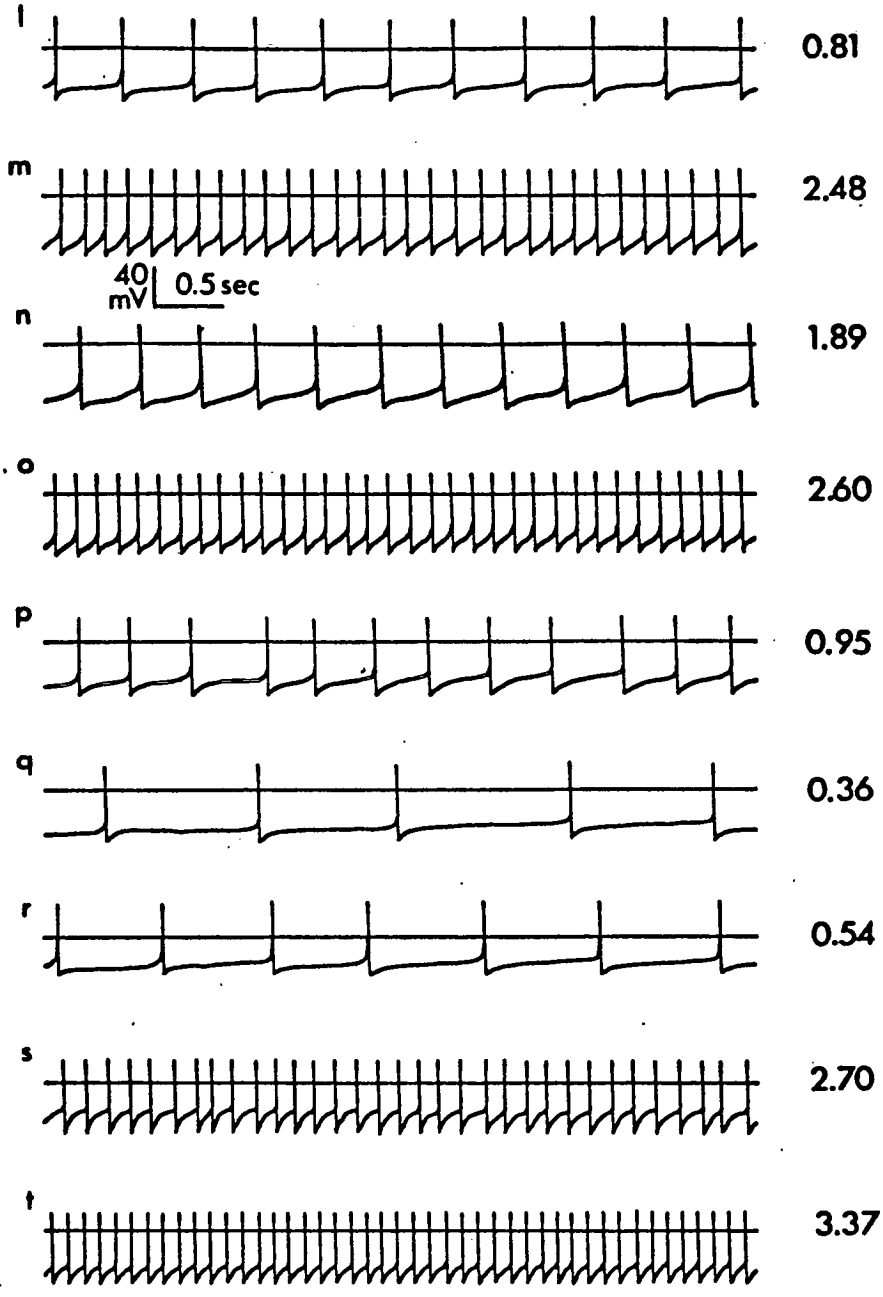

Scale bars in a apply to all records except k and n.
Mean frequencies indicated to right of each record.

Amplitude and frequency of spontaneous action potentials; 20 cell sample

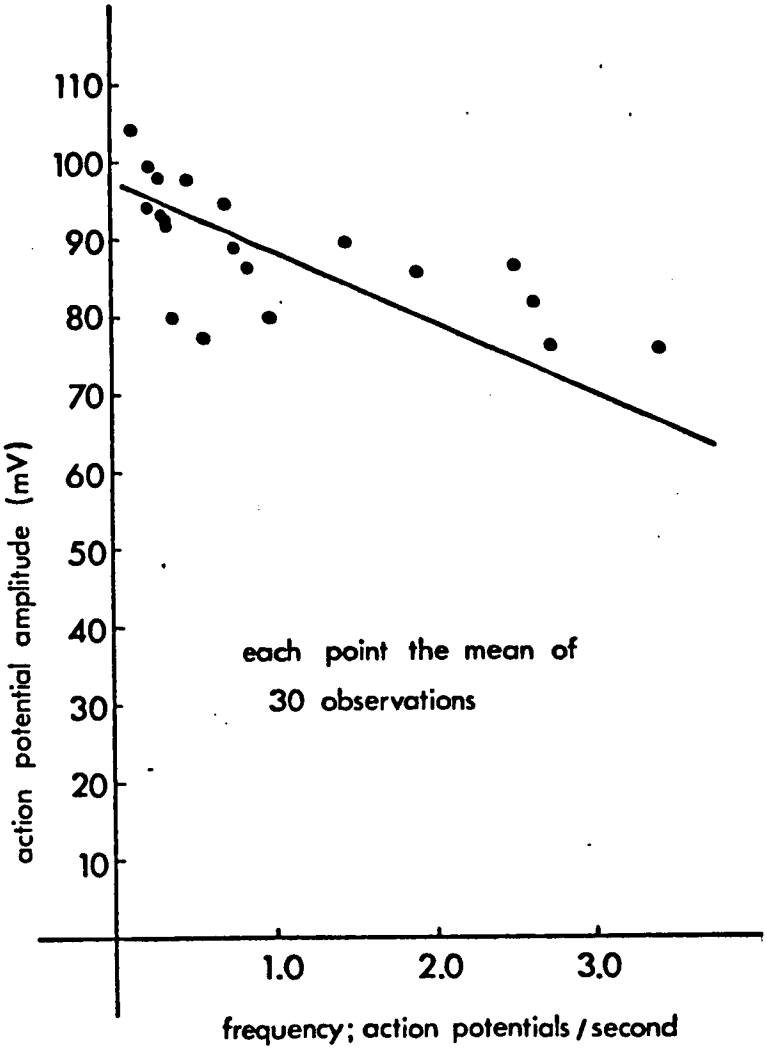

Components of action potential amplitude; 20 cell sample

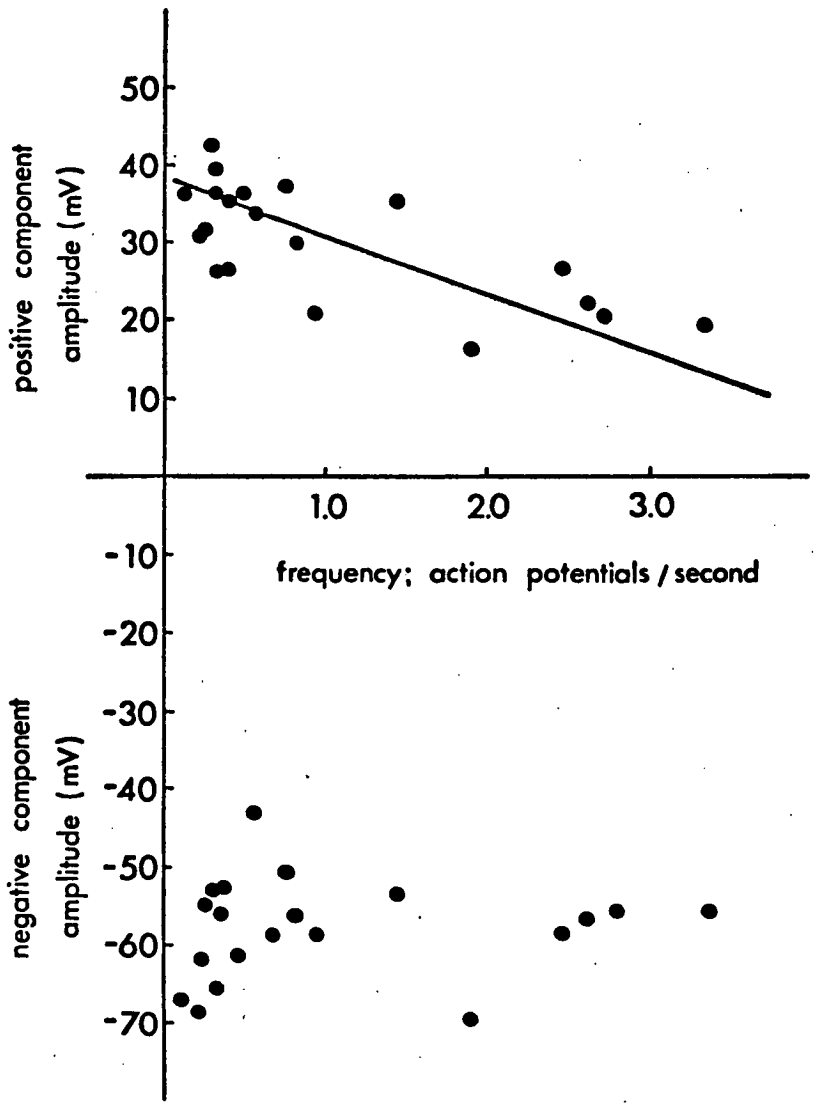

Amplitude and frequency of spontaneous action potentials;
Single cell

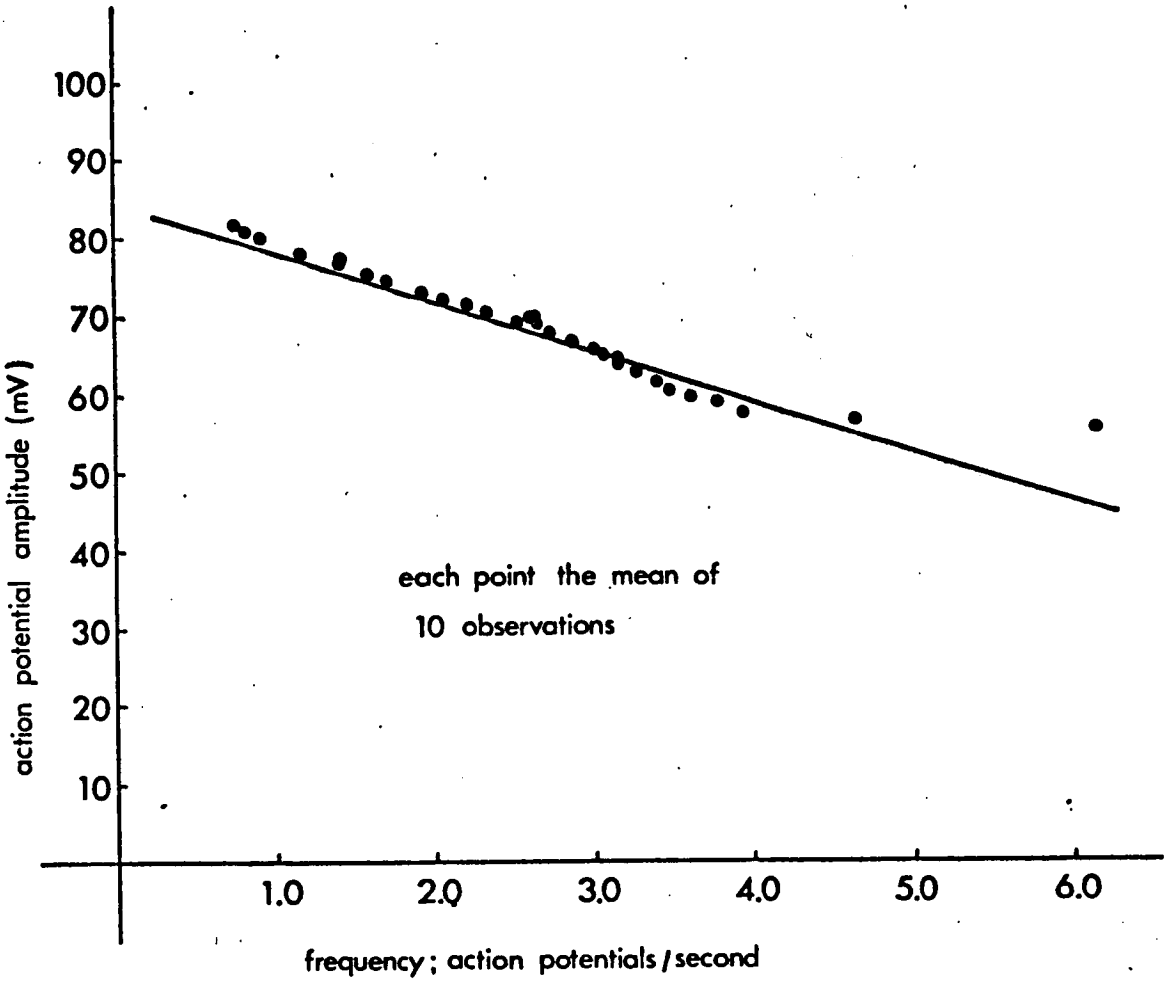

Components of action potential amplitude; Single cell;

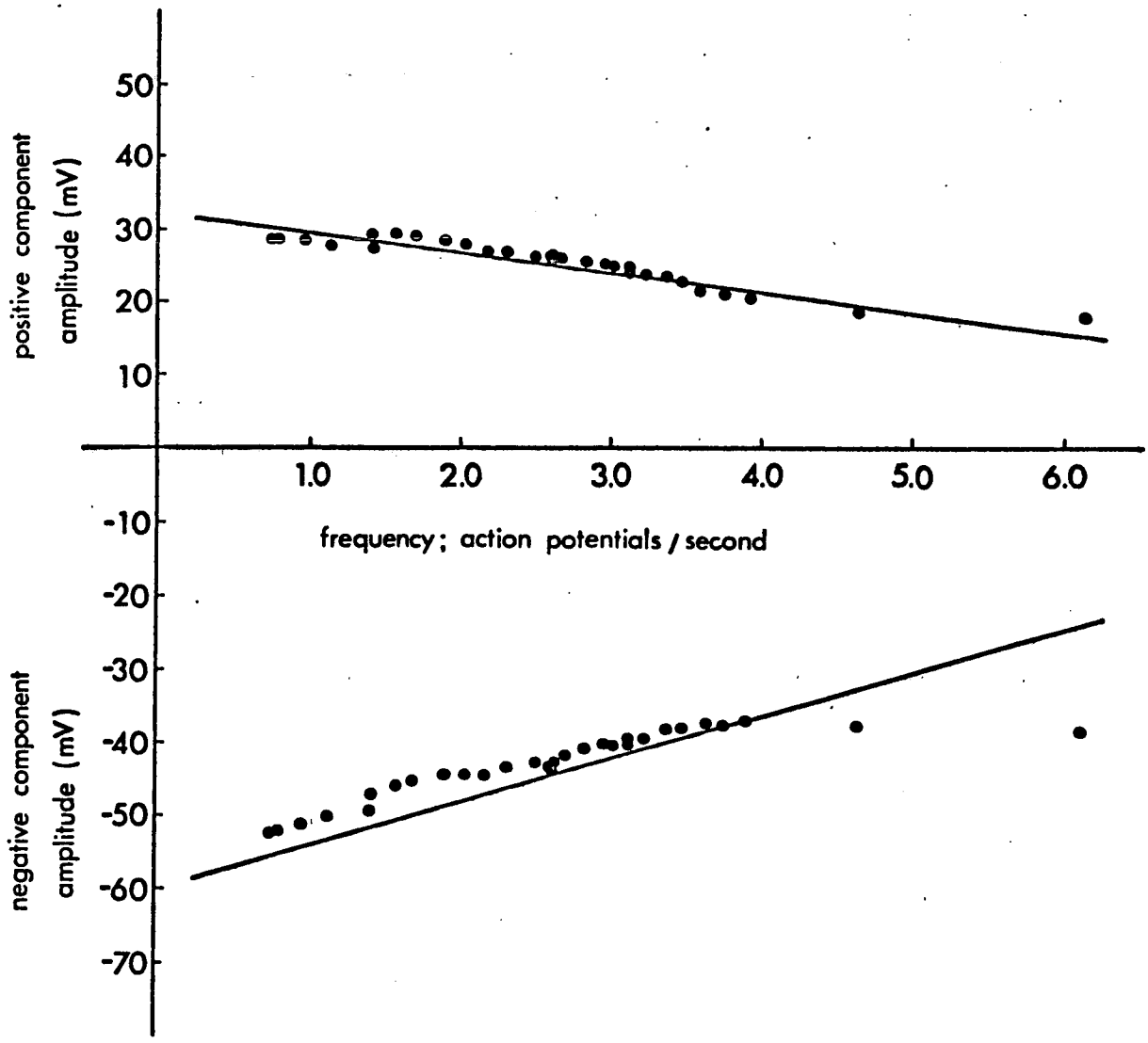

plotted as a function of spontaneous action potential frequency. The Pearson product-moment correlation coefficient calculated for these results was $r = -0.650$ (significant $p < 0.01$) indicating a definite negative relationship. Two regression lines can be found by linear regression analysis - one which corresponds to the prediction of action potential amplitude from the known spontaneous frequencies and another for which the reverse is true. The 'line of best fit' plotted in Figure 39 was obtained as the average of these two regression lines.

Figure 40 shows the mean positive and negative component amplitudes plotted against frequency for the same 20 cells. In this case the calculated correlation coefficient for the positive component amplitudes was $r = -0.686$ (significant $p < 0.001$) and for the negative component amplitudes $r = -0.078$ (insignificant). For the positive component values a line of best fit was plotted.

The occurrence of a relationship between action potential amplitude and frequency in a statistical sample of spontaneously active cells suggests that the same relationship might be apparent in single cells when intracellular recording with KCl electrodes is prolonged for periods of 30 minutes or more. Under these conditions hyperpolarization accompanied by a reduction in spontaneous frequency is often observed (KERKUT & MEECH, 1966). In fact when a prolonged recording is analyzed from the point of microelectrode penetration in the manner described above an extremely clear relationship can be demonstrated (Figures 41 and 42). In this case the negative component amplitudes (as well as the positive component and overall amplitudes) are closely correlated with spontaneous frequency ($p < 0.001$). The observed alterations in the

spontaneous activity may be related to the leakage of ions from the microelectrode tip. Chloride ions rather than potassium ions may be important (KERKUT & MEECH, 1966). However, since increases in the intracellular chloride concentration should lead to depolarization, the origin of the observed hyperpolarization remains obscure.

3) Discussion;

The distinct negative relationship between action potential amplitude and spontaneous frequency both in single cells and in a statistical sample of cells is consistent with the idea that pacemaker function may be partly determined by the distribution of ions across the nerve cell membrane. In the statistical case, the relationship appears to be associated more with the positive component of an action potential than with its negative component. The membrane conductance to sodium ions during the overshoot of an action potential is much higher than that to potassium ions and provided that the ratio of the two conductances at the peak of the overshoot can be regarded as fairly constant, the amplitude of the positive component should provide a relative estimate of the equilibrium potential for sodium ions across the membrane. If the positive component is large, a relatively low intracellular sodium concentration is indicated; if it is small a relatively high intracellular concentration is indicated.

Applying this argument to the experimental results produces the paradoxical inference that a reduction in the sodium equilibrium potential will lead to an increase in spontaneous action potential frequency and membrane excitability. Since sodium ions contribute to an inward and depolarizing current during the

action potential and the magnitude of this current is directly dependent on the sodium equilibrium potential, this inference cannot be true. The initial assumption that the conductance ratio at the peak of an action potential is relatively constant from cell to cell is therefore incorrect.

Pacemaker frequency cannot therefore be interpreted in simple terms and before proceeding to further experiments it is essential to consider in more detail the mechanisms which underly the generation of the action potential. This leads to an examination of the Hodgkin-Huxley theory and subsequent relevant work.

Chapter 4

THEORETICAL DEVELOPMENT

A) The Hodgkin-Huxley Theory;

1) Current-voltage curves;

The Hodgkin-Huxley equations represent an attempt to describe mathematically the membrane currents associated with action potential production and propagation in nerve.

The equations are dervied largely from voltage clamp studies on the giant axons of the squid, Loligo (HODGKIN, HUXLEY & KATZ, 1952; HODGKIN & HUXLEY, 1952a; 1952b; 1952c; 1952d). The method depends on the use of a feedback amplifier to maintain a uniform membrane potential over a definite area of membrane. Step function changes in membrane potential from one holding level to another can be applied and the current supplied by the amplifier in 'clamping' membrane potential at a constant level after a step function change provides a direct measure of the transmembrane current.

The basic circuit for voltage clamping is given in Figure 43(A). The amplifier detects differences between the control voltage (E_c) and the membrane potential (E_m). Any discrepancy is amplified and a current is driven across the membrane such that E_m is brought into parity with E_c.

Figure 43(B) shows a typical series of records for a membrane clamped at resting potential and then hyperpolarized or depolarized to a new holding level. The transmembrane current (I_c) can be divided into a capacitative component and an ionic component. The capacity current flows as a brief surge at the start of each record and its amplitude is directly proportional to the alteration

A; Basic voltage clamp circuit;

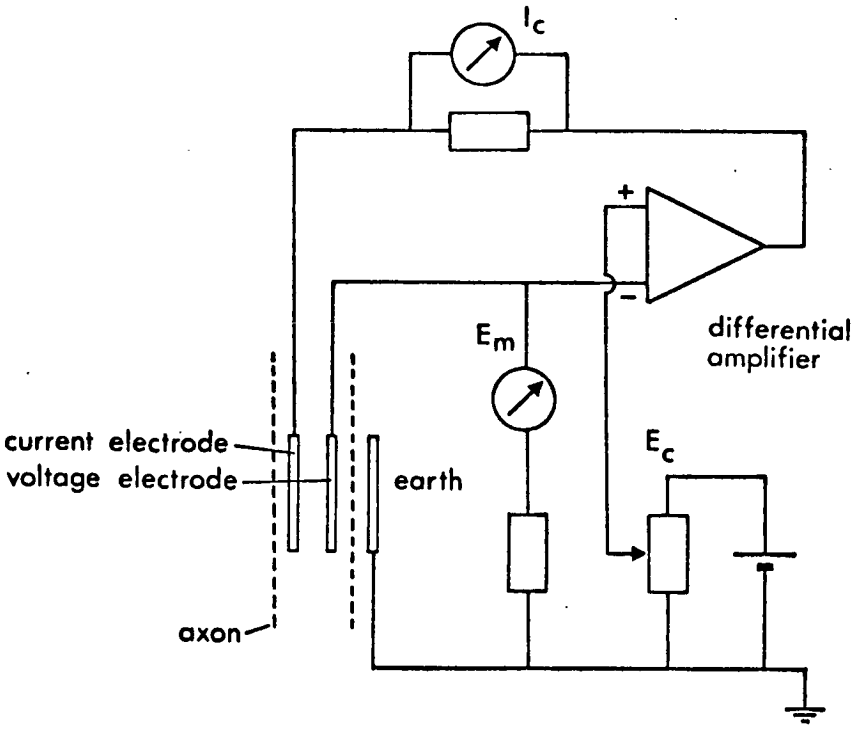

B; Typical voltage clamp records;

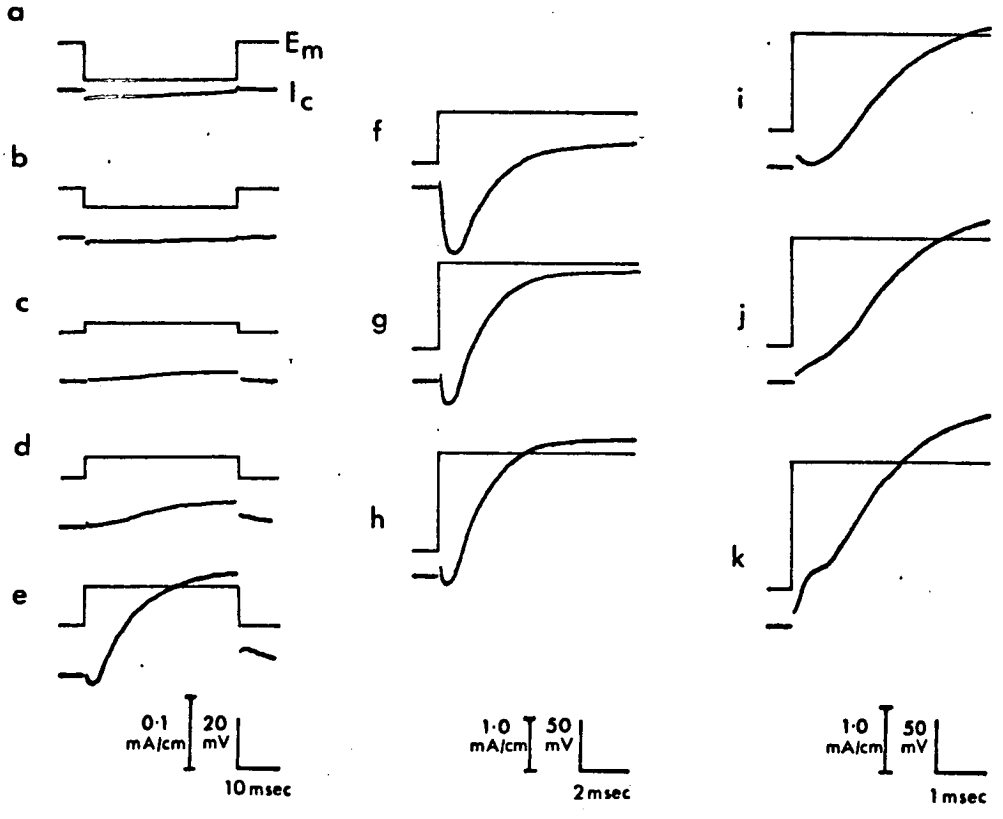

After Hodgkin, Huxley & Katz, 1952; for explanation see text.

Membrane current-voltage relation;

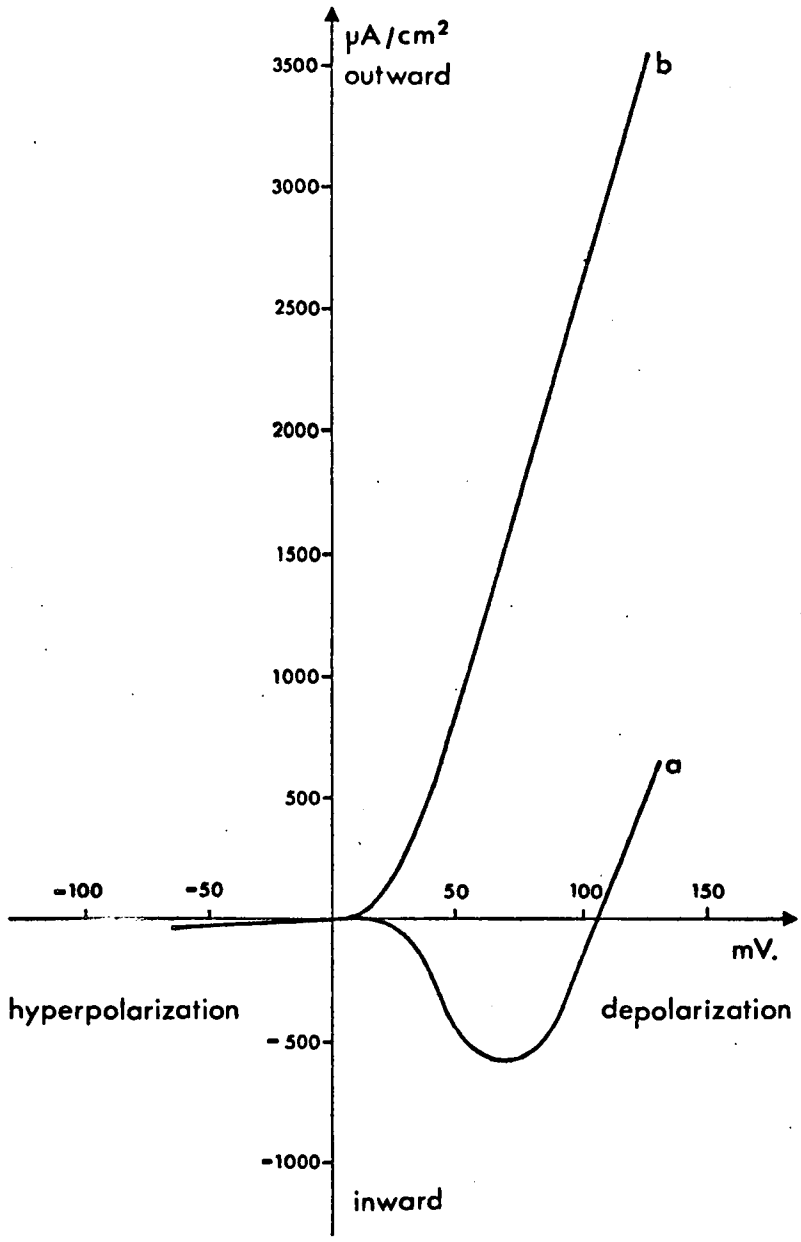

After Hogkin, Huxley & Katz, 1952; for explanation see text.

in membrane potential (HODGKIN, HUXLEY & KATZ, 1952). On the other hand, the sign and time course of the ionic current vary considerably with membrane potential. Hyperpolarizing displacements give small inward currents (records a,b). Small depolarizations give outward currents which are small initially but increase with time (records c,d). With intermediate depolarizations (records e,f) an initial phase of inward current changes after a short delay into a large and prolonged outward current. As the depolarizing step is further increased (records g-k) the phase of inward current is reduced, disappears and is then replaced by an outward current (record k).

During intermediate depolarizations the prolonged outward current reaches a stable level at which it can apparently be maintained more or less indefinitely. When large depolarizations are applied there is a slow decline in maintained outward current for reasons which are obscure. However, since membrane potential is strongly depolarized only briefly during the normal action potential it can be assumed that this decline has little physiological significance.

The relationship between membrane current density and membrane potential derived from voltage clamp records is illustrated in Figure 44. The two curves refer to membrane current density shortly after step displacement of the membrane potential (curve a) and to the maximum maintained ('steady state') current density (curve b).

It can be inferred from these results that there is a continuous relationship between transmembrane current and membrane

potential and that the response of the membrane to depolarization takes the form of voltage-dependent alterations in ionic 'conductance'.

Voltage clamp experiments with giant axons in solutions of differing ionic composition show that the early inward current associated with intermediate depolarizations can be attributed to sodium ions while the prolonged outward current can be attributed to potassium ions. In addition there is a small 'leakage' current of other ions (HODGKIN & HUXLEY, 1952a).

The movement of these ions through the membrane is determined in each case by a driving force which is the resultant of the concentration difference of the ion on the two sides of the membrane and the electrical potential difference (E) across the membrane. Thus the driving force for sodium ions is given by $(E-E_{Na})$ where E_{Na} is the equilibrium potential, derived from the Nernst equation, for sodium ions. Similarly the driving force for potassium ions is $(E-E_K)$.

The magnitude of the transmembrane ionic currents, denoted by I_{Na}, I_K and I_l, depend on these driving forces and also on the freedom with which the membrane allows ions to pass. This 'permeability' factor is expressed in terms of ionic conductance; g_{Na}, the sodium conductance is defined by $\frac{I_{Na}}{(E-E_{Na})}$, g_K, the potassium conductance is defined by $\frac{I_K}{(E-E_K)}$ and g_l, the leakage conductance, by $\frac{I_l}{(E-E_l)}$.

Provided that appropriate values can be determined for the ionic equilibrium potentials E_{Na} and E_K, and the ionic currents I_{Na} and I_K, these relationships can be used to estimate, g_{Na} and g_K as

functions of time during voltage clamp. The large depolarization at which the early inward current disappears (Figure 43(B), record j) provides an estimate of E_{Na}. The estimation of E_K is more complex and depends on raising the potassium conductance to a maximal level by a clamped depolarization of a fixed duration and then repolarizing to a new holding level. The current which flows after a step function repolarization consists of a brief capacitative component which is followed, depending on the repolarized holding potential, by an exponentially declining inward or outward current carried by potassium ions. The repolarized potential at which the potassium current is absent is an estimate of E_K (HODGKIN & HUXLEY, 1952b). The ionic currents I_{Na} and I_K can be estimated by comparing voltage clamp records obtained for each of two solutions of differing ionic composition (HODGKIN & HUXLEY, 1952a).

Figures 45(A) and 46(A) show the changes in potassium conductance and sodium conductance calculated in this way for a series of voltage clamped depolarizations.

The mathematical description of these relationships is the essential feature of the Hodgkin-Huxley theory.

2) The potassium conductance;

The potassium conductance is the simpler case and is assumed to be dependent on the state of a unitless variable n which may take values between 0 and 1. The n 'reaction' can be written as;

$$(1-n) \underset{\beta_n}{\overset{\alpha_n}{\rightleftharpoons}} n \qquad (1)$$

The reaction obeys first order kinetics and its mathematical description is;

$$\frac{dn}{dt} = \alpha_n(1-n) - \beta_n n \qquad (2)$$

where α_n and β_n are the rate constants of the forward and reverse reactions. These rate constants are assumed to be functions of temperature and membrane potential but not of time. When a sudden change in voltage is applied to the system, α_n and β_n instantaneously take up new values and n approaches its steady state value n_∞ along a simple exponential time course. At equilibrium;

$$n_\infty = \frac{\alpha_n}{(\alpha_n+\beta_n)} \qquad (3)$$

The time constant, τ_n, of the reaction is given by;

$$\tau_n = \frac{1}{(\alpha_n+\beta_n)} \qquad (4)$$

For $n = n_o$ when $t = 0$ equation (2) has the solution;

$$n = n_\infty - (n_\infty - n_o).\exp(-\frac{t}{\tau_n}) \qquad (5)$$

where exp denotes the natural exponential function i.e. $\exp(-\frac{t}{\tau_n}) = e^{(-\frac{t}{\tau_n})}$.

In order to produce theoretical curves which can be satisfactorily fitted to the experimental results of Figure 45(A) the potassium conductance is assumed to take values such that;

$$g_K = \bar{g}_K n^4 \qquad (6)$$

where $\bar{g}_K$ is a constant and is the maximum possible potassium conductance of the membrane corresponding to a value of $n = 1$.

Using this relationship equation (5) can be transformed to allow comparison with the experimental data;

$$g_K = ((g_{K_\infty})^{\frac{1}{4}} - ((g_{K_\infty})^{\frac{1}{4}} - (g_{K_o})^{\frac{1}{4}}).\exp(-\frac{t}{\tau_n}))^4 \qquad (7)$$

where g_{K_o} is the conductance at $t = 0$ and g_{K_∞} is the value which

the conductance attains during a given depolarization. Experimental values of g_{K_o} and g_{K_∞} can be substituted into this equation and τ_n is then the only unknown. Theoretical curves of potassium conductance are produced using values of τ_n selected to give the best fit.

The theoretical curves of Figure 45(A) were derived in this way and are in reasonable agreement with the experimental results except that the latter show more initial delay.

The usefulness of these approximations is extended if expressions can be found relating the rate constants, α_n and β_n, to membrane potential.

If a value can be assigned to $\bar{g}_K$, n_∞ can be calculated from equation (6), using experimental values of g_K, for any given depolarization. α_n and β_n can then be obtained from the following relationships derived from equations (3) and (4);

$$\alpha_n = \frac{n_\infty}{\tau_n} \tag{8}$$

$$\beta_n = \frac{(1-n_\infty)}{\tau_n} \tag{9}$$

An arbitrary value of $\bar{g}_K$ 20% greater than the value of g_{K_∞} for a depolarization of 100 mV was chosen. Using values of τ_n approximated for best fit as above, α_n and β_n can be calculated from conductance curves such as those of Figure 45(A). Plotting these values for the rate constants against membrane potential provides continuous relationships which are closely approximated by the following equations;

$$\alpha_n = \frac{0.01(V+10)}{\exp\frac{V+10}{10} - 1} \tag{10}$$

A;

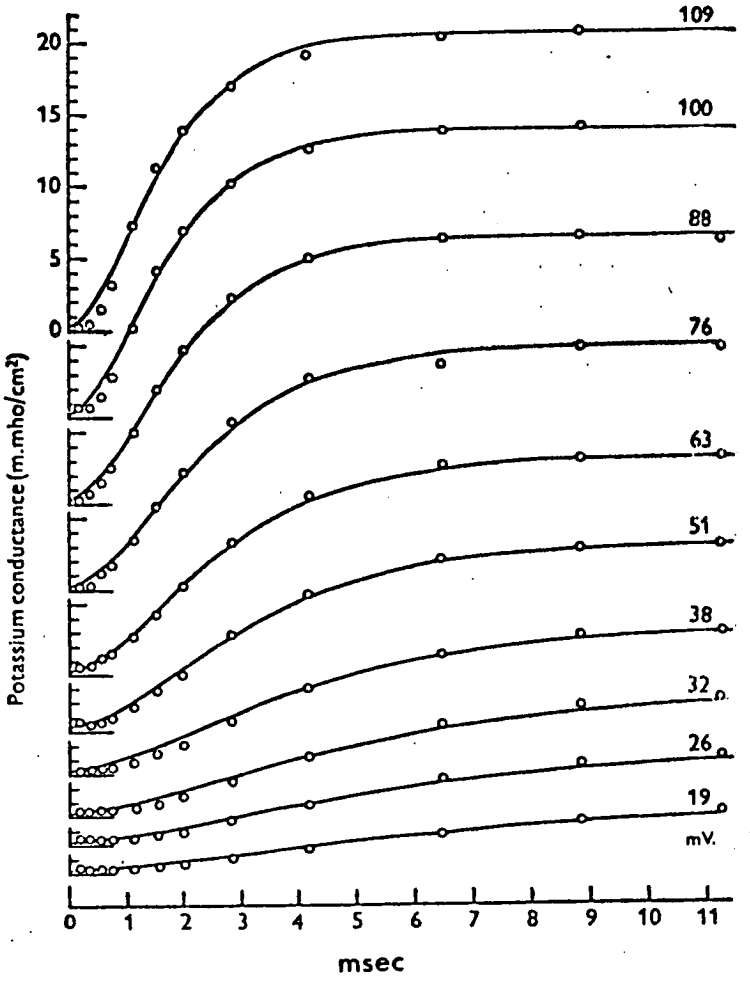

Rise of potassium conductance associated with different depolarizations. The circles give experimental estimates of potassium conductance; the smooth curves were calculated according to equation (7) as described in the text. The number on each curve gives the depolarization relative to resting potential in mV.

After Hodgkin & Huxley, 1952d.

B;

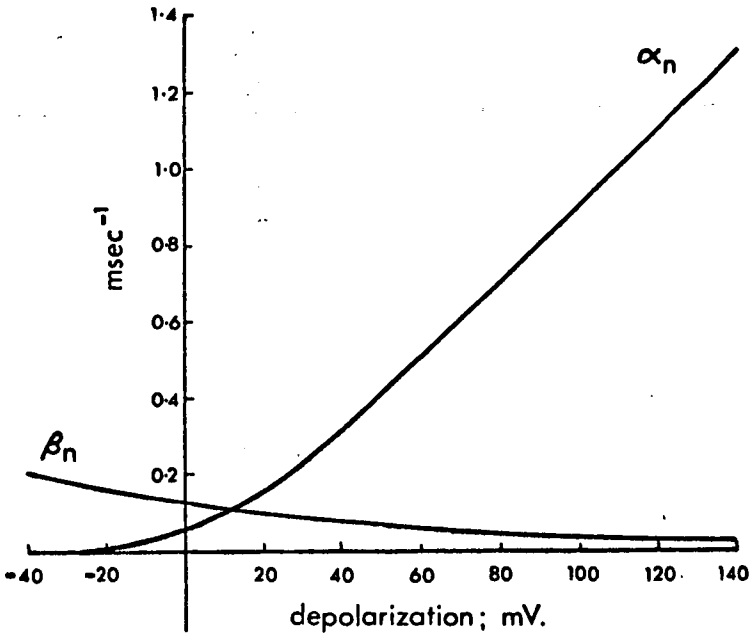
1·4
1·2
1·0
0·8
0·6
0·4
0·2
msec⁻¹
α_n
β_n
-40
-20
20
40
60
80
100
120
140
depolarization; mV.

C;

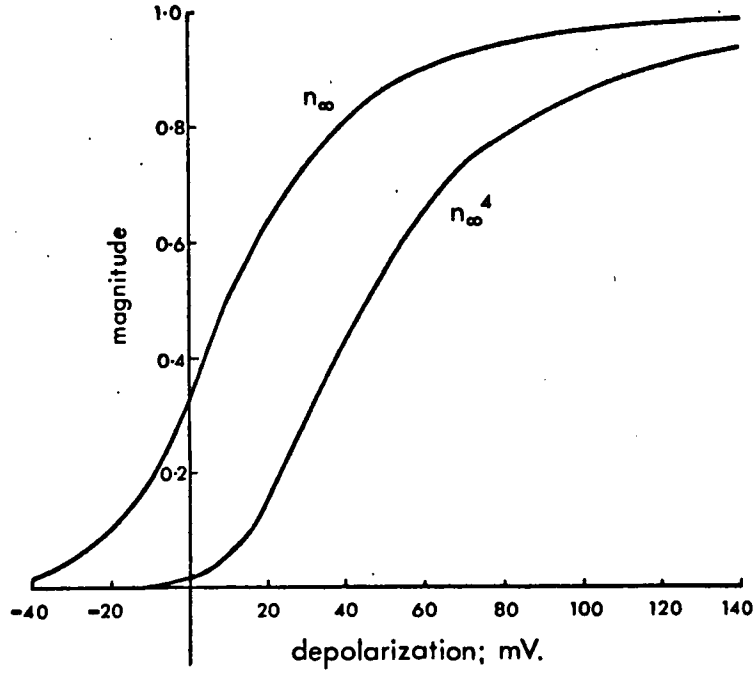
1·0
0·8
0·6
0·4
0·2
magnitude
n_∞
n_∞^4
-40
-20
20
40
60
80
100
120
140
depolarization; mV.

$$\beta_n = 0.125\exp(\frac{V}{80}) \qquad (11)$$

where α_n and β_n are given in reciprocal msec and V is the displacement of the membrane from its resting level in mV (depolarization negative). Figure 45(B) illustrates these relationships and Figure 45(C) shows n_∞, calculated from equation (3) and n_∞^4 as functions of membrane potential.

Collectively these equations are an adequate description of the observed properties of the potassium conductance (HODGKIN & HUXLEY, 1952d). Temperature effects can be accounted for by assuming a Q_{10} of about 3.0 for the rate constants.

While the system is hypothetical it may be given some physical basis by supposing that potassium ions can only cross the membrane when four similar particles occupy a certain region ('site') of the membrane. If n is the proportion of particles in the appropriate place (or having the appropriate configuration) then n^4 will be the proportion of effective sites and will determine the potassium conductance.

The magnitude of the potassium current, I_K, at any time is given by;

$$I_K = \bar{g}_K n^4 (V - V_K) \qquad (12)$$

where V is the displacement of the membrane from resting potential (E_r) and $V_K = -(E_K - E_r)$.

3) The sodium conductance;

The changes in sodium conductance associated with depolarization (Figure 46(A)) can be described in terms of their

dependence on two variables, each of which obeys a first order equation. The sodium activation variable is denoted by m and the m 'reaction' can be written as;

$$(1-m) \underset{\beta_m}{\overset{\alpha_m}{\rightleftharpoons}} m \tag{13}$$

The appropriate mathematical description is;

$$\frac{dm}{dt} = \alpha_m(1-m) - \beta_m m \tag{14}$$

where α_m and β_m are the rate constants of the forward and reverse reactions. As in the case of the n reaction, these rate constants are assumed to be functions of temperature and membrane potential but not of time. Under a clamped depolarization m approaches its steady state value m_∞ along a simple exponential time course. At equilibrium;

$$m_\infty = \frac{\alpha_m}{(\alpha_m+\beta_m)} \tag{15}$$

The time constant, τ_m, of the reaction is given by;

$$\tau_m = \frac{1}{(\alpha_m+\beta_m)} \tag{16}$$

For $m = m_o$ when $t = 0$ equation (14) has the solution;

$$m = m_\infty - (m_\infty - m_o).\exp(-\frac{t}{\tau_m}) \tag{17}$$

The sodium inactivation variable is denoted by h and is defined by a corresponding set of expressions. The h 'reaction' can be written as;

$$(1-h) \underset{\beta_h}{\overset{\alpha_h}{\rightleftharpoons}} h \tag{18}$$

and its mathematical expression is;

$$\frac{dh}{dt} = \alpha_h(1-h) - \beta_h h \tag{19}$$

where α_h and β_h are the rate constants. The steady state value of h is given by;

$$h_\infty = \frac{\alpha_h}{(\alpha_h+\beta_h)} \tag{20}$$

and the time constant of the reaction is given by;

$$\tau_h = \frac{1}{(\alpha_h+\beta_h)} \tag{21}$$

For $h = h_o$ when $t = 0$ equation (19) has the solution;

$$h = h_\infty - (h_\infty - h_o).\exp(-\frac{t}{\tau_h}) \tag{22}$$

In order to produce theoretical curves which can be satisfactorily fitted to the experimental results the sodium conductance is assumed to take values such that;

$$g_{Na} = \bar{g}_{Na} m^3 h \tag{23}$$

where $\bar{g}_{Na}$ is a constant corresponding to the maximum possible sodium conductance and m and h are unitless variables which can take values between 0 and 1.

For depolarizations greater than 30 mV m_o is negligible compared to m_∞ and equation (17) can be simplified to;

$$m = m_\infty(1-\exp(-\frac{t}{\tau_m})) \tag{24}$$

Under similar conditions, inactivation is very nearly complete and h_∞ can therefore be considered negligible, equation (22) simplifying to;

$$h = h_o.\exp(-\frac{t}{\tau_h}) \tag{25}$$

Substituting in equation (23) the sodium conductance for larger depolarizations can be written as;

$$g_{Na} = \bar{g}_{Na} m_\infty^3 h_o (1-\exp(-\frac{t}{\tau_m}))^3.\exp(-\frac{t}{\tau_h}) \tag{26}$$

Theoretical conductance curves, produced by estimating $\bar{g}_{Na} m_\infty^3 h_o$ (i.e. the level which g_{Na} would attain if h remained at

A;

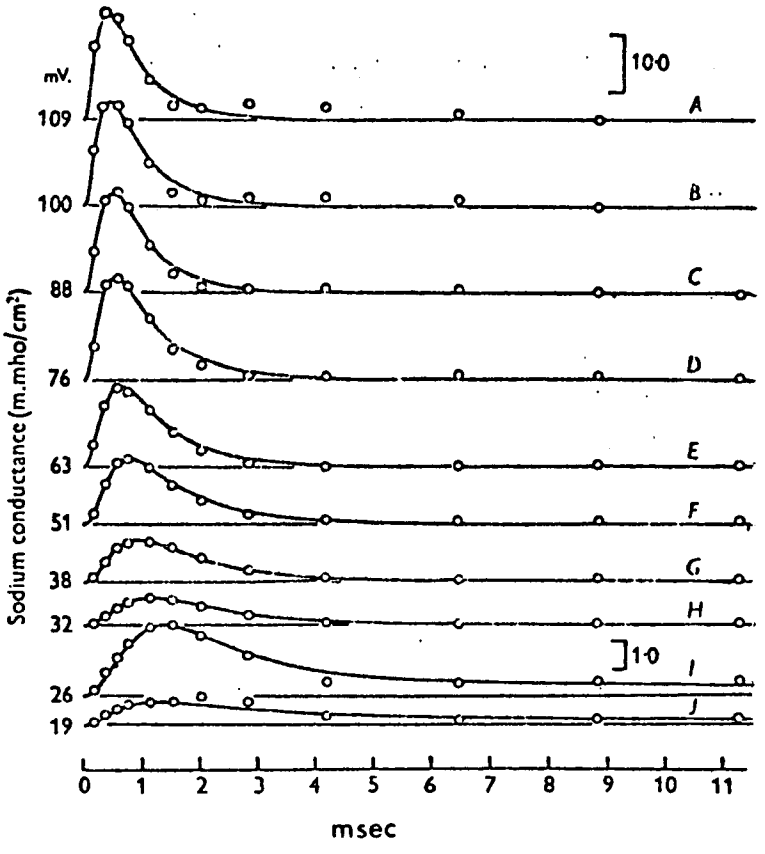

Changes in sodium conductance associated with different depolarizations. The circles give experimental estimates of sodium conductance; the smooth curves were calculated according to equation (26) as described in the text. The number on each curve gives the depolarization relative to resting potential in mV. The upper scale bar applies to curves A–H, the lower scale bar to curves I and J; both scale bars in m.mho/cm^2.

After Hodgkin & Huxley, 1952d.

B:

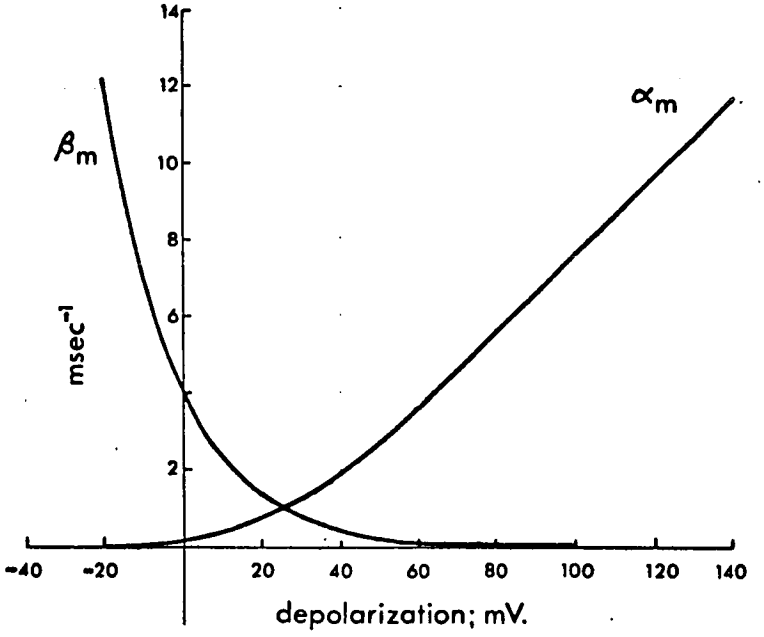
14
12
10
8
6
2
α_m
β_m
msec^{-1}
-40
-20
20
40
60
80
100
120
140
depolarization; mV.

C:

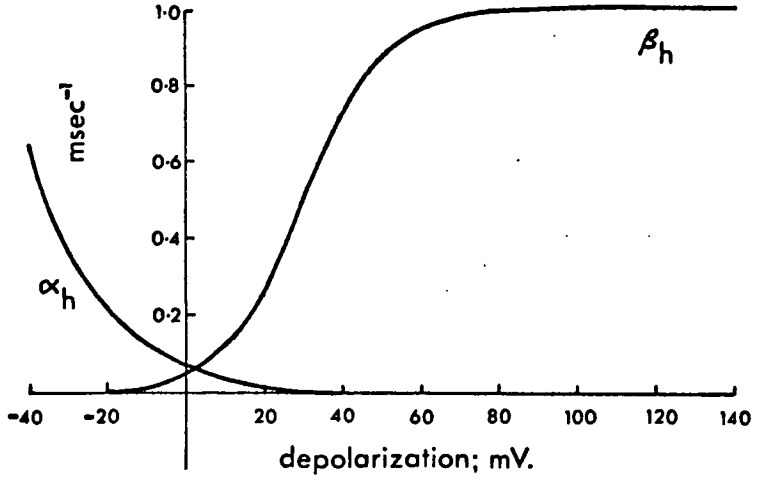
1·0
0·8
0·6
0·4
0·2
β_h
α_h
msec^{-1}
-40
-20
20
40
60
80
100
120
140
depolarization; mV.

D;

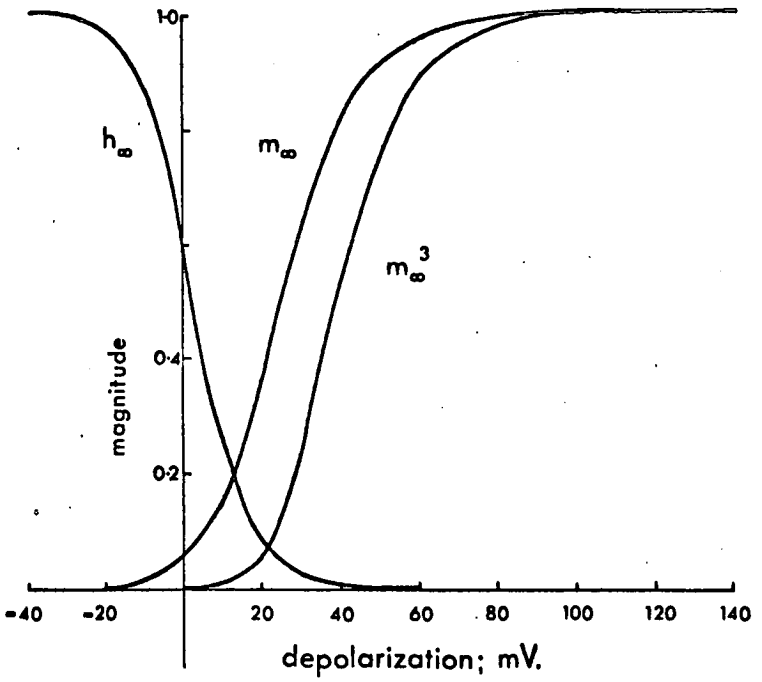
1·0
0·4
0·2
magnitude
h_∞
m_∞
m_∞^3
-40
-20
20
40
60
80
100
120
140
depolarization; mV.

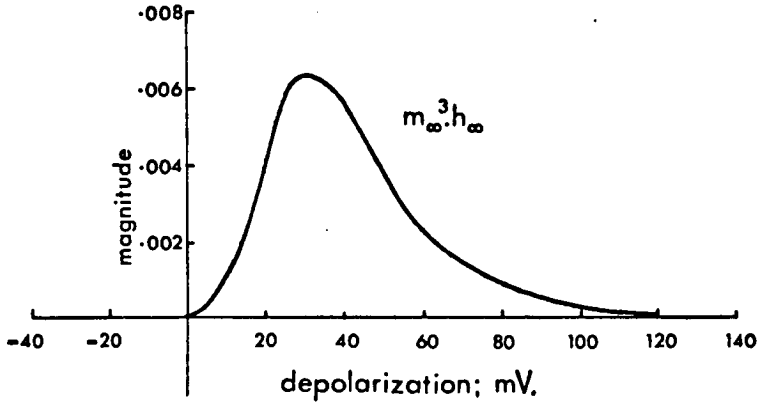
·008
·006
·004
·002
magnitude
$m_\infty^3 h_\infty$
-40
-20
20
40
60
80
100
120
140
depolarization; mV.

its resting level h_o) for each depolarization and selecting values for the time constants τ_m and τ_h for best fit, are in good agreement with experimental observations (Figure 46(A)).

For smaller depolarizations experimentally derived estimates of h_∞ and τ_h are necessary before good agreement is obtained (HODGKIN & HUXLEY, 1952c).

As in the case of the potassium conductance, suitable approximations relating the rate constants to membrane potential can be found (HODGKIN & HUXLEY, 1952b; 1952c; 1952d). The derived expressions are;

$$\alpha_m = \frac{0.1(V+25)}{\exp\frac{V+25}{10} - 1} \tag{27}$$

$$\beta_m = 4\exp(\frac{V}{18}) \tag{28}$$

$$\alpha_h = 0.07\exp(\frac{V}{20}) \tag{29}$$

$$\beta_h = \frac{1}{\exp\frac{V+30}{10} + 1} \tag{30}$$

where the rate constants are given in reciprocal msec and V is the displacement of the membrane from its resting level in mV (depolarization negative). Temperature effects can be accounted for by assuming a Q_{10} of about 3.0.

Figure 46(B) and Figure 46(C) illustrate these relationships and Figure 46(D) shows the steady state values of m_∞, m_∞^3, h_∞, $m_\infty^3 h_\infty$, calculated from equations (15) and (20), and plotted against membrane potential.

In physical terms it can be supposed that sodium ions can only cross the membrane at a 'site' occupied by three 'activating'

particles and that this transfer can be blocked at a given site by a single 'inactivating' particle. If m represents the proportion of activating particles in the appropriate place (or having the appropriate configuration) then m^3 will be the proportion of available sites. If h represents the proportion of these which are not inactivated then m^3h represents the overall proportion of effective sites and will determine the sodium conductance.

The magnitude of the sodium current (I_{Na}) at any time is given by;

$$I_{Na} = \bar{g}_{Na} m^3 h (V - V_{Na}) \qquad (31)$$

where V is the displacement of the membrane from resting potential (E_r) and $V_{Na} = -(E_{Na} - E_r)$.

4) The leakage conductance;

In addition to the relatively large sodium and potassium currents associated with voltage dependent conductance changes, a small 'leakage' current can be identified. This can be attributed to chloride ions, diffusion through any damaged areas of membrane and, possibly, ions transferred by metabolism against concentration gradients. Although of a composite nature the leakage current, denoted by I_l, has a conductance g_l and an apparent equilibrium potential, E_l, at which I_l is zero. The leakage conductance is assumed to have a constant value irrespective of temperature and membrane potential (HODGKIN & HUXLEY, 1952b).

The magnitude of the leakage current at any time is given by;

$$I_l = g_l (V - V_l) \qquad (32)$$

where V is membrane potential displacement as before and $V_l = -(E_l - E_r)$.

5) Reconstruction of the action potential;

As previously indicated the transmembrane current consists of a capacitative and an ionic component i.e.;

$$I_m = C_m \cdot \frac{dV}{dt} + I_i \qquad (33)$$

where I_m is the total transmembrane current, C_m is the membrane capacity and I_i is the total ionic current, all referred to unit area.

Using the relationships derived above for potassium, sodium and leakage currents (equations (12), (31) and (32) respectively) this equation can be expanded as follows;

$$I_m = C_m \cdot \frac{dV}{dt} + \bar{g}_K n^4 (V - V_K) + \bar{g}_{Na} m^3 h (V - V_{Na}) + g_l (V - V_l) \qquad (34)$$

Together with all the expressions relating n, m and h to membrane potential this equation forms a complete mathematical description of the transmembrane current (HODGKIN & HUXLEY, 1952d; NOBLE, 1966).

In the case of a 'membrane' action potential (defined as one in which membrane potential is uniform at any point in time over the entire area involved in the active response) there is no lateral spread of current and hence the whole of the ionic current must be involved in charging or discharging the membrane capacity, i.e. the net transmembrane current is always zero. The response of the membrane to a given depolarization is then calculated by equating equation (34) to zero and solving for V as a function of time. Such a solution depends on a relatively complex integration procedure

but provides an action potential reconstruction which is in good agreement with experimental results.

In the case of a propagated action potential a proportion of the transmembrane current flows laterally since the potential across the membrane is not uniform along its length. Action potential reconstruction depends on equating equation (34) to an expression defining the proportion of lateral current and involves a similar integration procedure. These results are also in good agreement with experimental measurements.

Figure 47(A) shows a theoretical propagated action potential and the predicted variations in sodium conductance, potassium conductance and overall conductance against time. The overall conductance changes are in close agreement with those determined by experiment (COLE & CURTIS, 1939).

Figure 47(B) shows the familiar electrical membrane analogue which summarizes the membrane properties described by the Hodgkin-Huxley equations.

6) Discussion;

The Hodgkin-Huxley theory can be expanded to account for very many of the observed properties of excitable membranes (HODGKIN & HUXLEY, 1952d; NOBLE, 1966). The equations accurately predict the amplitude, threshold and shape of the action potential, its rate of propagation, sub-threshold excitatory phenomena, refractoriness and temperature effects. Because of this the theory provides a valuable basis of interpretation for a wide range of experimental data.

A; Theoretical propagated action potential;

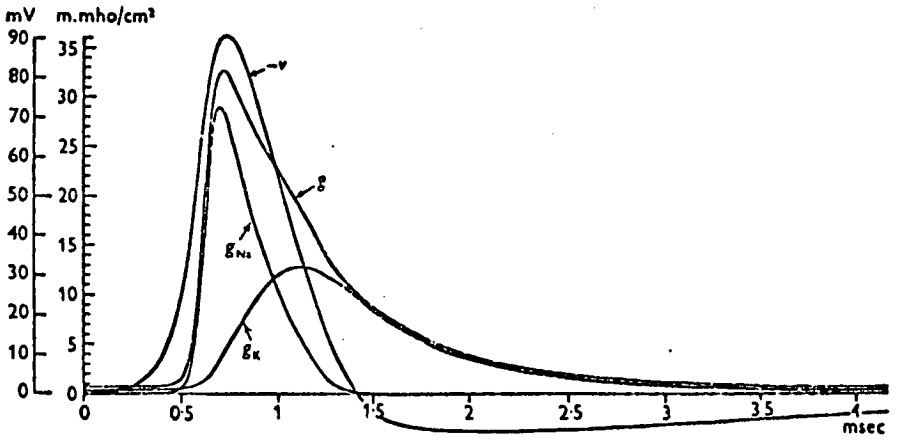

After Hodgkin & Huxley (1952d)

B; Membrane analogue;

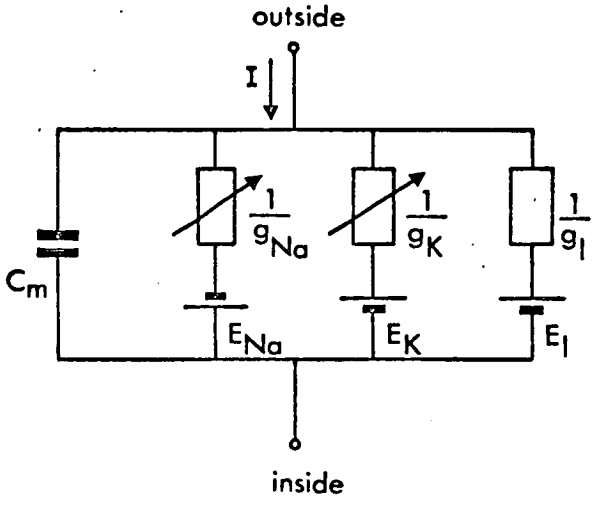

In some membranes the active response is determined not only by changes in sodium conductance and potassium conductance but also by changes in the conductance for other ions. For example voltage-dependent changes in calcium conductance contribute to the active response in Helix aspersa neurons (CHAMBERLAIN & KERKUT, 1969), in Anisidoris neurons (CONNOR & STEVENS, 1971a) and in Lymnea stagnalis neurons, where changes in magnesium conductance may also be involved (JERELOVA, KRASTS & VEPRINTSEV, 1971). At least in the case of Anisidoris, the calcium and sodium conductances can be pooled and the Hodgkin-Huxley equations adapted to provide an accurate mathematical description of the system (CONNOR & STEVENS, 1971a). In addition conductance changes of a type not included in the Hodgkin-Huxley formulation(q.v.) can be described in an analogous manner (NEHER, 1971; CONNOR & STEVENS, 1971b; 1971c).

While the range of application of the theory is considerable it should not be accepted uncritically since rather little is known of the mechansims which underly changes in membrane conductance. What can be said is that the theory provides an adequate conceptual framework for the discussion of the properties of excitable membranes.

B) Absolute potential rate constant equations;

The Hodgkin-Huxley rate constant equations depend on a quantity V which is defined as the difference between membrane potential (E) and resting potential (E_r). Depolarizing displacements are regarded as negative and hyperpolarizing displacements as positive i.e. $V = -(E-E_r)$ where E and E_r are absolute potential values ('inside' relative to 'outside'). V = 0 defines resting potential irrespective of its absolute value. This terminology was adopted for practical reasons; firstly, because the absolute resting potential could not be measured with any accuracy since relatively large junction potentials were associated with the recording electrodes and, secondly, because results from different axons could be grouped more easily.

If the 'reactions' which determine the conductance of the membrane are to depend on membrane potential, it is clearly more probable that the absolute potential, rather than the potential relative to resting, will be significant. In this context, it is relevant that voltage-dependent conductance changes similar to those in nerve can be produced in artificial bimolecular lipid and protein membranes under an applied electric field (MUELLER & RUDIN, 1968), which suggests that the physical membrane reactions may be subject to ordinary kinetic principles. In real nerve therefore, the rate constants of conductance determining reactions are likely to be continuous functions of absolute membrane potential.

The Hodgkin-Huxley rate constant equations (equations (10), (11), (27), (28), (29) and (30)) are easily converted to an absolute potential form assuming a representative value for the absolute resting potential. Recorded resting potentials are normally around

-50 mV and, allowing for a junction potential of about 10 mV at the recording electrode, a value of -60 mV is a reasonable estimate of the absolute resting potential (HODGKIN & KATZ, 1949). Hence V can be represented as V = -(E+60) and the rate constant equations become;

$$\alpha_n = \frac{0.01(-(E+60) + 10)}{\exp\frac{-(E+60) + 10}{10} - 1} \tag{35}$$

$$\beta_n = 0.125\exp(\frac{-(E+60)}{80}) \tag{36}$$

$$\alpha_m = \frac{0.1(-(E+60) + 25)}{\exp\frac{-(E+60) + 25}{10} - 1} \tag{37}$$

$$\beta_m = 4\exp(\frac{-(E+60)}{18}) \tag{38}$$

$$\alpha_h = 0.07\exp(\frac{-(E+60)}{20}) \tag{39}$$

$$\beta_h = \frac{1}{\exp\frac{-(E+60) + 30}{10} + 1} \tag{40}$$

where E is the absolute membrane potential 'inside' relative to 'outside'.

The composite Hodgkin-Huxley equation for transmembrane current (equation (34)) may also be expressed in an absolute potential form;

$$I_m = C_m \cdot \frac{dE}{dt} + \bar{g}_K n^4 (E-E_K) + \bar{g}_{Na} m^3 h (E-E_{Na}) + g_l (E-E_l) \tag{41}$$

(Note that inward currents calculated from equation (34) will be positive in sign while, calculated from equation (41), inward currents will be negative in sign and will therefore correspond to the more normal convention.)

It is significant that the rate constants calculated from equations (35) - (40), and hence the ionic conductances of the membrane, do not have fixed values at resting potential if this is

subject to variation. This means that equation (41) can be applied to membranes exposed to abnormal ionic environments which may produce large alterations in resting potential and in the resting ionic conductances (see BAKER, HODGKIN & SHAW, 1962b). It is not valid to assume, as is implied by equation (34), that the resting ionic conductances have fixed values irrespective of the absolute value of the resting potential. Equation (34), with its corresponding rate constant equations, is only applicable under strictly normal conditions when its solution is, in any case, identical to that calculated from absolute potential rate constant equations and equation (41).

For theoretical purposes at least, absolute potential equations are much more useful than those expressed in relative potential terms.

C) Reconstruction of membrane current-voltage relationships;

1) Theoretical basis;

While the solution of equation (41) for E with respect to time either for 'membrane' or propagated action potentials involves conceptually complex mathematics, it is relatively simple to solve for I_m with respect to time, substituting appropriate values for E. This can be done to produce theoretical voltage clamp records which are in good agreement with experimental records (HODGKIN & HUXLEY, 1952d). Theoretical curves of ionic current density (I_i) with respect to membrane potential could be derived from such reconstructions. Alternatively, if suitable values can be assigned to the unitless variables n, m and h, theoretical 'current-voltage' curves can be produced directly.

Under a maintained voltage clamp, the unitless variables tend towards their steady state values and, after a time, $n = n_\infty$, $m = m_\infty$ and $h = h_\infty$. Since $I_m = C_m \cdot \frac{dE}{dt} + I_i$ and under voltage clamped conditions $C_m \cdot \frac{dE}{dt} = 0$, the theoretical steady state current-voltage relation (corresponding to curve b of Figure 44) can be plotted according to;

$$I_i \simeq \bar{g}_K n_\infty^4 (E-E_K) + \bar{g}_{Na} m_\infty^3 h_\infty (E-E_{Na}) + g_l (E-E_l) \qquad (42)$$

The non-linear variations in current shortly after step displacement of membrane potential in real nerve are largely the result of changes in sodium conductance. The Hodgkin-Huxley equations accomodate this observation by assuming that the sodium activation variable (m) approaches its steady state value (m_∞) much more rapidly than either the potassium activation variable (n) or the sodium inactivation variable (h). Assuming that n and h remain

at their resting values ($n = n_o$, $h = h_o$) theoretical curves of ionic current density shortly after step displacement of membrane potential (corresponding to curve a of Figure 44) can be produced according to;

$$I_i = \bar{g}_K n_o^4 (E-E_K) + \bar{g}_{Na} m_\infty^3 h_o (E-E_{Na}) + g_l (E-E_l) \qquad (43)$$

The magnitude of ionic currents calculated from this expression are likely to overestimate observed currents to some extent because n and h are assumed to be constant. Nevertheless qualitative predictions derived from theoretical results should still be valid.

Reconstruction of the steady state current-voltage relation is achieved by substituting appropriate values for $\bar{g}_K$, $\bar{g}_{Na}$, g_l, E_K, E_{Na} and E_l in equation (42). For a particular value of E, α_n, β_n, α_m, β_m, α_h and β_h are calculated according to equations (35) - (40) and the corresponding steady state values n_∞, m_∞ and h_∞ calculated according to equations (3), (15) and (20) respectively. Using these values, the solution of equation (42) is the value of I_i which corresponds to the selected value of E i.e. these values of I_i and E are the coordinates of a point on the theoretical steady-state current-voltage relation. This can be plotted by repeating the calculations for other values of E taken at intervals over the desired range.

Since no explicit assumptions regarding the absolute magnitude of the resting potential (E_r) are necessary for the calculation of the theoretical steady state current-voltage relation, the values of n_o and h_o appropriate for equation (43) are not prespecified. However the steady state current (I_i) will be equal to zero at the resting potential which is therefore defined

by the intersection of the steady-state current-voltage relation on the voltage axis (i.e. $E = E_r$ when $I_i = 0$). Using this value of E, $\alpha_n, \beta_n, \alpha_h$ and β_h are calculated according to equations (35), (36), (39) and (40) and the appropriate values of n_o and h_o are found from equations (3) and (20) respectively.

Reconstruction of the 'early' current-voltage relation is achieved by entering the derived values of n_o and h_o as constants in equation (43) and substituting appropriate values for $\bar{g}_K$, $\bar{g}_{Na}$, g_l, E_K, E_{Na} and E_l as in the case of the steady-state current-voltage relation; m_∞ is the only remaining variable and is voltage dependent. For a particular value of E, α_m and β_m are calculated according to equations (37) and (38) and m_∞ is found from equation (15). Using this value, the solution of equation (43) is the value of I_i corresponding to the selected value of E. The theoretical early current-voltage relation is plotted by repeating the calculations for other values of E taken at intervals over the desired range.

2) Computer analysis;

Since the calculations involved in producing theoretical current-voltage relations are rather tedious, computer analysis was desirable. A suitable programme, written in Algol W, is given in Appendix 1 and was run on an IBM system/360 Model 44 computer.

The following data were entered on punched cards; EMIN, EMAX, EINC specifying the range of the calculation and the interval between successive values of E; EK, ENA, EL, G_K, G_NA and GL specifying appropriate parameter values.

The STEADY_STATE calculation was performed first. As

indicated above, resting potential is given by the intersection of the steady-state relation on the voltage axis. The computer selected the two values of E between which the steady-state current first became positive (i.e. outwardly directed) and the calculation was repeated with new values of EMIN and EMAX including these values in a reduced range. EINC was reduced to a tenth of its original value. The new value of E at which the steady-state current first becomes positive gives an estimate of resting potential which can be improved by successive repetitions of the calculation. The accuracy of the final estimate was controlled by a term EINCMIN. In this case the intercept was determined to within $\pm$ 0.01 mV.

The EARLY calculation was carried out with n and h constant throughout at the values (NREST, HREST) calculated for the estimated intercept. The early current-voltage relation typically crosses the voltage axis at three points (HODGKIN, HUXLEY & KATZ, 1952). Each of these intersections was also estimated by successive approximation.

Computer output was transferred to a line printer and consisted of the punched card data followed by the results of the steady-state calculations comprising values of E over the selected range with corresponding values of I_i, I_K, I_{Na} and I_l. In trial programmes the values of α_n, β_n, n, n^4, α_m, β_m, m, m^3, m^3h, α_h, β_h and h were also printed. The estimated (resting potential) intersection was indicated and in some cases corresponding values for the potassium conductance, sodium conductance and conductance ratio were calculated. In the case of the early calculations the output produced was similar except that in the trial programmes the n and h variables were omitted (since these are constant throughout)

and that three intersections were identified.

As a check on the accuracy of the approximations for the steady-state and early currents expressed in equations (42) and (43) the programme was run with parameter values corresponding to those typical for squid giant axons (HODGKIN & HUXLEY, 1952d). Figure 48 shows the resultant theoretical current-voltage relationships and Table 3 gives the parameter values used; these have been converted into absolute potential values where appropriate by assuming a resting potential of -60 mV. These results are comparable to the experimentally derived relationships given in Figure 44 except that the theoretical curves are referred to an absolute potential axis. It can be seen that reasonable agreement is obtained. The theoretical steady-state current closely approximates the experimental results. In the case of the early currents the theoretical values overestimate observed values as anticipated. Closer agreement could be obtained by calculating values for n, m and h at a fixed (short) time interval after the outset of the voltage step. However, since the theoretical treatment envisaged was essentially qualitative, it was decided to tolerate this discrepancy and the approximation of equation (43) was retained.

The calculated variations in α_n, β_n, n_∞ and n_∞^4 with absolute membrane potential are shown in Figure 49, (A) and (B). Figure 50 illustrates the comparable relationships for α_m, β_m, m_∞ and m_∞^3 and Figure 51 for α_h, β_h, h_∞ and $m_\infty^3 h_\infty$. These relationships are identical to those previously given in Figures 45 and 46 except that the various parameters are in this instance referred to an absolute potential axis.

Table 3.

Parameter values used in calculating theoretical current-voltage curves.

EMIN =	-100 mV	EK =	-72 mV	G_K =	36.0 m.mho/cm^2
EMAX =	80 mV	ENA =	+55 mV	G_{NA} =	120.0 m.mho/cm^2
EINC =	1 mV	EL =	-60 mV	GL =	0.3 m.mho/cm^2

After Hodgkin & Huxley (1952d).

Hodgkin-Huxley model;
Theoretical current-voltage relationships;

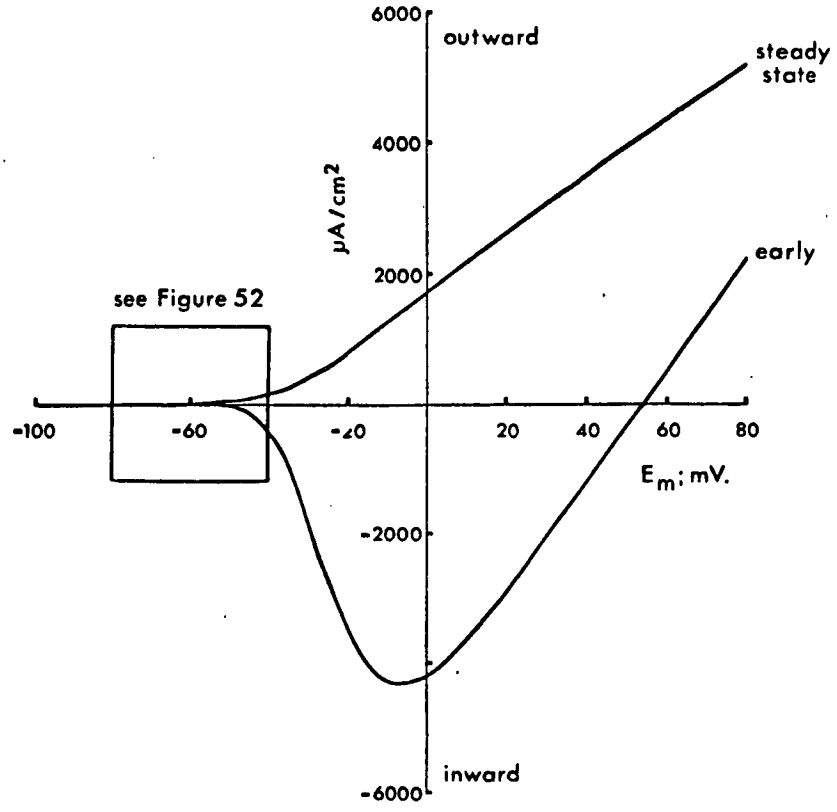

A;

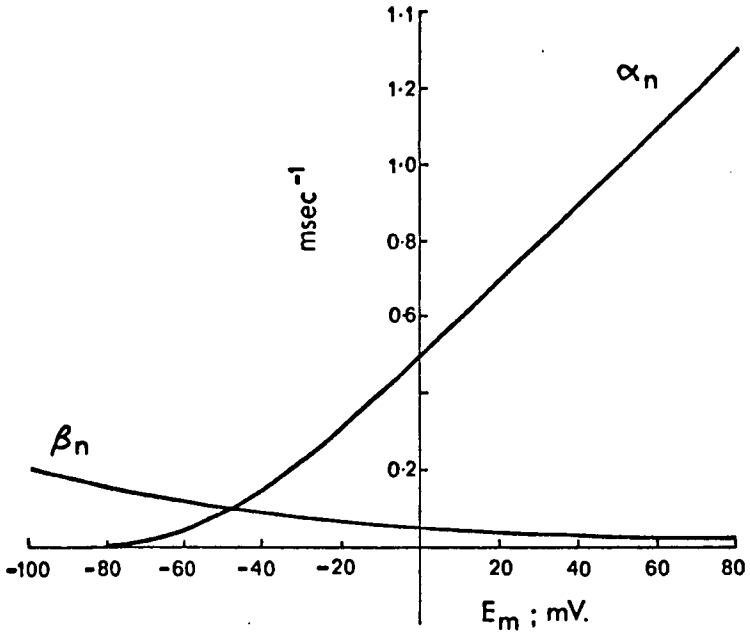
1·1
1·2
1·0
0·8
0·6
0·2
msec⁻¹
α_n
β_n
-100
-80
-60
-40
-20
20
40
60
80
E_m ; mV.

B;

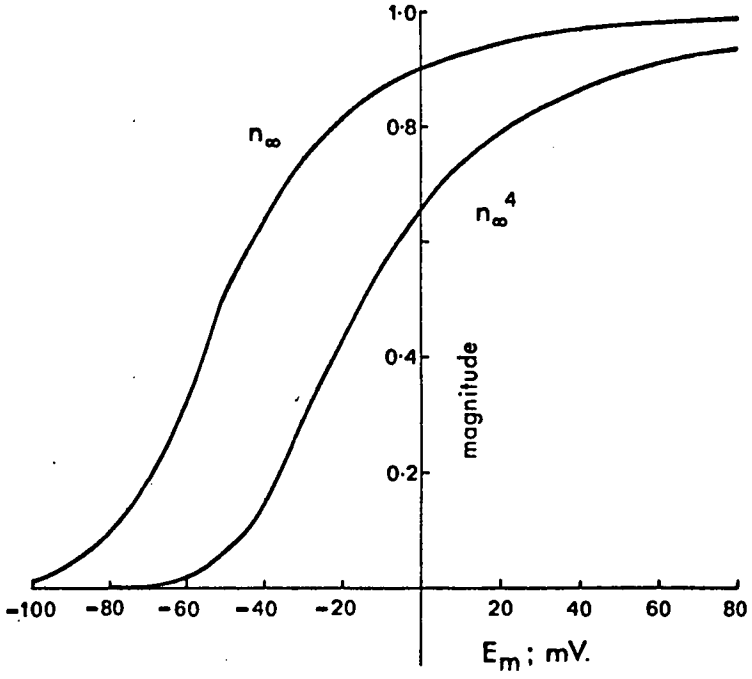
1·0
0·8
0·4
0·2
magnitude
n_∞
n_∞^4
-100
-80
-60
-40
-20
20
40
60
80
E_m ; mV.

A;

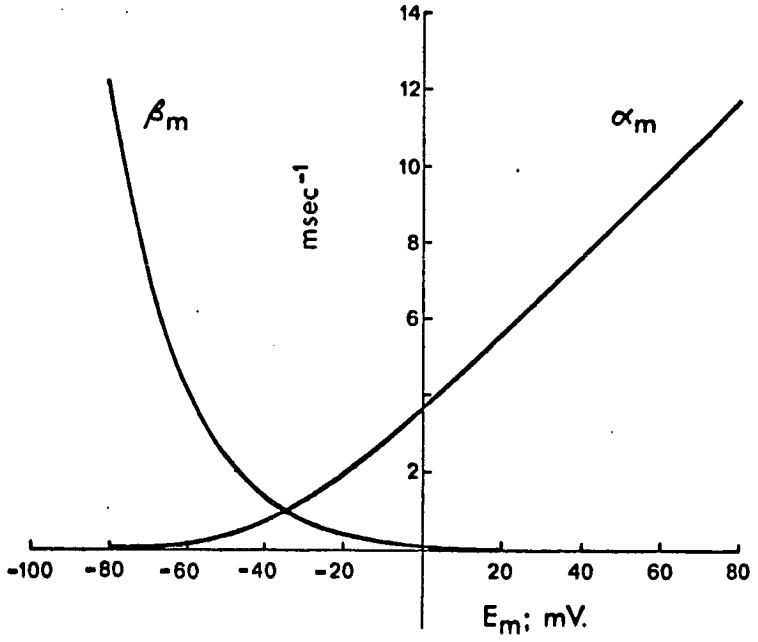
14
12
10
8
6
2
β_m
α_m
msec^{-1}
-100
-80
-60
-40
-20
20
40
60
80
E_m; mV.

B;

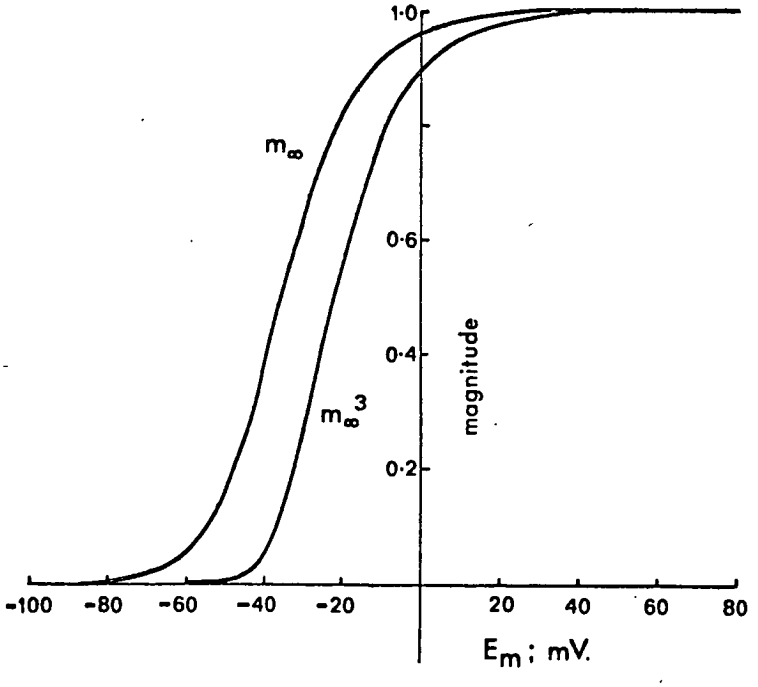
1·0
0·6
0·4
0·2
m_∞
m_∞^3
magnitude
-100
-80
-60
-40
-20
20
40
60
80
E_m; mV.

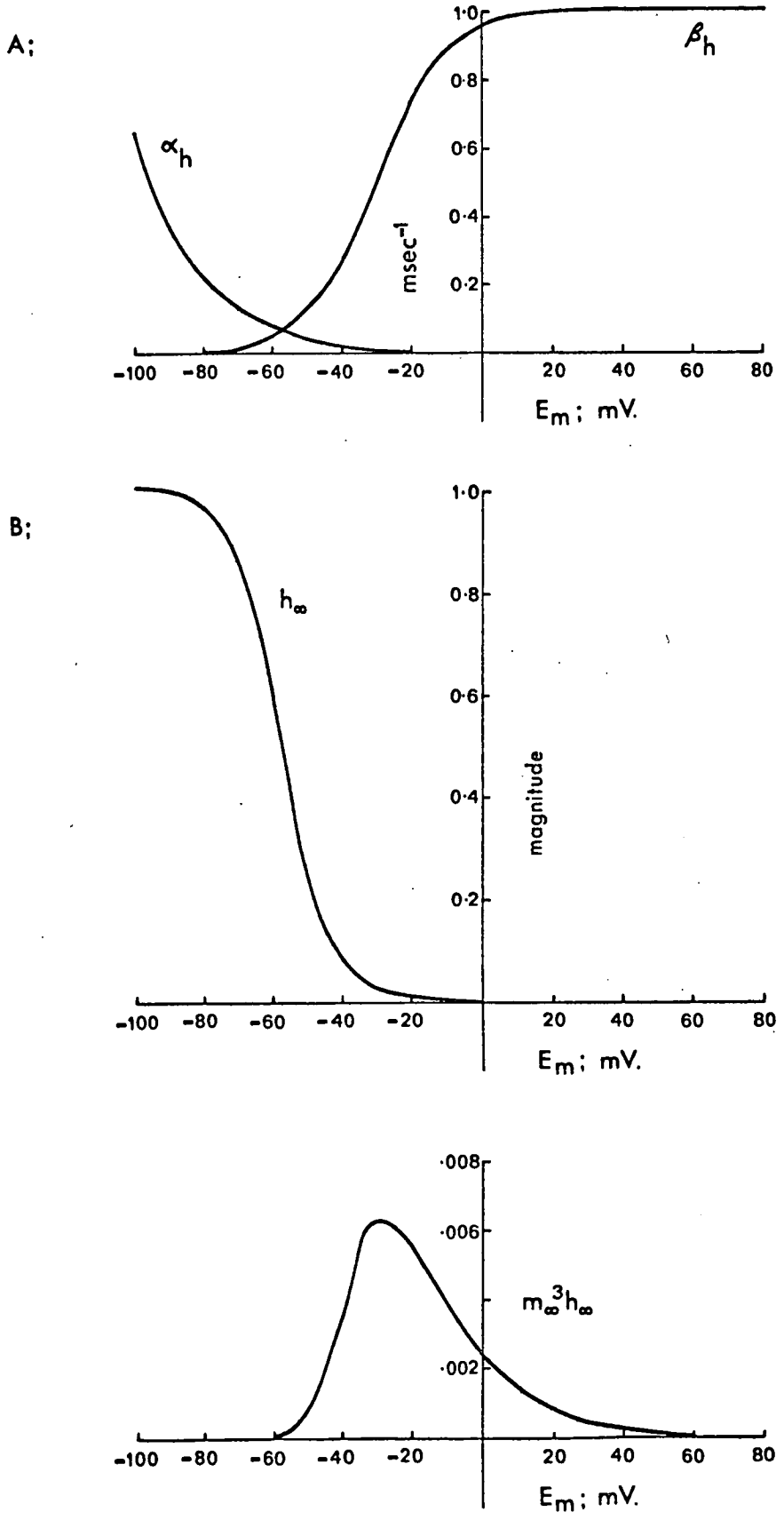
A;
α_h
β_h
msec^{-1}
1·0
0·8
0·6
0·4
0·2
-100 -80 -60 -40 -20
20 40 60 80
E_m; mV.
B;
h_∞
magnitude
1·0
0·8
0·6
0·4
0·2
-100 -80 -60 -40 -20
20 40 60 80
E_m; mV.
·008
·006
·002
$m_\infty^3 h_\infty$
-100 -80 -60 -40 -20
20 40 60 80
E_m; mV.

FIGURE 52; p 83

Hodgkin-Huxley model;
Theoretical early current intersections;

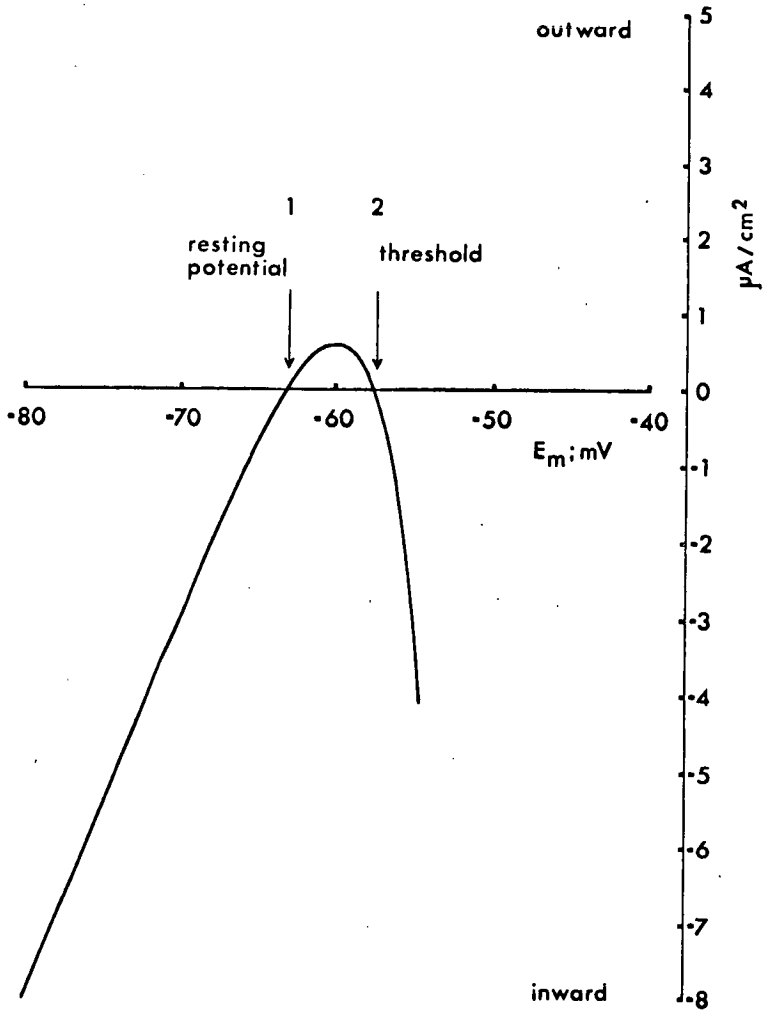

It is now necessary to consider the significance of the three intersections of the early current-voltage curve on the voltage axis. Figure 52 shows the theoretical early current plotted against an expanded axis to illustrate the first and second intersections more clearly. The first intersection coincides with the steady-state current intersection and defines the resting potential of the system. The second intersection corresponds to the voltage threshold for a uniformly stimulated membrane (i.e. the applied stimulation produces no lateral current flow). This is clear since the balance of early current flow is outward and therefore hyperpolarizing if E has a value between that at the first intersection and that at the second. Thus if stimulation is discontinued with E in this range the membrane will become repolarized. For values of E greater than that at the second intersection the balance of early current will be inward and therefore depolarizing. Thus, if stimulation is discontinued, depolarization will continue, become regenerative and an action potential will be produced. The third intersection provides an estimate of the maximum value of E which can be attained during an action potential. It is clear that the action potential peak cannot exceed E_{Na}, the equilibrium potential for sodium ions, and the intersection is close to but always somewhat less than E_{Na}. The discrepancy is accounted for by the leakage conductance and the potassium conductance both of which permit the flow of small outward currents.

Thus for given values of E_K, E_{Na}, E_l, $\bar{g}_K$, $\bar{g}_{Na}$ and g_l the solution of equations (42) and (43) in the manner described provides estimates of the resting potential, threshold and action

potential peak expected for the 'membrane' action potential of a system to which the same parameter values apply. Repeating the calculations with new parameter values makes it a simple matter for example to determine the theoretical variation in threshold accompanying variations in E_K or the variation in action potential peak or resting potential accompanying variations in E_{Na}. In addition, it should be possible to correlate changes in activity (e.g. in pacemaker cells) with predicted changes in membrane properties. For example if the theoretical threshold depolarization is increased by increasing E_K then reducing the external concentration of potassium ions would be expected to lead to a reduction in the firing rate of a pacemaker cell. Clearly, theoretical current-voltage curves based on an absolute potential system of equations can be produced to predict the changes in membrane properties to be expected for a wide variety of experimental situations.

D) Action potential simulation;

Although theoretical current-voltage curves are clearly useful in assessing the likely effect of experimental changes in ion concentrations the advantage of a full action potential simulation is that changes in activity can be predicted more directly. In addition, the significance of the interpretation placed on theoretical current-voltage curves is increased if the predictions produced are confirmed through simulation. Taken together these two theoretical techniques can provide a definite indication of exactly what type of changes in membrane properties, in response to alterations in experimental conditions, are predicted by the Hodgkin-Huxley equations.

While conceptually more complex than theoretical current-voltage curve production, action potential simulation involves essentially the same calculations except that these are solved for membrane potential with respect to time rather than for ionic current with respect to membrane potential.

At $t = 0$ membrane potential is taken as equal to resting potential (i.e. $E_o = E_r$) and the unitless variables are assumed to have their steady-state resting values (i.e. $n = n_o$, $m = m_o$, $h = h_o$). For these values the net transmembrane ionic current (I_i) will be equal to zero and therefore will not produce any alteration in the parameter values. If now a stimulus current (denoted by I_{stim}) is applied, a change in membrane potential will be produced. For the purpose of simulating a 'membrane' action potential the stimulus current is considered to be exclusively involved in altering the charge on the membrane capacitance. The potential (E) across a

capacitance (C) is related to its charge (Q) according to;

$$E = \frac{Q}{C} \tag{44}$$

Since charge has the dimensions of current (I) multiplied by time (t) this equation is equivalent to;

$$E = \frac{I \times t}{C} \tag{45}$$

In terms of this relationship it is clear that the initial change in membrane potential $\partial E_{m_1} = E_1 - E_o$ produced by the stimulus current after a short time interval (∂t) will be;

$$\partial E_{m_1} = \frac{I_{stim} \times \partial t}{C_m} \tag{46}$$

The membrane potential at the end of this interval (E_1) can be written as;

$$E_1 = E_o + \partial E_{m_1} \tag{47}$$

We now have a new value for membrane potential such that $E \neq E_r$ and it is no longer valid to assume that $I_i = 0$ as in the case of the timestep $t_o \rightarrow t_1$. The value of the ionic current (I_{i_1}) appropriate for the timestep $t_1 \rightarrow t_2$ can be found using suitable values for n, m and h such that $n = n_1$, $m = m_1$ and $h = h_1$ and entering these along with E_1 in the composite equation for transmembrane current when;

$$I_{i_1} = \bar{g}_K n_1^4 (E_1 - E_K) + \bar{g}_{Na} m_1^3 h_1 (E_1 - E_{Na}) + g_1 (E_1 - E_1) \tag{48}$$

Suitable values for the unitless variables are found by calculating the various rate constants for the new potential E_1 (equations (35) - (40)) and n_1, m_1 and h_1 are then given by the following relationships derived from equations (2), (14) and (19);

$$n_1 = n_o + \partial t(\alpha_{n_1}.(1-n_o) - \beta_{n_1}.n_o) \quad (49)$$

$$m_1 = m_o + \partial t(\alpha_{m_1}.(1-m_o) - \beta_{m_1}.m_o) \quad (50)$$

$$h_1 = h_o + \partial t(\alpha_{h_1}.(1-h_o) - \beta_{h_1}.h_o) \quad (51)$$

∂E_{m_2} the change in membrane potential during the timestep $t_1 \rightarrow t_2$ is given by;

$$\partial E_{m_2} = \frac{(I_{stim} - I_{i_1})\partial t}{C_m} \quad (52)$$

E_2 the membrane potential at the end of the second timestep ($t = t_2$) can be written;

$$E_2 = E_1 + \partial E_{m_2} \quad (53)$$

In general terms membrane potential at any point in time ($E_{(t)}$) can be determined according to;

$$E_{(t)} = E_{(t_o)} + \frac{(I_{stim} - I_{i_{(t_o)}}).\partial t}{C_m} \quad (54)$$

where t_o is any instant in time such that $t - t_o = \partial t$.

The accuracy of the integration procedure implicit in equation (54) is limited by the magnitude of ∂t, the interval between successive timesteps. If ∂t is too large the solution for $E_{(t)}$ may run off to infinity. In practice a value $\partial t = 0.01$ msec was found to provide satisfactory action potential simulations while $\partial t = 0.1$ msec was found to be too large.

With integration intervals as small as this, computer analysis is clearly essential if the simulation is to span any reasonable time interval. A suitable programme written in Algol W is given in Appendix 2. The computer output was in this case

Table 4.

Paramameter values used for action potential simulation

$I\_STIM = 40\ \mu A/cm^2$

T_STIM = 1 msec	EK = −72 mV	G_K = 36.0 m.mho/cm^2
T_MAX = 10 msec	ENA = +55 mV	G_NA = 120.0 m.mho/cm^2
DT = 0.01 msec	EL = −60 mV	GL = 0.3 m.mho/cm^2

After Hodgkin & Huxley (1952d).

Hodgkin-Huxley model; action potential simulation;

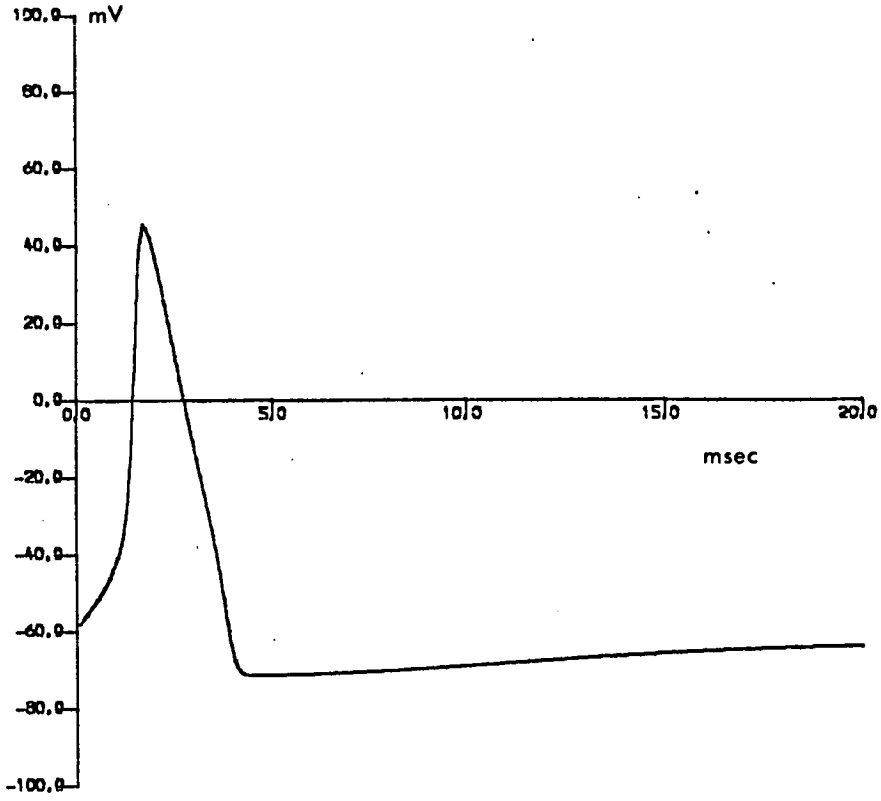

Hodgkin-Huxley model; simulated membrane responses;

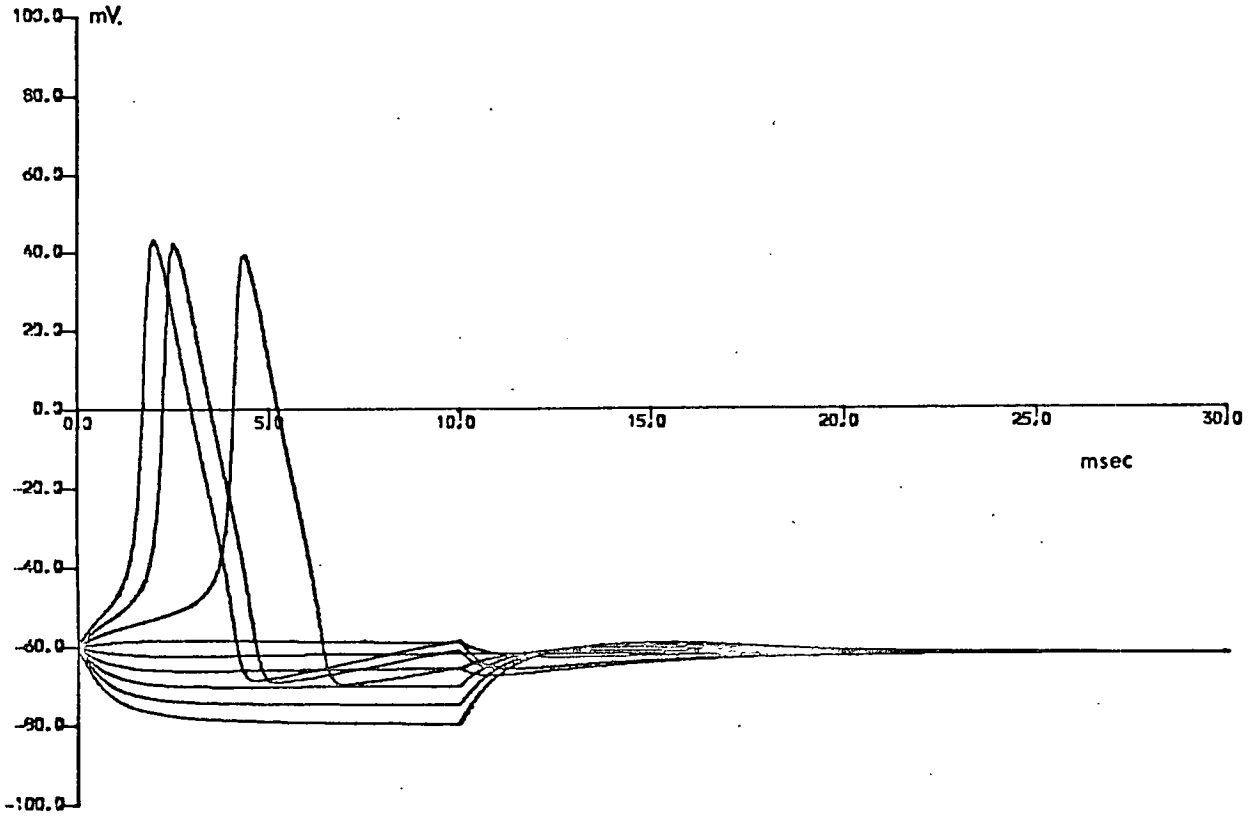

transferred to an XY plotter (CIL 6011) and simulation results were thus obtained directly.

The data required as input for the simulation were as follows; I_STIM, T_STIM, T_MAX, DT specifying the stimulus current, its duration, the total simulation interval and the integration interval; E_K, E_{Na}, E_l, $\bar{g}_K$, $\bar{g}_{Na}$, g_l specifying appropriate parameter values and EREST specifying the resting potential (E_r) such that $E_o = E_r$ at $t = 0$. The appropriate value for EREST was derived from the theoretical current-voltage curve programme (Appendix 1) run with the same parameter values. Figure 53 shows the results of a simulation using the parameter values given in Table 4. The value of EREST in this case was derived from the theoretical current-voltage curves given in Figure 48. Figure 54 shows a series of simulated membrane responses for a series of stimuli all of 10 msec duration but of an intensity varied between -20 and +20 $\mu A/cm^2$ in steps of 5 $\mu A/cm^2$. The membrane parameters correspond to those given in Table 4.

E) Transient outward currents;

While the Hodgkin-Huxley theory has proved adequate to describe very many of the properties of excitable membranes (NOBLE, 1966) more recent studies have revealed additional properties not included in the Hodgkin-Huxley formulation. In particular transient outward currents have been found which are dependent on conductance changes additional to those associated with the normal delayed outward current carried by potassium ions (NEHER & LUX, 1971; NEHER, 1971; CONNOR & STEVENS, 1971a; 1971b; 1971c).

In Helix pomatia neurons voltage clamp records can be obtained from a limited patch of the soma membrane by applying a conventional (two-microelectrode) clamp to the cell interior and additionally placing a two-chambered semi-micropipette on the exposed soma. The pipette interior is held close to ground potential by feedback control. When a voltage pulse is applied to the cell interior only those clamp currents which cross the patch of membrane covered by the pipette can be measured in the current chamber of the pipette (NEHER & LUX, 1969). Records obtained by this elegant technique are uncontaminated by currents flowing in unclamped areas of membrane distal to the clamping microelectrodes.

'Patch' clamp records obtained for a membrane held at resting potential and then stepped to a more depolarized holding potential (Figure 55(A)) are essentially similar to those obtained in the case of the squid giant axon (Figure 43). However, if the membrane is clamped at a hyperpolarized potential or if a hyperpolarizing prepulse is delivered prior to depolarization then there is an alteration in the time course and magnitude of the

Voltage clamp records from somatic membrane patches of Helix pomatia neurons;

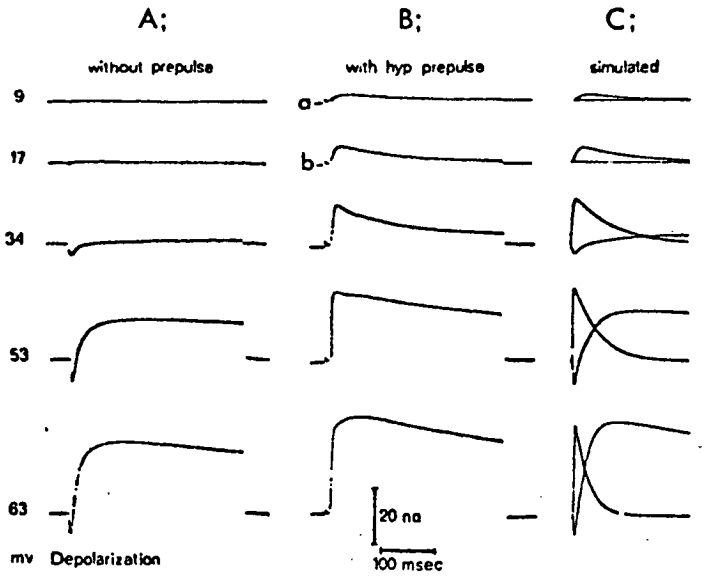

After Neher (1971); for explanation see text

recorded clamp current (Figure 55 (B)). During a hyperpolarizing prepulse there are only very small time-independent leakage currents. On the other hand, during a subsequent clamped test pulse there are transient outward currents of appreciable magnitude even for clearly subthreshold potentials (Figure 55(B) records a,b). The transient current inactivates completely within 300–400 msec and can always be represented as a mere additive superposition on the normal currents (NEHER, 1971). Figure 55(C) shows analogue computer simulations which effect a separation of the transient and delayed outward currents on this basis.

In Anisodoris and Archidoris a transient outward current can be demonstrated under identical experimental conditions (CONNOR & STEVENS, 1971b). The kinetics and magnitude of this transient current are closely similar to those determined in the case of Helix pomatia. The peak amplitude is dependent both upon the (hyperpolarized) holding potential and the test step potential while the time courses of development and decay of the current are relatively independent of these parameters. The developing and decaying phases are approximated by exponentials leading to a time constant for development of 10–25 msec and for decay of 220–600 msec.

In both cases if the external concentration of potassium ions is altered there is a corresponding alteration in the equilibrium potential for the transient outward current. In addition, the equilibrium potentials of the transient and the normal outward currents are very nearly equal and change by the same amount under altered ionic conditions. Neither value is influenced by substitution of acetate for external chloride ions. These observations strongly suggest that the transient outward current

is carried by potassium ions. However, both in Helix pomatia and in Archidoris addition of tetraethylammonium (TEA) to the bathing solution in concentrations which substantially alter the normal potassium current leave the transient current relatively little affected. It can be concluded that the transport mechanism for the transient current is at least operationally distinct from the mechanism underlying delayed (normal) outward current.

Both studies indicate that the properties and kinetics of the transient outward current can be described mathematically in a manner exactly analogous to that adopted for the other membrane currents under the Hodgkin-Huxley formulation (NEHER, 1971; CONNOR & STEVENS, 1971c).

Following the terminology of Connor & Stevens (1971c) the formal assumptions describing the transient outward current conductance (denoted by g_A) can be written;

$$g_A(V,t) = \bar{g}_A . A_A^4(V,t) B_A(V,t) \qquad (55)$$

where $\bar{g}_A$ is the peak conductance, A_A is a unitless 'activation' term taking values between 0 and 1 and B_A is a similar 'inactivation' term. These activation and inactivation terms are described by the first order differential equations;

$$\tau_{AA}(V) . \frac{dA_A(V,t)}{dt} + A_A(V,t) = A_A(V,\infty) \qquad (56)$$

$$\tau_{BA}(V) . \frac{dB_A(V,t)}{dt} + B_A(V,t) = B_A(V,\infty) \qquad (57)$$

where τ_{AA} is the time constant for activation and $A_A(V,\infty)$ is the steady-state value; similarly τ_{BA} is the time constant for inactivation and $B_A(V,\infty)$ the steady-state value.

Following the terminology of Hodgkin & Huxley (1952d) these relationships are exactly equivalent to;

$$g_A = \bar{g}_A \cdot a^4 b \tag{58}$$

$$\tau_a \cdot \frac{da}{dt} + a = a_\infty \tag{59}$$

$$\tau_b \cdot \frac{db}{dt} + b = b_\infty \tag{60}$$

The consistency of these formal assumptions with those describing the other membrane conductances can be easily demonstrated. Thus equation (59) can be written as;

$$\frac{da}{dt} = \frac{a_\infty - a}{\tau_a} \tag{61}$$

By analogy with equations (3), (15) and (20), a_∞ can be expressed in terms of rate constants such that;

$$a_\infty = \frac{\alpha_a}{(\alpha_a + \beta_a)} \tag{62}$$

Similarly, by analogy with equations (4), (16) and (21), τ_a can be written;

$$\tau_a = \frac{1}{(\alpha_a + \beta_a)} \tag{63}$$

Substitution in equation (61) leads to;

$$\frac{da}{dt} = \frac{\dfrac{\alpha_a}{(\alpha_a + \beta_a)}}{\dfrac{1}{(\alpha_a + \beta_a)}} - \frac{a}{\dfrac{1}{(\alpha_a + \beta_a)}} \tag{64}$$

whence

$$\frac{da}{dt} = \alpha_a - a(\alpha_a + \beta_a) \tag{65}$$

Rearrangement of the right-hand side of this expression provides;

$$\frac{da}{dt} = \alpha_a(1-a) - \beta_a a \qquad (66)$$

Similarly;

$$\frac{db}{dt} = \alpha_b(1-b) - \beta_b b \qquad (67)$$

These two relationships are exact mathematical analogies of equations (2), (14) and (19) the formal assumptions necessary for description of the other membrane conductances.

Clearly the assumptions implicit in the Connor & Stevens description of g_A, the transient outward current (equations (55), (56) and (57)), are equivalent to those implicit in its description after the method of Hodgkin & Huxley.

In Archidoris the normal transient inward current associated with intermediate depolarizations does not appear to be carried exclusively by sodium ions as in the case of Loligo (CONNOR & STEVENS, 1971a). Thus if the external sodium is replaced by choline or if tetrodotoxin (TTX) is added to the bathing medium, the form and time course of the action potential are little affected. On the other hand, action potentials are abolished and, under voltage clamp conditions, transient inward currents are completely suppressed if external sodium and calcium are both replaced. This suggests that both calcium and sodium ions may contribute to a composite inward current as, for example, in Helix aspersa neurons (CHAMBERLAIN & KERKUT, 1969) and Aplysia neurons (GEDULDIG & GRUENER, 1970).

Nevertheless, the transient inward current can be described mathematically in terms of its corresponding membrane conductance (denoted by g_I) such that;

$$g_I(V,t) = \bar{g}_I \cdot A_I^3(V,t) B_I(V,t) \tag{68}$$

$$\tau_{AI}(V) \cdot \frac{dA_I(V,t)}{dt} + A_I(V,t) = A_I(V,\infty) \tag{69}$$

$$\tau_{BI}(V) \cdot \frac{dB_I(V,t)}{dt} + B_I(V,t) = B_I(V,\infty) \tag{70}$$

As before the formal assumptions necessary in describing this conductance are equivalent to those necessary for the comparable Hodgkin-Huxley formulation. In addition equations (68), (69) and (70) describe a system which is clearly not only formally but also directly equivalent to that determining transient inward current (carried exclusively by sodium ions) in Loligo.

This is an important result since it suggests that the Hodgkin-Huxley equations for transient inward current can be applied with little modification whether or not inward current is carried exclusively by sodium or is of a composite nature.

The normal outward current in Anisodoris, as in Loligo, appears to be carried exclusively by potassium ions. However its corresponding conductance (denoted by g_K) was found to be more adequately described in terms of its dependence on two first order variables rather than on only one as in the Hodgkin-Huxley formulation. Thus;

$$g_K(V,t) = \bar{g}_K \cdot A_K^2(V,t) B_K(V,t) \tag{71}$$

$$\tau_{AK}(V) \cdot \frac{dA_K(V,t)}{dt} + A_K(V,t) = A_K(V,\infty) \tag{72}$$

$$\tau_{BK}(V) \cdot \frac{dB_K(V,t)}{dt} + B_K(V,t) = B_K(V,\infty) \tag{73}$$

In this case both A_K and B_K can be thought of as activation variables. The improvement achieved by a two parameter reconstruction of voltage clamp currents is marginal for the rise in potassium conductance associated with depolarizing commands but is more significant for the fall in conductance associated with hyperpolarizing commands (CONNOR & STEVENS, 1971c).

Clearly the Connor & Stevens analysis of the currents involved in action potential production for Archidoris is very similar to the Hodgkin-Huxley analysis for Loligo. In actual simulation terms however, there is a difference in method which prevents the direct expansion of the Hodgkin-Huxley equations to include the additional transient outward current channel. Essentially the Connor & Stevens simulation depends on the time constants of activation and inactivation of the various conductances; equations describing the rate constants of the determinant variables are not derived. On the other hand, rate constant equations are fundamental for the Hodgkin-Huxley simulation.

The significance of the transient outward current lies in its contribution to membrane currents during repetitive activity. Its conductance, g_A, becomes less inactivated on hyperpolarization relative to resting potential. In ordinary circumstances, activation will be appreciable only during the undershoot of the action potential. Since the decay time constant of the current is relatively large its effect will be to delay the recovery of membrane potential from the undershoot and the frequency of action potential production in response to an applied current will be substantially lower than that expected from the Hodgkin-Huxley equations. On the other hand, the Connor & Stevens simulation

predicts action potential frequencies which are in good agreement with experimental results. A more detailed discussion of repetitive activity will be given in a later section.

F) Additional rate constant equations;

In order to expand the Hodgkin-Huxley equations to include the additional potassium conductance, g_A, it is necessary to derive suitable rate constant equations. This can be done from results available for both Helix pomatia (NEHER, 1971) and Anisidoris (CONNOR & STEVENS, 1971c). Both studies provide experimentally derived estimates of the variations in the steady-state values of the activation variable (denoted by a) and the inactivation variable (denoted by b) associated with alterations in membrane potential. These relationships are reproduced in Figure 56(A) and (B).

Considering the inactivation variable (b) first, it can be supposed, by analogy with equations (3), (15) and (20), that the steady-state value (b_∞) can be expressed in terms of rate constants such that;

$$b_\infty = \frac{\alpha_b}{(\alpha_b+\beta_b)} \tag{74}$$

By analogy with equations (4), (16) and (21) the inactivation time constant τ_b can be written;

$$\tau_b = \frac{1}{(\alpha_b+\beta_b)} \tag{75}$$

It is clear from equation (74) that, for the membrane potential corresponding to a value of $b_\infty = 0.5$, the rate constants will be equal. From equation (75) the value of each at this potential can be determined according to;

$$\alpha_b = 0.5\frac{1}{\tau_b} \tag{76}$$

$$\beta_b = 0.5\frac{1}{\tau_b} \tag{77}$$

Experimentally derived relationships;

A;

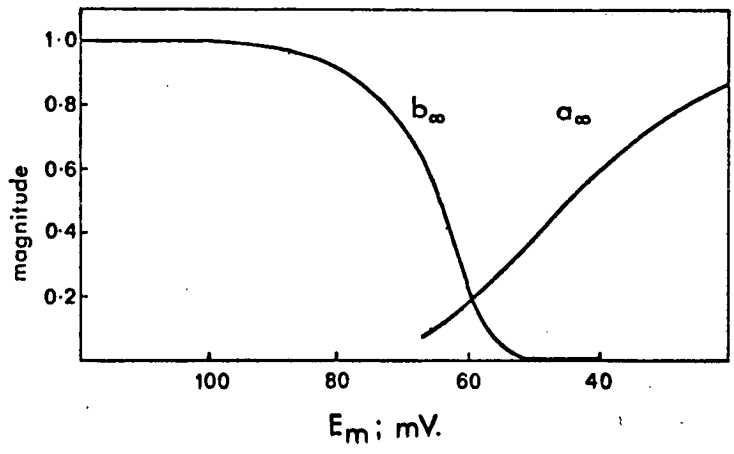

After Neher (1971)

B;

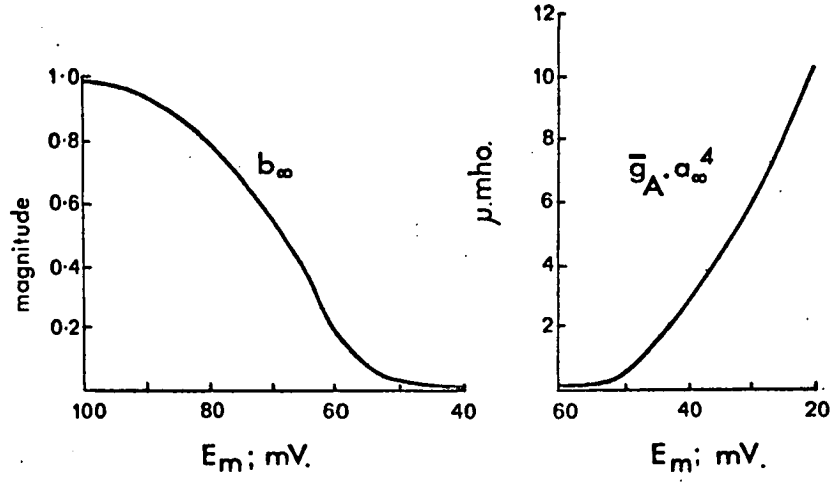

After Connor & Stevens (1971c); for explanation see text

From the relationships given in Figure 56 the membrane potential value $E = -70$ mV is a reasonable estimate for that corresponding to $b_\infty = 0.5$. Taking $\tau_b = 235$ msec (the value used for action potential simulation after the method of Connor & Stevens (1971c)) as a suitable approximation, the rate constants have the values $\alpha_b = 0.002128$, $\beta_b = 0.002128$.

By direct analogy with the Hodgkin-Huxley rate constant equations, (35) and (37), β_b can now be written as follows;

$$\beta_b = \frac{0.0002128(-(E+60) - 10)}{\exp\frac{-(E+60) - 10}{10} - 1} \tag{78}$$

(Note that equations (35) and (37) refer to α_n and α_m respectively while equation (78) refers to β_b. This is correct since n_∞ and m_∞ decrease with hyperpolarization while b_∞ increases.)

In an ideal first order reaction the rate constants would be symmetrical about their intersection (HODGKIN & HUXLEY, 1952d). Assuming that this applies in the present case α_b can be written;

$$\alpha_b = \frac{0.0002128(-(E+60) - 10)}{1 - \exp(-(\frac{-(E+60) - 10}{10}))} \tag{79}$$

A similar derivation for the action variable rate constants provides;

$$\alpha_a = \frac{0.004167(-(E+60) + 10)}{\exp\frac{-(E+60) + 10}{10} - 1} \tag{80}$$

$$\beta_a = \frac{0.004167(-(E+60) + 10)}{1 - \exp(-(\frac{-(E+60) + 10}{10}))} \tag{81}$$

These latter equations can be regarded only as approximate since, in the case of the Connor & Stevens analysis it was found difficult to obtain separate estimates for a_∞ and $\bar{g}_A$: the second

A;

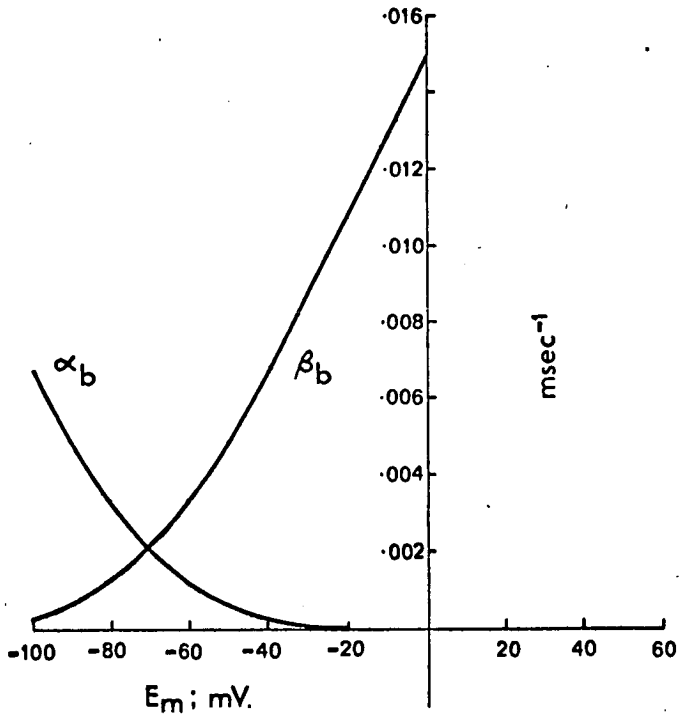
·016
·012
·010
·008
·006
·004
·002
msec⁻¹
α_b
β_b
-100
-80
-60
-40
-20
20
40
60
E_m; mV.

B;

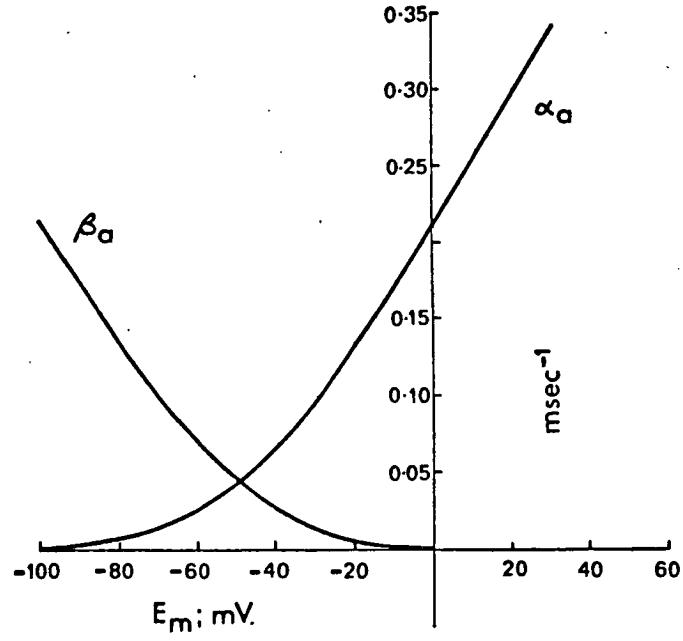
0·35
0·30
0·25
0·15
0·10
0·05
msec⁻¹
α_a
β_a
-100
-80
-60
-40
-20
20
40
60
E_m; mV.

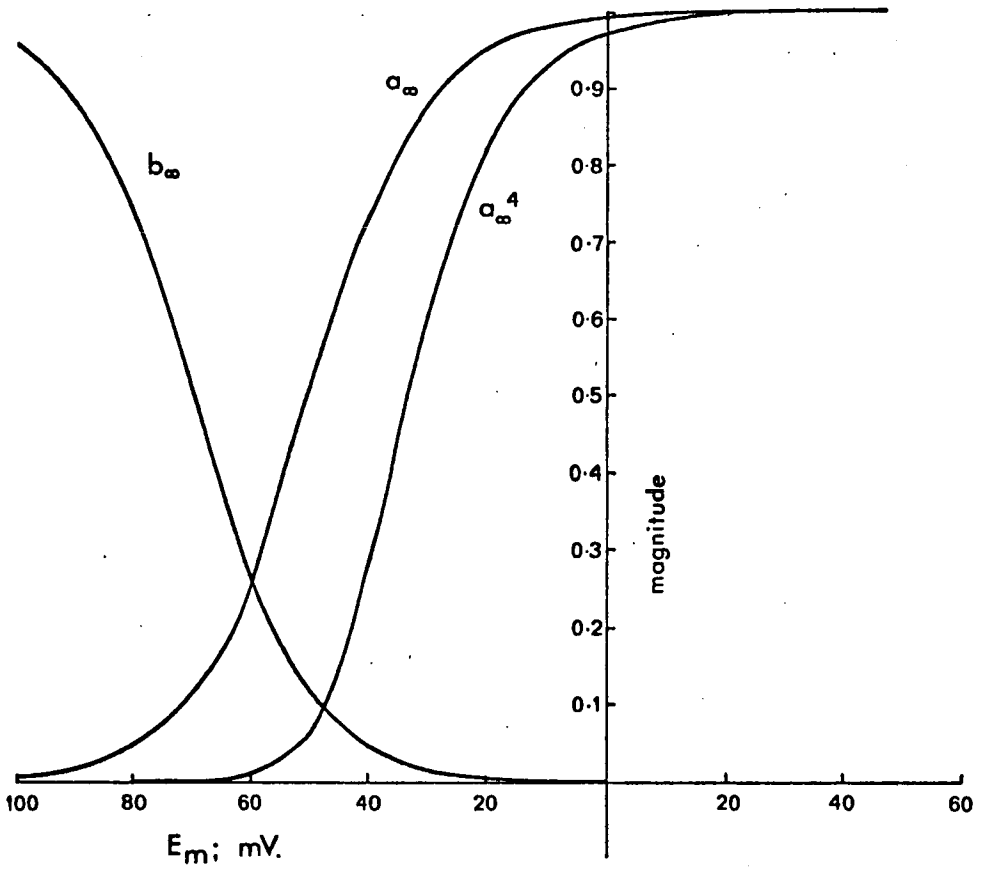
a_∞
b_∞
a_∞^4
0·9
0·8
0·7
0·6
0·5
0·4
0·3
0·2
0·1
magnitude
100
80
60
40
20
20
40
60
E_m; mV.

curve shown in Figure 56(B) gives $a_\infty^4 . \bar{g}_A$ as a function of membrane potential. Because of this there is some doubt as to the potential for which $a_\infty = 0.5$.

The relationships between membrane potential and α_b and β_b the rate constants calculated from equations (79) and (78) are given in Figure 57(A) and the derived values for b_∞ calculated according to equation (74) in Figure 58.

Figure 57(B) shows α_a and β_a calculated from equations (80) and (81) and the resultant values of a_∞ and a_∞^4 (calculated according equation (62)) are shown in Figure 58.

These curves of a_∞ and b_∞ as functions of membrane potential are in tolerable agreement with the experimentally derived curves of Figure 56 and would at any rate seem adequate for theoretical purposes. Accordingly the composite Hodgkin-Huxley equation for membrane current (equation (41)) can be expanded as follows;

$$I_m = C_m . \frac{dE}{dt} + \bar{g}_K n^4 (E-E_K) + \bar{g}_A a^4 b (E-E_A) + \bar{g}_{Na} m^3 h (E-E_{Na}) + g_l (E-E_l) \quad (82)$$

It was decided to retain the Hodgkin-Huxley description of g_K in this equation since its alteration to the form proposed by Connor & Stevens (equation (71)) would require the further derivation of rate constant equations. This procedure can at best be regarded as somewhat approximate when full numerical data for the variation in the steady-state values of the unitless variables with membrane potential are not available.

Equation (82) can be used as the basis for the production of theoretical current-voltage curves as in the case of equation (41). In this case, the early current is calculated by assuming

Table 5.

Parameter values used for calculation of theoretical current-voltage curves and action potential simulation with Hodgkin-Huxley equations expanded to include a transient outward current channel.

EMIN =	-100 mV	EK =	-72 mV	G_K =	36.0 m.mho/cm^2
EMAX =	80 mV	ENA =	+55 mV	G_NA =	120.0 m.mho/cm^2
EINC =	1 mV	EL =	-60 mV	GL =	0.3 m.mho/cm^2
		EA =	-72 mV	G_A =	40.0 m.mho/cm^2

I_STIM = 40 μA/cm^2

T_STIM = 1 msec T_MAX = 20 msec DT = 0.01 msec

See text for explanation.

Expanded model;
Theoretical current-voltage relationships;

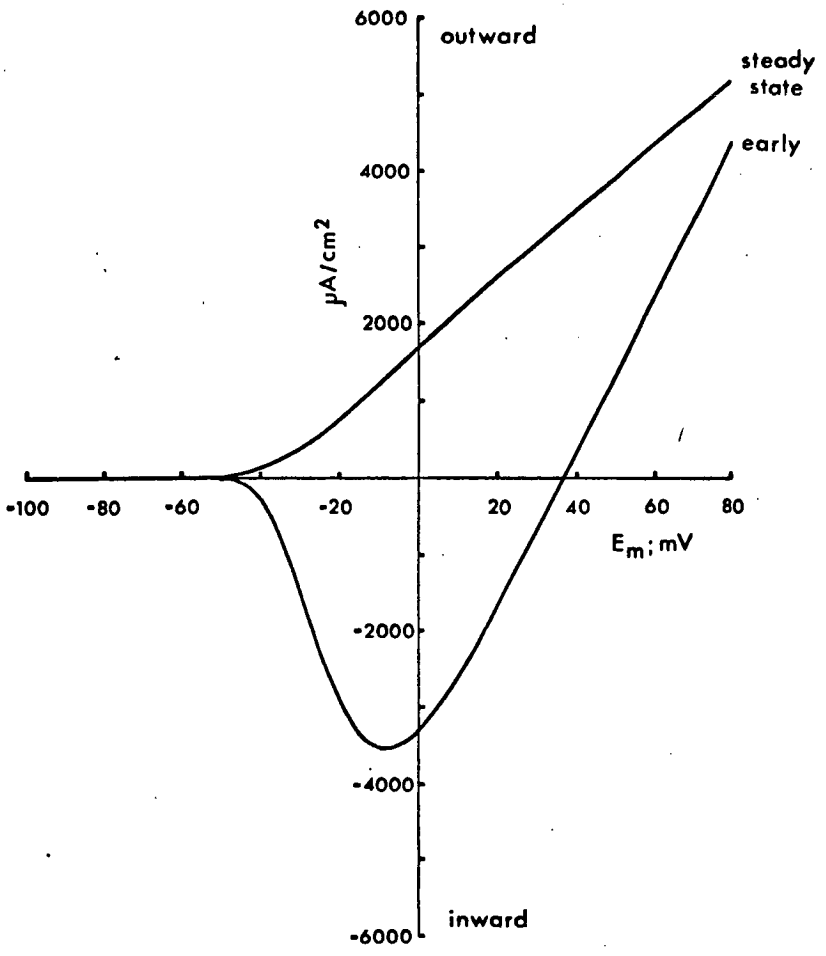

Expanded model; action potential simulation;

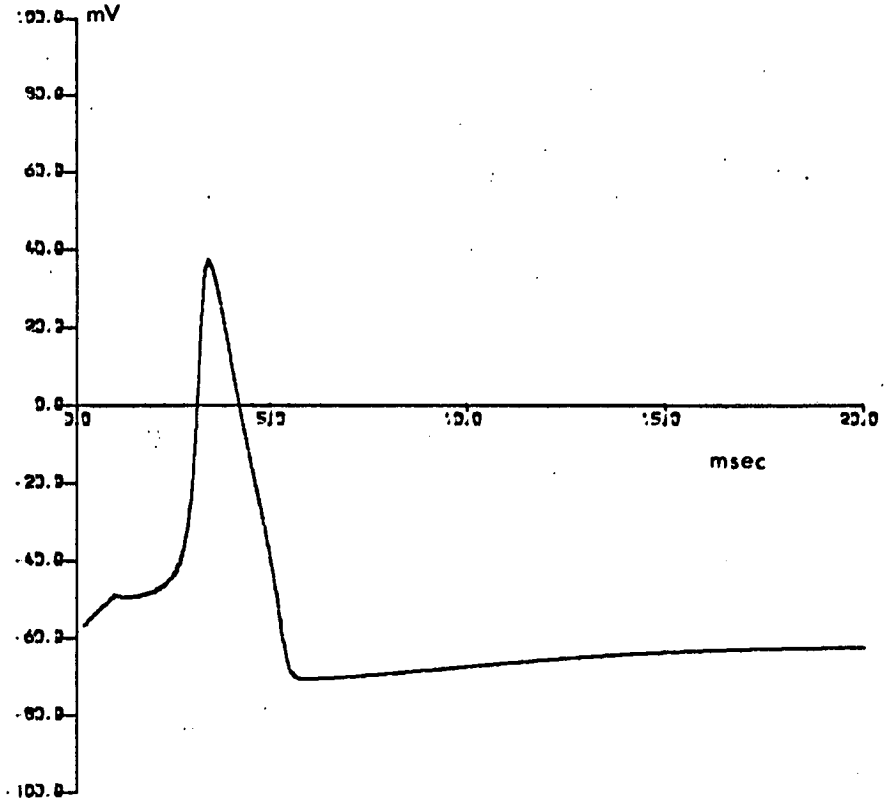

FIGURE 61; p100

Expanded model; simulated membrane responses;

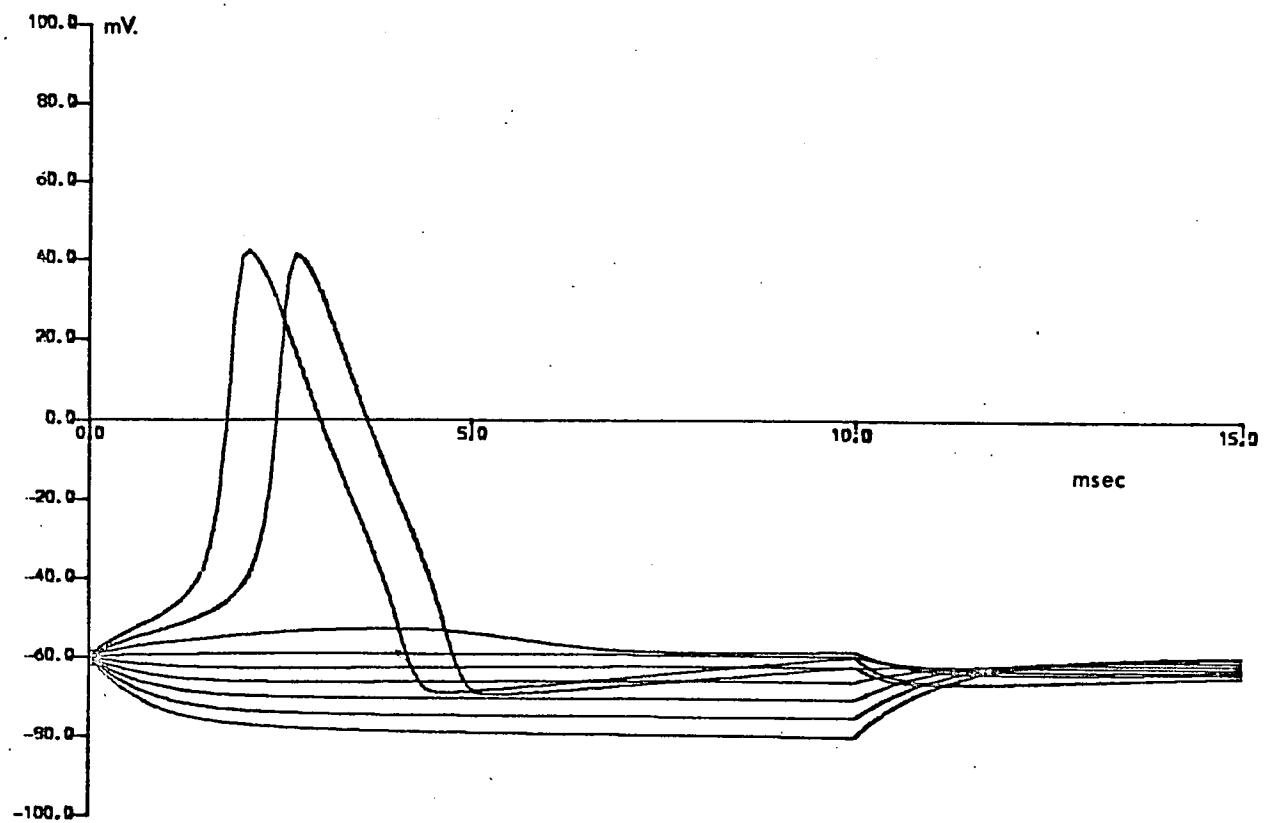

that the inactivation variable (b) for the transient outward current remains constant at its resting value ($b = b_o$) while the activation variable (a) reaches its steady-state value ($a = a_\infty$). A suitable computer programme, written in Algol W and incorporating these assumptions in addition to those described for theoretical current-voltage curve production using the Hodgkin-Huxley equations, is given in Appendix 3. Figure 59 shows the results obtained for the parameter values given in Table 5. The values used for $\bar{g}_K$, E_K, $\bar{g}_{Na}$, E_{Na}, g_l and E_l are the same as those used for calculation of the theoretical current-voltage curves of Figure 48. In line with the observation that the transient outward current is carried by potassium ions, E_A was given the same value as E_K. The value used for $\bar{g}_A$ was chosen so that the ratio $\bar{g}_A : \bar{g}_{Na}$ had the value implicit in the Connor & Stevens analysis.

Action potential simulation with the expanded equation is also possible and a suitable programme is given in Appendix 4. Figure 60 shows the results obtained for the parameter values already given (Table 5). Figure 61 shows a series of membrane responses also simulated with the parameter values given in Table 5 but with a stimulus duration of 10 msec and a stimulus intensity varied between -20 and +20 $\mu A/cm^2$ in steps of 5 $\mu A/cm^2$.

The four programmes now available (Appendices 1-4) provide the means for fairly comprehensive predictions of alterations in membrane properties expected in response to altered ionic environments and for comparison between the alterations expected on the basis of the Hodgkin-Huxley equations and the Hodgkin-Huxley equations expanded to include the transient outward current channel.

Chapter 5

THEORETICAL EVALUATION

A) Introduction;

Although the absolute potential conversion of the Hodgkin-Huxley equations is a fairly obvious possibility, its consequences do not appear to have been studied in any depth and predictions of alteration in membrane properties based on the equations expressed in absolute potential terms are largely lacking in the literature. In view of this it is essential to evaluate the predictions of the theoretical approach developed above with reference to already available experimental results before the theory can be applied with confidence to less well documented situations. This evaluation and the generation of suitable predictions for subsequent experimental test are the main aims of this section.

B) Resting potential and extracellular potassium concentrations;

1) The constant-field equation;

The description of alterations in the resting membrane potential in response to changes in external potassium concentration by means of the constant-field equation has become a standard experimental technique (MARMOR & GORMAN, 1970; MORETON, 1968; 1969; 1972). The equation was derived by Hodgkin & Katz (1949) and has the form;

$$E = \frac{RT}{F} \ln \frac{P_K \cdot K_o^+ + P_{Na} \cdot Na_o^+ + P_{Cl} \cdot Cl_i^-}{P_K \cdot K_i^+ + P_{Na} \cdot Na_i^+ + P_{Cl} \cdot Cl_o^-} \qquad (83)$$

where E is the resting potential; P_K, P_{Na}, P_{Cl} refer to the membrane permeabilities for the various ions; K_o^+, Na_o^+, Cl_o^- are the extracellular ion concentrations and K_i^+, Na_i^+, Cl_i^- are the intracellular concentrations; R, T and F have their normal significance.

It is often assumed that chloride ions are in equilibrium across the membrane and can therefore be omitted from the equation (HODGKIN, 1958) which can then be written;

$$E = \frac{RT}{F} \ln \frac{K_o^+ + b \cdot Na_o^+}{K_i^+ + b \cdot Na_i^+} \qquad (84)$$

where b is the permeability ratio P_{Na}: P_K. When a value for b is obtained from tracer-flux measurements the calculated resting potential is in good agreement with observed values (KATZ, 1966).

In applying the equation to the changes in membrane potential produced by alterations in the external potassium concentration, this permeability ratio is assumed to remain constant

at its resting value.

When neither the membrane permeabilities nor the intracellular ion concentrations are known the equation can be applied in a modified form (MORETON, 1968). Equation (83) is exponential in form but a linear expression can be derived;

$$\exp\left(\frac{EF}{RT}\right) = \frac{P_K \cdot K_o^+ + P_{Na} \cdot Na_o^+ + P_{Cl} \cdot Cl_i^-}{P_K \cdot K_i^+ + P_{Na} \cdot Na_i^+ + P_{Cl} \cdot Cl_o^-} \qquad (85)$$

This can be simplified by omission of the chloride terms as before. It can also be assumed that the resting potassium conductance of the cell membrane is much greater than that to sodium and that the intracellular sodium concentration is small. The term $P_{Na} \cdot Na_i^+$ is then negligible compared to $P_K \cdot K_i^+$ and can be omitted. Thus;

$$\exp\left(\frac{EF}{RT}\right) = \frac{K_o^+}{K_i^+} + \frac{P_{Na} \cdot Na_o^+}{P_K \cdot K_i^+} \qquad (86)$$

This expression implies that the relationship between $\exp\left(\frac{EF}{RT}\right)$ and extracellular potassium concentration plotted using experimental values for E can be estimated by linear regression. The slope of the line of best fit obtained in this way provides an estimate of K_i^+ and the ratio P_{Na}: P_K can be found from its intercept when Na_o^+ is known. These values can be substituted in equation (86) in its equivalent exponential form;

$$E = \frac{RT}{F} \ln \frac{K_o^+ + \frac{P_{Na}}{P_K} \cdot Na_o^+}{K_i^+} \qquad (87)$$

This description of the relationship between resting

membrane potential and extracellular potassium concentration is in reasonable agreement with experimental results in Helix aspersa (MORETON, 1968) and in Anisodoris (MARMOR & GORMAN, 1970).

2) Absolute potential predictions;

As already mentioned, the Hodgkin-Huxley equations expressed in absolute potential terms require no explicit assumptions regarding the absolute magnitude of the resting potential for the calculation of theoretical steady-state current-voltage curves. On the contrary, the theoretical resting potential is defined by the intersection of the steady-state curve on the voltage axis. This means that the relationship between resting potential and extracellular potassium concentration can be predicted by calculating steady-state current-voltage curves for a range of values of the potassium equilibrium potential, E_K, finding their resting potential intersections and plotting these values against extracellular potassium concentration. Since the potassium equilibrium potential rather than the extracellular potassium concentration is used in this calculation it is necessary to assume a suitable value for the intracellular concentration and find the extracellular concentration corresponding to each value of the equilibrium potential from the Nernst equation before the relationship can be plotted. In effect, each resting potential value obtained is the solution for E of equation (42), such that $I_i = 0$, for a particular value of E_K when E_{Na}, E_l, $\bar{g}_K$, $\bar{g}_{Na}$ and g_l are kept constant.

The constant-field equation describes the actual relationship between extracellular potassium concentration and membrane potential with some accuracy. It is therefore a crucial

test of the absolute potential equations that the relationship predicted should resemble that predicted by the constant-field equation.

Table 6 gives the resting potential values computed from the Hodgkin-Huxley theoretical current-voltage curve programme (Appendix 1) for a range of values of the potassium equilibrium potential with the other parameters kept constant at the values previoulsy given in Table 3. Corresponding values for the extracellular potassium concentration (K_o^+) were calculated from the Nernst equation on the assumption that the intracellular potassium concentration (K_i^+) was constant at 100 m$\bar{M}$. (This value was chosen partly for convenience but is close to that estimated for Helix aspersa neurons, (MORETON, 1968).) Figure 62 shows the derived relationship between resting potential and extracellular potassium concentration. The corresponding variation in the potassium equilibrium potential (E_K) is indicated for comparison.

The 'constant-field' approximation to these results was obtained by treating the Hodgkin-Huxley derived values as experimental points, substituting in $\exp(\frac{EF}{RT})$ and plotting the resultant values against a linear scale of extracellular potassium concentration as in Figure 63. A linear regression analysis was carried out to determine a line of best fit. (Two regression lines can be obtained from such an analysis; one in which the magnitudes of the dependent variable (y-axis) are predicted from those of the independent variable (x-axis) and one in which the reverse is true. The term 'line of best fit' is used here to denote the average of these two regression lines.) The equation for the line of best fit corresponds to the best fit constant-field equation for the Hodgkin-

Table 6.

Hodgkin-Huxley model; theoretical relationship between resting potential and extracellular potassium concentration.

E_K (mV)	(K_o^+) (mM)	H-H resting potential (mV)	Constant-field approximation (mV)
90	2.81	66.50	69.14
80	4.18	65.20	64.29
70	6.21	62.95	58.47
67	7.00	61.90	56.53
65	7.57	60.95	55.20
63	8.20	59.75	53.83
60	9.23	57.10	51.72
57	10.40	52.95	49.53
55	11.26	49.70	48.04
53	12.20	46.60	46.51
50	13.74	42.75	44.17
47	15.48	39.55	41.77
43	18.14	35.90	38.48
40	20.43	33.45	35.97
37	23.01	31.15	33.40
33	26.98	28.10	29.90
30	30.39	25.80	27.24
20	45.20	17.95	18.15
10	67.23	9.33	8.77

For explanation see text.

Theoretical relationships between resting membrane potential and extracellular potassium concentration;

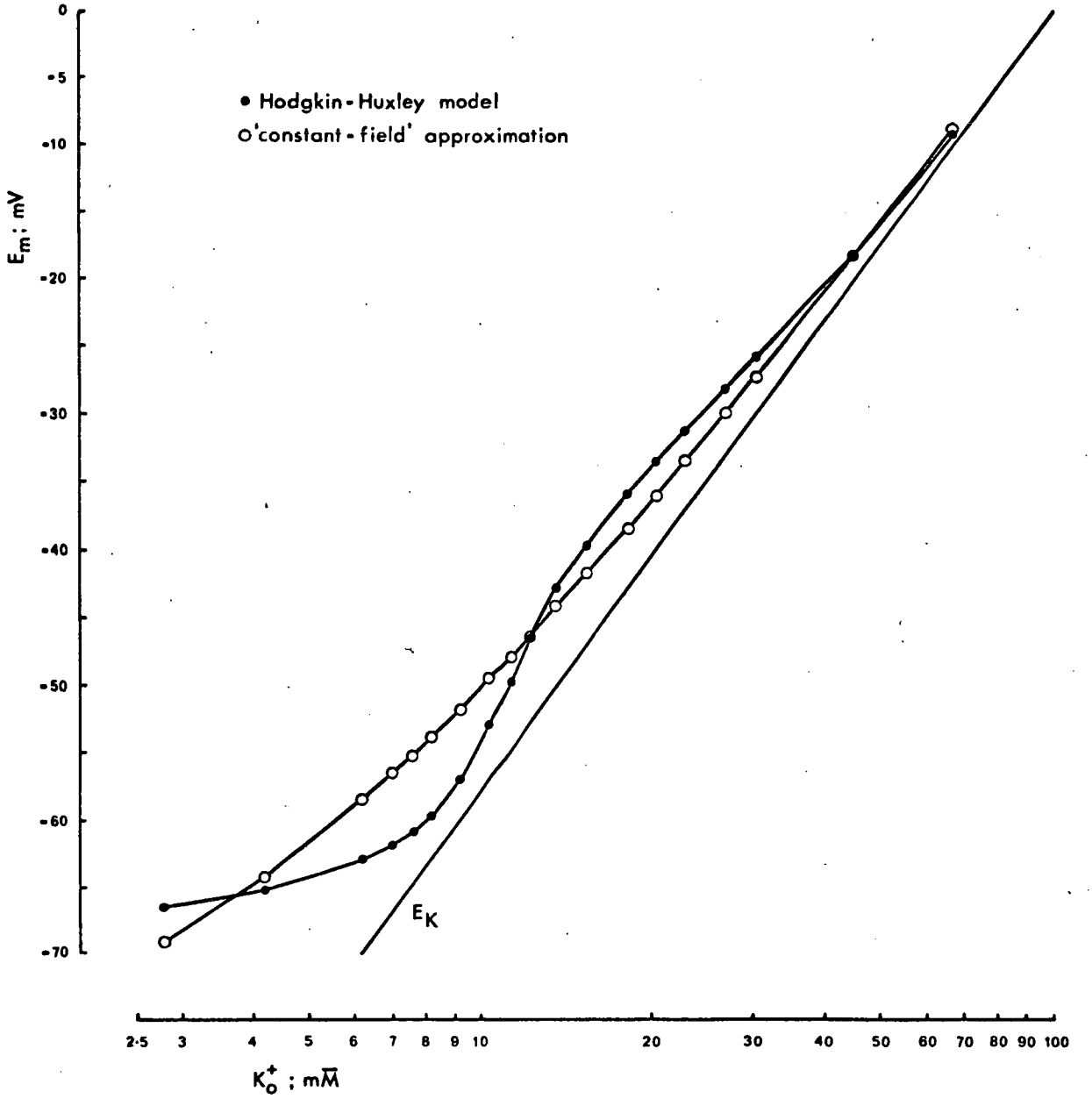

for explanation see text

Hodgkin-Huxley model; 'constant-field' linear regression

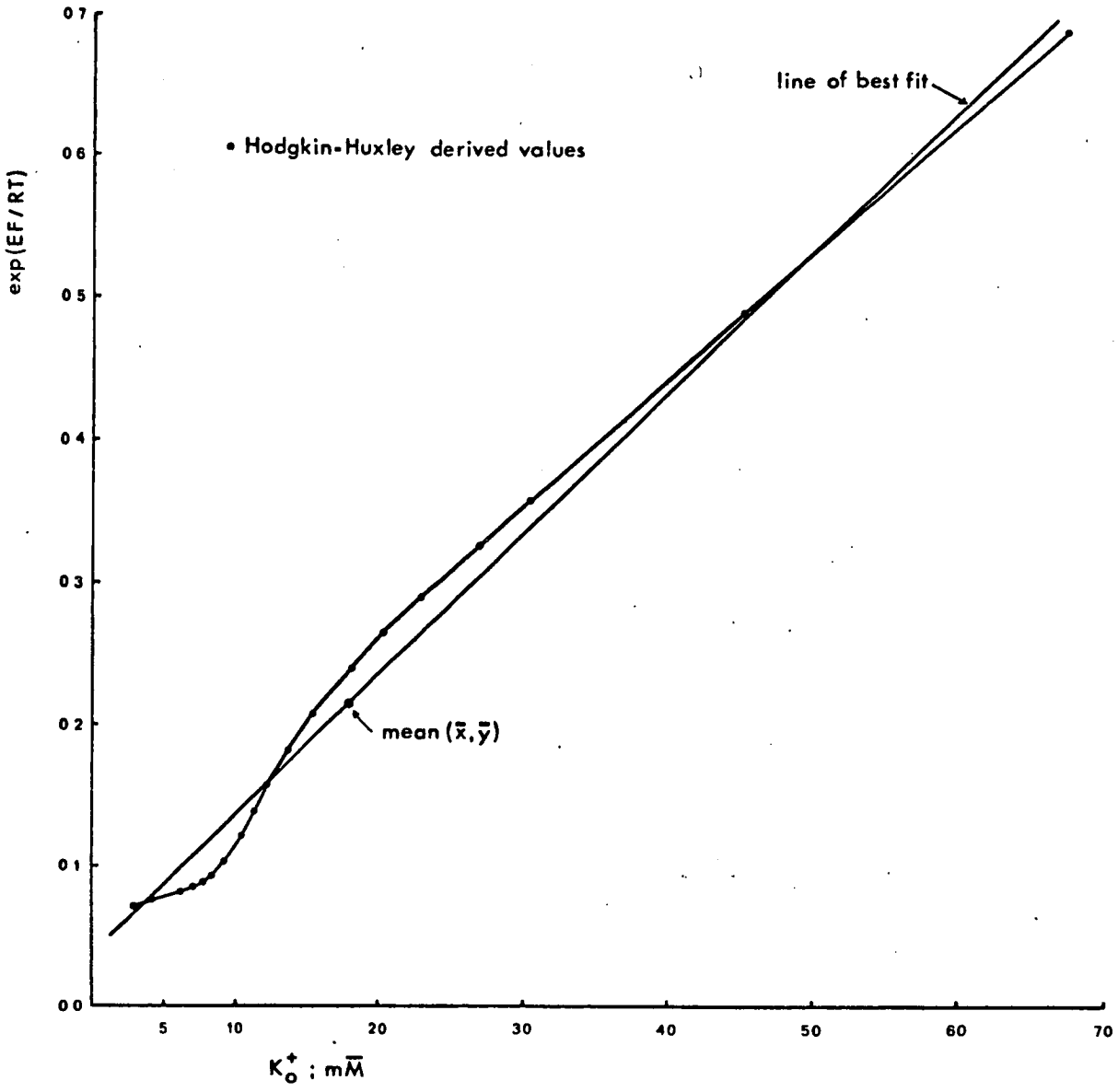

Huxley derived values . If the value $x = \exp(\frac{EF}{RT})$, corresponding to a particular value of K_o^+ is found from the line of best fit, then $E = \frac{RT}{F} \ln(x)$ gives the appropriate resting potential value for the constant-field approximation plotted in Figure 62.

The expanded model predictions were derived from the programme of Appendix 3 in an exactly similar way and are given in Table 7 and illustrated in Figures 64 and 65.

3) Discussion;

It is clear from both sets of results that the form of the relationship predicted by the absolute potential equations is in reasonable, but not excellent, agreement with the form of the relationship predicted by the constant-field equation, over the range of values chosen. The mean difference between the absolute potential equation derived values and the corresponding constant-field approximation values was found to be 2.67 mV in the case of the Hodgkin-Huxley model and 2.42 mV in the case of the expanded model. Deviation of the absolute potential predictions from the constant-field approximations is most pronounced at lower extracellular potassium concentrations (2-10 m$\bar{M}$, Figures 62 and 64). However, if the analysis were restricted to values within this range, or if fewer values at higher concentrations were used, as would normally be the case in an experimental study (e.g. MORETON, 1968; GORMAN & MARMOR, 1970a; 1970b) then agreement between the two curves in this region would be substantially improved. Thus, the form of the relationship predicted from the absolute potential equations cannot be regarded as inconsistent with that predicted from the constant-field equation.

Table 7.

Expanded model; theoretical relationship between resting potential and extracellular potassium concentration.

E_K (mV)	(K_o^+) (mM)	Expanded resting potential (mV)	Constant-field approximation (mV)
90	2.81	66.9	71.8
80	4.17	65.5	66.3
70	6.21	63.2	59.9
65	7.57	61.2	56.4
63	8.20	60.0	54.9
60	9.24	57.5	52.6
57	10.40	53.9	50.3
55	11.26	50.8	48.7
53	12.20	47.7	47.1
50	13.74	43.7	44.7
47	15.48	40.5	42.2
45	16.75	38.5	40.5
43	18,13	36.7	38.8
40	20.43	33.7	36.1
35	24.92	29.8	31.7
30	30.39	25.9	27.2
20	45.20	18.0	17.9
10	67.23	9.3	8.4

For explanation see text.

Theoretical relationships between resting membrane potential and extracellular potassium concentration;

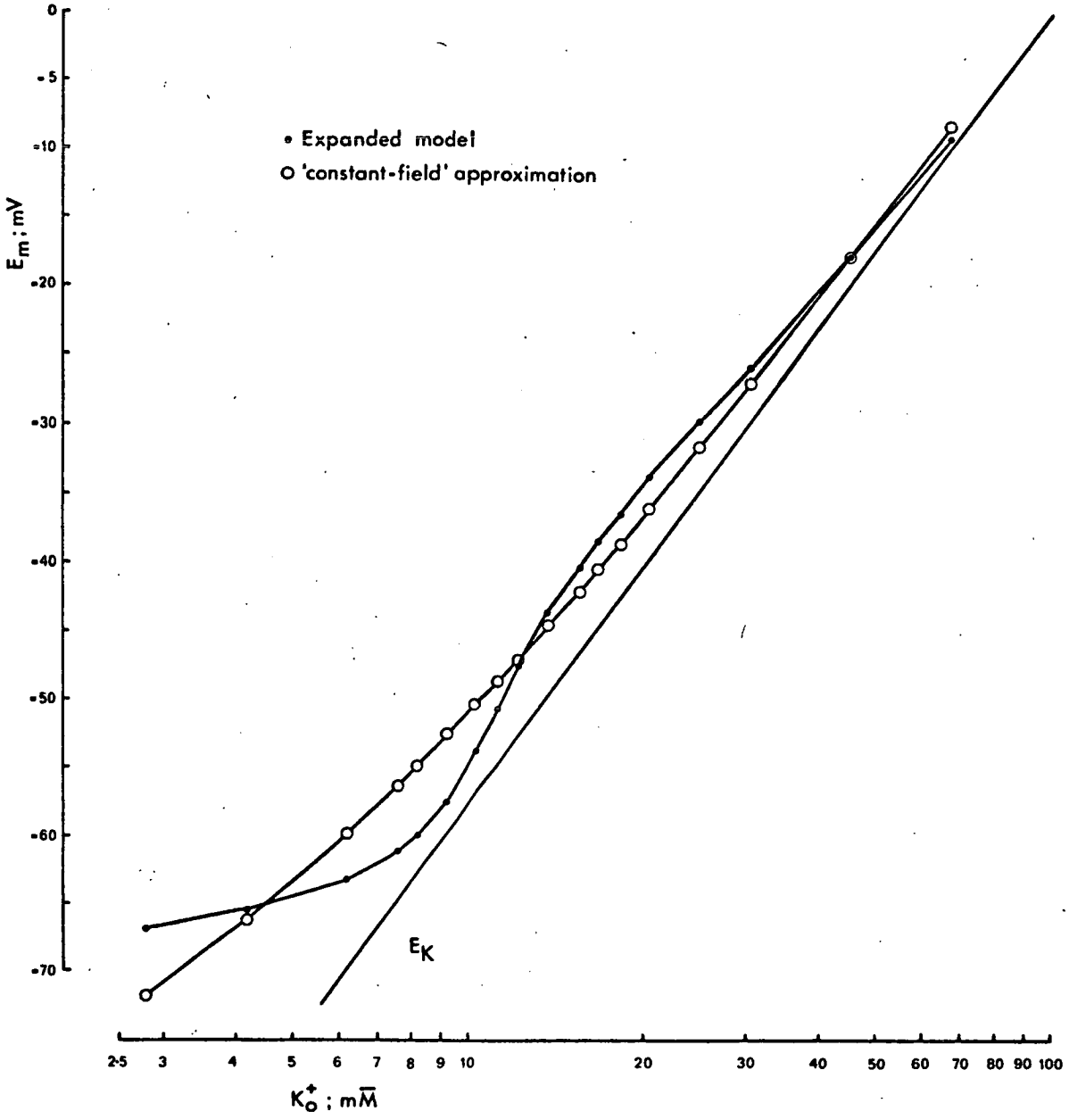

for explanation see text

Expanded model; 'constant-field' linear regression

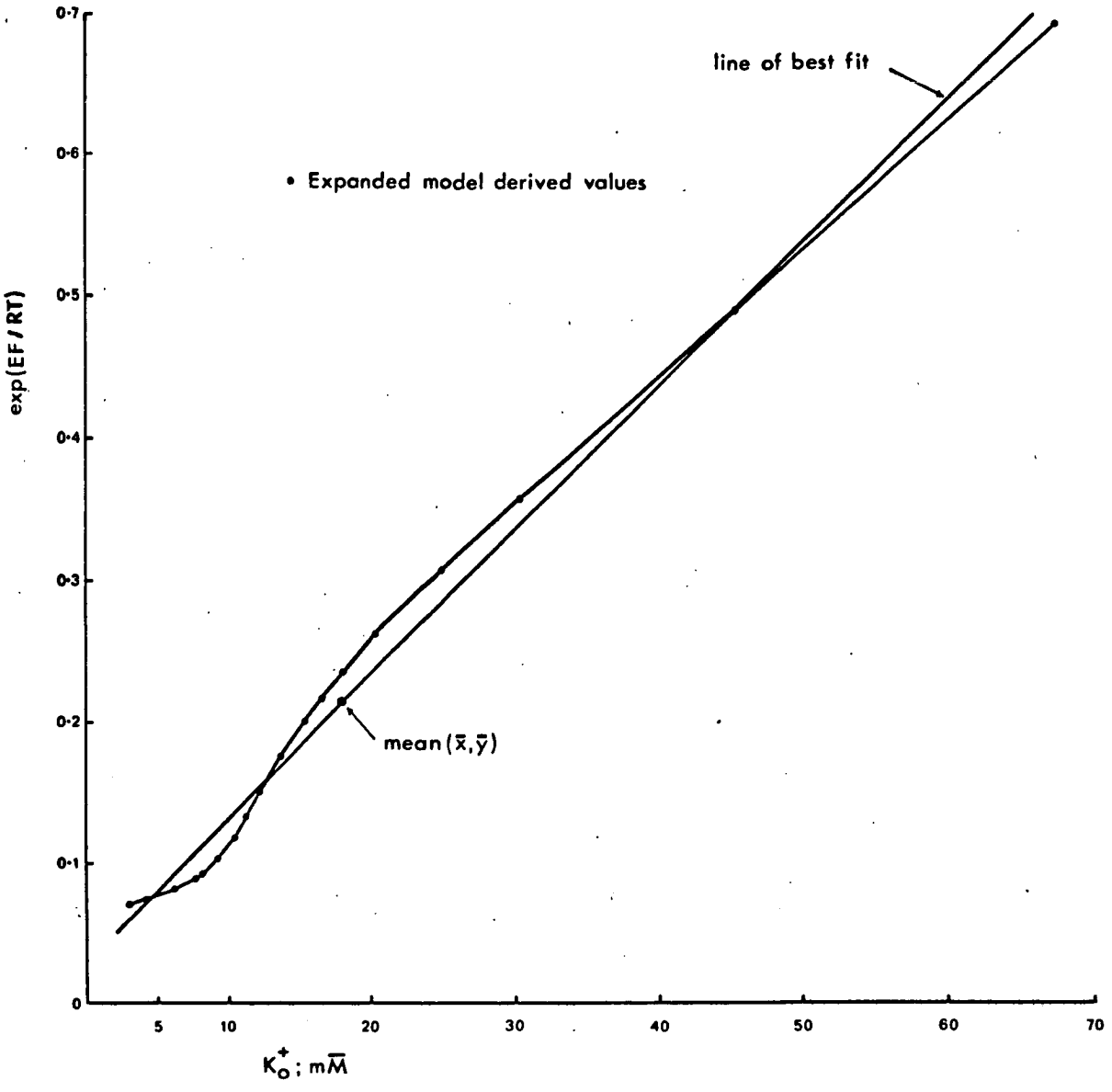

A;

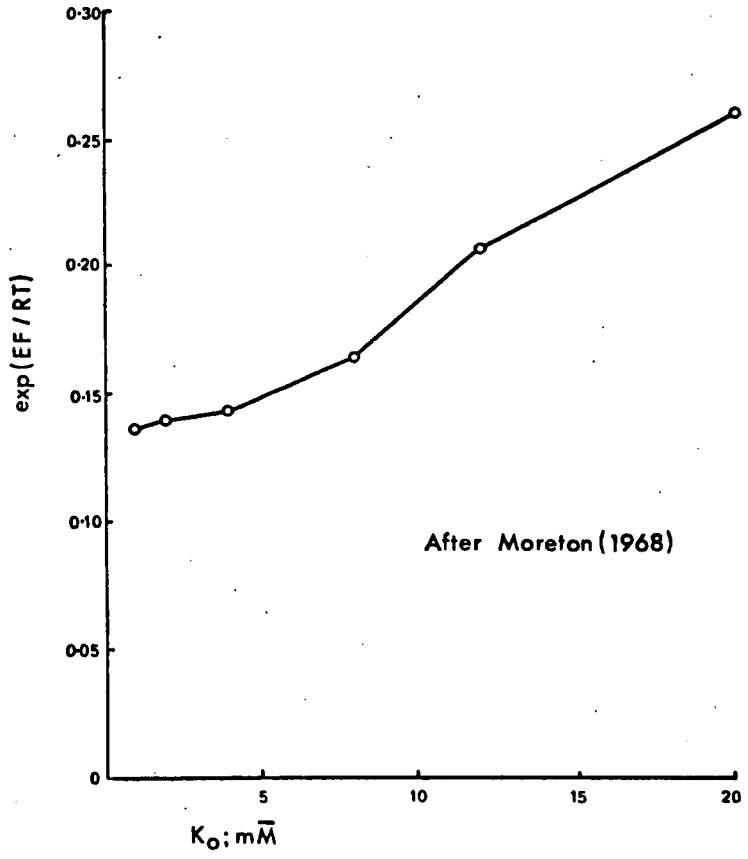
0·30
0·25
0·20
0·15
0·10
0·05
0
exp(EF/RT)
5
10
15
20
K_o; mM
After Moreton (1968)

B;

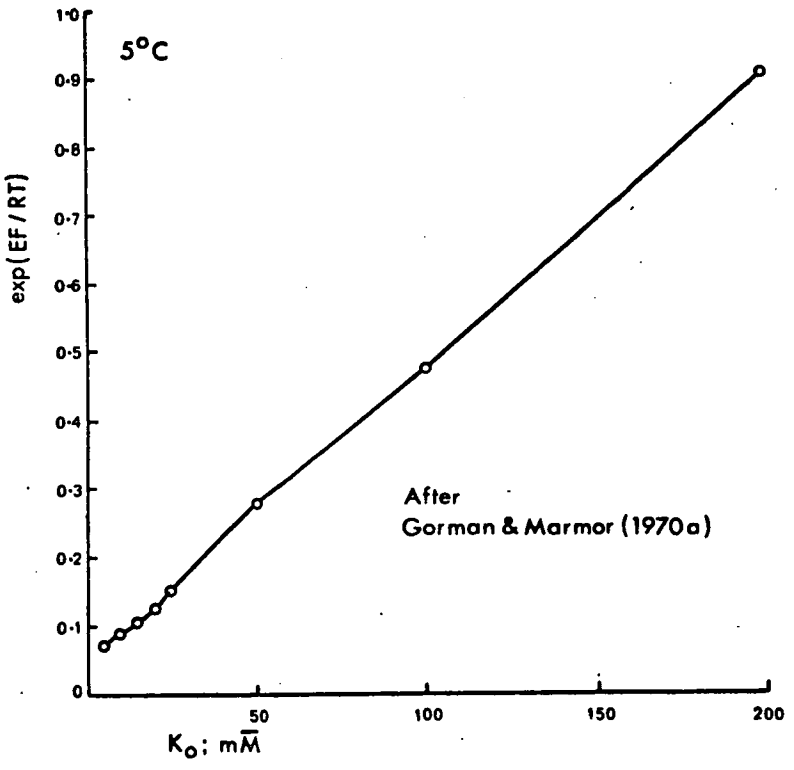
5°C
1·0
0·9
0·8
0·7
0·6
0·5
0·4
0·3
0·2
0·1
0
exp(EF/RT)
50
100
150
200
K_o; mM
After
Gorman & Marmor (1970a)

What is more significant in assessing the validity of the absolute potential approach is that the deviations from the constant-field equation apparent in an experimental context are typically of exactly the same type as those predicted by the absolute potential equations. Figure 66 shows two plots of $\exp(\frac{EF}{RT})$ using experimental values of E from Moreton (1968), (A), and Gorman & Marmor (1970a), (B). Similar nonlinearities in the region of low extracellular potassium concentration are clearly present. Thus it seems that the form of the actual relationship between resting potential and extracellular potassium concentration may be better described by the absolute potential equations than by the constant-field equation.

This suggestion is further supported by results obtained from perfused squid giant axons where theoretical curves of resting potential for membranes exposed to a variety of ionic environments, apparently based on the Hodgkin-Huxley equations expressed in absolute potential terms, are in reasonable agreement with experimental results (BAKER, HODGKIN & SHAW, 1962b).

In applying the constant-field equation, the permeability ration P_{Na}: P_K is assumed to remain constant at the value corresponding to the resting potential when the extracellular potassium concentration is normal. In the case of the Hodgkin-Huxley model, the conductance ratio g_{Na}: g_K is roughly equivalent to this permeability ratio. The conductance ratio at each resting potential can be obtained from the absolute potential analysis and the values determined are plotted as a function of extracellular potassium concentration in Figure 67. In the case of the expanded model the equivalent of the permeability ratio should include the additional potassium channel and the appropriate conductance ratio

Theoretical conductance ratios ;

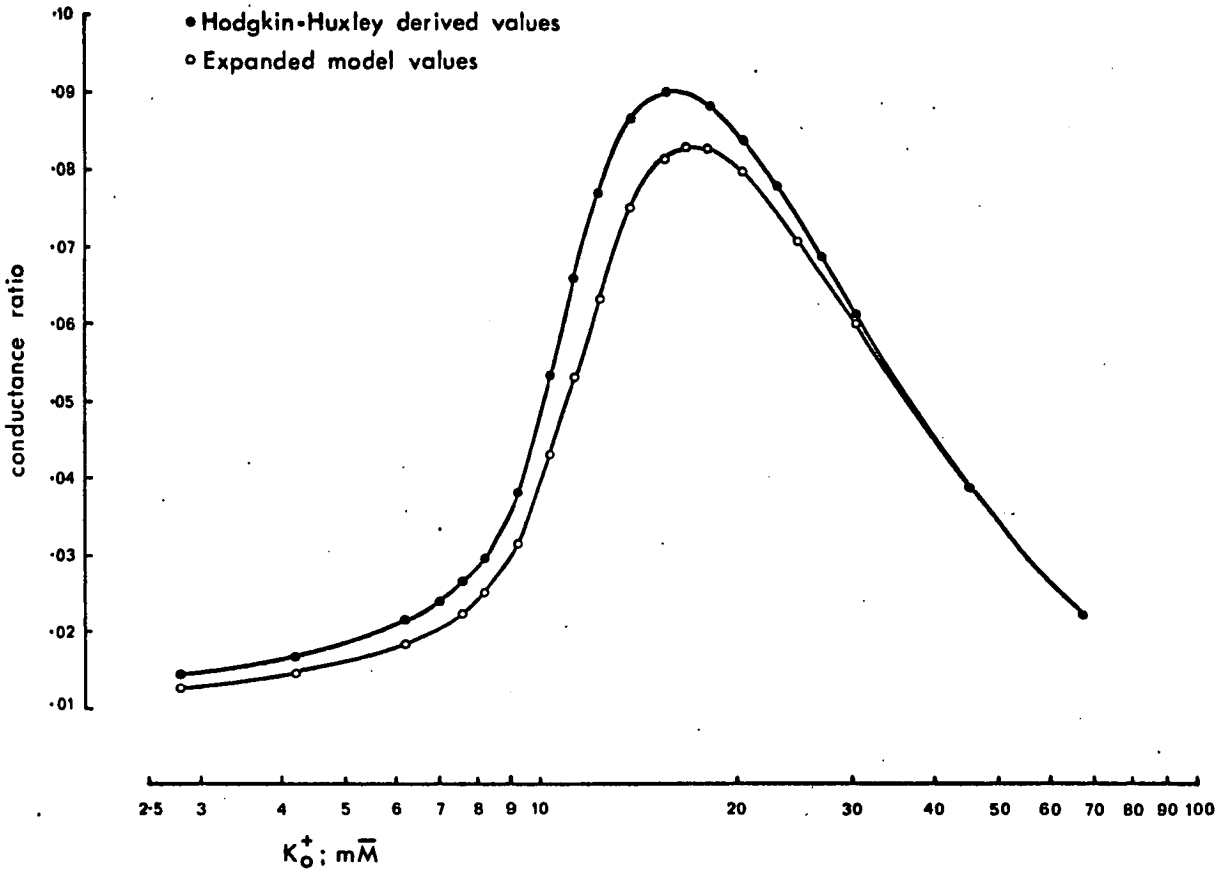

is therefore g_{Na}: $(g_K + g_A)$. The values obtained for this ratio have also been plotted.

Far from being constant, both series of conductance ratios calculated undergo practically an order of magnitude alteration within the range of extracellular potassium concentrations used. This large variation is barely reflected in the resting potentials predicted by the absolute potential equations for two reasons. Firstly, the ratio is always small and the influence of the sodium equilibrium potential on resting potential is therefore limited. Secondly, the leakage conductance (g_l) predominates for lower extracellular potassium concentrations in both cases. This has the effect of damping the changes in resting potential which would otherwise take place. The alteration in the calculated conductance ratio can be largely attributed to a rise in sodium conductance associated with the absolute potential variation of $m_\infty^3 h_\infty$ (Figure 46(D)). The peak value of $m_\infty^3 h_\infty$ is approximately 0.006, corresponding to a maximum possible resting (steady-state) sodium conductance of 0.72 m.mho/cm^2. This compares with a constant leakage conductance of 0.30 m.mho/cm^2, clearly sufficient to appreciably damp its effect.

The parallel between the leakage conductance and the chloride conductance is obvious. However, the two terms cannot be considered as synonymous. The leakage conductance can be regarded as of a composite, nonspecific, nature (HODGKIN & HUXLEY, 1952b) and it is probable that a 'leakage' component will contribute to membrane potential even when the chloride conductance is sufficient to allow equilibration of chloride ions across the membrane under altered ionic conditions. In muscle fibres equilibration has been

shown to take place (HODGKIN & HOROWICZ, 1959), but in other cases the chloride equilibrium potential is more stable and may contribute significantly to membrane potential (CHRISTOFFERSEN, 1973; KERKUT & MEECH, 1966).

Another feature of the theoretical results illustrated in Figure 67 is that the effect of including the additional potassium conductance channel in the expanded model has been to reduce the range of variation in the calculated conductance ratio to some extent. This is reflected in reduced deviations of the absolute potential predicted values from their corresponding constant-field approximations both in the case of the resting potential and $\exp(\frac{EF}{RT})$ plots (Figures 64 and 65). This reduction of the conductance ratio occurs because the increase of g_{Na} with absolute potential is partially offset by a simultaneous increase in g_A, the latter having a similar pattern of variation with absolute potential. Thus, if the proportion of $\bar{g}_A$ in the total potassium conductance was higher, the absolute potential $\exp(\frac{EF}{RT})$ plot would approximate more closely to a linear function.

The absolute potential equations can also be used to predict the relationship between membrane resistance and the extracellular potassium concentration. Figure 68 shows the predictions obtained. Clearly, membrane resistance falls rapidly with increasing extracellular potassium levels. This does happen in the experimental situation. For example, the experimentally derived relationship for Helix pomatia illustrated in Figure 69 (KOSTYUK, 1968) is obviously similar to the theoretical result. The corresponding variations in resting potential are also given and show deviations from the constant-field pattern similar to those predicted by the absolute potential

Theoretical membrane resistance;

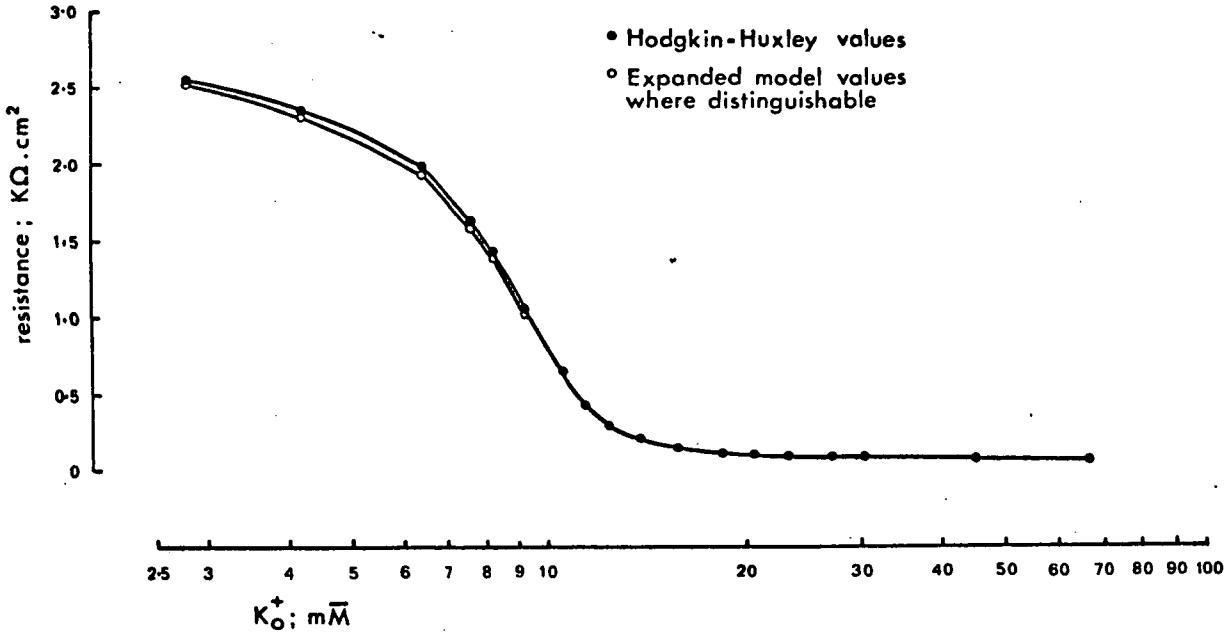

Experimentally determined membrane resistance;

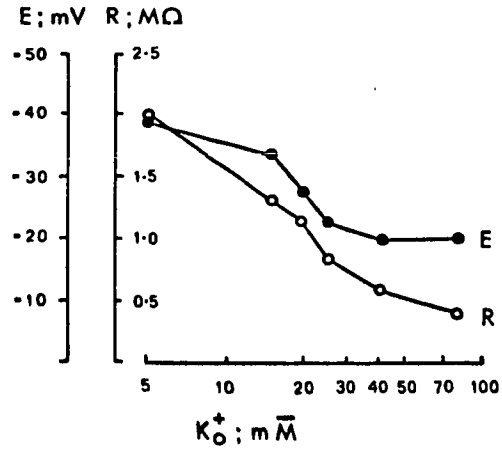

After Kostyuk (1968)

analysis (Figures 62 and 64). More detailed comparison is not possible however, since the extracellular potassium concentration in this case was raised by equimolar substitution of sodium; the relationship is therefore less steep at higher extracellular concentrations than would otherwise be expected.

These considerations lead to the conclusion that the variations in resting membrane properties with extracellular potassium conductance predicted by the Hodgkin-Huxley equations in absolute potential form, and by expansion to include an additional potassium conductance, are not inconsistent with experimental results and may possibly provide a better description of such variations than that afforded by the constant-field equation. Furthermore, the application of the constant-field equation may tend to obscure interactions of considerable subtlety between the various ionic conductance channels of the resting membrane.

In the experimental context, the main advantage of the constant-field equation is that it provides a simple empirical description of the changes in membrane properties associated with alterations in external ion concentrations. The direct experimental test of the quantitative validity of the absolute potential equations would, on the other hand, be an extremely complex undertaking.

In the first instance, an accurate description would be required for all the parameters on which the equations depend. This information is only available in a very limited number of cases. In addition, there is a strong possibility that the parameters will have different values for different individual cells in some preparations.

This is likely to be true in the suboesophageal ganglion of Helix aspersa where the proportion of sodium and calcium ions constituting the inward current differs markedly from cell to cell (KERKUT & GARDNER, 1967; CHAMBERLAIN & KERKUT, 1969) and widely different intracellular chloride concentrations can also be demonstrated (KERKUT & MEECH, 1966). As determined from the constant-field approach, considerable variation in intracellular potassium concentrations is also present (MORETON, 1968).

Secondly, there is some uncertainty over the assumption that the equilibrium potential for one ion will remain constant when the extracellular concentration of another is altered since this may change the osmotic equilibrium of the cell or interfere with an equilibrium dependent on the Donnan distribution of ions across the membrane. Thus, the intracellular concentration of ions is likely to be reduced by water uptake if the extracellular solution is made hypotonic or increased if it is made hypertonic. In either case the effect will depend on the elasticity of the cell membrane and an equilibrium will be reached when the hydrostatic pressure developed counterbalances the difference in osmotic pressure across the membrane. The possible re-equilibration of chloride ions across the membrane when its potential is altered presents a similar problem. In the absence of specific information it is difficult to see how theoretical calculations can allow for these effects. The situation is further complicated by the fact that intracellular ion activities as opposed to concentrations may be difficult to measure. In addition, there is the problem of whether changes in the ionic composition of the bathing solution are fully reflected at the cell surface.

Finally, there is a problem associated with the metabolic sodium 'pump' responsible for extruding any excess intracellular sodium ions and accumulating potassium ions from the surrounding medium. If the pump exchanges one sodium ion for one potassium ion then it will be electroneutral and will not contribute directly to membrane potential. However, if the ratio of exchange differs from unity the pump will become electrogenic and will make a direct contribution to membrane potential (THOMAS, 1969; CARPENTER & ALVING, 1968). The magnitude of this contribution will depend on the net pump current and also upon the resistance of the membrane. In terms of transmembrane current the appropriate description of the resting condition will now be $I_K + I_{Na} + I_l + I_p = 0$ where I_p is the pump current. This adds a further complication to theoretical analysis. When the sodium pump is electrogenic it is normal for sodium ion transport to predominate and the net pump current therefore makes a hyperpolarizing contribution to resting potential (KERKUT & YORK, 1971). The pump can be effectively inhibited by reducing the extracellular potassium concentration to zero, by cooling or by the application of ouabain (GORMAN & MARMOR, 1970a). Either of the latter techniques allows changes in membrane potential associated with alterations in external ion concentrations to be measured independently of any sodium pump contribution. However, in the longer term the intracellular sodium concentration will rise and that of potassium will fall.

In view of all these difficulties the qualitative rather than the quantitative test of the absolute potential predictions would seem appropriate.

C) Theoretical current-voltage predictions;

1) Introduction;

The prediction of changes in resting membrane properties in response to altered extracellular potassium concentrations by means of the absolute potential approach is sufficiently consistent with experimental observations to justify the extension of the approach of other situations. As previously indicated, theoretical current-voltage curves can be used to predict the threshold and the action potential peak in addition to the resting potential. The effect on each of these parameters of varying the equilibrium potential and the maximum possible conductance has been assessed for each of the ionic conductance channels. The varied parameters for the Hodgkin-Huxley analysis were E_{Na}, $\bar{g}_{Na}$, E_K, $\bar{g}_K$, E_l and g_l. Additional variables for the expanded model analysis were E_A, which was taken to vary with E_K, and $\bar{g}_A$ which was varied independently. With both systems of equations each parameter was varied in turn while all of the other parameters were kept constant. The resultant theoretical current-voltage curves and the corresponding predictions of alteration in resting potential, threshold and action potential peak are given in Figures 70 to 88. These provide a comprehensive description of the changes in membrane properties to be expected on the basis of the absolute potential approach when the ionic environment differs from normal or when the ionic conductances of the membrane are altered.

2) The sodium channel;

The effects of varying the sodium channel parameters are illustrated in Figures 70 to 75.

Hodgkin-Huxley model;

Theoretical current-voltage curves; effect of E_{Na} variation.

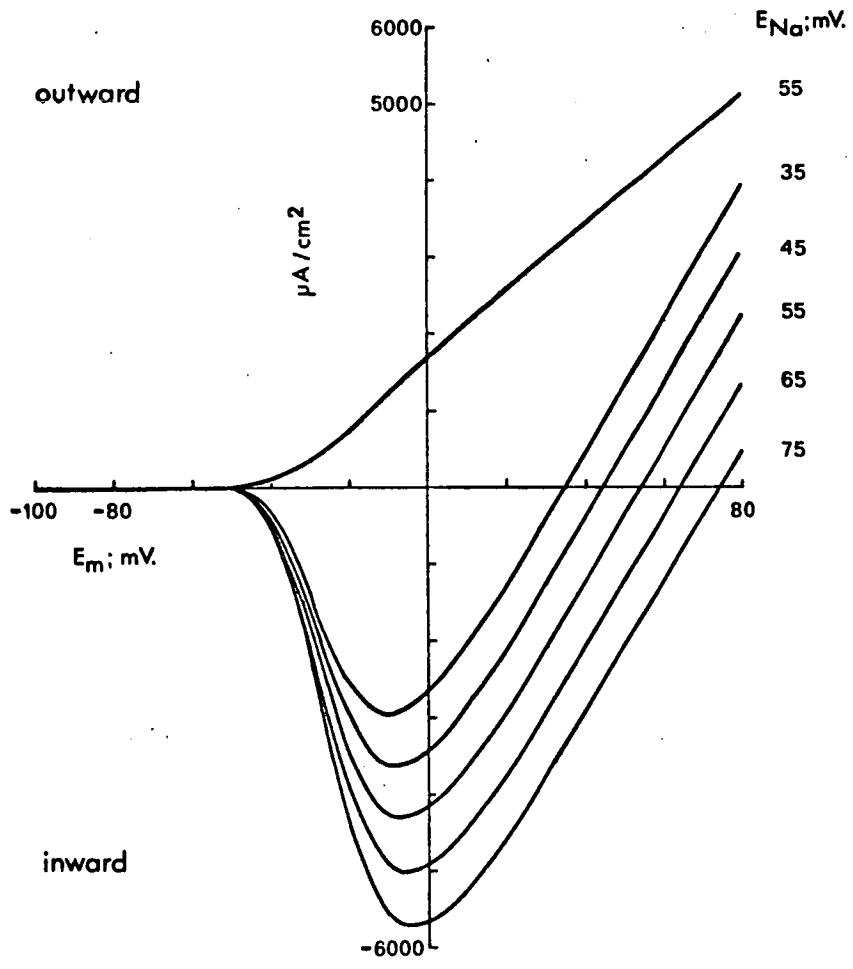

	mV.		m.mho/cm²
E_K	-72	$\bar{g}_K$	36·0
E_l	-60	$\bar{g}_{Na}$	120·0
		g_l	0·3

Hodgkin-Huxley model;

Theoretical current-voltage curves; effect of $\bar{g}_{Na}$ variation

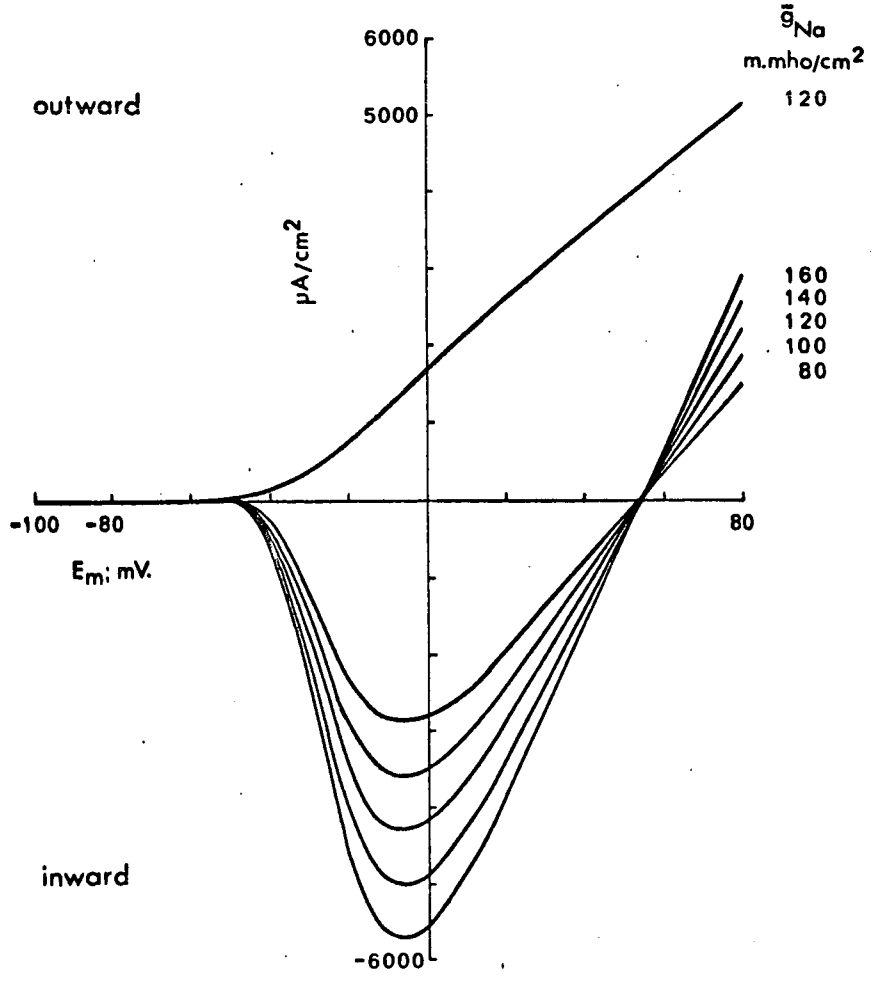

	mV.		m.mho/cm²
E_K	-72	$\bar{g}_K$	36.0
E_{Na}	55	g_l	0.3
E_l	-60		

Hodgkin-Huxley model ; current-voltage curve predictions

A;

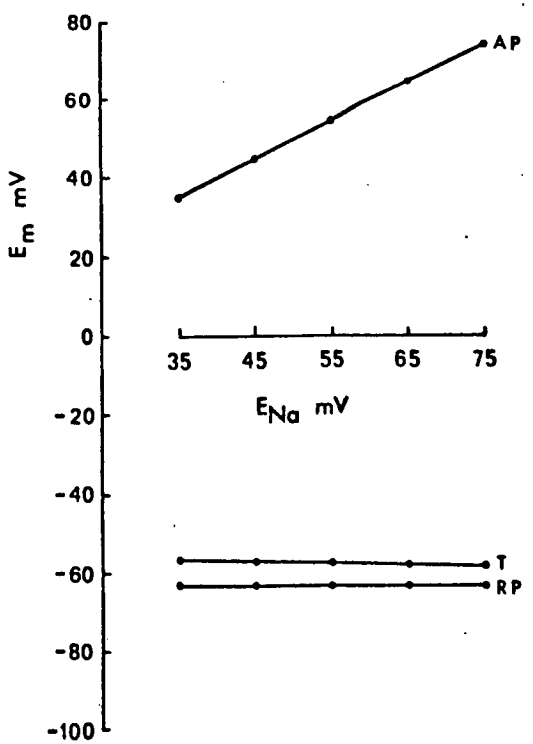

B;

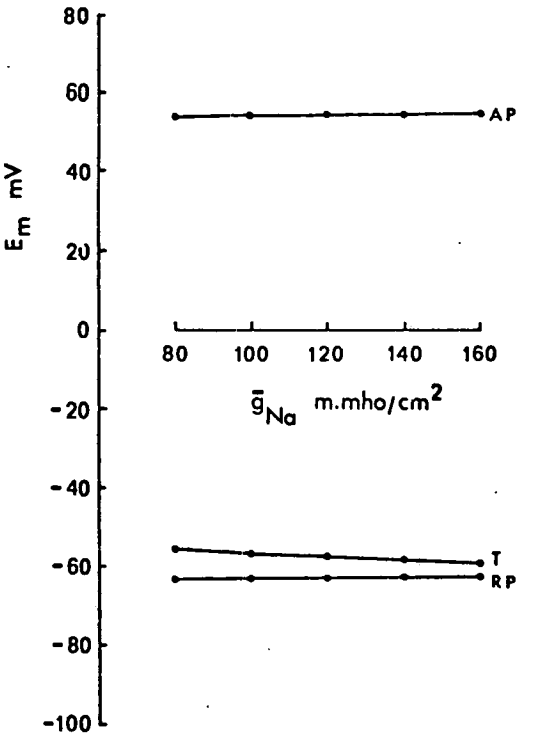

Expanded model;

Theoretical current-voltage curves; effect of E_{Na} variation

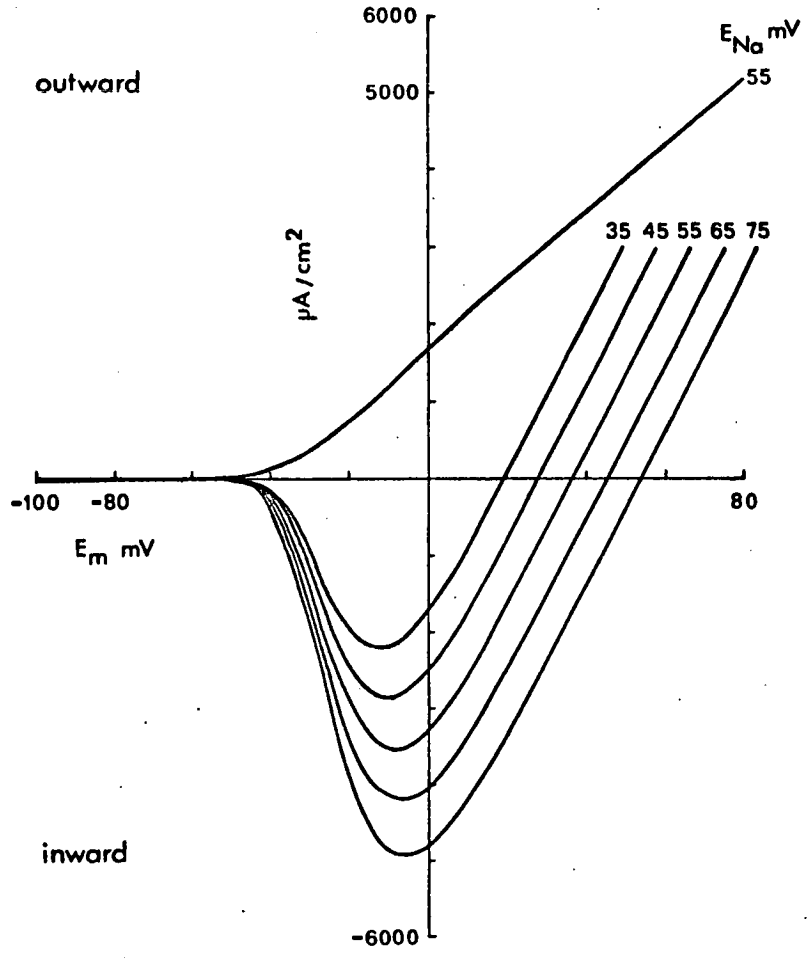

	mV		m.mho/cm²
E_K	-72	$\bar{g}_K$	36·0
E_A	-72	$\bar{g}_{Na}$	120·0
E_l	-60	$\bar{g}_A$	40·0
		g_l	0·3

Expanded model;

Theoretical current-voltage curves; effect of $\bar{g}_{Na}$ variation

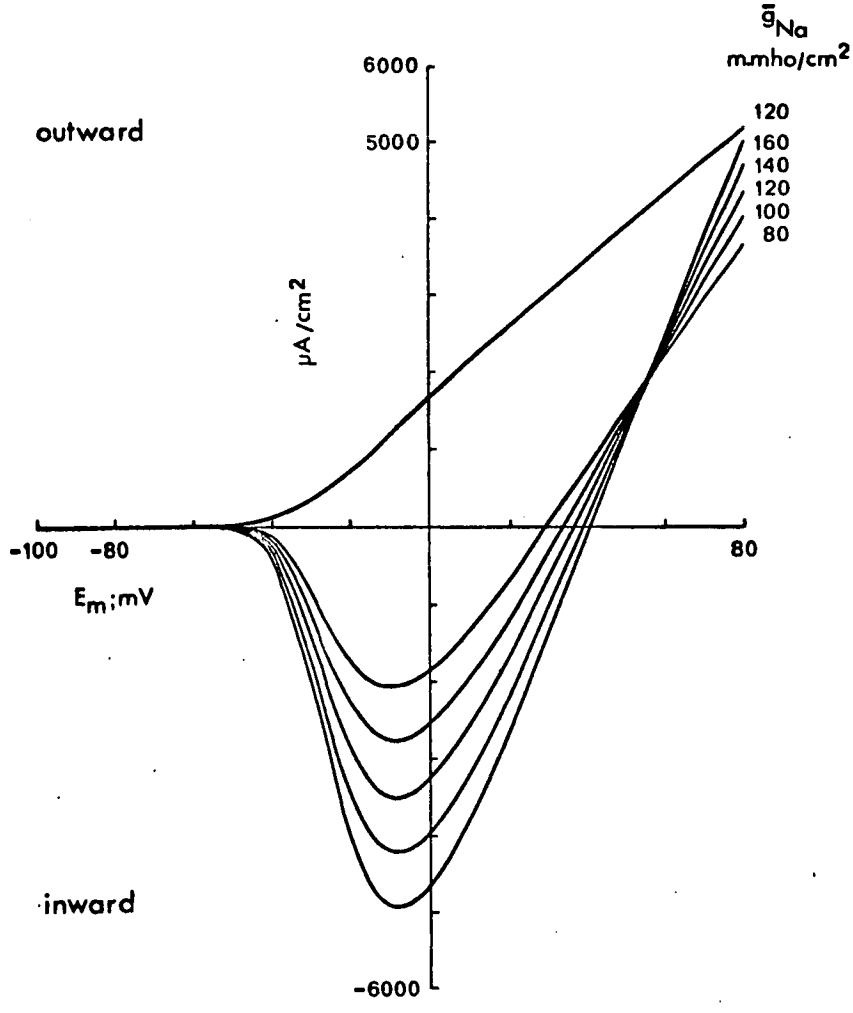

	mV		m.mho/cm²
E_K	-72	$\bar{g}_K$	36·0
E_{Na}	55	$\bar{g}_A$	40·0
E_A	-72	g_l	0·3
E_l	-60		

Expanded model; current-voltage curve predictions

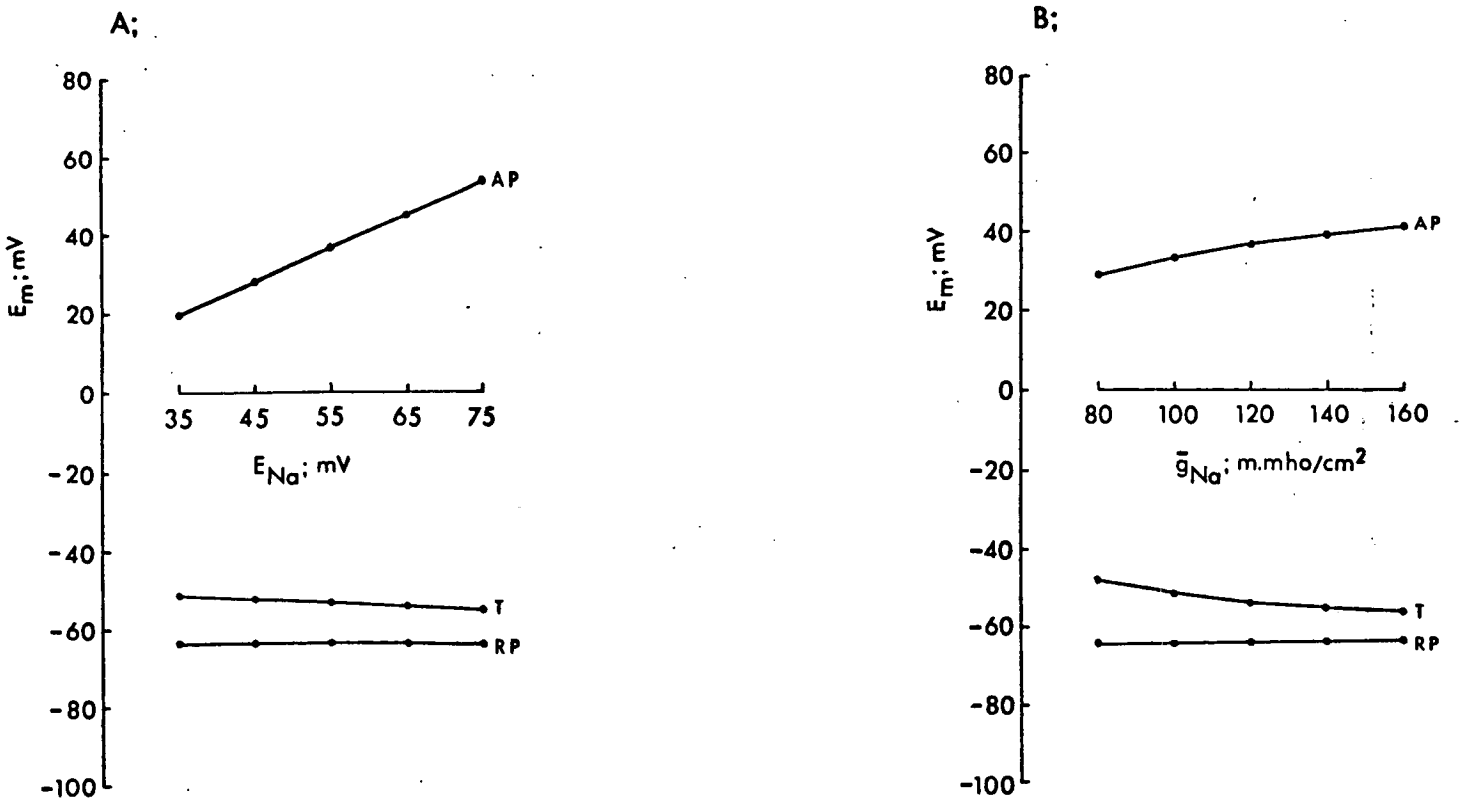

For the Hodgkin-Huxley model, varying the sodium equilibrium potential (E_{Na}) has a pronounced effect on the action potential peak and comparatively little effect on the threshold and resting potential (see Figures 70 and 72(A)). Over the range examined the relationship between E_{Na} and the action potential peak is approximately linear and has a slope corresponding to a 57.7 mV change per tenfold change in extracellular sodium concentration. This is marginally less than the 58 mV per decade change in the equilibrium potential calculated from the Nernst equation because the potassium and leakage conductances, as well as the sodium conductance, contribute to membrane potential at the action potential peak.

The experimentally derived relationship (HODGKIN & KATZ, 1949) is very similar for increased extracellular sodium concentrations but shows larger than predicted reductions in action potential peak for lower concentrations. However, the rate of rise of the action potential was shown to be related to the extracellular sodium concentration so that the action potential peak occurred later in sodium deficient solutions. This discrepancy can therefore be attributed to the time dependent rise in potassium conductance in the experimental case; in the theoretical analysis the potassium conductance was assumed to remain constant at its resting level.

The expanded model results for variation of E_{Na} (Figures 73 and 75(A)) show that the effect of including the additional potassium channel has been to substantially reduce the magnitude of the action potential peak. This is because the potassium conductance, g_A, rises simultaneously with the sodium conductance, g_{Na}; for the theoretical early current-voltage curves both have been assumed to reach maximum values corresponding to $a_\infty^4 b_o \cdot \bar{g}_A$ and $m_\infty^3 h_o \cdot \bar{g}_{Na}$

respectively. The slope of the derived relationship between E_{Na} and the action potential peak corresponds to a 50.1 mV change per tenfold change in extracellular sodium concentration. This differs more from the equilibrium potential slope than in the case of the Hodgkin-Huxley model because of the increased importance of potassium currents in determining membrane potential. The larger difference between threshold and resting potential can be accounted for in a similar way.

In Helix aspersa a tenfold change in extracellular sodium concentration has been shown to result in an average change in action potential peak of only 29 mV (KERKUT & GARDNER, 1967). This cannot be explained simply in terms of increased potassium conductance during the action potential but argues the involvement of some other ion in the maintenance of the 'overshoot' potential. In fact, calcium ions were shown to contribute, a tenfold change in extracellular calcium producing an average change of 16 mV in the action potential peak. The importance of calcium ions has been confirmed by voltage-clamp experiments (CHAMBERLAIN & KERKUT, 1969).

While sodium and calcium ions can be considered as making an additive contribution to a single inward current channel (CONNOR & STEVENS, 1971c), the situation is complicated by the observation that calcium ions affect the 'stability' of the membrane conductance channels (FRANKENHAEUSER & HODGKIN, 1957). Changes in external calcium concentration will therefore lead to alterations in the absolute potential dependency of the theoretical conductance determining variables. The Hodgkin-Huxley equations can be modified to accomodate this effect (HUXLEY, 1959) but if the proportions of calcium and sodium ions constituting the inward current are unknown

or variable, prediction of the relationship between the action potential peak and the extracellular concentrations of sodium ions and calcium ions will be little improved. The absolute potential approach can therefore only be applied with caution in this particular instance.

The effects on the theoretical current-voltage curves of varying $\bar{g}_{Na}$ are illustrated in Figures 71 and 74. These results compare very favourably with experimental curves for membranes exposed to tetrodotoxin or tarichatoxin (TAKATA et al, 1966; CUERVO & ADELMAN, 1970; MOORE et al, 1967) both of which specifically inhibit the inward current conductance channel. In the theoretical and also in the experimental situation the late steady-state currents are virtually unaffected by alterations in the sodium conductance. Resting potential is therefore barely affected (Figures 72(B) and 75(B)). For the Hodgkin-Huxley model the threshold and action potential peak are also relatively invariant. Changes in these two parameters are more pronounced for the expanded model as a result of the inclusion of the additional potassium conductance channel.

The significance of these results for the validity of the absolute potential approach is somewhat limited since the absolute magnitude of the resting potential is comparatively little affected by alterations in E_{Na} and $\bar{g}_{Na}$. Predictions based on the unmodified equations, while plotted against differing axis, would therefore differ only slightly in form from the absolute potential predictions.

3) The potassium channel;

The theoretical effect of alteration in E_K on resting potential has already been discussed in some detail. The corresponding changes in the theoretical current-voltage curves are illustrated in Figures 76 and 79. The derived relationships between E_K and the threshold and action potential peak are given in Figures 78(A) and 82(A).

The theoretical early current-voltage curves show that the maximum inward current is slightly increased when the potassium equilibrium potential is made more negative and markedly reduced when it is made more positive. The theoretical values for early current correspond to those expected for a voltage-clamped membrane stepped from resting potential to a series of new holding potentials. The peak early current measured in each case being plotted against the holding potential to derive the early current-voltage curve. The resting potential value appropriate for each theoretical early current-voltage curve is defined by the intersection of the corresponding theoretical steady-state current-voltage curve. Since the theoretical resting potential is strongly dependent on the value of the potassium equilibrium potential, the initial voltage-clamped level for each of the theoretical early current-voltage curves will be different. If, on the other hand, the initial voltage-clamped level were constant it would be a prediction of the absolute potential equations that the maximum inward current would be little affected by changes in E_K.

In the experimental situation, increases in extracellular potassium concentration lead to reductions in the early transient

Hodgkin-Huxley model;

Theoretical current-voltage curves; effect of E_K variation

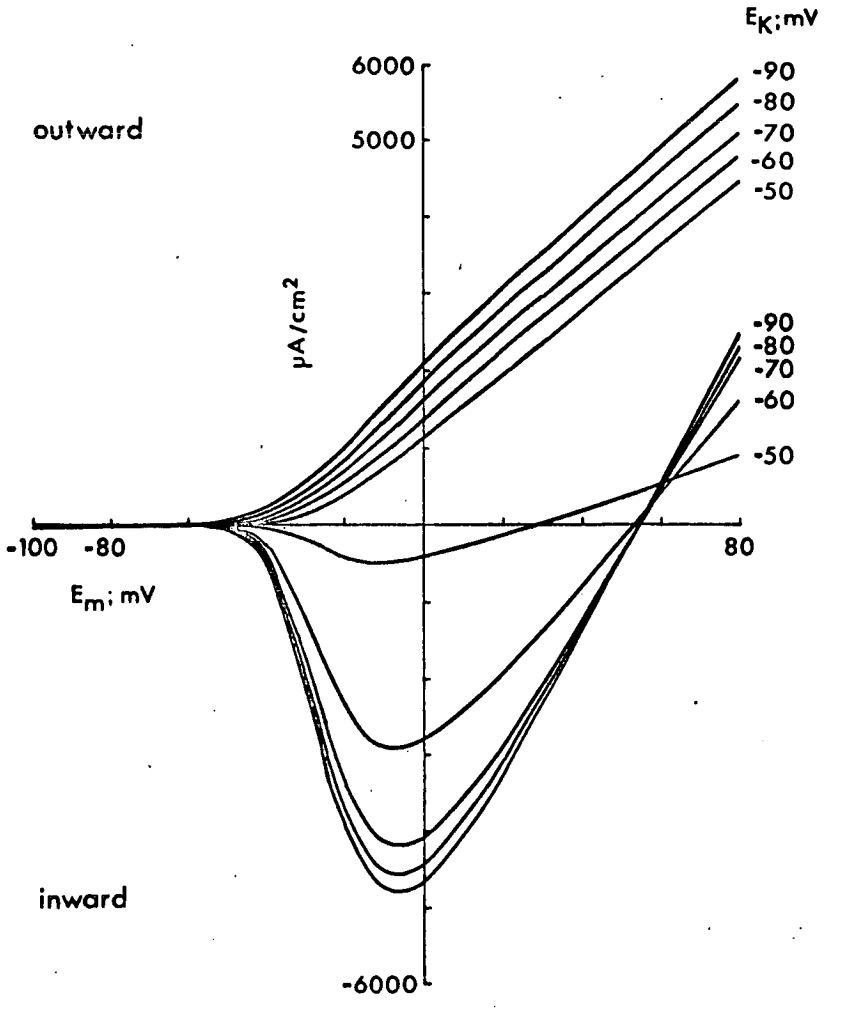

	mV		m.mho/cm²
E_{Na}	55	$\bar{g}_K$	36·0
E_l	-60	$\bar{g}_{Na}$	120·0
		g_l	0·3

Hodgkin-Huxley model;

Theoretical current-voltage curves; Effect of $\bar{g}_K$ variation

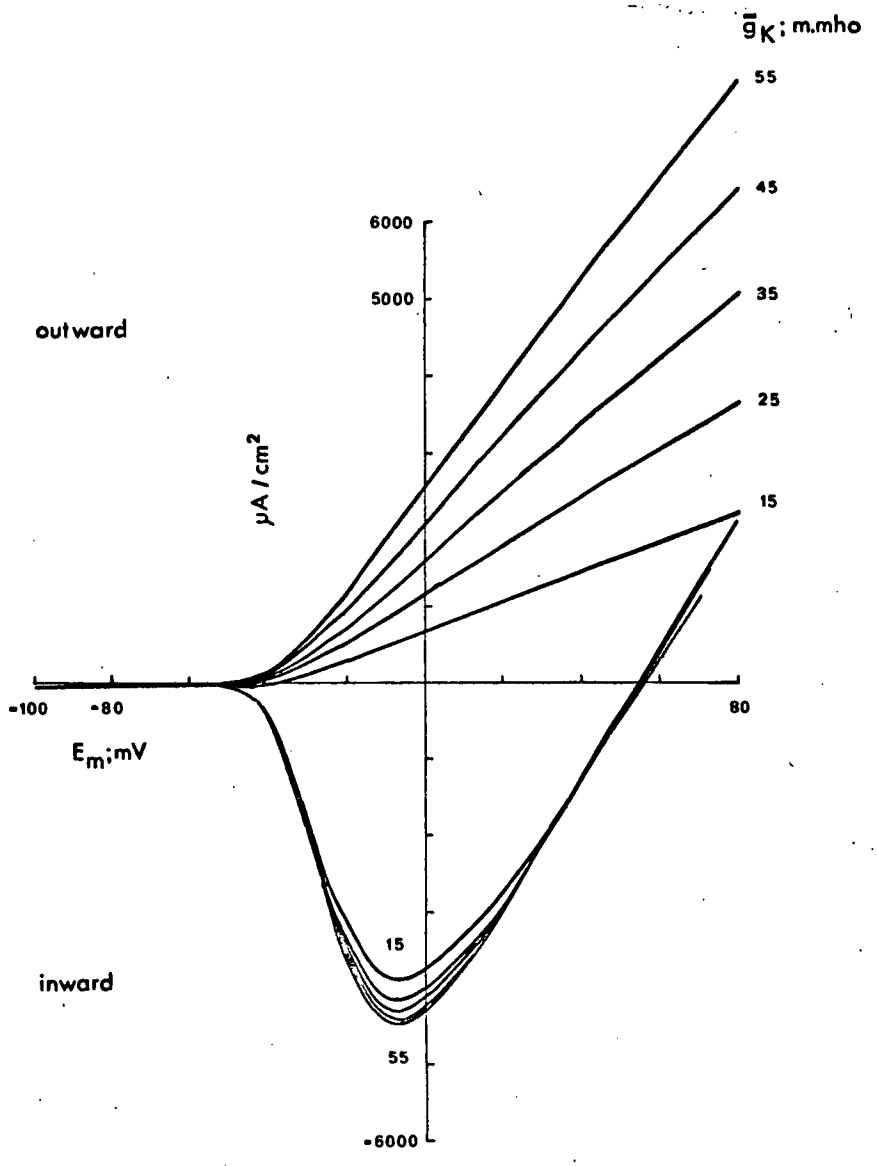

	mV		m.mho/cm²
E_K	-72	$\bar{g}_{Na}$	36·0
E_{Na}	55	g_l	0·3
E_l	-60		

Hodgkin-Huxley model; current-voltage curve predictions

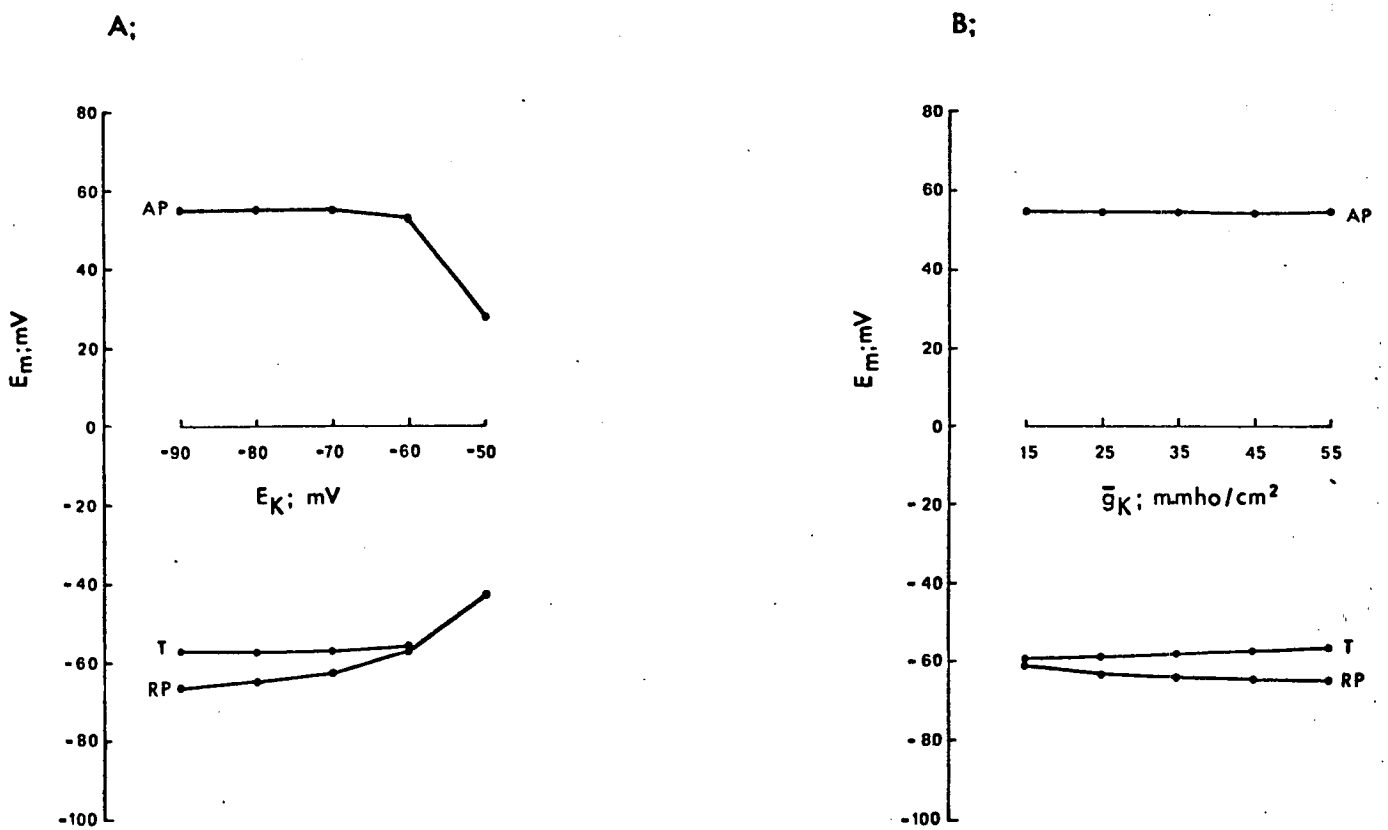

Expanded model;

Theoretical current-voltage curves; effect of E_K, E_A variation

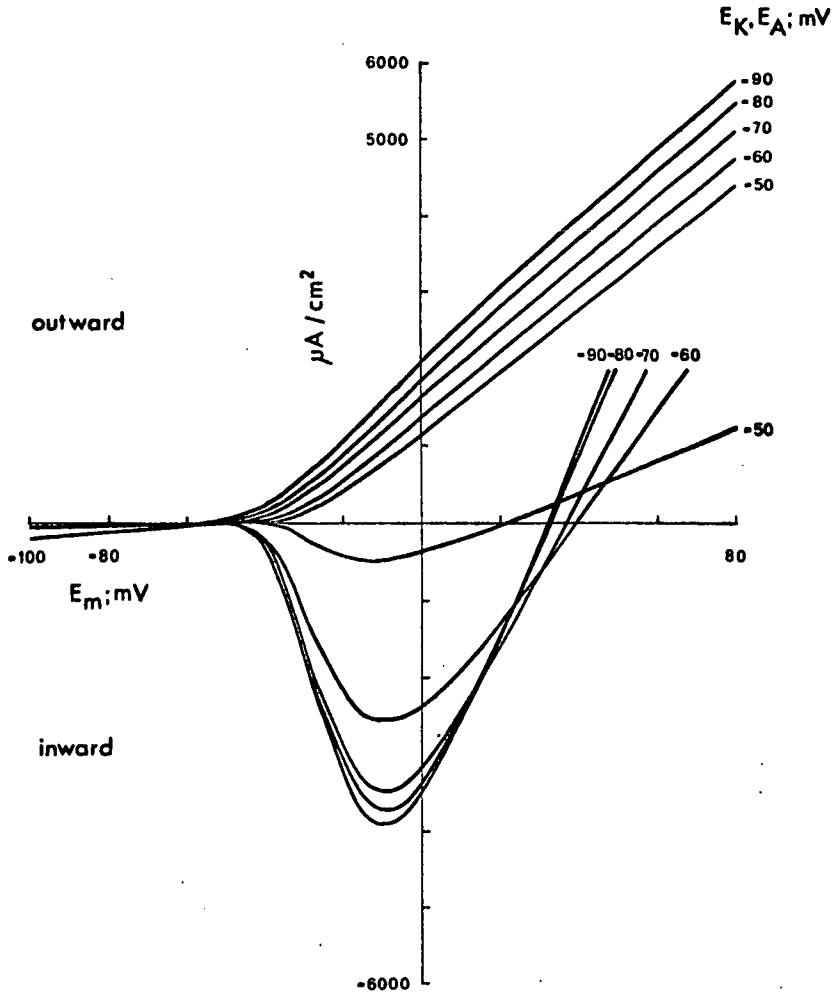

	mV		m.mho/cm²
E_{Na}	55	$\bar{g}_K$	36·0
E_l	-60	$\bar{g}_{Na}$	120·0
		$\bar{g}_A$	40·0
$E_A = E_K$		g_l	0·3

Expanded model;

Theoretical current-voltage curves; effect of $\bar{g}_K$ variation

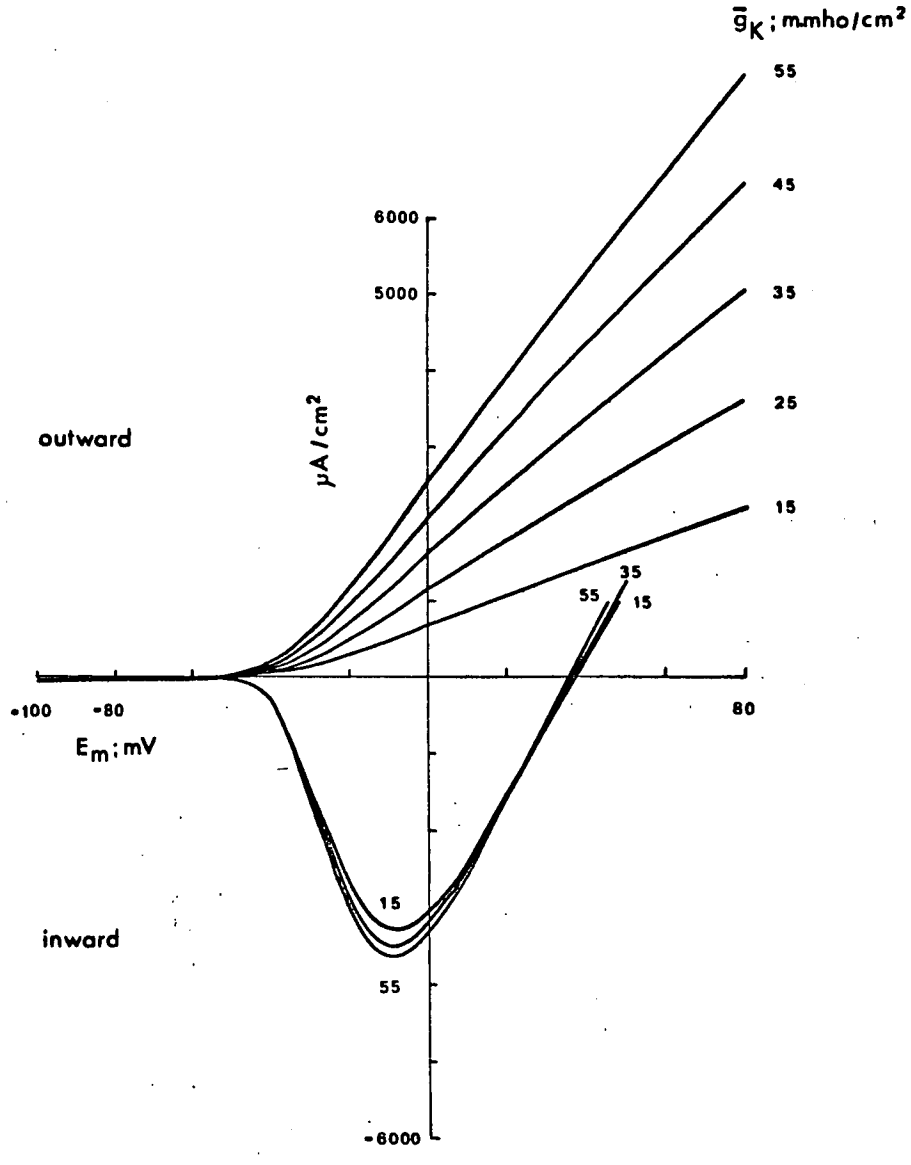

E_K	-72	$\bar{g}_{Na}$	120·0
E_{Na}	55	$\bar{g}_A$	40·0
E_A	-72	g_l	0·3
E_l	-60		

Expanded model;

Theoretical current-voltage curves; effect of $\bar{g}_A$ variation

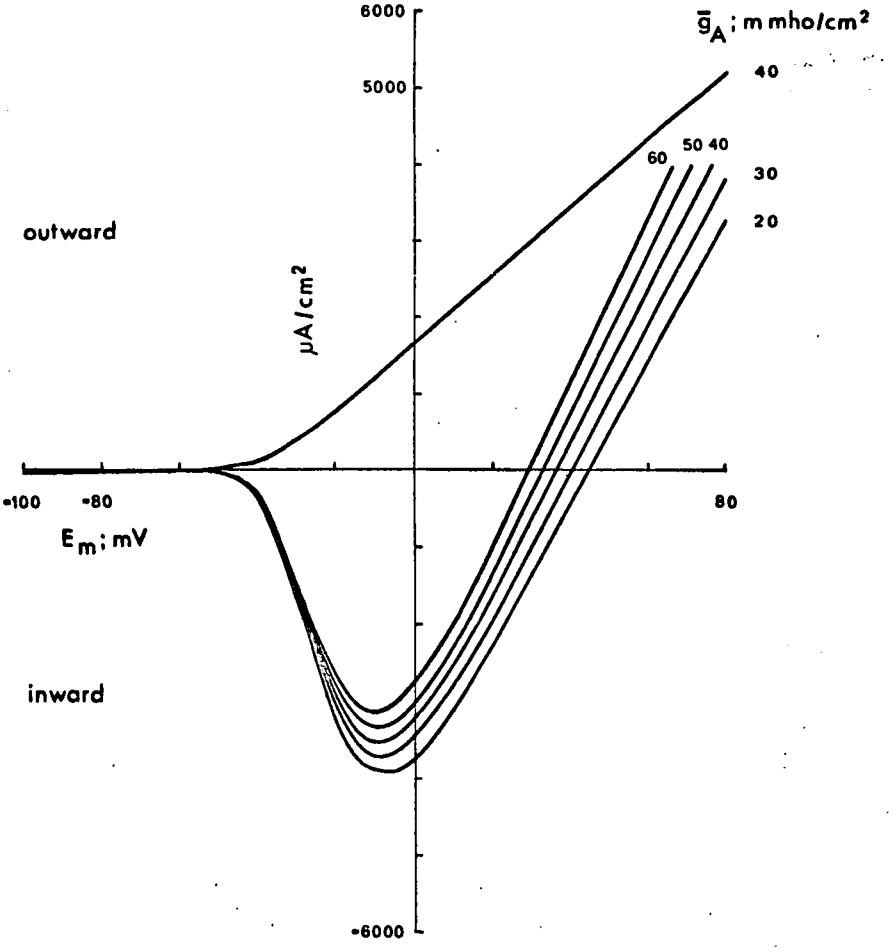

	mV		m.mho/cm²
E_K	-72	$\bar{g}_K$	36·0
E_{Na}	55	$\bar{g}_{Na}$	120·0
E_A	-72	g_l	0·3
E_l	-60		

Expanded model; current-voltage curve predictions

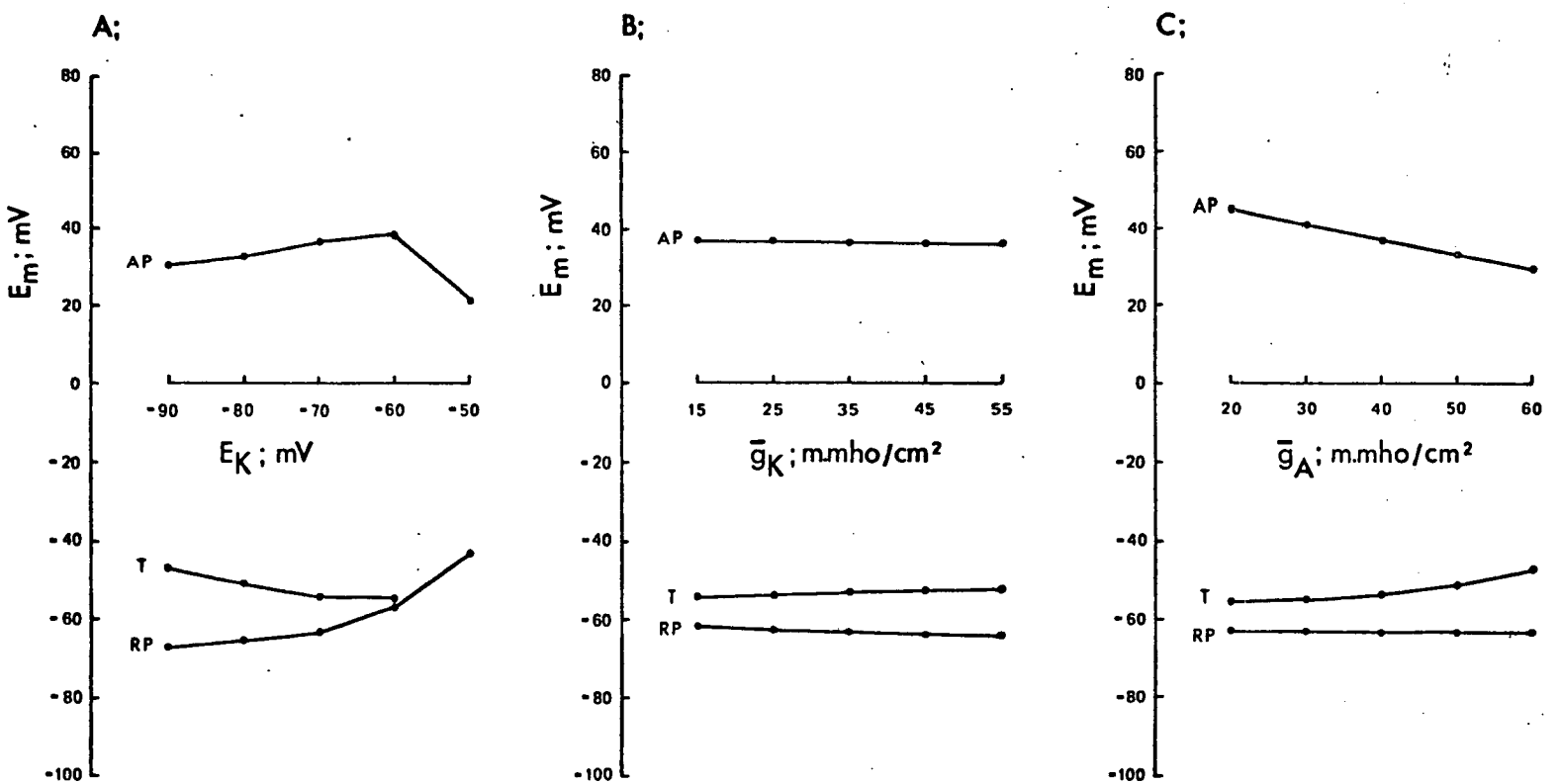

currents in the squid giant axon when the initial voltage-clamped potential corresponds to resting potential, as in the theoretical case (ADELMAN & PALTI, 1969a; 1969b). However, for high potassium solutions the reductions are larger than expected and when the initial voltage-clamped potential is constant the early currents are not restored to their normal level. In effect, the maximum steady-state value (taken as unity when $K_o^+ = 0$) of the sodium inactivation variable, h_∞, is reduced in potassium enriched solutions. Thus, when extracellular potassium is varied, the applicability of the absolute potential equations to the early current-voltage curve is restricted to a fairly narrow range of concentrations close to the normal value. The applicability to the steady-state current-voltage curve will however cover a much wider range since sodium currents contribute comparatively little to the total steady-state current. Thus, even large changes in the magnitude of h_∞ will barely affect resting potential values.

In contrast to this situation, voltage-clamp experiments on perfused giant-axons show clearly that the steady-state values for the sodium inactivation variable are not reduced by reductions in the intracellular potassium concentration, and in addition that the absolute potential dependency of steady-state inactivation is constant provided that the ionic strength of the perfusing solution is constant at its normal level (CHANDLER, HODGKIN & MEVES, 1965). When isotonic sucrose was substituted for internal potassium chloride, the inactivation curve was shifted along the voltage axis in a positive direction. However, if the internal potassium chloride was replaced by sodium chloride, choline chloride or rubidium chloride at equivalent concentration there was no change in the derived relation-

ships between h_∞ and absolute potential. These ionic changes would produce large alterations in resting potential in the unclamped axon and it can be concluded that the absolute potential equations should be applicable over a wide range of potassium equilibrium potential values when the intracellular, rather than the extracellular, potassium concentration is altered.

The convergence of the theoretical threshold and resting potential for less negative values of the potassium equilibrium potential is of special interest and will be discussed fully in a subsequent section.

The differences between the theoretical current-voltage curves produced for the Hodgkin-Huxley model and those for the expanded model are similar to those described in the case of the sodium channel. Thus the threshold is raised and the action potential peak reduced by the inclusion of the additional potassium channel.

The effects on the theoretical current-voltage curves of alterations in $\bar{g}_K$ are illustrated in Figures 77 and 80. The effects on resting potential, threshold and action potential peak are summarised in Figures 78(B) and 82(B). Clearly the steady-state current is strongly dependent on $\bar{g}_K$ while early currents are barely affected. These predictions are entirely consistent with experimental observations which show that delayed potassium currents can be totally abolished by tetraethylammonium (TEA) ions without affecting transient early currents or leakage currents in any way (HILLE, 1967). In low TEA concentrations small delayed currents remain with normal time constants.

For the expanded model, variations in $\bar{g}_A$ have the effects illustrated in Figures 81 and 82(C). These show that the maximum inward current and the action potential peak are reduced by increases in $\bar{g}_A$ and the theoretical current-voltage curves are therefore somewhat similar to those obtained for E_{Na} variations. Although resting potential is only slightly altered, the effect on threshold is more pronounced than in the case of E_{Na} variations.

There is as yet no standard experimental method for blocking the additional potassium channel. Its independence from the normal delayed potassium conductance channel is indicated by its insensitivity to TEA ions (CONNOR & STEVENS, 1971b).

4) The leakage channel;

Predictions for the leakage channel have been included partly for completeness and are illustrated in Figures 83 to 88.

When E_l is made more positive, resting potential is little altered but when it is made more negative the effect on resting potential is more pronounced. The threshold and action potential peak are barely affected in either case. The relationship between the leakage equilibrium potential and the chloride equilibrium potential (E_{Cl}) is difficult to assess and experimental observations on Helix aspersa are not entirely consistent with a simple interdependence. For example, diffusion of chloride ions from a 3 M KCl intracellular microelectrode may cause hyperpolarization rather than the expected depolarization (KERKUT & MEECH, 1966). This may be related in some way to a Donnan equilibrium in the distribution of potassium ions and chloride ions across the membrane (see Chapter 6).

Hodgkin-Huxley model;
Theoretical current-voltage curves; effect of E_l variation

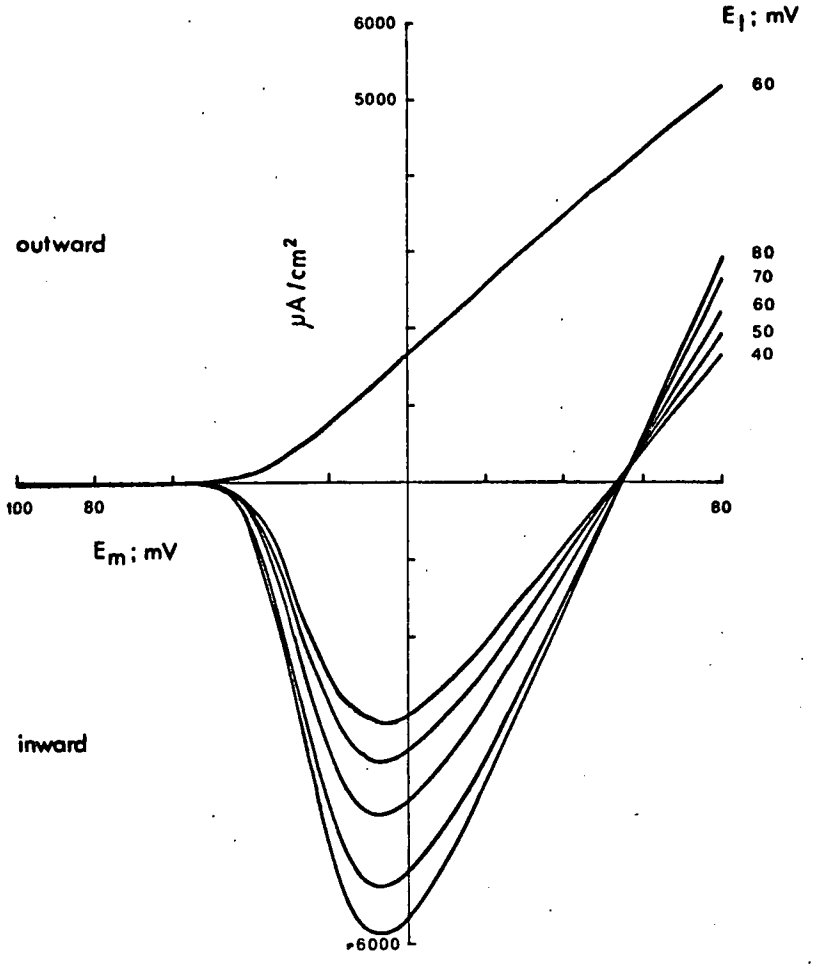

	mV		m.mho/cm²
E_K	-72	$\bar{g}_K$	36·0
E_{Na}	55	$\bar{g}_{Na}$	120·0
		g_l	0·3

Hodgkin-Huxley model;

Theoretical current-voltage curves; effect of g_l variation.

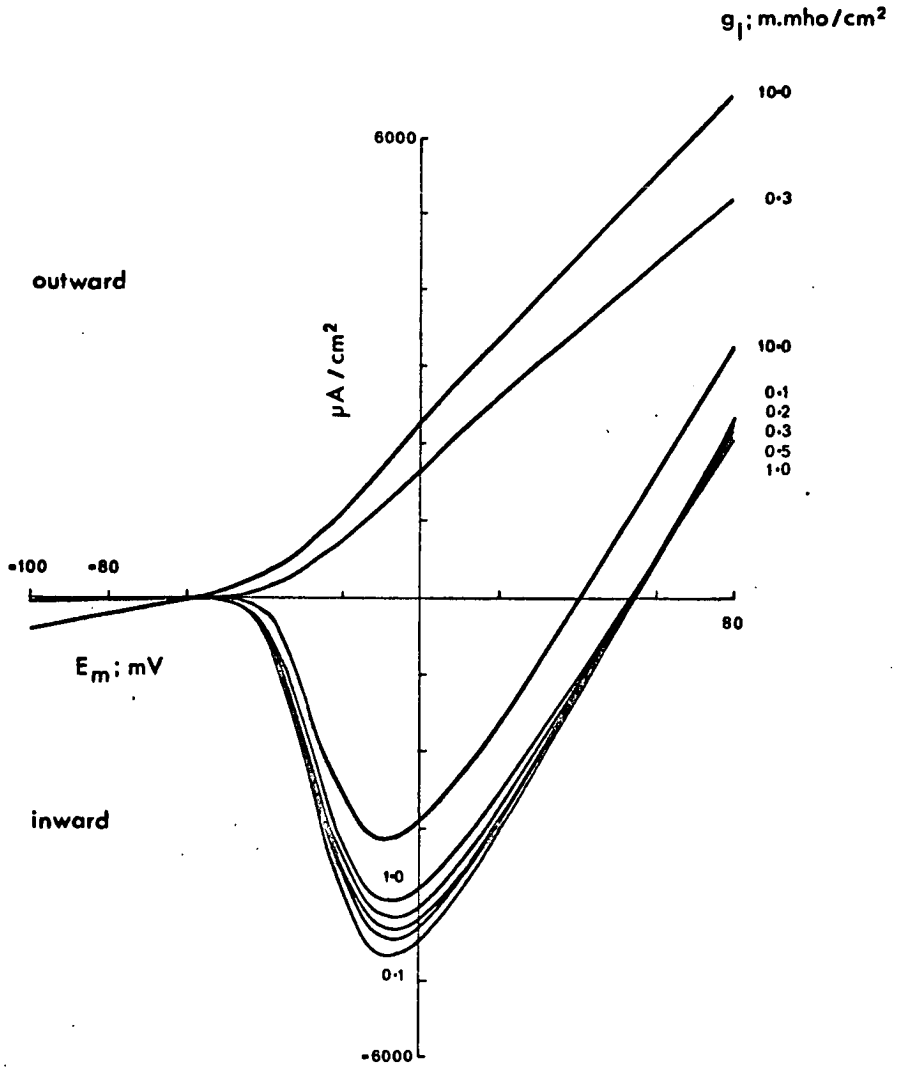

	mV		m.mho/cm²
E_K	-72	$\bar{g}_K$	36·0
E_{Na}	55	$\bar{g}_{Na}$	120·0
E_l	-60		

FIGURE 85; p 121

Hodgkin-Huxley model; current-voltage curve predictions

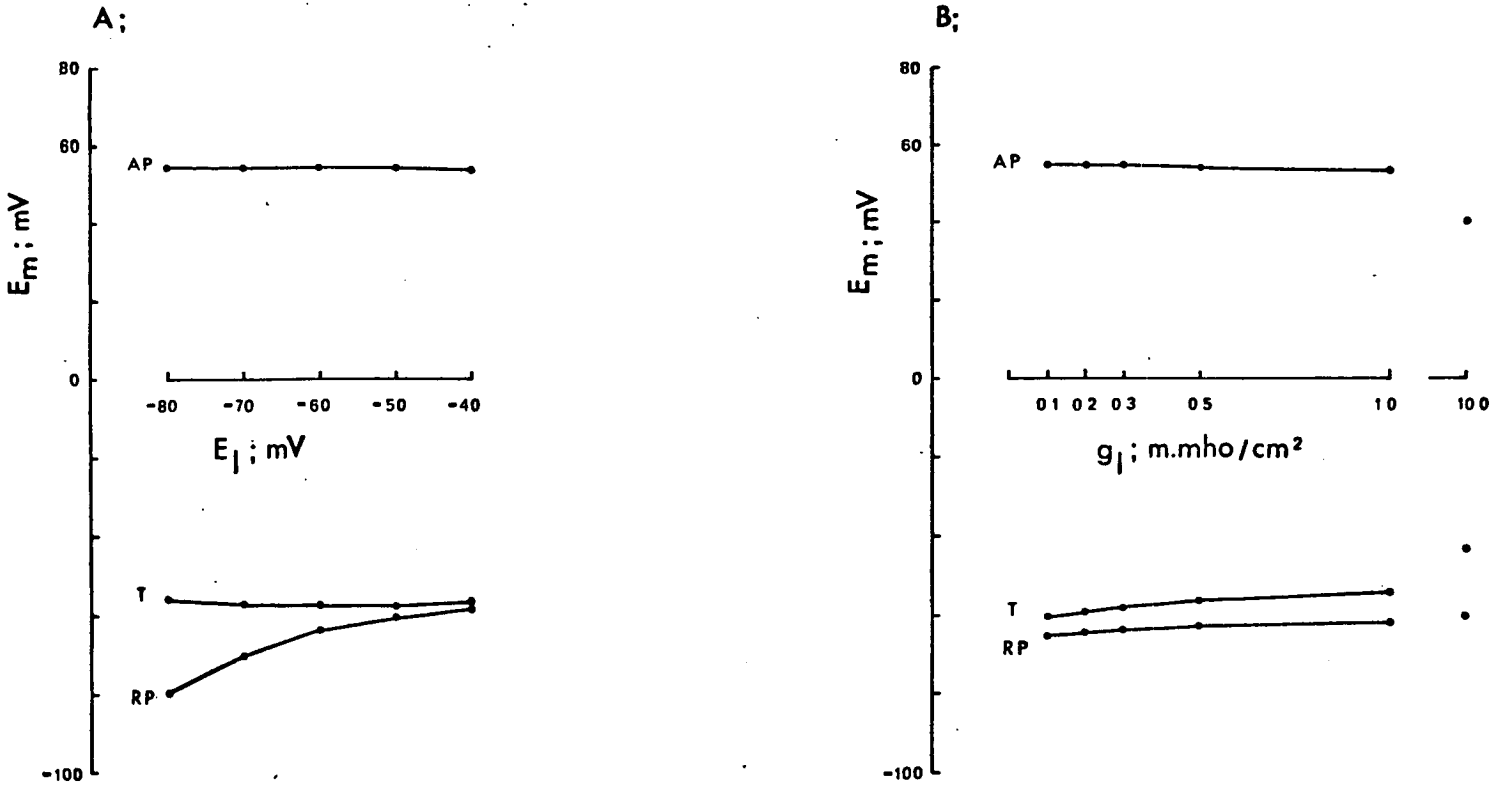

Expanded model;

Theoretical current-voltage curves; effect of E_l variation

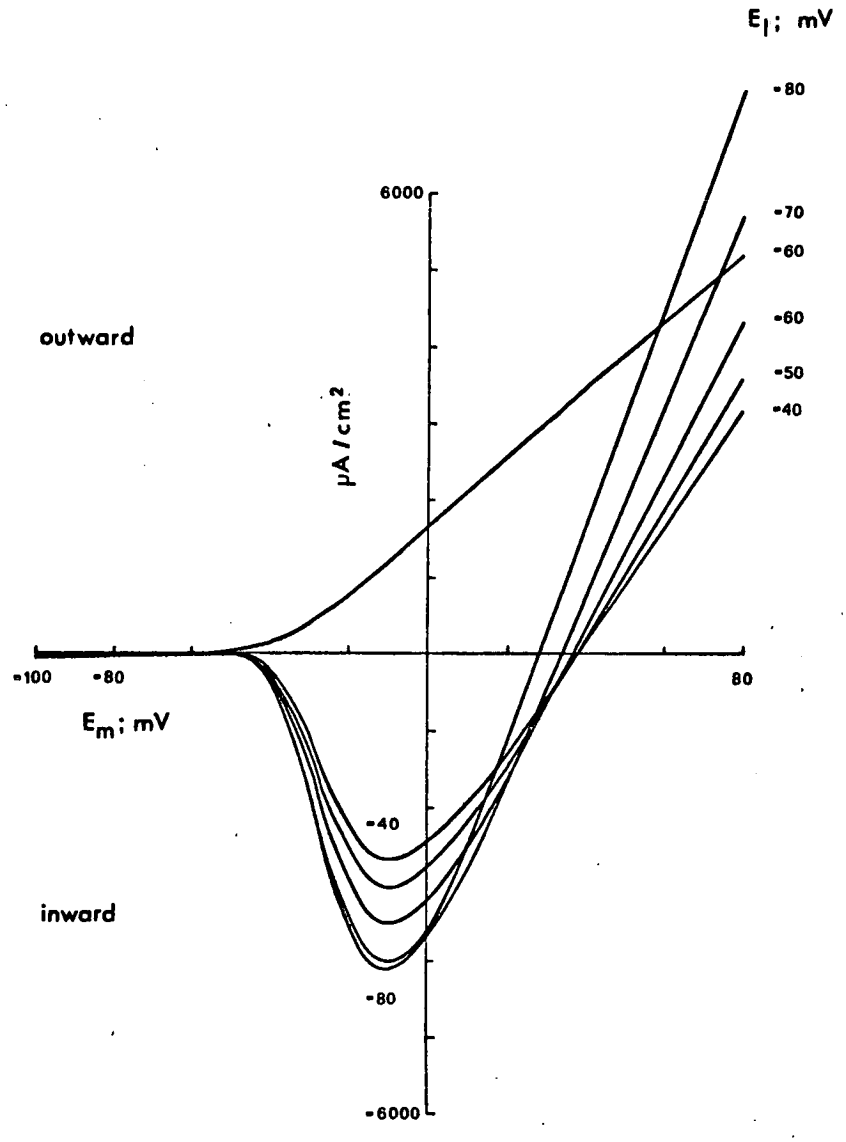

	mV		mmho/cm²
E_K	-72	$\bar{g}_K$	36·0
E_{Na}	55	$\bar{g}_{Na}$	120·0
E_A	-72	$\bar{g}_A$	40·0
		g_l	0·3

Expanded model;

Theoretical current-voltage curves; effect of g_l variation

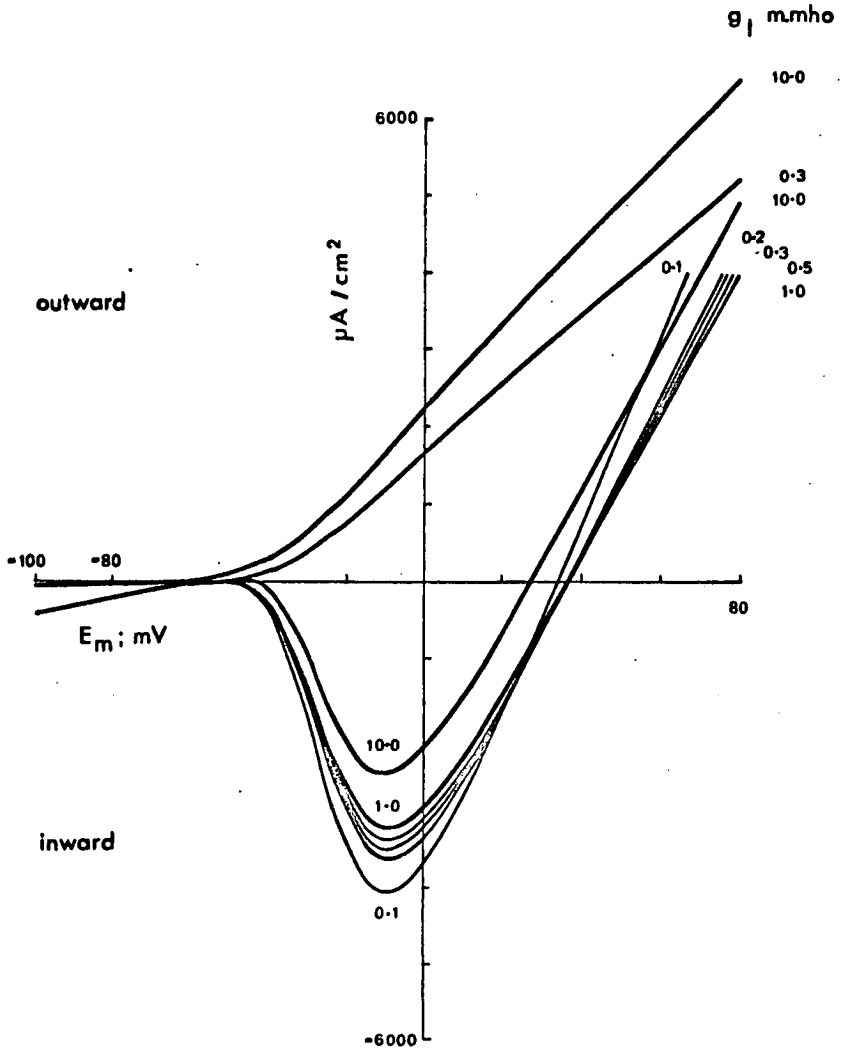

	mV		mmho/cm²
E_K	-72	$\bar{g}_K$	36·0
E_{Na}	55	$\bar{g}_{Na}$	120·0
E_A	-72	$\bar{g}_A$	40·0
E_l	-60		

Expanded model; current-voltage curve predictions

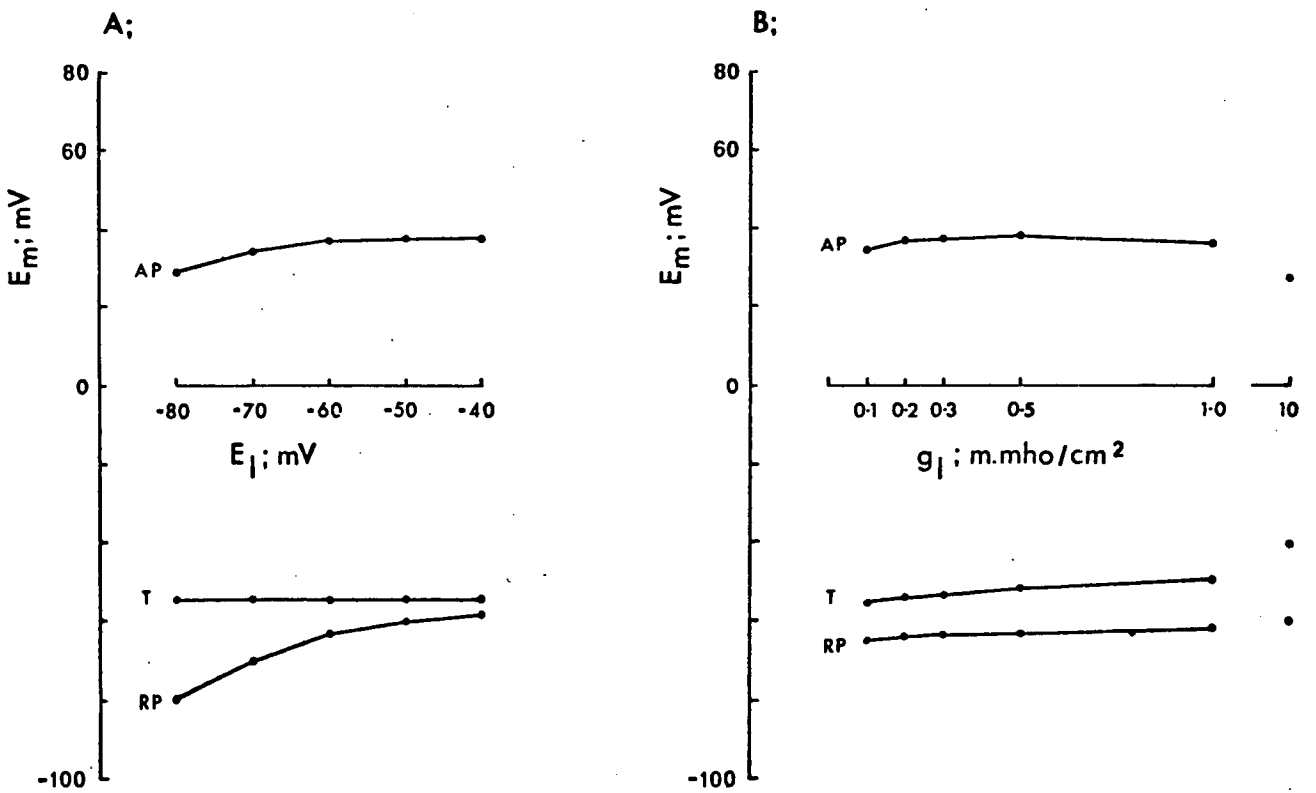

Complete replacement of chloride ions by acetate ions in the extracellular solution has little effect on the threshold and action potential peak (KERKUT & GARDNER, 1967).

The closest experimental parallel for variations in g_1 is afforded by the effects of cell damage on microelectrode penetration. However, since there is no guarantee that the relative importance of the various factors contributing to the leakage conductance will be preserved during damage, the two situations are not really comparable. A slow hyperpolarization and a reduction in any spontaneous activity usually follow penetration.

5) Discussion;

The overall conclusion which can be drawn from the comparisons between the predictions of the absolute potential equations and available experimental results given above is that, cautiously applied, the absolute potential equations can provide a valid description of changes in membrane properties associated with alterations in ionic conductances and equilibrium potentials. In particular, if the analysis is restricted to relatively small changes in the values of the various parameters from their normal levels, the validity of the absolute potential approach seems in little doubt.

One feature of the experimental results which is not predicted by the theoretical analysis is that, in terms of its effect on membrane properties, the alteration in extracellular ion concentration which produces a given change in the corresponding ionic equilibrium potential is not necessarily equivalent to the alteration in intracellular ion concentration which produces the

same change in equilibrium potential. When experimental alterations in external ion concentrations are relatively large it may be difficult to interpret the observed changes in membrane properties in terms of the absolute potential approach. However, the physiological range of changes in external ion concentrations is likely to be rather restricted and any naturally-occurring variation in ionic equilibrium potential is therefore more likely to be associated with variations in intracellular ion concentrations. In this case the corresponding differences in membrane properties should be adequately described by the absolute potential approach.

D) Prediction of intrinsic 'pacemaker' activity;

1) Introduction;

In some spontaneously active nerve cells, no extrinsic driving current seems to be available by which repetitive, 'pacemaker' activity could be maintained. For example, in Aplysia spontaneous activity may persist in neuron somata isolated by ligatures from the synaptic regions of the axon (ALVING, 1968). Totally isolated somata obtained by trypsin treatment of Aplysia ganglia can also show pacemaker activity and where individual cells can be followed throughout trypsin treatment and subsequently isolated, recovery to the normal pattern of spontaneous activity in the intact ganglion can be demonstrated (CHEN, Von BAUMGARTEN & TAKEDA, 1971). Thus pacemaker activity in some cells must be considered an intrinsic property of the somatic membrane.

The fact that intrinsic pacemaker activity can be predicted by applying the absolute potential equations represents the most significant feature of the absolute potential approach. The unmodified equations imply that repetitive activity can only be produced by the application of a depolarizing current.

2) Pacemaker current-voltage curves;

The convergence of the theoretical threshold and resting potential values apparent for more positive values of the potassium equilibrium potential (Figures 76 and 79) was studied in more detail by plotting theoretical current-voltage curves for a wider range of E_K values against an expanded current axis. The theoretical steady-state current-voltage curves obtained in this way for the Hodgkin-

Hodgkin-Huxley model;

Steady-state currents; effect of E_K variation;

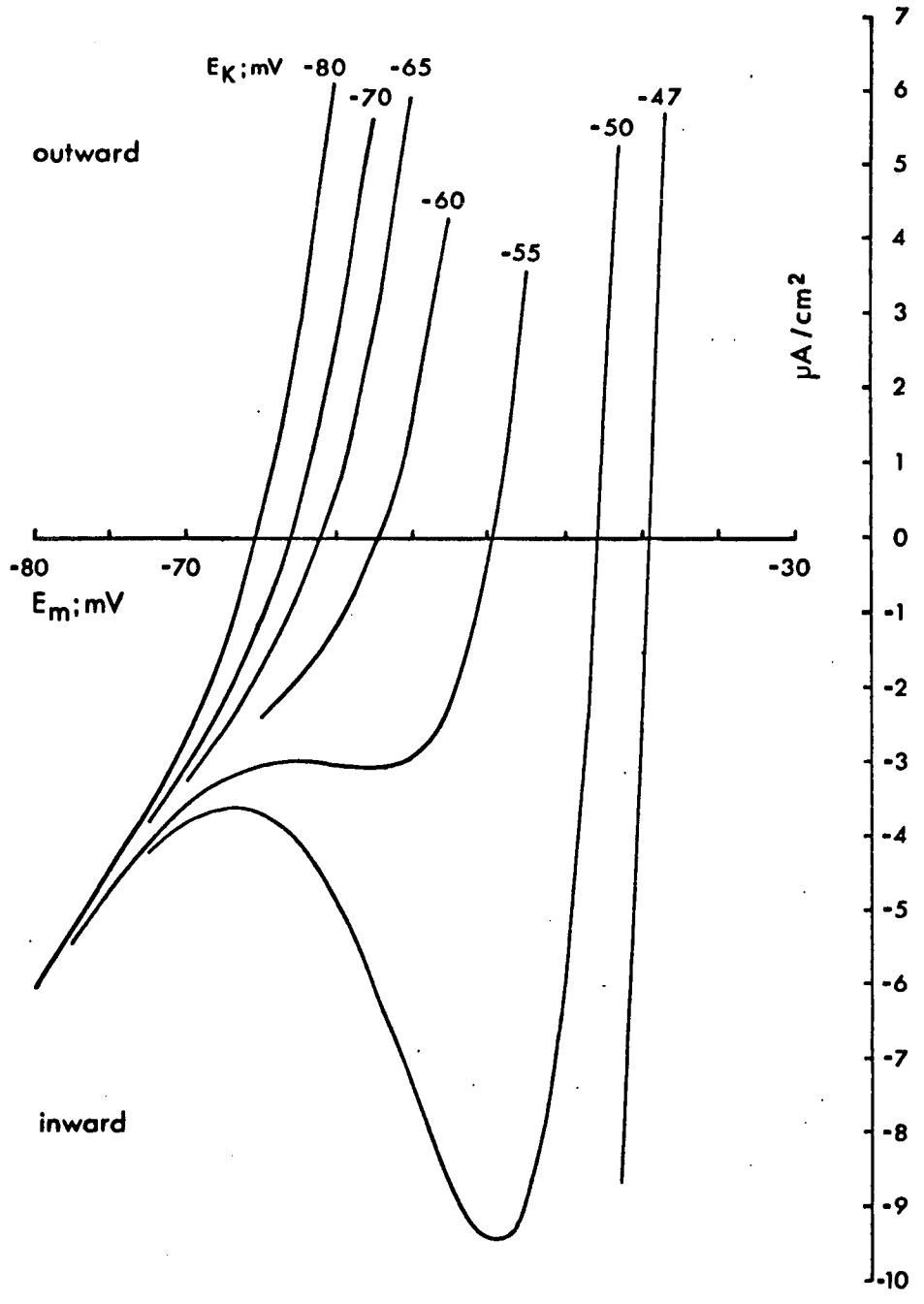

Hodgkin-Huxley model;

Early currents; effect of E_K variation

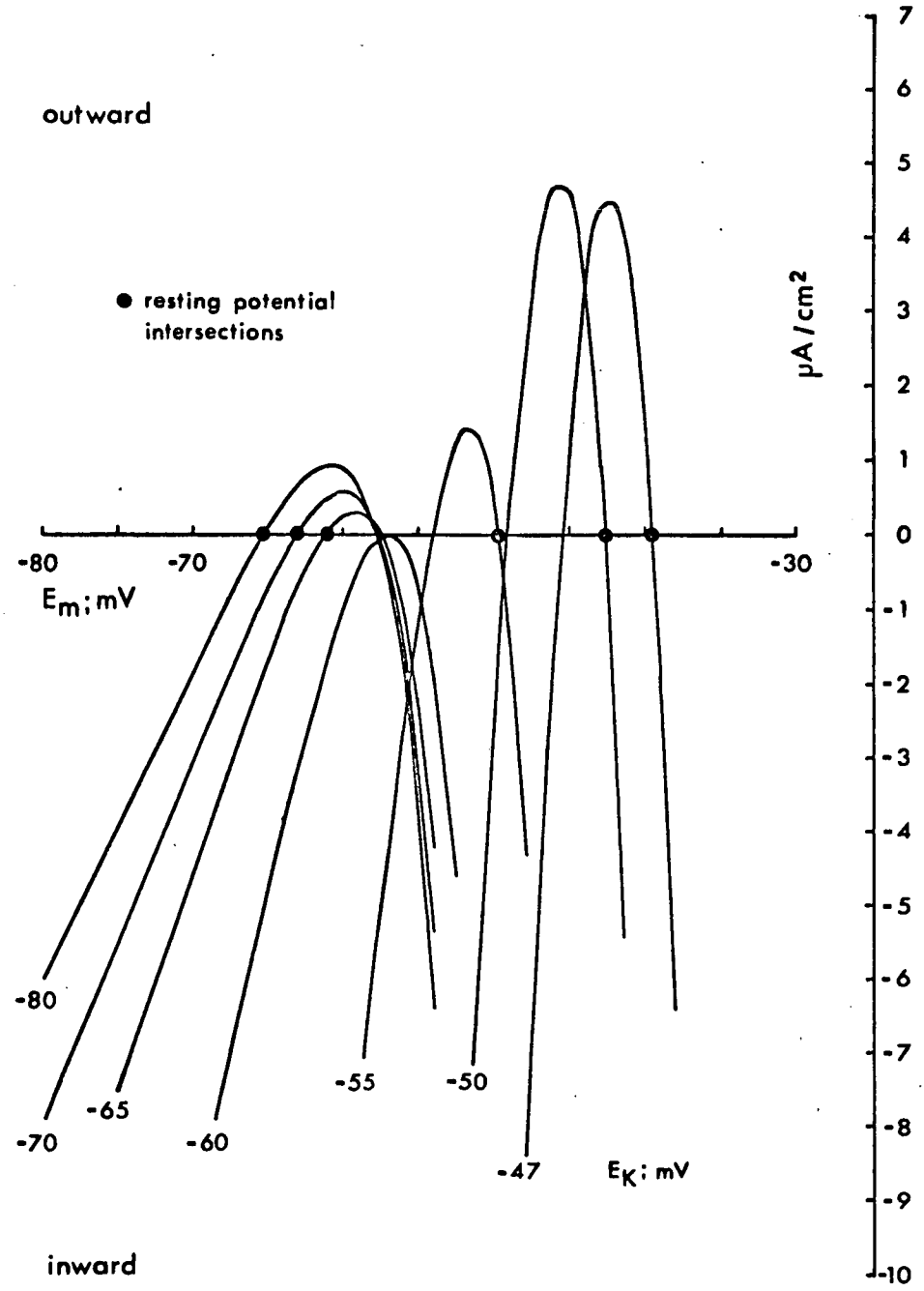

Expanded model;

Steady-state currents; effect of E_K variation ($E_A = E_K$)

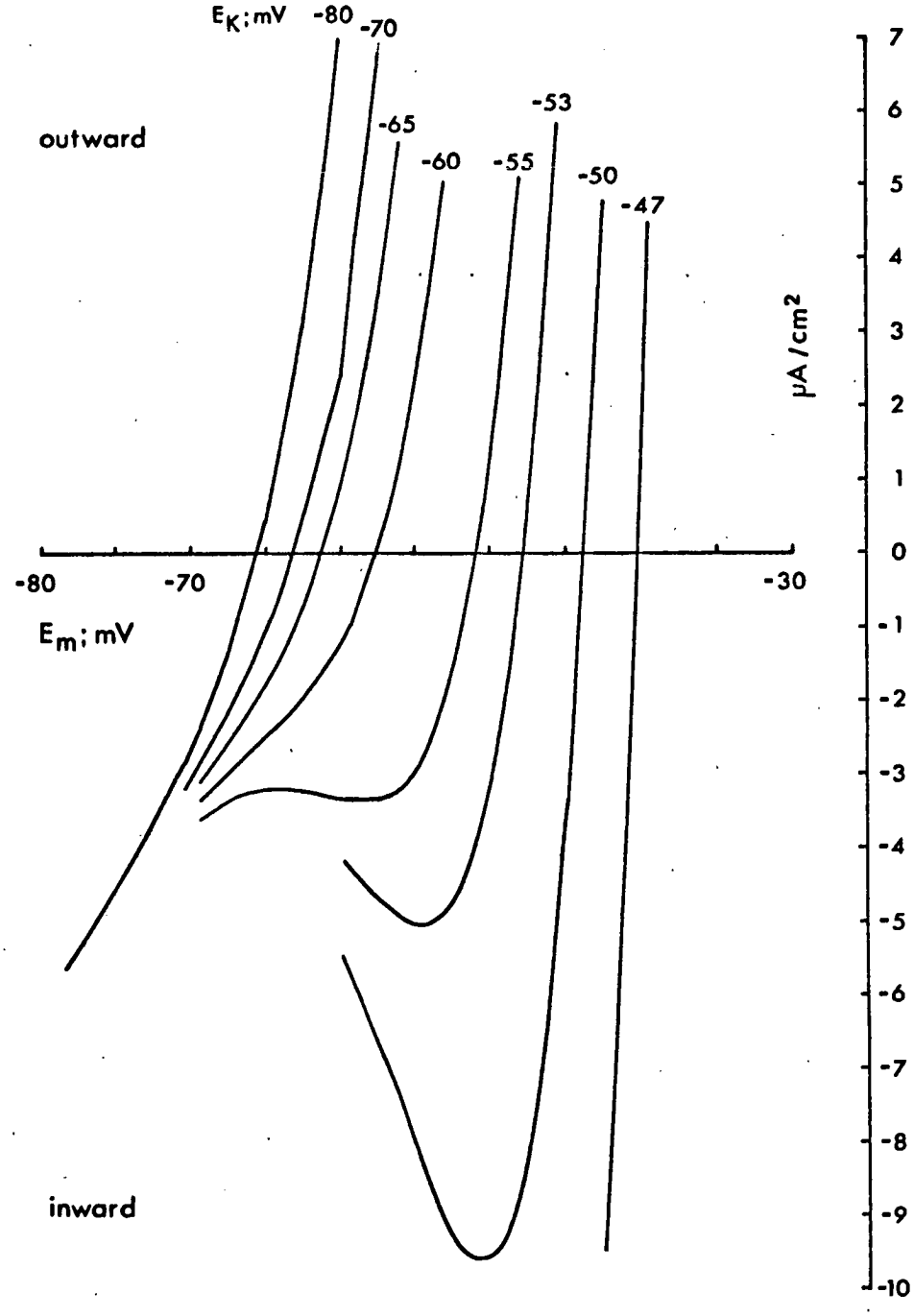

Expanded model;

Early currents; effect of E_K variation ($E_A = E_K$)

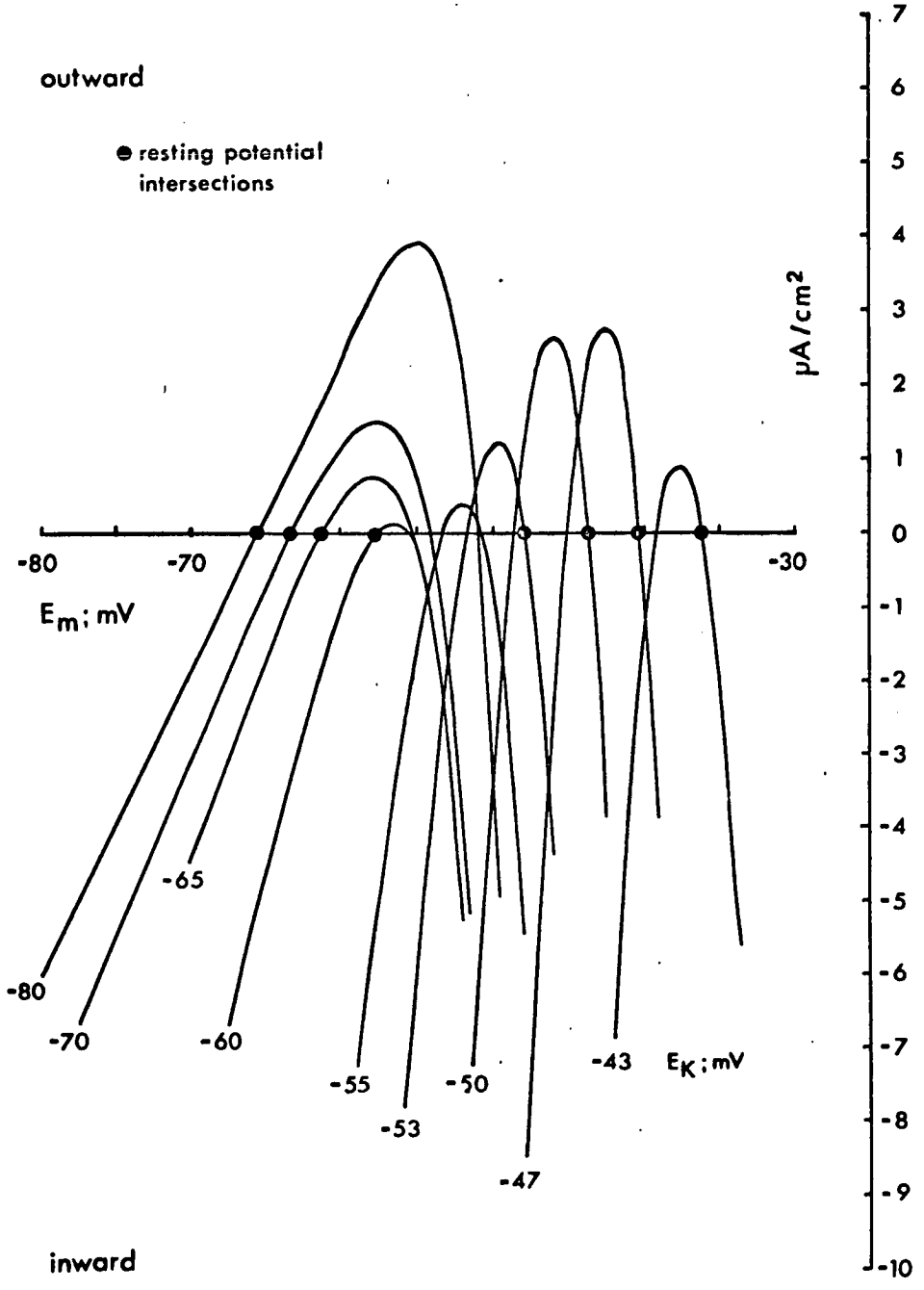

Huxley model are shown in Figure 89 and the corresponding early current-voltage curves in Figure 90. Similarly derived curves for the expanded model are shown in Figures 91 and 92.

It is clear from both sets of results that the effect of small increments in E_K relative to its normal value is to depress the early outward currents associated with small depolarizations from resting potential. For intermediate increments there may be virtually no early outward current while it appears to be restored for larger increments. However, when the early current-voltage curves for larger increments are compared with the corresponding steady-state current-voltage curves it is clear that the steady-state (resting potential) intersection now coincides not with the first intersection of the early current-voltage curve but with its second (threshold) intersection.

When resting potential corresponds to the first early curve intersection the balance of early current associated with a small depolarization will be outward and therefore hyperpolarizing; the system will therefore return to resting potential. However, when resting potential corresponds to the second intersection the balance of early current will be inward and therefore depolarizing even for the smallest depolarization. The system is therefore unstable and an action potential will be produced for any depolarizing deviation from resting potential. This is clearly the current-voltage curve requirement for intrinsic pacemaker activity.

(The progressive development of a negative resistance region in the steady-state current-voltage curves (Figures 89 and 91) is of some interest in the context of recent results obtained from bursting neurons and is discussed in Chapter 6.)

3) Action potential simulations;

The prediction of intrinsic pacemaker activity by the absolute potential current-voltage curves has been confirmed by action potential simulation. Figure 93 shows the result obtained with the Hodgkin-Huxley simulation programme (Appendix 2) for E_K = -60 mV. A brief (10 msec) stimulus at the beginning of the simulated time (200 msec) initiates a single action potential as expected from the corresponding theoretical early current-voltage curve. When E_K = -57 mV and resting potential coincides with the second early curve intersection pacemaker activity is initiated and continues throughout the simulated time (Figure 94). If E_K is further increased to -55 mV there is an increase in the frequency of spontaneous activity and a reduction in action potential amplitude (Figure 95).

The expanded model simulation programme (Appendix 4) generates a similar set of results. However, the critical value for E_K in this case is somewhat higher. The simulation for E_K = -57 mV (Figure 96) does not show spontaneous activity. A series of damped subthreshold oscillations can nevertheless be identified; these occur at a frequency which is similar to but lower than that of the spontaneous action potentials present when the simulation is carried out with E_K = -55 mV (Figure 97). With E_K = -53 mV (Figure 98) there is an increase in action potential frequency and a reduction in amplitude.

The difference between the frequencies of spontaneous action potentials predicted by the two models is rather slight. This indicates that the maximum value assigned to the additional

FIGURE 93; p126

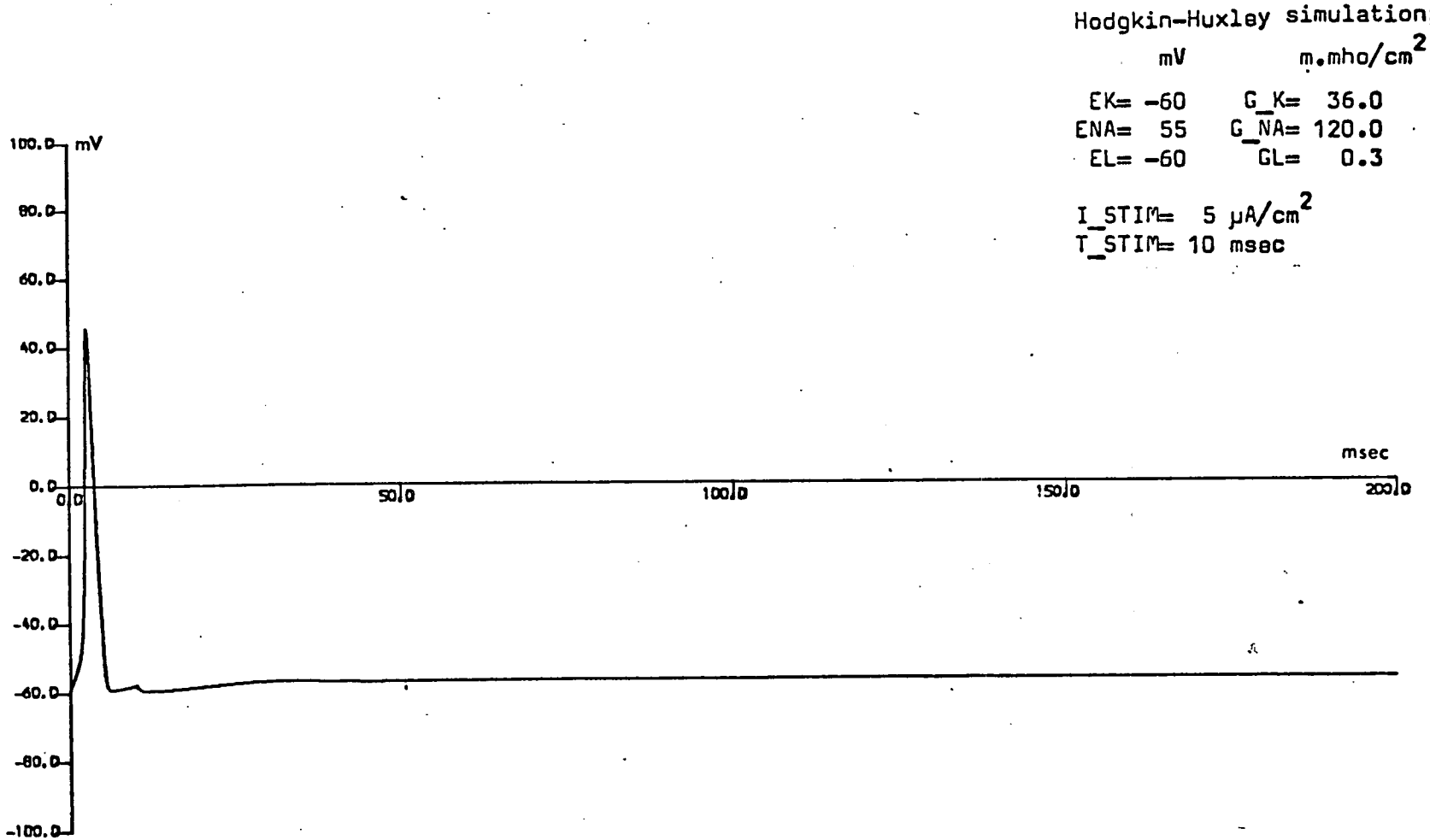

FIGURE 94; p126

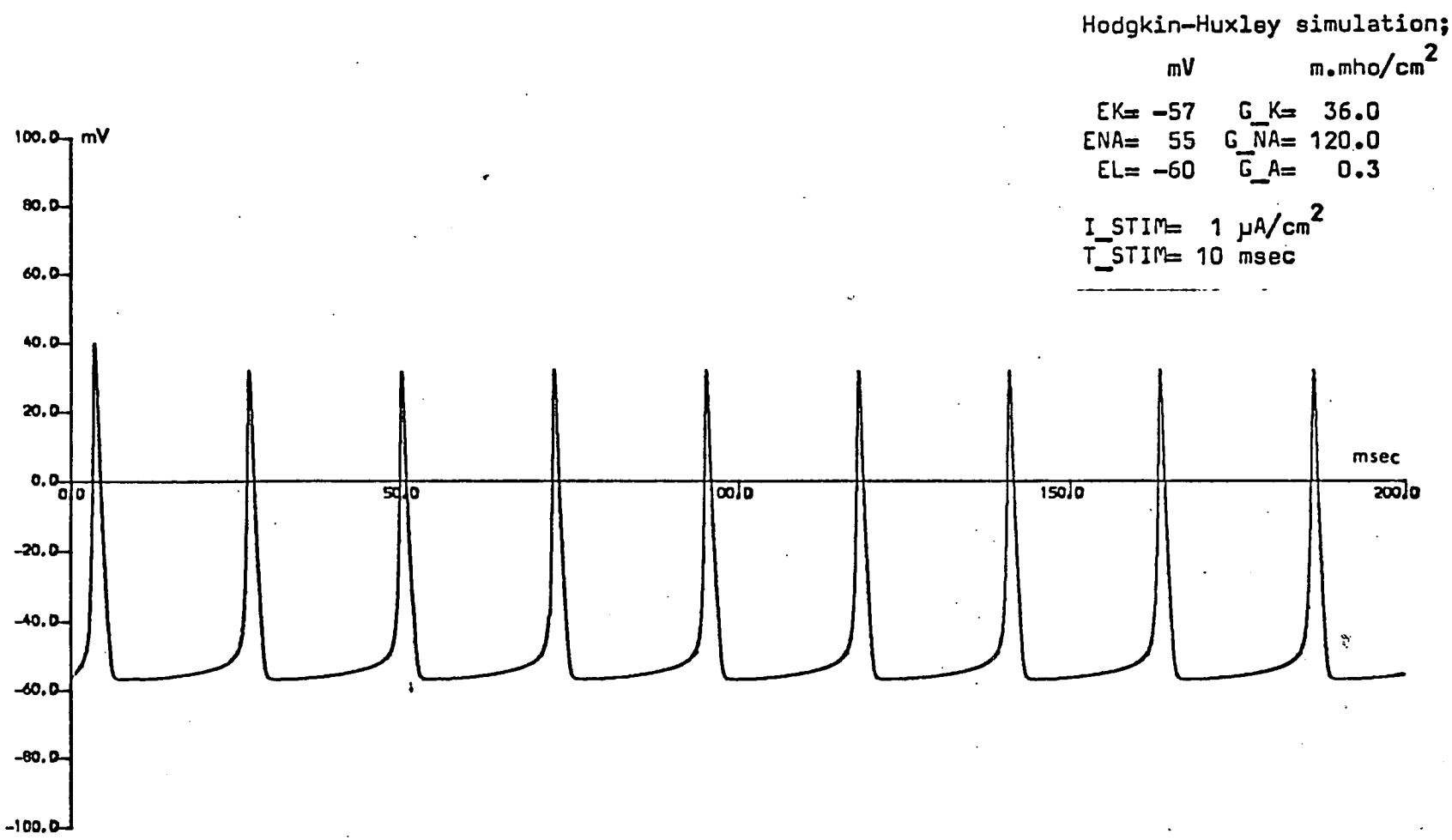

FIGURE 95; p 126

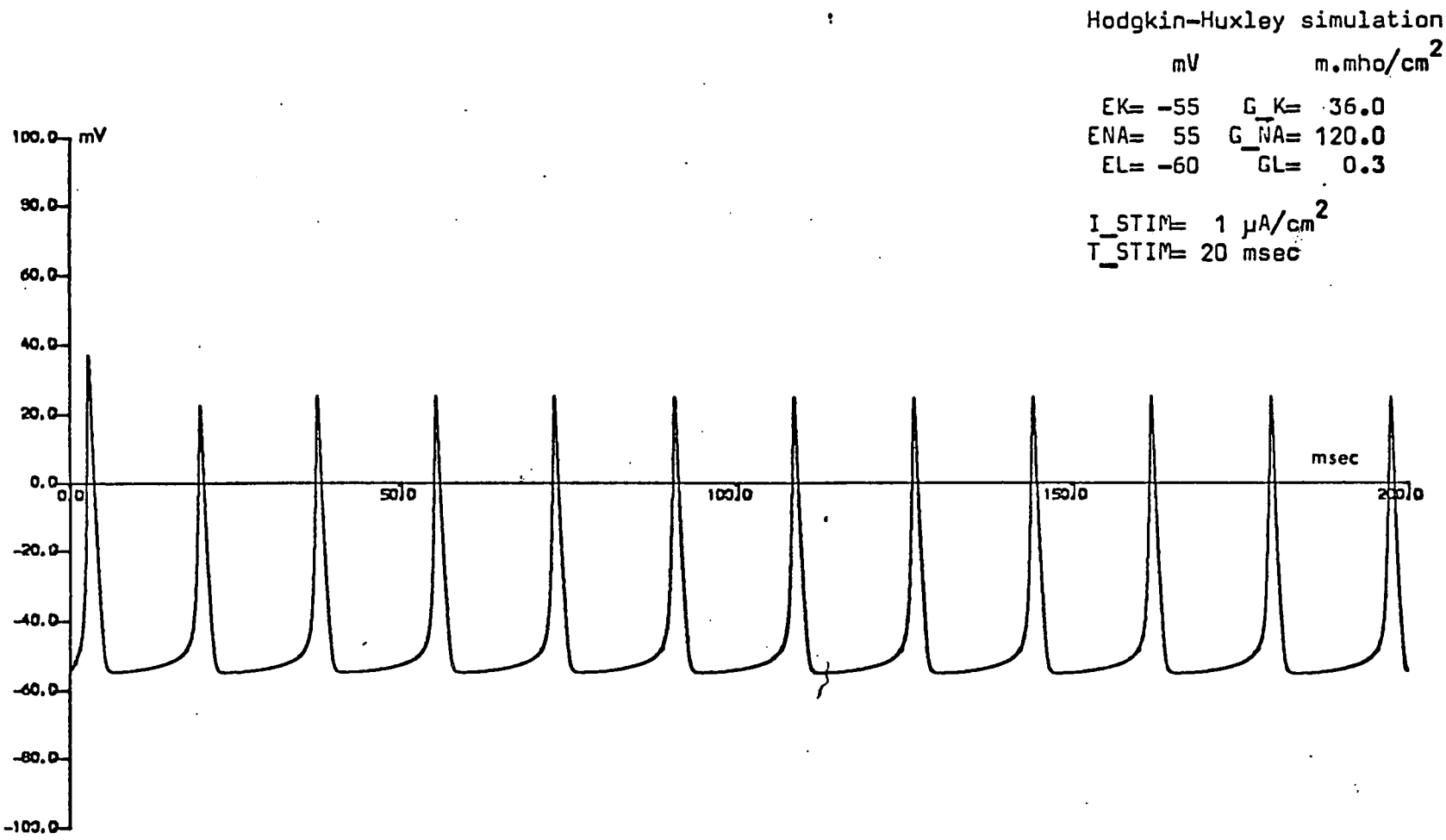

FIGURE 96; p126

Expanded model simulation;

	mV		m.mho/cm^2
EK=	-57	G_K=	36.0
ENA=	55	G_NA=	120.0
EA=	-57	G_A=	40.0
EL=	-60	GL=	0.3

I_STIM= 10 μA/cm^2
T_STIM= 10 msec

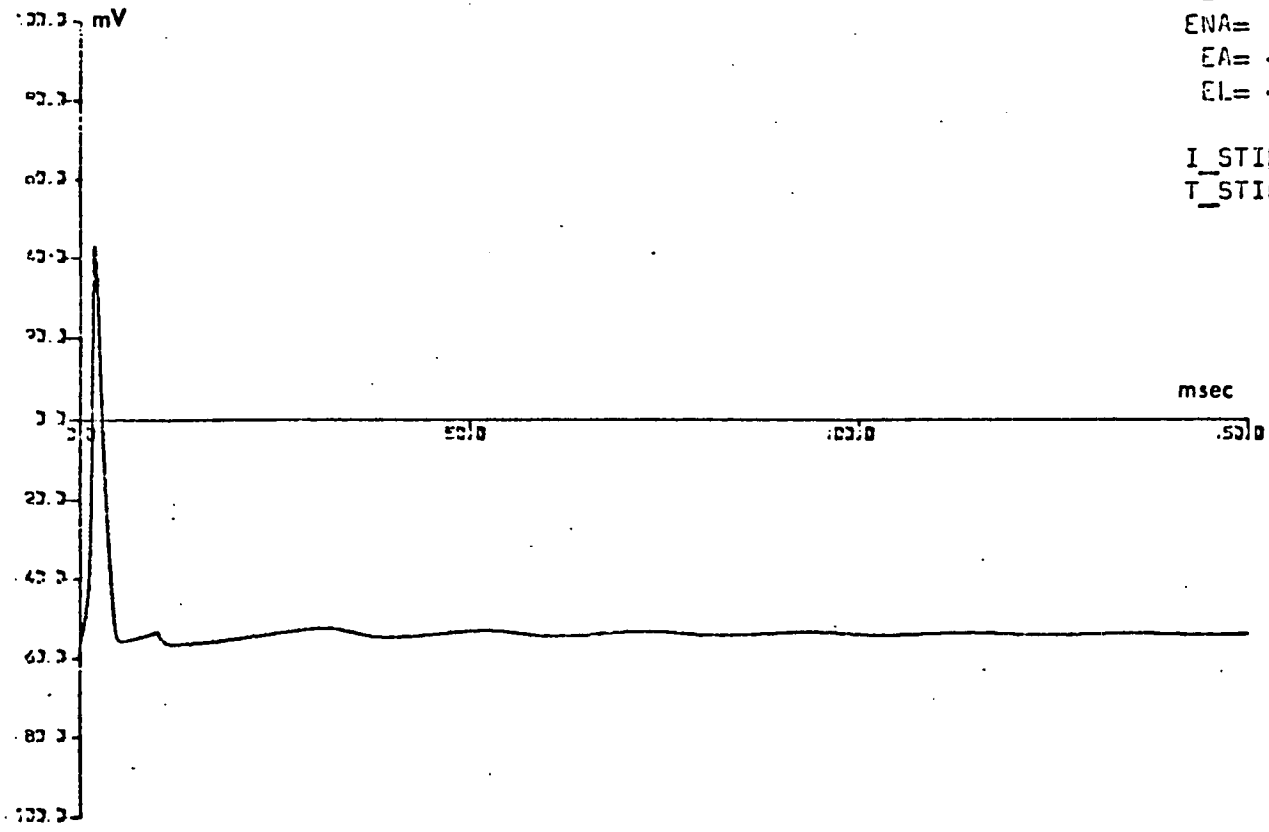

FIGURE 97; p126

Expanded model simulation;

mV		m.mho/cm^2	
EK=	-55	G_K=	36.0
ENA=	55	G_NA=	120.0
EA=	-55	G_A=	40.0
EL=	-60	GL=	0.3

I_STIM= 10 μA/cm^2
T_STIM= 10 msec

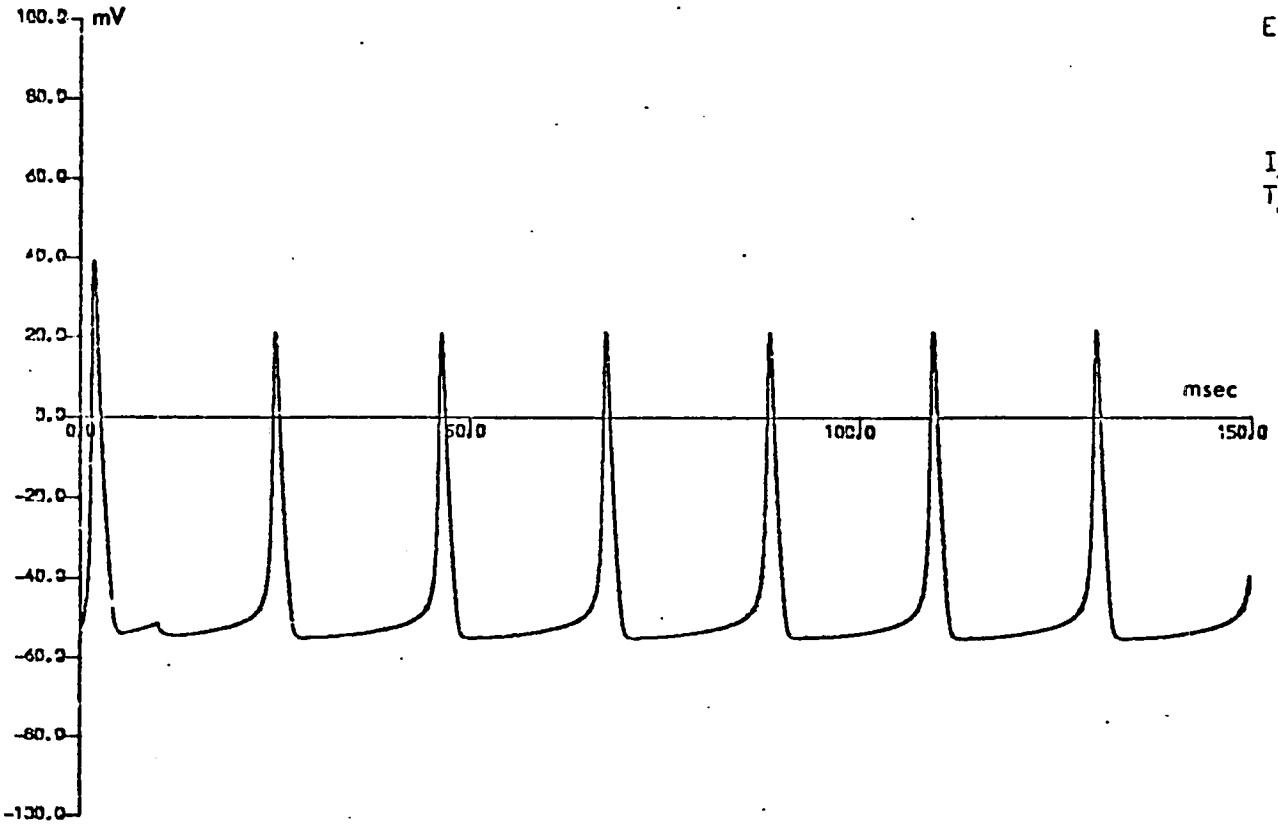

FIGURE 98; p126

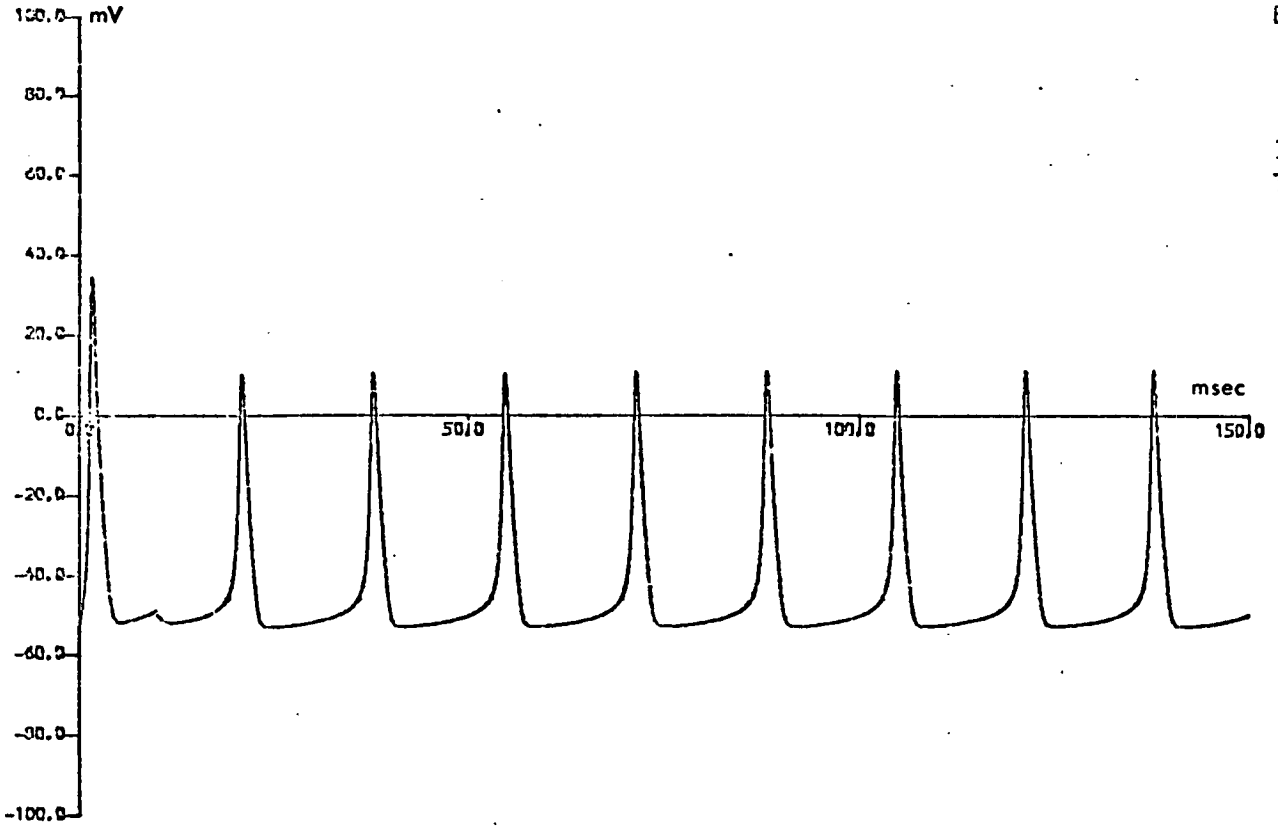

Expanded model simulation;

mV		m.mho/cm^2	
EK=	-53	G_K=	36.0
ENA=	55	G_NA=	120.0
EA=	-53	G_A=	40.0
EL=	-60	GL=	0.3

I_STIM= 10 μA/cm^2
T_STIM= 10 msec

potassium conductance $\bar{g}_A$ is insufficient to offset spontaneous oscillations between the Hodgkin-Huxley variables. These oscillations are seen in the $E_K = -57$ mV situation of Figure 96 apparently superimposed on another change in membrane potential with a much longer time-constant. The value chosen as appropriate for $\bar{g}_A$ for the purposes of the theoretical current-voltage curve calculations is in approximately the same proportion to $\bar{g}_{Na}$ as that indicated by the Connor & Stevens (1971c) analysis for Archidoris. The other parameter values for the expanded model were not correspondingly altered so that the effect of the additional conductance channel could be assessed independently of other changes.

The Connor & Stevens (1971c) analysis was carried out for a neuron soma with a capacitance of 14 pF. If the specific membrane capacity for Archidoris is assumed to be 1.0 $\mu F/cm^2$ a new set of parameter values more appropriate for the expanded model analysis can be derived by scaling the maximum conductance values accordingly. In addition, the time-constants estimated for the conductance-determining variables in Archidoris are rather different from those derived by Hodgkin & Huxley (1952d). The expanded model can be modified to take account of these differences simply by multiplying each of the rate constants by the appropriate (constant) quantity.

When these modifications are made and the expanded model simulations repeated with the new parameter values the predicted frequency of spontaneous action potentials is substantially reduced. Figures 99 to 105 show the simulations obtained for a range of values of E_K. The results are summarized in Figure 106 and the variations in the peak to peak amplitude and in the positive and negative component amplitudes of the simulated action potentials with frequency are shown in Figure 107.

FIGURE 99; p127

Expanded model simulation;

	mV		m.mho/cm^2
EK=	-69	G_K=	15.0
ENA=	55	G_NA=	150.0
EA=	-69	G_A=	85.0
EL=	-40	GL=	0.4

E(initial)= -57.00925
E(final) = -56.05629

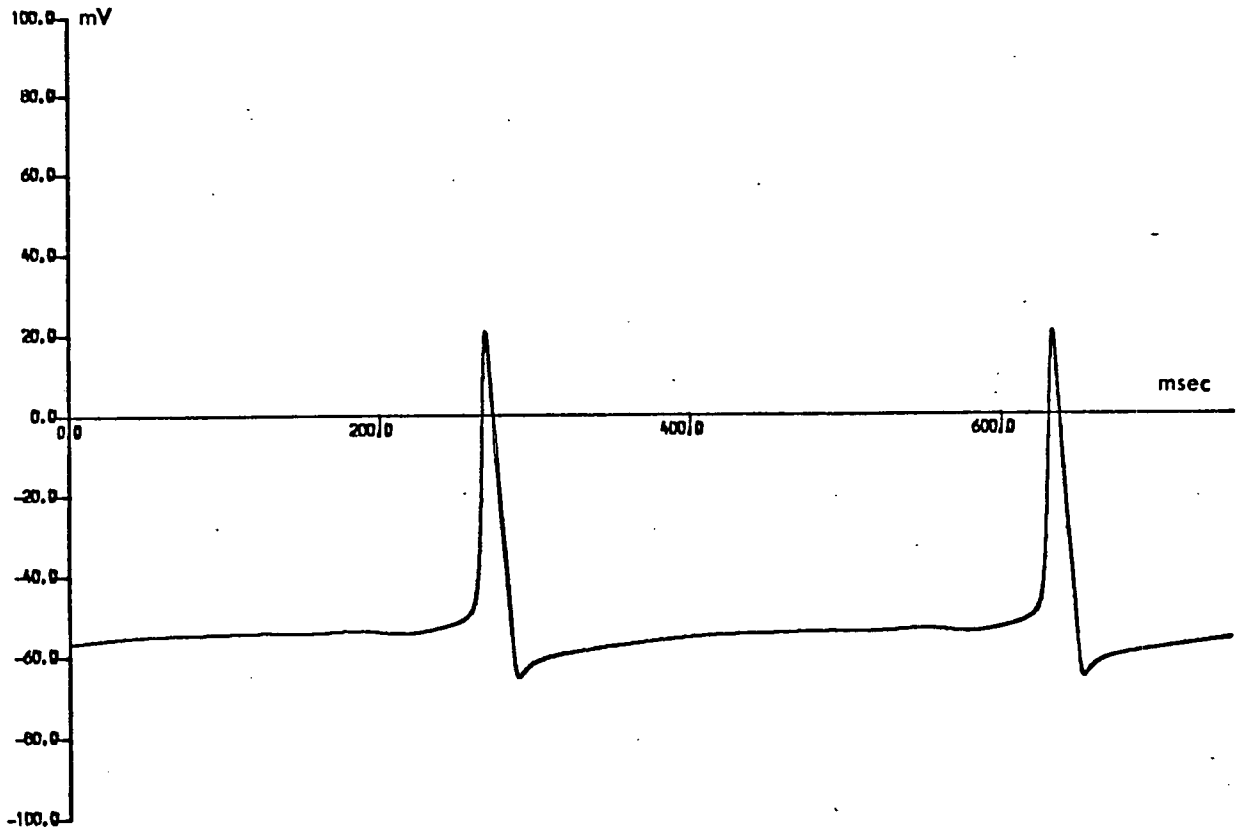

FIGURE 100; p127

Expanded model simulation;

mV		m.mho/cm^2	
EK=	-67	G_K=	15.0
ENA=	55	G_NA=	150.0
EA=	-67	G_A=	85.0
EL=	-40	GL=	0.4

E(initial)= -58.52632
E(final) = -55.57855

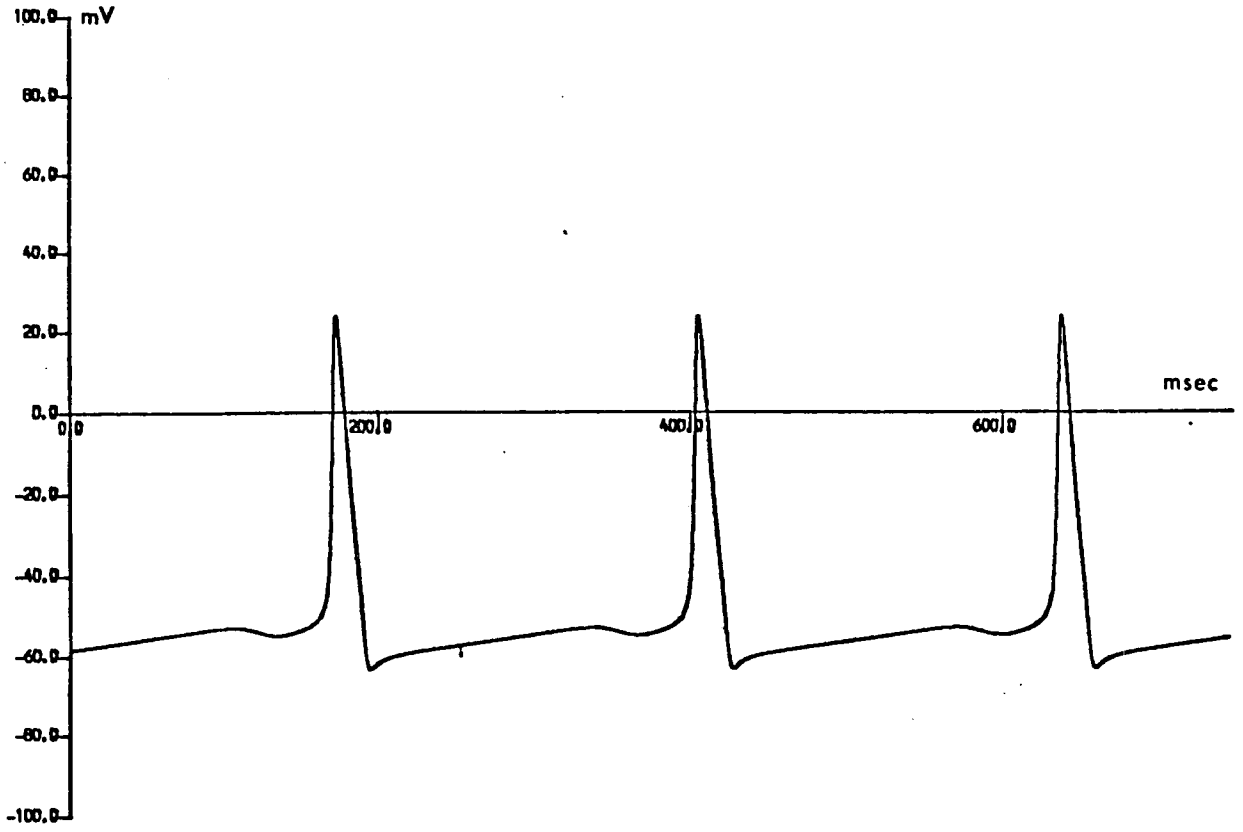

Expanded model simulation;

mV		m.mho/cm^2	
EK=	-65	G_K=	15.0
ENA=	55	G_NA=	150.0
EA=	-65	G_A=	85.0
EL=	-40	GL=	0.4

E(initial)= -56.60599
E(final) = -57.71846

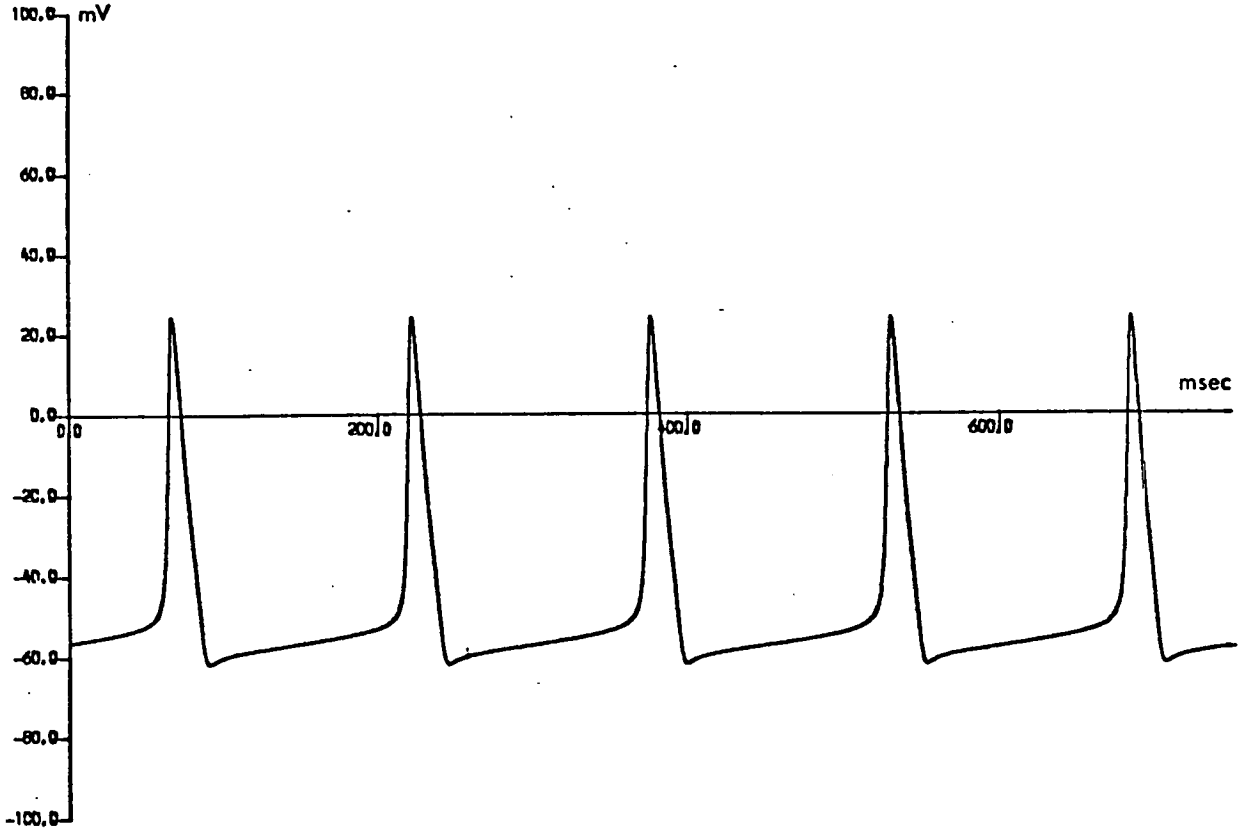

FIGURE 102; p 127

Expanded model simulation;

	mV		$m.mho/cm^2$
EK=	-63	G_K=	15.0
ENA=	55	G_NA=	150.0
EA=	-63	G_A=	85.0
EL=	-40	GL=	0.4

E(initial)= 3.532157
E(final) = -57.48357

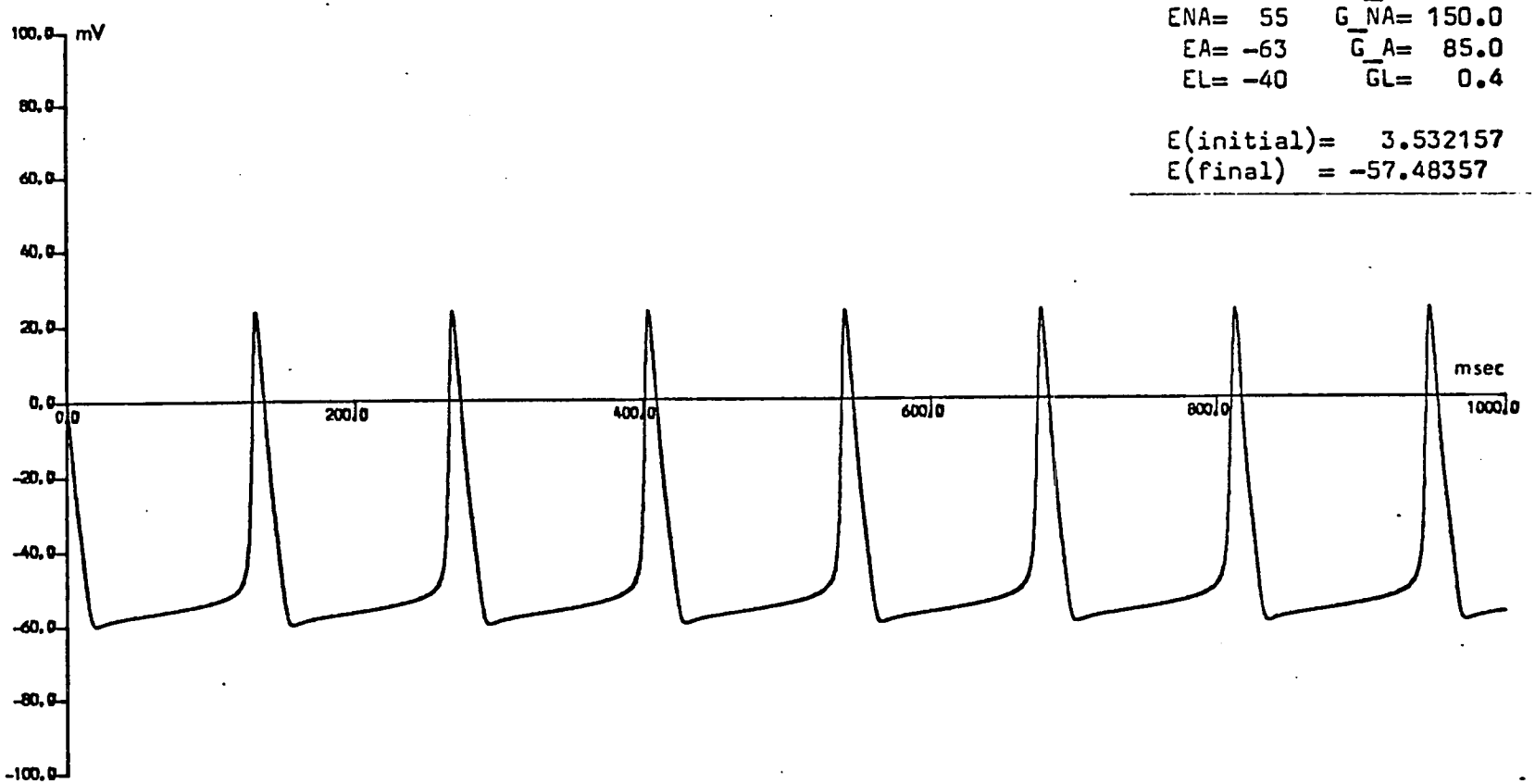

FIGURE 103: p127

Expanded model simulation;

mV		m.mho/cm^2	
EK=	-60	G_K=	15.0
ENA=	55	G_NA=	150.0
EA=	-60	G_A=	85.0
EL=	-40	GL=	0.4

E(initial)= -48.00568
E(final) = -53.83565

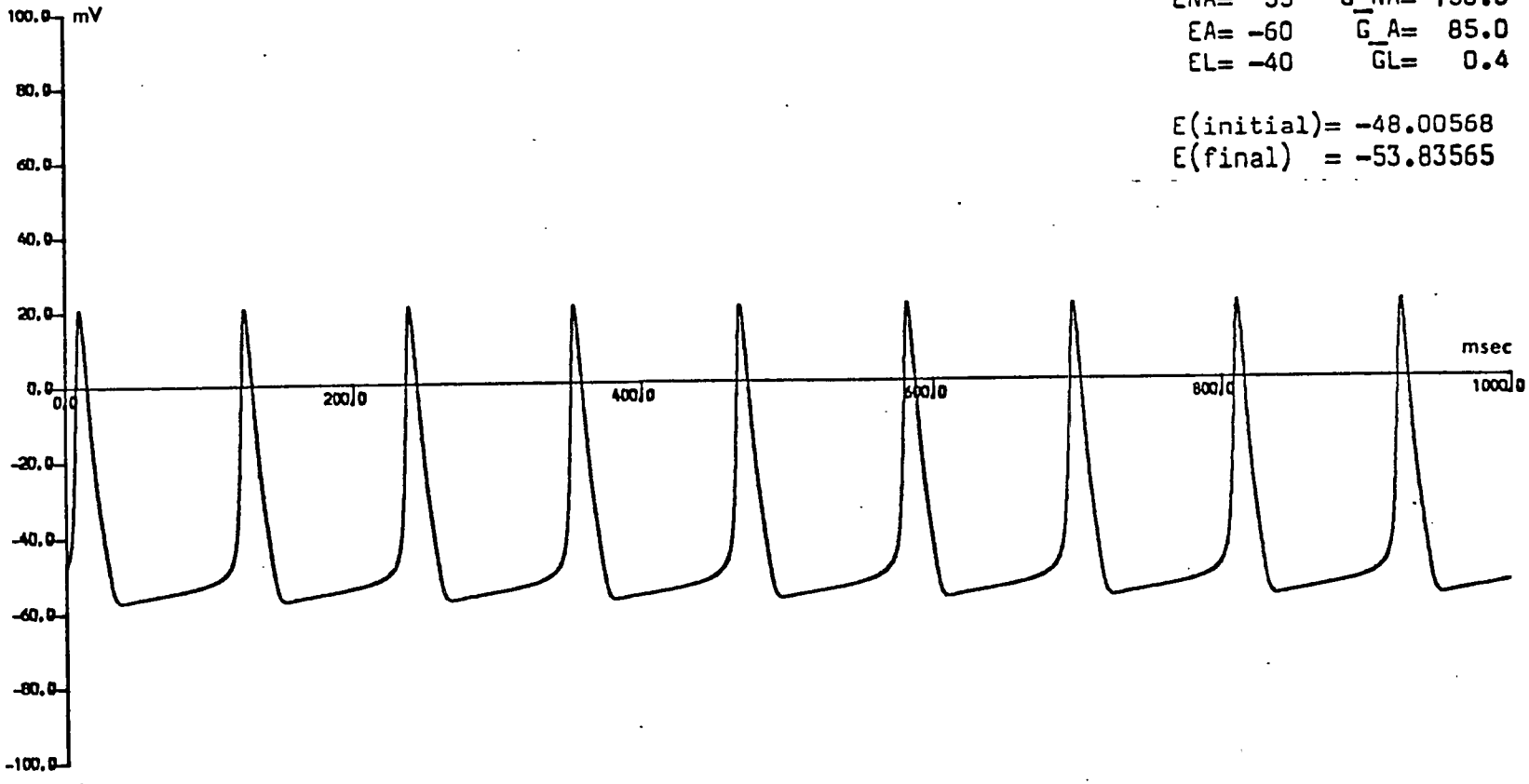

FIGURE 104; p 127

Expanded model simulation;

mV		m.mho/cm^2	
EK=	-57	G_K=	15.0
ENA=	55	G_NA=	150.0
EA=	-57	G_A=	85.0
EL=	-40	GL=	0.4

E(initial)= -47.59358
E(final) = -54.32216

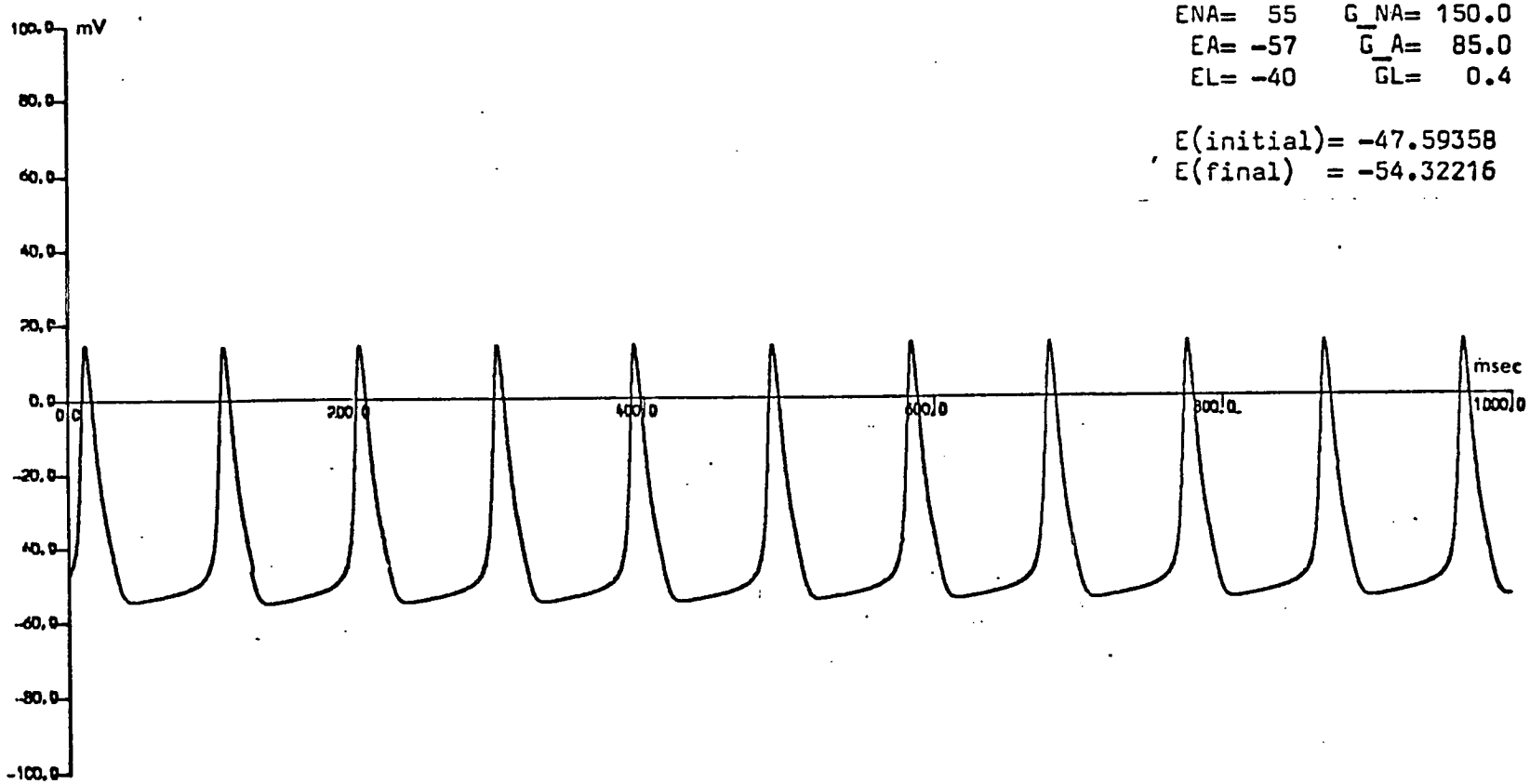

FIGURE 105; p 105

Expanded model simulation;

mV		m.mho/cm^2	
EK=	-55	G_K=	15.0
ENA=	55	G_NA=	150.0
EA=	-55	G_A=	85.0
EL=	-40	GL=	0.4

E(initial)= -51.95717
E(final) = -44.35284

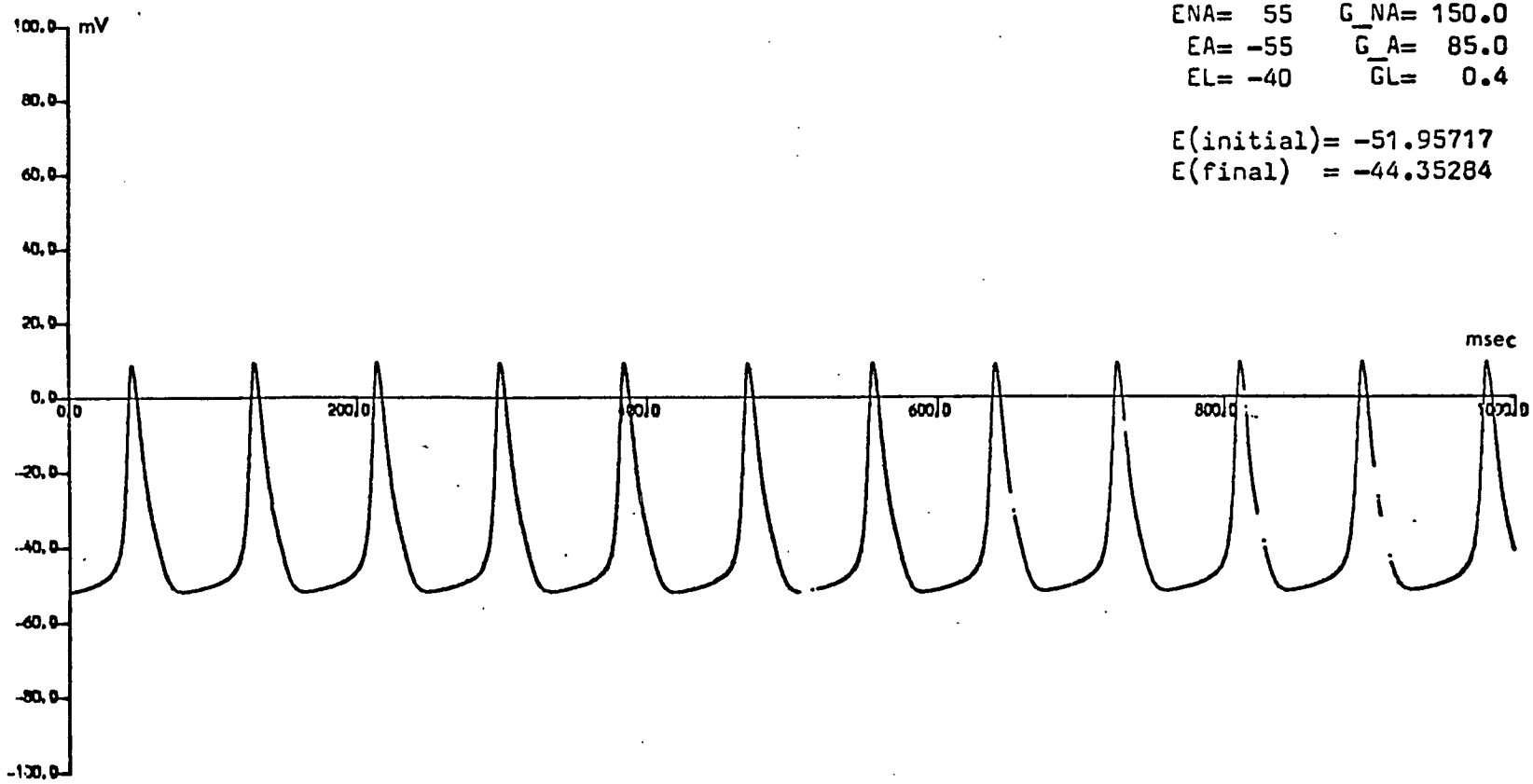

Expanded model;

Relationship between E_K, E_A and spontaneous frequency of simulated action potentials

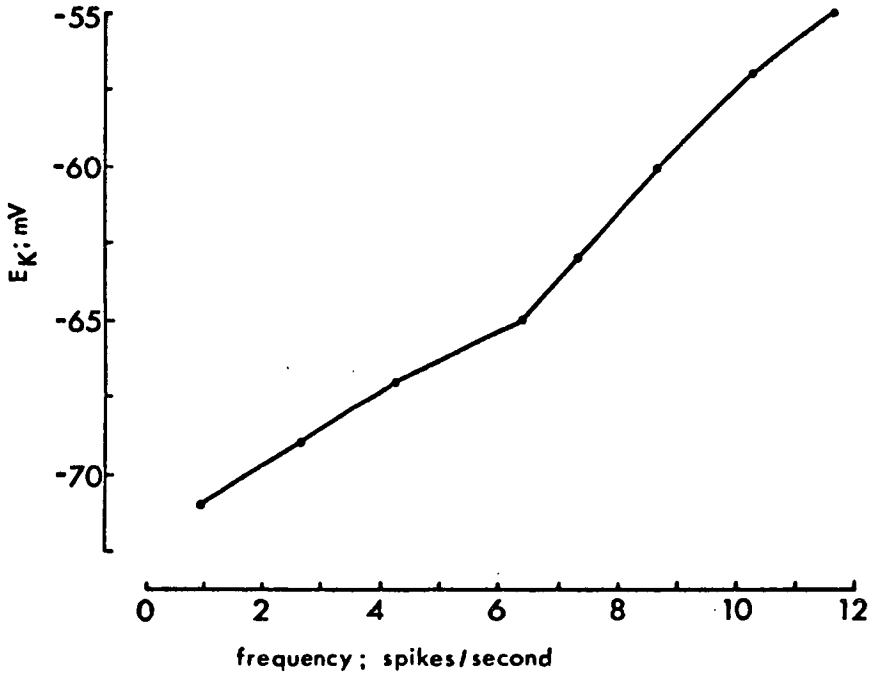

Expanded model;

Relationships between spontaneous frequency and amplitude of simulated action potentials

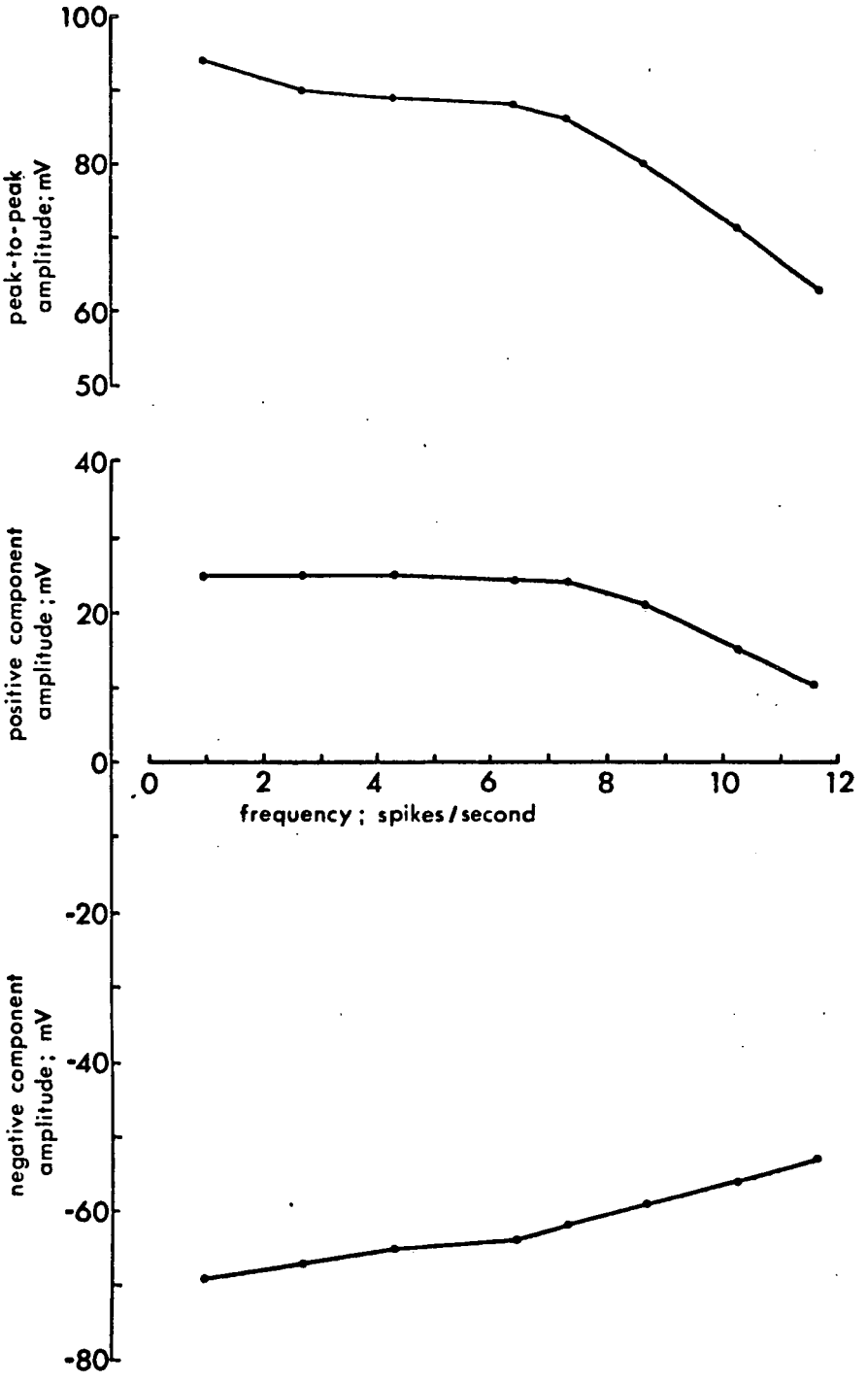

4) Discussion;

These theoretical relationships between the frequency of spontaneous action potentials and their amplitude are not dissimilar in form to thse demonstrated experimentally for spontaneously active cells in the suboesophageal ganglia of Helix aspresa (Figures 38 to 42). This observation leads to the hypothesis that the occurrence and frequency of intrinsic pacemaker activity in the experimental case may also be controlled by variations in the potassium equilibrium potential.

The discrepancy between the magnitudes of the observed and predicted spontaneous frequencies does not present a serious objection to the validity of this hypothesis. Thus the maximum inactivation time-constant (τ_b) for the additional potassium conductance channel implicit in the expanded model calculations, from which the theoretical relationship was derived, was 235 msec corresponding to the value given by Connor & Stevens (1971c) for Archidoris. The maximum inactivation time-constant value in Helix pomatia however may be as high as 1000 msec (NEHER, 1971). If this latter value is nearer to that appropriate for Helix aspersa neurons, as is probable, then much better agreement between predicted and observed frequencies could be obtained. In addition if the activation time-constant (τ_a) for the additional potassium channel were similarly increased, the slope of the relationship between overshoot (positive component) amplitudes and frequency would be greater at lower frequencies and increased overshoot amplitudes would be observed.

It is significant that, for a single value of the

inactivation time-constant (τ_b), the range of spontaneous frequencies available with the expanded model analysis seems entirely adequate to account for the full range of spontaneous frequencies observed experimentally. With the Hodgkin-Huxley analysis however, the minimum spontaneous frequency which can be predicted is moderately high. This situation is paralleled in the unmodified equations for which it has been shown that repetitive activity in response to applied currents occurs either at a high frequency or not at all (STEIN, 1967). However, if random fluctuations in the various parameter values about their steady-state values are allowed to take place, the minimum frequency of repetitive activity can be substantially reduced although the interval between successive action potentials becomes rather variable. While the postulation of such fluctuations seems unnecessary to account for observed frequencies of repetitive activity with the expanded model analysis it may be that naturally-occurring spontaneous activity is dependent to some extent on small random alterations in conductance. In this case, very low frequencies of spontaneous activity could be maintained.

Since there seems to be no particular difficulty in accounting for the range and magnitudes of observed spontaneous frequencies in terms of the expanded model absolute potential equations when the potassium equilibrium potential is varied the problem is now whether the required alterations in intracellular potassium concentrations are within the probable physiological range. The simulation results suggest that a difference of approximately 20 mV between the minimum and maximum values of E_K should be sufficient to provide a complete range of cell types including 'silent' as well as spontaneously active cells.

As previously mentioned, the constant-field approach can be used to estimate intracellular potassium concentrations. While the method may depend on an over-simplified view of changes in resting membrane properties with extracellular potassium concentration, there is no reason to suppose that the approximation for K_i^+ obtained from the slope of the $\exp(\frac{EF}{RT})$ plot will be qualitatively misleading. Thus the slope of the $\exp(\frac{EF}{RT})$ plot derived from the absolute potential equations would vary with intracellular potassium concentration in the same manner as that implied by the constant-field equation. Estimates of variations in K_i^+ derived from the constant-field approach can therefore be regarded as reasonable.

The mean value for K_i^+ in Helix aspersa neurons, as determined by the constant-field approach, is approximately 93 mM (MORETON, 1968). A 20 mV difference between the minimum and maximum values of E_K would require a variation in intracellular potassium concentration of $\pm$ 45 mM with respect to this mean value. In fact the observed variations overlap this range to some extent (MORETON, 1968) and it can be concluded that the variations in intracellular potassium concentration required for the validity of the absolute potential hypothesis of intrinsic pacemaker activity are within the physiological range. The large variations observed in the resting potentials of Helix aspersa neurons are also consistent with a variable intracellular potassium concentration (KERKUT & WALKER, 1961; KERKUT & MEECH, 1966; MORETON, 1968).

Although intracellular potassium concentrations are likely to be much more significant in determining the potassium equilibrium potential, in Aplysia there is some evidence that the extracellular space around pacemaker cells is restricted such that

the immediate extracellular concentration of potassium ions may be higher than that in the extracellular fluid as a whole (ALVING, 1969; EATON, 1972). The accumulation of ions seems to be associated with extensive infoldings of the neuron membrane. However, in Anisodoris, similar membrane infoldings seem to represent only a relatively minor restriction to diffusion (MIROLLI & GORMAN, 1973) and it is suggested that a difference larger than 2 mM between the potassium concentration of the bathing solution and that of the fluid layer adjacent to the neuron membrane cannot be maintained under most conditions. While this difference seems small the alteration in E_K relative to the value expected from the concentration of potassium in the bathing solution could be as much as 5 or 10 mV if the bathing concentration is fairly low. The possibility that a restricted extracellular space could, in some cases, make a significant contribution to pacemaker activity cannot be definitely excluded. It is tempting to suggest that membrane invagination represents an adaptation for intrinsic activity per se but it is more likely that the higher rate of potassium efflux from spontaneously active cells requires a slight restriction to extracellular diffusion such that accumulating potassium ions can be transported back across the membrane by means of the metabolic Na-K exchange pump.

It is significant that the variations required in the potassium equilibrium potential and in the naturally-occurring intracellular and extracellular potassium concentrations are not extreme and therefore should not have any appreciable effect on the absolute potential dependency of the conductance determining variables. On the other hand, the alterations in sodium and/or

calcium equilibrium potentials required for the production of theoretical pacemaker current-voltage curves are very large, outwith the probable physiological range and liable to affect absolute potential dependencies. Although large reductions in extracellular calcium concentration can initiate spontaneous activity (FRANKENHAEUSER & HODGKIN, 1957) this is most unlikely to be of physiological significance. In addition, the observed relationship between spontaneous action potential amplitude and frequency cannot be interpreted in terms of E_{Na} variation since this implies an increase in amplitude with frequency.

The importance of the leakage equilibrium potential is less easy to assess. The theoretical current-voltage curves suggest that, over a certian range, the contribution of E_l in determining membrane potential is comparable to that of E_K. Essentially, variations in E_l over this range could mimic the effect of variations in E_K. This suggestion seems consistent with the experimental observations of Figures 41 and 42. Clearly, changes in chloride equilibrium potential could modulate spontaneous frequencies. However, variations in intracellular chloride concentration cannot fully account for intrinsic activity since, at least in the case of Helix aspersa, the chloride equilibrium potential of spontaneously active cells may lie above or below 'resting' potential (KERKUT & MEECH, 1966).

The theoretical current-voltage curves (Figures 70-88) show that variations in the maximum ionic conductances affect resting potential and threshold comparatively little except in the case of $\bar{g}_A$. Since the contribution of the additional potassium channel to membrane potential is always hyperpolarizing, variations

in $\bar{g}_A$ cannot account for the occurrence of intrinsic activity but can only alter the frequency of action potentials produced by an already spontaneously active membrane. This method of control would also predict an increase in amplitude with frequency and is therefore inconsistent with the observed relationship. A final possibility, that pacemaker frequency is controlled by the time-constants of g_A, seems improbable since this would appear to require a distinct membrane structure for each spontaneous frequency.

While variation in any of the above parameters could alter pacemaker frequency to some extent, it remains probable that the potassium equilibrium potential is the significant determinant for pacemaker activity and that the effect of variation in other parameters is secondary.

It has been suggested that a relatively high 'resting' sodium conductance may account for the occurrence of Purkinje fibre pacemaker potentials (TRAUTWEIN & KASSEBAUM, 1961) and more recently a similar explanation has been advanced for intrinsic activity in molluscan neurons (CARPENTER, 1973). Since depolarization can only occur when the flow of inward currents exceeds the flow of outward currents such explanations in effect state a truism; clearly the current associated with the 'resting' sodium conductance must exceed that associated with the 'resting' potassium conductance, otherwise intrinsic activity would not occur. Thus, a relatively high 'resting' sodium conductance (g_{Na}) does not necessarily imply a correspondingly high maximum conductance ($\bar{g}_{Na}$). Within the framework of the absolute potential equations and the potassium equilibrium potential hypothesis the relatively high 'resting' sodium conductance necessary for intrinsic activity occurs as a

result of the depolarization associated with reductions in intracellular potassium concentration.

Throughout the theoretical analysis it has been assumed that the functions describing the changes in the rate constants of the conductance determining variables with time and voltage can be regarded as constant for a given preparation. If this were not the case then alternative mechanisms of intrinsic activity could be proposed. However, there is no experimental evidence to suggest that individual pacemaker cells differ significantly in respect of the time and voltage dependency of the rate constants. Although such mechanisms cannot be definitely excluded, the potassium equilibrium potential hypothesis is much more economic and, as shown above, is consistent with all the available experimental evidence.

The direct test of the predicted relationship between intracellular potassium concentration and spontaneous action potential frequency using ion-sensitive electrodes is an obvious possibility. Some attempt was made to manufacture ion-sensitive electrodes after the method described by Neher & Lux (1973) using an ion-exchange oil (Corning K^+ ion-exchanger No. 477317). The method involves rendering the tip of the microelectrode hydrophobic by treatment with a 4% solution of dichlorodimethylsilane in CCl_4. The electrodes are then filled with methanol under reduced pressure and immediately transferred to distilled water. After 3–4 hours the water is replaced by a 1 M KCl solution. Before use the electrode tips are dipped in ion-exchange oil and should fill spontaneously or when suction is applied. No particular difficulty was experienced in preparing electrodes according to this schedule; treated electrodes

which failed to become hydrophobic could be identified by their relatively low resistance (20-30 megohms) while the resistance of hydrophobic electrodes was so high that it could not be estimated with available equipment. When the tip of a hydrophobic electrode was filled with the ion-exchange oil its resistance fell sufficiently for its magnitude to be estimated but it was nevertheless exceedingly high - typically exceeding 10 gigaohms. Accurate potential measurement through such an immense electrode resistance would require an amplifier input impedance of at least 10^{14} ohms. The amplifiers described in the Materials and Methods section fall appreciably short of this requirement and a suitable alternative device was not readily available. In view of this and the additional technical problems associated with very high impedance recording circuits and also because of the obvious need for careful calibration of ion-sensitive electrodes and the relative difficulty of inserting the two intracellular microelectrodes necessary for measuring intracellular potassium concentrations, it was clear that the direct test of the potassium equilibrium potential hypothesis would be a rather time consuming process. The hypothesis could also be tested rather less directly using the constant-field equation to estimate intracellular potassium concentration. This method although technically easier would be scarcely less protracted than that using ion-sensitive electrodes and is of doubtful accuracy as previously indicated. The test of the hypothesis by either method is therefore outwith the scope of the present project.

5) Temperature effects;

Any examination of temperature effects has been excluded from the theoretical analysis. The original Hodgkin-Huxley

equations and their absolute potential equivalents refer to a temperature of 6.3°C while the Connor & Stevens equations were obtained for 5°C. This difference is slight and was disregarded in developing the expanded model described above. A common Q_{10} is usually assumed for all the rate constants and in this case the effect of increases in temperature is simply to contract the time scale of predicted activity. This assumption satisfactorily accounts for the temperature dependent alterations in the frequency of repetitive activity elicited from the squid giant axon in response to depolarizing stimuli (GUTTMAN & BARNHILL, 1970). The situation is less clear in Aplysia where temperature changes can have a rather variable effect on spontaneous activity (MURRAY, 1966).

Chapter 6

BURSTING PACEMAKERS

A) Introduction:

The development of a satisfactory theoretical explanation of intrinsic monotonic pacemaker activity using the Hodgkin-Huxley equations in an absolute potential form poses the question of whether the theoretical analysis can be extended to account for the activity of a second category of intrinsic pacemakers - those showing a bimodal or bursting pattern of action potential generation. While the characteristic activity pattern of bursting neurons is well known, the bursting cycle is sometimes rather irregular and the distinction between the two categories of pacemaker can best be illustrated in terms of the frequency distribution of interspike intervals. Thus, the distribution of interspike intervals from a monotonic pacemaker is continuous and usually slightly skewed or normal in form with the intervals distributed about a single modal value (KISS, 1973). On the other hand, the distribution of interspike intervals from a bursting pacemaker may be discontinuous and is always clearly bimodal in form. Characterized in this way, bursting neurons can be identified even in the absence of a regular activity cycle.

As a preliminary to further theoretical analysis, the properties of the Big-D cell of Helix aspersa have been studied in some detail. This cell frequently shows a regular bursting rhythm of action potential discharge and, as previously stated, can be identified in a majority of preparations.

B) Big-D cell properties;

1) Range of spontaneous activity;

The range of spontaneous activity which can be recorded from the Big-D cell is illustrated in Figure 108; record (A) shows a pattern of discharge which can be regarded as typical, with more or less regularly spaced bursts each consisting of a relatively constant number of action potentials. Usually the number of spikes present in each burst lies in the range 6-12 but occasionally the number may exceed 20 as in record (C). In a proportion of cases, Big-D cell activity is less regular and individual bursts appear to be prolonged as in record (E). Alternatively, the discharge may be so irregular that no clear bursting rhythm can be identified although hyperpolarizations of a typically interburst form are clearly present (record (B)). Less commonly, as in record (D), such hyperpolarizations are completely absent and the Big-D cell fires monotonically. However, a bursting rhythm usually develops in cells of this type when recording is prolonged for 30 minutes or more.

2) Characteristics of burst generation;

In cells which show a regular bursting cycle the characteristics of the action potentials which constitute an individual burst are not constant but change progressively within the burst. These changes are more obvious in cells which show a particularly well developed bursting rhythm and for this reason the characteristics of burst generation have been quantified by analysis of the photographic record obtained from such a cell. Burst duration, interburst interval, the maximum interburst hyperpolarization and the

Big-D cell; Range of spontaneous activity

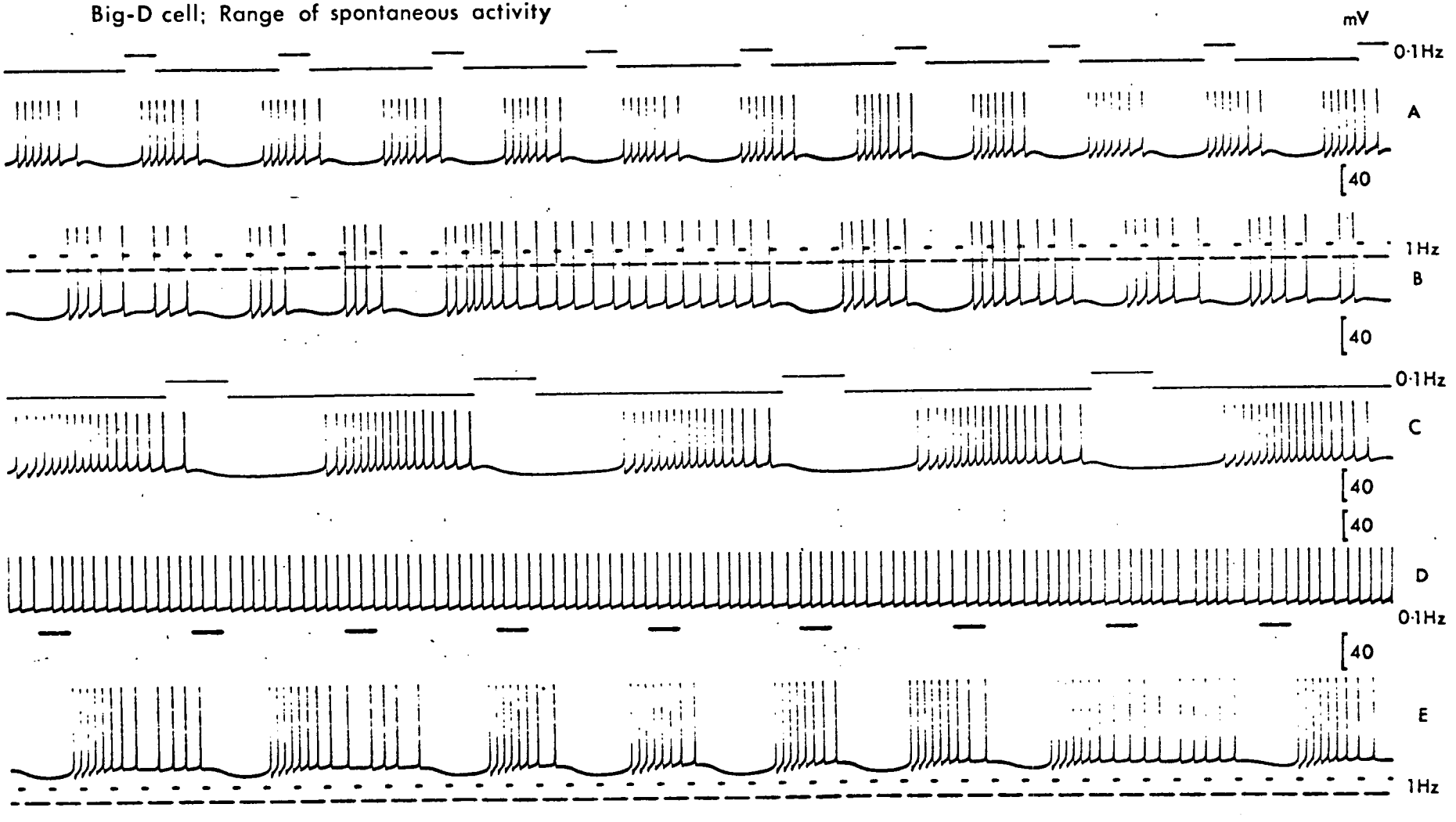

potential level at the termination of the burst were measured for each of the 20 consecutive bursts shown in Figure 109. The prespike interval, overall amplitude, positive component(overshoot) amplitude and negative component (undershoot) amplitude were measured for each of the 24 or 25 action potentials in each burst and the results were grouped according to action potential serial number within the burst. Table 8 gives the mean values determined for all these parameters; the range of observation (2 standard deviations) is indicated where appropriate. Instantaneous action potential frequency was obtained as the reciprocal of the mean prespike interval in each case. The components of action potential amplitude were measured initially with respect to the base level of a time calibration trace and were corrected according to the extracellular (zero) potential level determined both before and after the intracellular recording. As previously, all measurements were made with vernier calipers.

The results of Table 8 were plotted in the manner shown in Figure 110 to provide a statistical bursting pattern representative of this example of Big-D cell activity. The bursting rhythm has a period of about 12 sec. consisting of an interburst interval of 6.5 sec. and a burst duration of 5.5 sec. Action potential amplitude is at a maximum at the beginning of the burst and declines rapidly at first but shows a slight recovery towards the end of the burst. These alterations are largely the result of changes in the magnitude of the negative components of successive action potentials; the positive component (overshoot) amplitudes increase gradually throughout the burst. This increase in overshoot is unexpected; in terms of the Hodgkin-Huxley equations the sodium inactivation variable h should increase with hyperpolarization during the

Big-D cell; well developed bursting rhythm

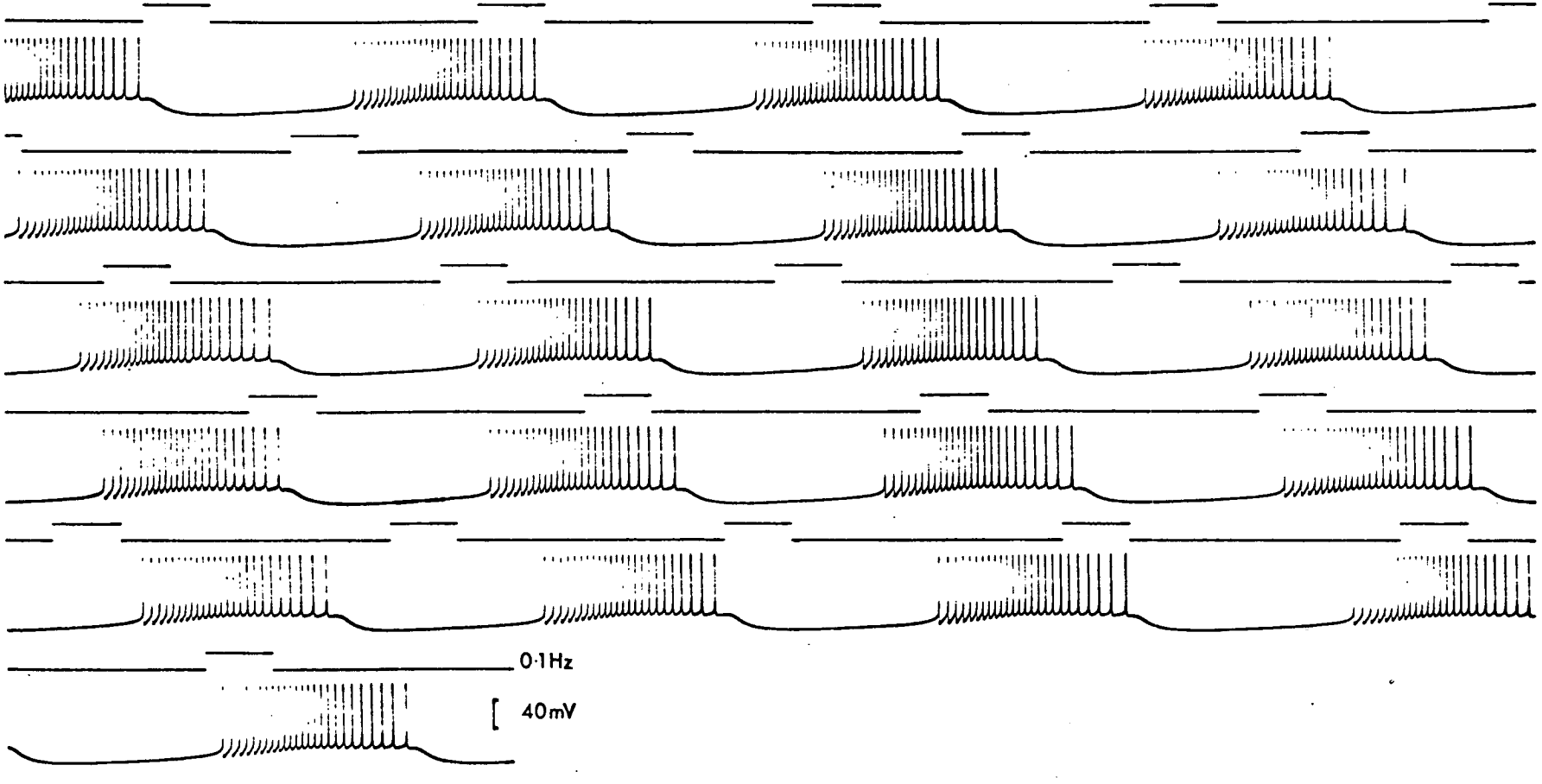

Table 8.

Characteristics of Big-D cell activity;

Burst duration	5359(354.60) msec
Interburst interval	6447(314.77) msec
Mean duration; interval ratio	0.83
Maximum pre-hyperpolarization	53.80(2.37) mV
Burst terminating level	36.64(2.52) mV

No.	Overall amplitude (mV)	Positive component (overshoot) amplitude (mV)	Negative component (undershoot) amplitude (mV)	Preepike interval (msec)	Hz	N
1	81.40(1.36)	34.16(2.55)	47.24(1.98)	6447(314.77)	0.16	20
2	81.00(1.46)	34.36(2.35)	46.64(1.81)	264 (20.93)	3.79	20
3	80.36(1.22)	34.56(2.57)	45.80(1.71)	242 (25.63)	4.13	20
4	79.92(1.26)	34.88(2.56)	45.04(1.88)	222 (22.10)	4.50	20
5	79.24(1.32)	34.96(2.49)	44.28(1.74)	206 (26.28)	4.85	20
6	78.68(1.19)	35.24(2.41)	43.44(1.88)	198 (17.89)	5.05	20
7	78.04(1.22)	35.52(2.67)	42.52(2.03)	189 (20.42)	5.29	20
8	77.36(1.28)	35.80(2.54)	41.56(1.98)	184 (20.93)	5.43	20
9	76.68(1.19)	36.12(2.76)	40.56(2.21)	182 (22.10)	5.49	20
10	75.80(1.14)	36.08(2.48)	39.72(2.09)	177 (19.57)	5.65	20
11	75.16(1.32)	36.28(2.61)	38.88(2.51)	173 (19.57)	5.78	20
12	74.60(1.26)	36.48(2.77)	38.12(2.34)	175 (17.77)	5.71	20
13	74.16(1.28)	36.48(2.95)	37.68(2.74)	177 (14.65)	5.65	20
14	73.76(1.34)	36.40(2.82)	37.36(2.60)	187 (23.49)	5.35	20
15	73.64(1.10)	36.44(2.29)	37.20(2.35)	189 (20.42)	5.29	20
16	73.48(0.78)	36.32(2.51)	37.16(2.46)	195 (17.77)	5.13	20
17	73.52(0.64)	36.40(2.29)	37.12(2.23)	210 (20.52)	4.76	20
18	73.72(0.94)	36.72(1.94)	37.00(1.79)	218 (17.89)	4.59	20
19	73.96(1.10)	36.96(1.69)	37.00(1.71)	234 (18.81)	4.27	20
20	74.24(1.34)	37.12(1.90)	37.12(1.83)	245 (22.00)	4.08	20
21	74.56(0.98)	37.40(2.00)	37.16(2.04)	270 (30.44)	3.70	20
22	74.84(1.22)	37.56(2.04)	37.28(2.10)	295 (34.03)	3.39	20
23	75.08(1.19)	37.60(2.20)	37.48(2.16)	327 (35.00)	3.06	20
24	75.40(1.14)	37.64(2.35)	37.76(2.18)	373 (99.92)	2.68	20
25	75.66(1.07)	37.94(1.73)	37.74(1.34)	415 (34.64)	2.41	12

Where given the figure in brackets after each mean value represents two standard deviations.

FIGURE 110; p 140

Big-D cell; Statistical bursting pattern;

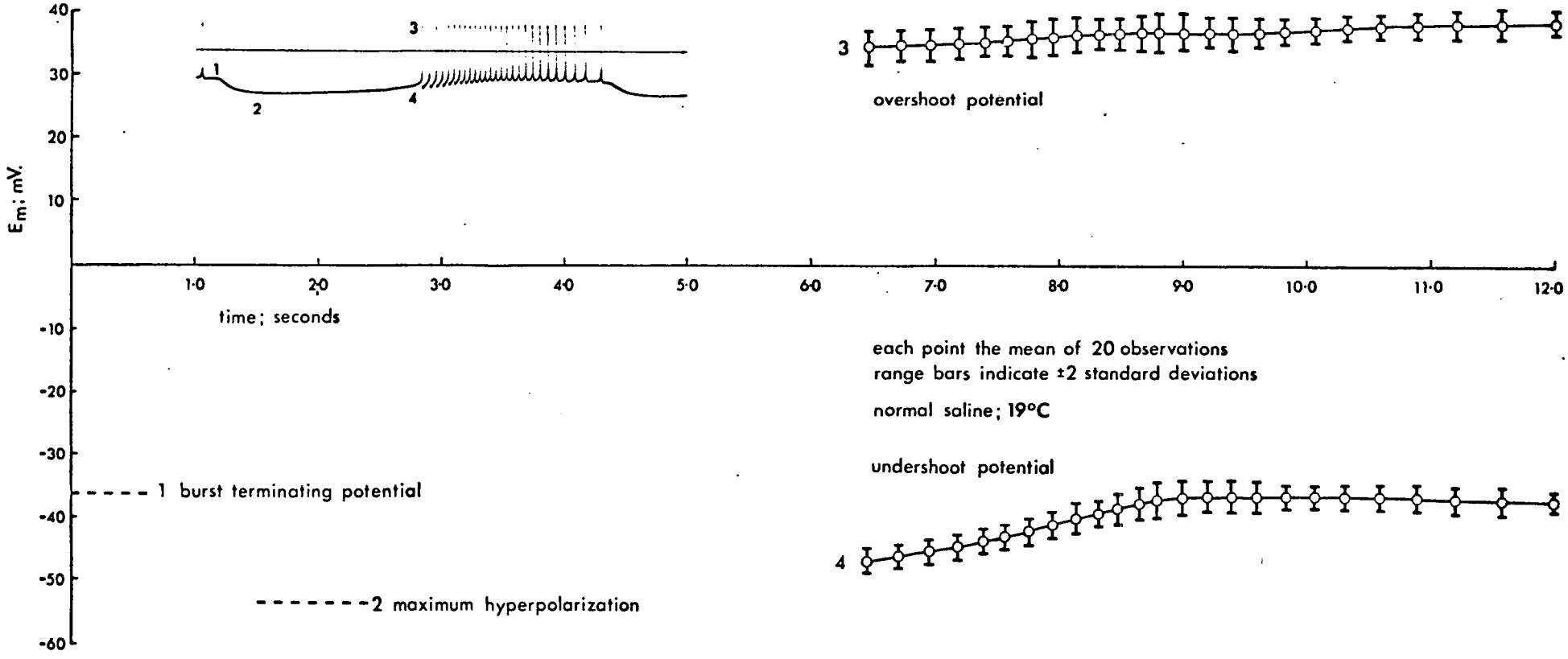

Distribution of successive pre-spike intervals in a representative burst;

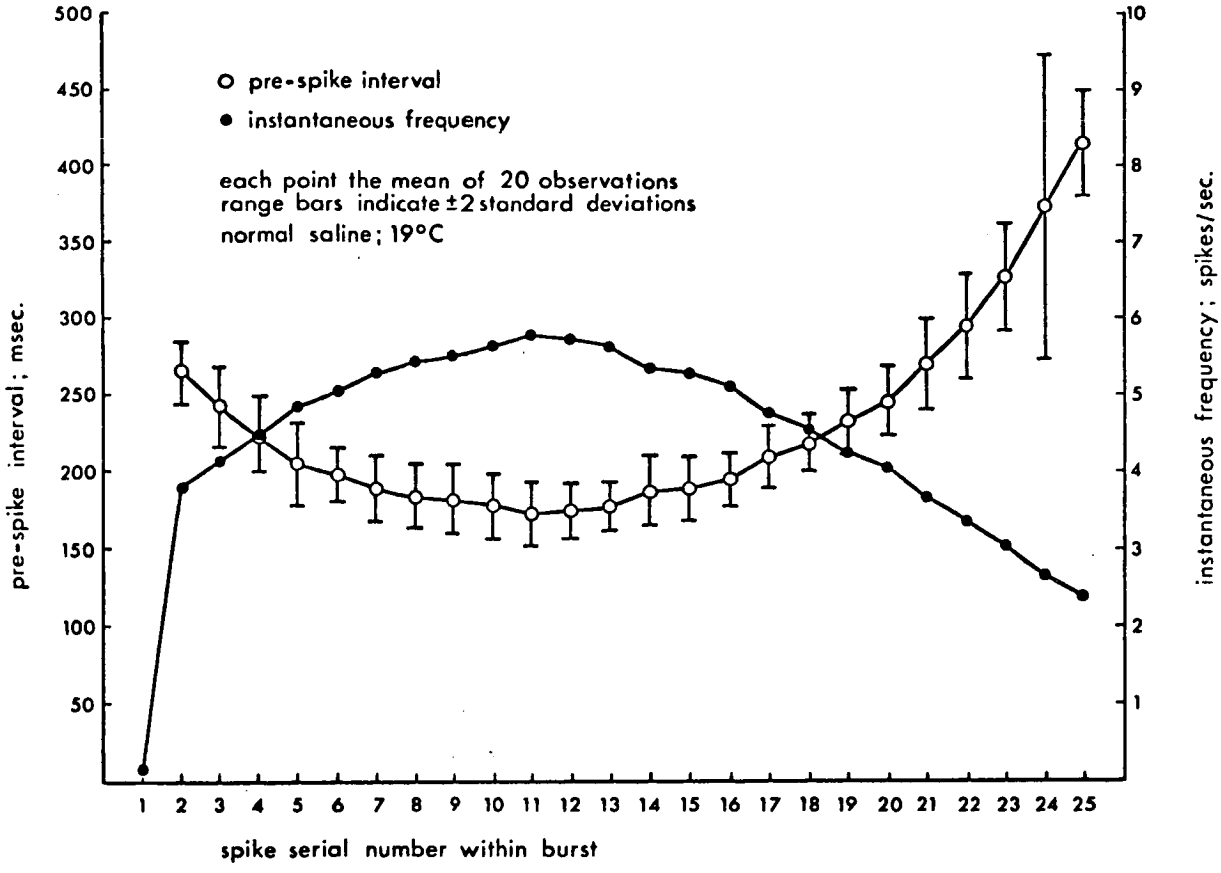

Big-D cell; Histogram of interspike intervals.

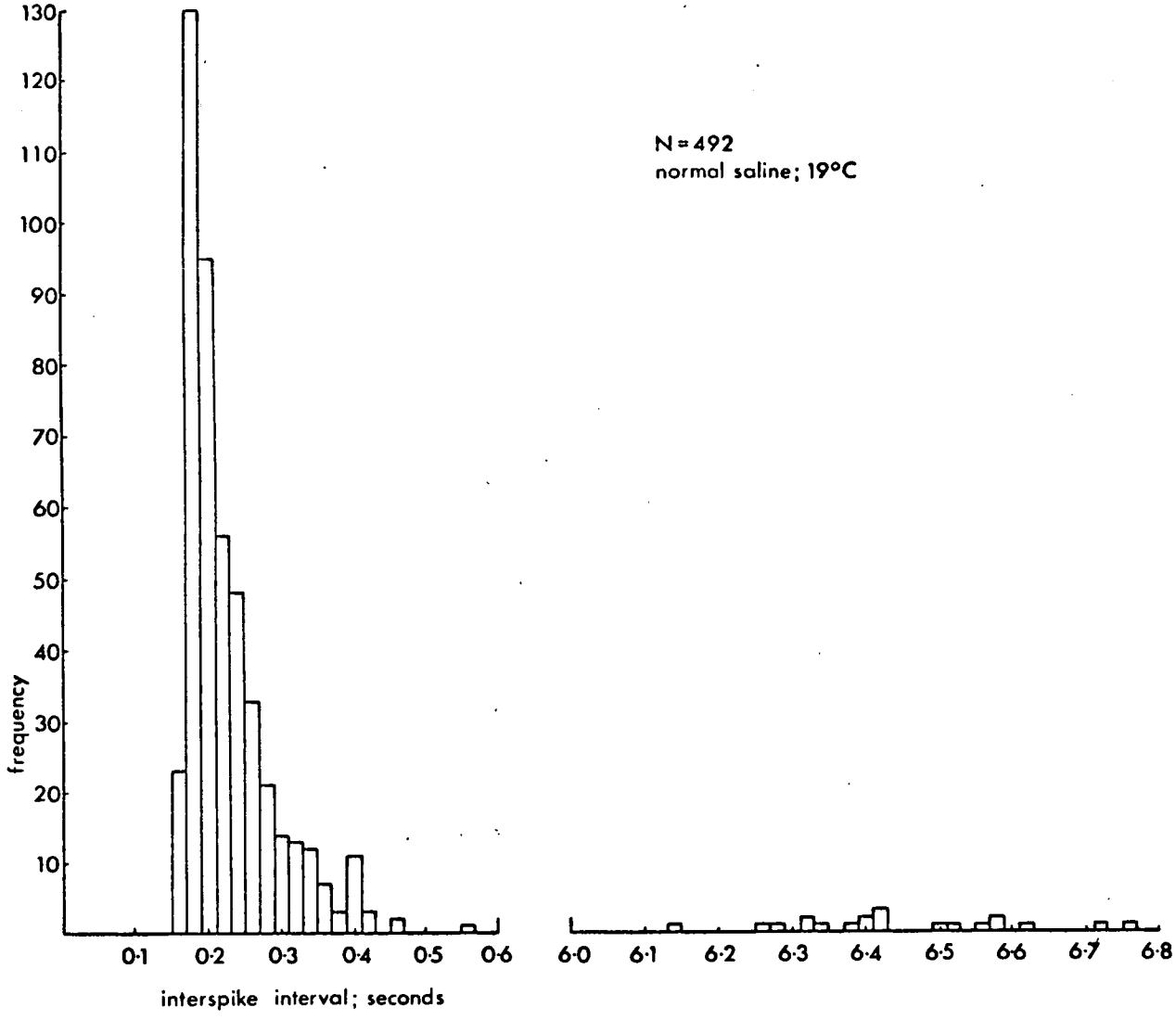

interburst interval and the product m^3h which is normally the most important factor in determining overshoot amplitude should therefore attain a higher peak value during the first action potential of a burst than during subsequent action potentials. This is an important observation and will be considered in more detail in a later section.

The statistical bursting pattern also shows that action potential frequency increases towards the middle of the burst and is subsequently reduced. The variation in action potential frequency is more clearly illustrated in Figure 111 which shows the mean prespike interval and instantaneous frequency plotted against action potential serial number within the burst. The form of this relationship corresponds closely with that demonstrated for identifiable bursting neurons in Helix pomatia (SALANKI, VADASZ & ELEKES, 1972) and in Aplysia (ARVANITAKI & CHALAZONITIS, 1968; STRUMWASSER, 1965) and can be regarded as characteristic of the bimodal type of activity.

Figure 111 also indicates that there is a tendency for larger standard deviations to be associated with higher mean prespike interval values. Thus, the pattern of action potential discharge is more variable from burst to burst during the latter part of the cycle when the intervals are longer than in the middle of the burst when the intervals are shorter. The frequency distribution of the individual intervals from which the mean values were derived is shown in the histogram of Figure 112 and reflects this situation in the skewed distribution of most of the intervals about a modal value of 0.20 sec. The overall distribution is discontinuous and a second group of observations with a modal value

of 6.42 sec. and corresponding to the interburst intervals is also present. As stated above, this method of describing the spontaneous activity of bursting neurons is especially useful since it can be used even in the absence of a regular bursting rhythm.

The relationship between the components of action potential amplitude and the instantaneous frequency of successive action potentials in the statistical bursting pattern is illustrated in Figure 113. The variations in the positive and negative component and overall amplitudes all show a definite hysteresis; that is their magnitude for a particular action potential depends on whether the corresponding instantaneous frequency value is larger or smaller than that of the preceding action potential. It is difficult to visualize the nature of the changes in membrane properties necessary to account for this hysteresis. The effect can also be demonstrated in monotonically active Big-D cells following artificial hyperpolarization. Figure 114 shows recordings obtained from such a cell for a series of hyperpolarizing stimuli varied in duration and intensity. A double-barrelled intracellular microelectrode was used for recording and stimulation and the stimulus current delivered to the cell was monitored differentially across a series resistance of 100 K.

When a brief (0.5 sec.) low intensity pulse of inward current is delivered (record (A)) spontaneous activity is suppressed during the small hyperpolarization produced and there is a perceptible increase in the amplitude and frequency of the first few subsequent action potentials. The increase in amplitude is accounted for mostly by changes in the undershoot but in this instance the overshoot is also very slightly enhanced. With a

Big-D cell; Relationships between components of action potential amplitude and instantaneous frequency of successive action potentials in a representative burst;

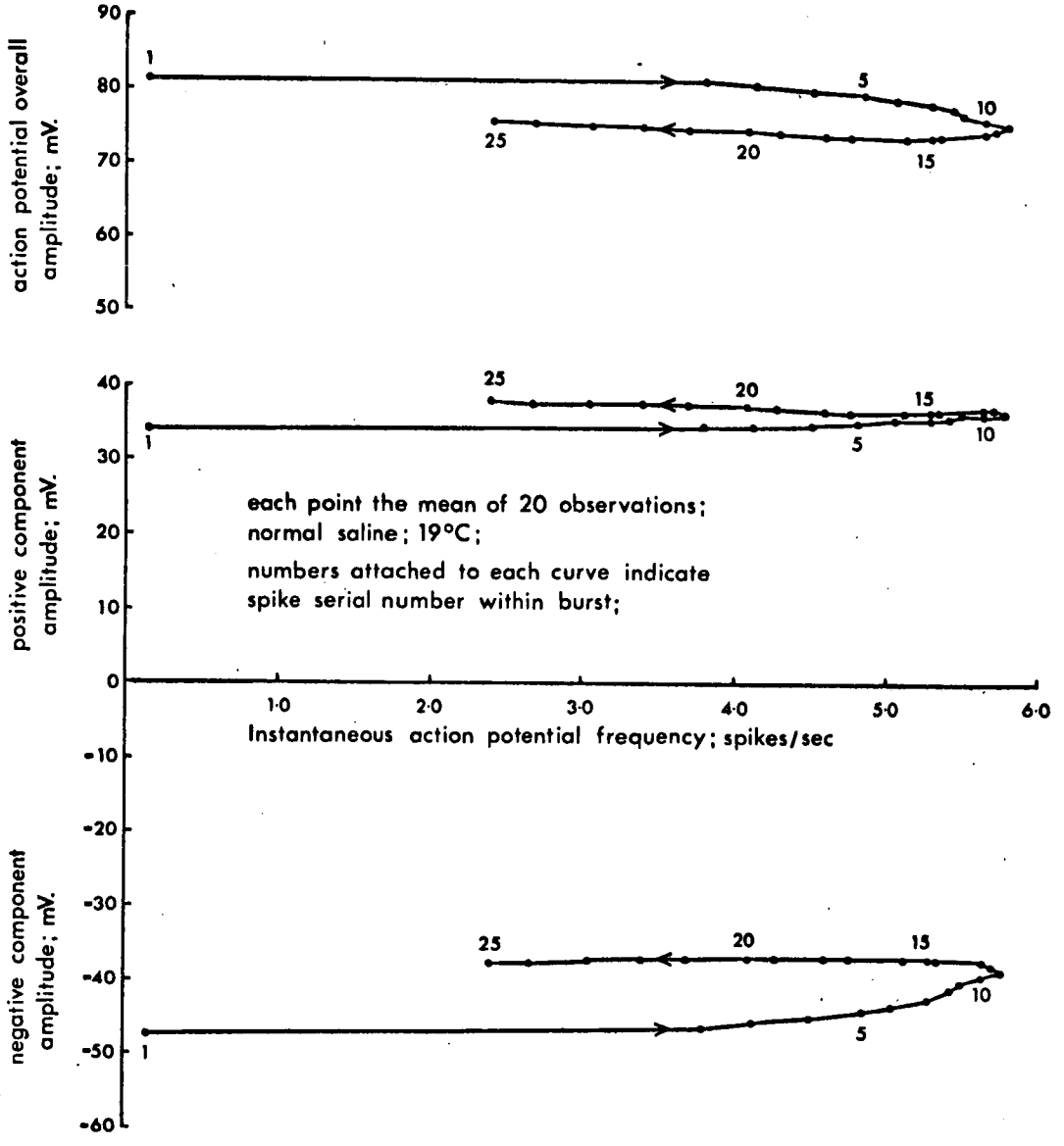

Big-D cell; Response of monotonically firing cell to hyperpolarizing stimuli;

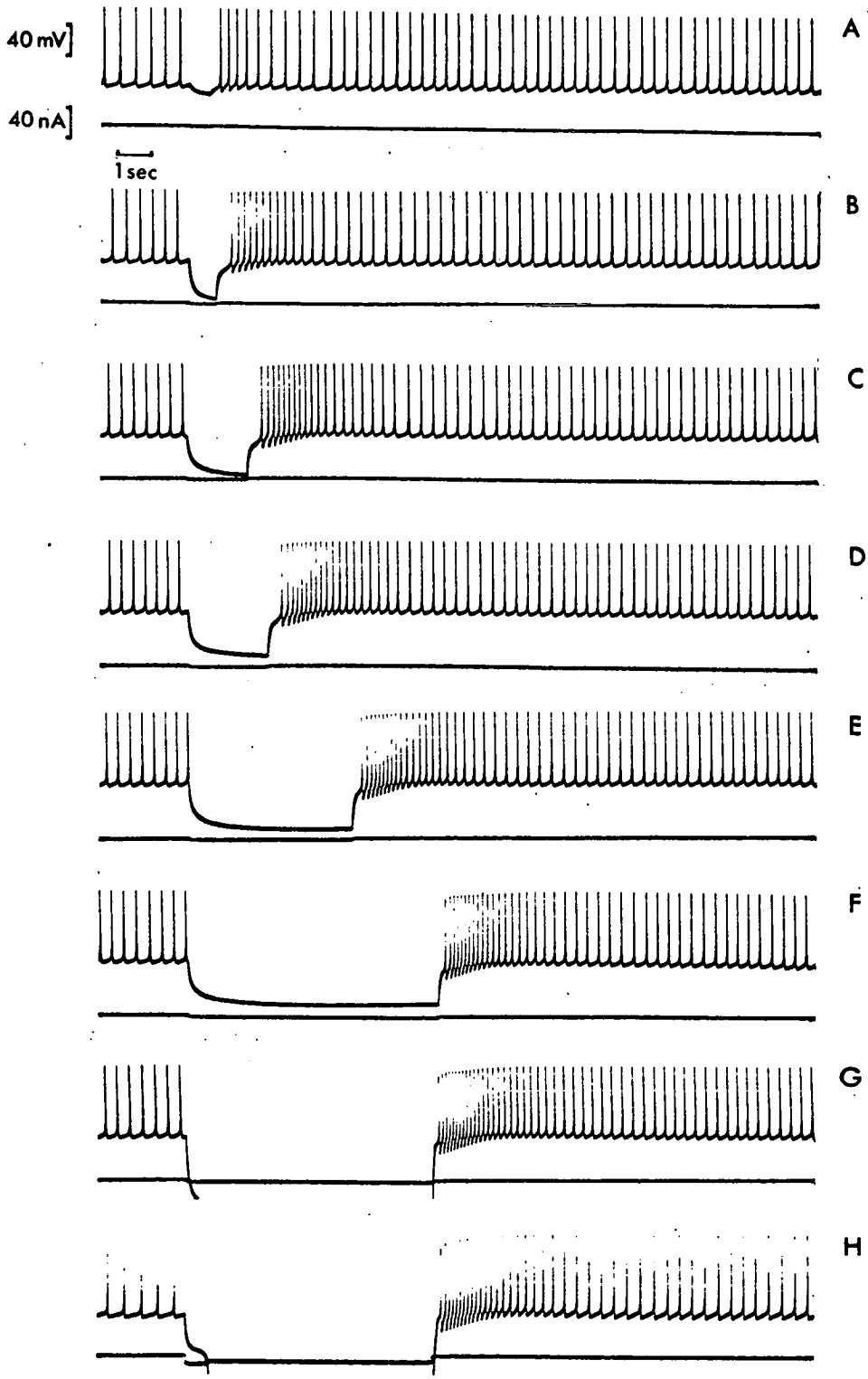

Silent cell; Response to stimulation;

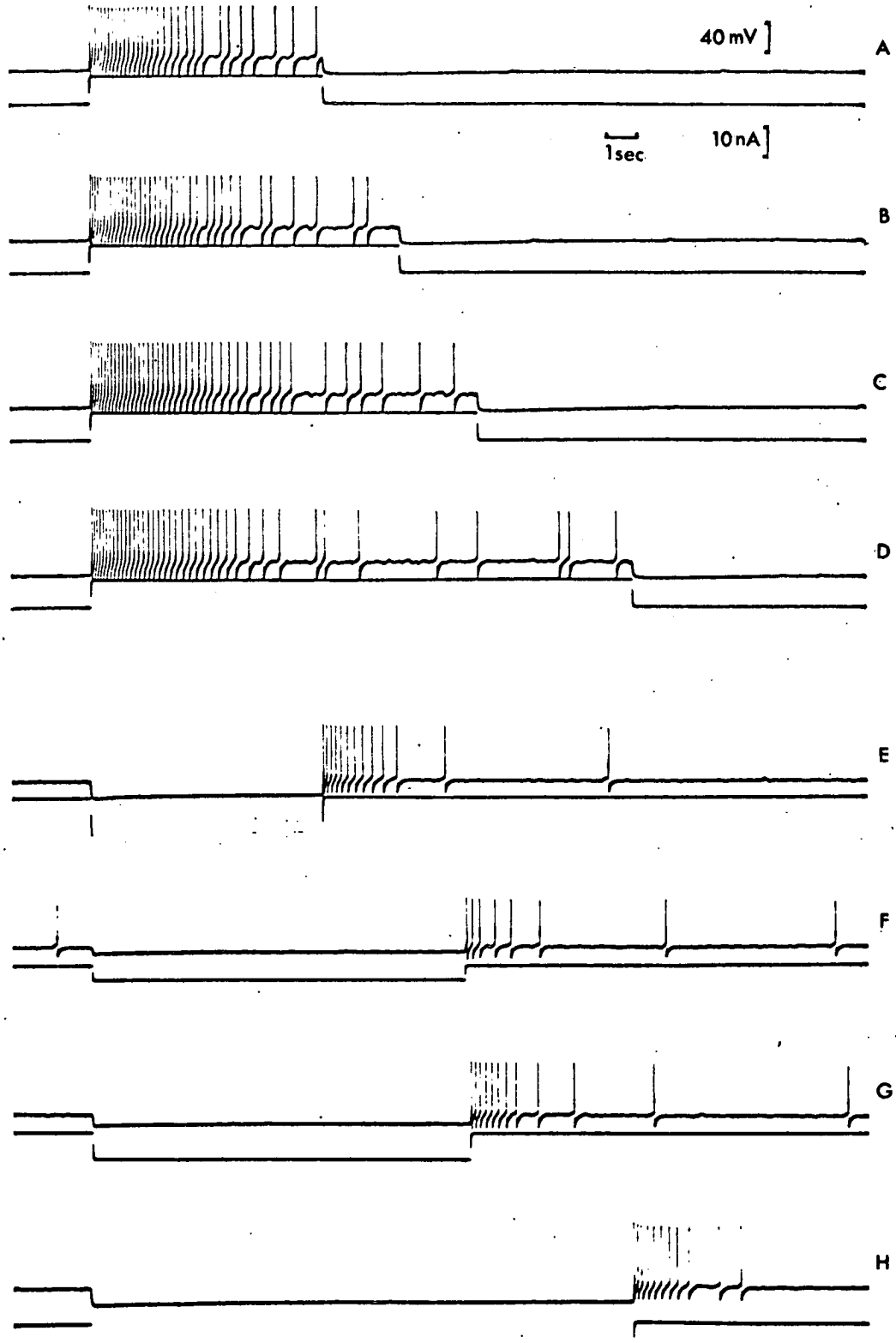

more intense current pulse of similar duration (record (B)) the initial overshoot following hyperpolarization is slightly depressed while the enhancement of the undershoot is more pronounced. This and the increase in frequency also affect a greater number of action potentials. As the duration and intensity of the hyperpolarizing pulses are progressively increased (records (C) - (H)) the suppression of subsequent overshoots becomes more obvious and may persist for several seconds before the normal pattern of activity is restored. In a similar manner the magnitude and duration of changes in action potential undershoot and frequency are progressively increased.

The maximum alterations in overshoot and undershoot are observed immediately after the hyperpolarizing stimulus and both effects have a similar time course. However, the magnitude of the initial increase in undershoot is always greater than that of the decrease in overshoot and it follows that the overall action potential amplitude reaches a maximum immediately after stimulation and subsequently declines. On the other hand, the peak instantaneous action potential frequency clearly follows moderate hyperpolarization only after some delay (records (C) - (H)) and in this case the relationship between instantaneous frequency and the components of action potential amplitude will show the hysteresis demonstrated for spontaneously bursting cells. Thus the pattern of action potential discharge which follows artificial hyperpolarization cannot be regarded as fundamentally different from that following spontaneous hyperpolarization. In the latter case the frequency of action potentials within a burst is related to the magnitude of the preceding (interburst) hyperpolarization in a similar manner (ARVANITAKI & CHALAZONITIS, 1968).

These results are in sharp contrast to those obtained by intracellular stimulation in the case of silent cells; Figure 115 shows a series of recordings. Maximum action potential frequency is observed with no delay at the onset of depolarizing stimuli and declines thereafter. In addition, action potential undershoot is barely affected by stimulation while overshoot shows a rapid reduction followed, as the interspike interval increases, by a gradual recovery towards its initial amplitude. The pattern of action potential discharge subsequent to hyperpolarizing stimuli (records (E) - (H)) has essentially the same characteristics. This type of response corresponds more closely to that expected on the basis of the Hodgkin-Huxley equations than that of the Big-D cell and can also be demonstrated in silent cells in Helix pomatia (GOLA, 1974.

3) Inhibition of bursting rhythm by cooling and by ouabain;

In the R 15 or 'parabolic burster' cell of Aplysia (FRAZIER et al, 1967; STRUMWASSER, 1965) it has been suggested that interburst hyperpolarization is primarily the result of the cyclic activation of an electrogenic sodium pump probably coupled to a metabolic chloride ion pump (STRUMWASSER, 1968). To examine this possibility for the Big-D cell of Helix aspersa recordings were obtained of the alterations in spontaneous activity produced by cooling and by treatment with ouabain. The occurrence of electrogenic pump activity in the Big-D cell has been demonstrated (KERKUT & YORK, 1969) and both cooling and ouabain are known to inhibit the electrogenic sodium pump (GORMAN & MARMOR, 1970a; 1970b; KERKUT & YORK, 1971).

FIGURE 116; p 145

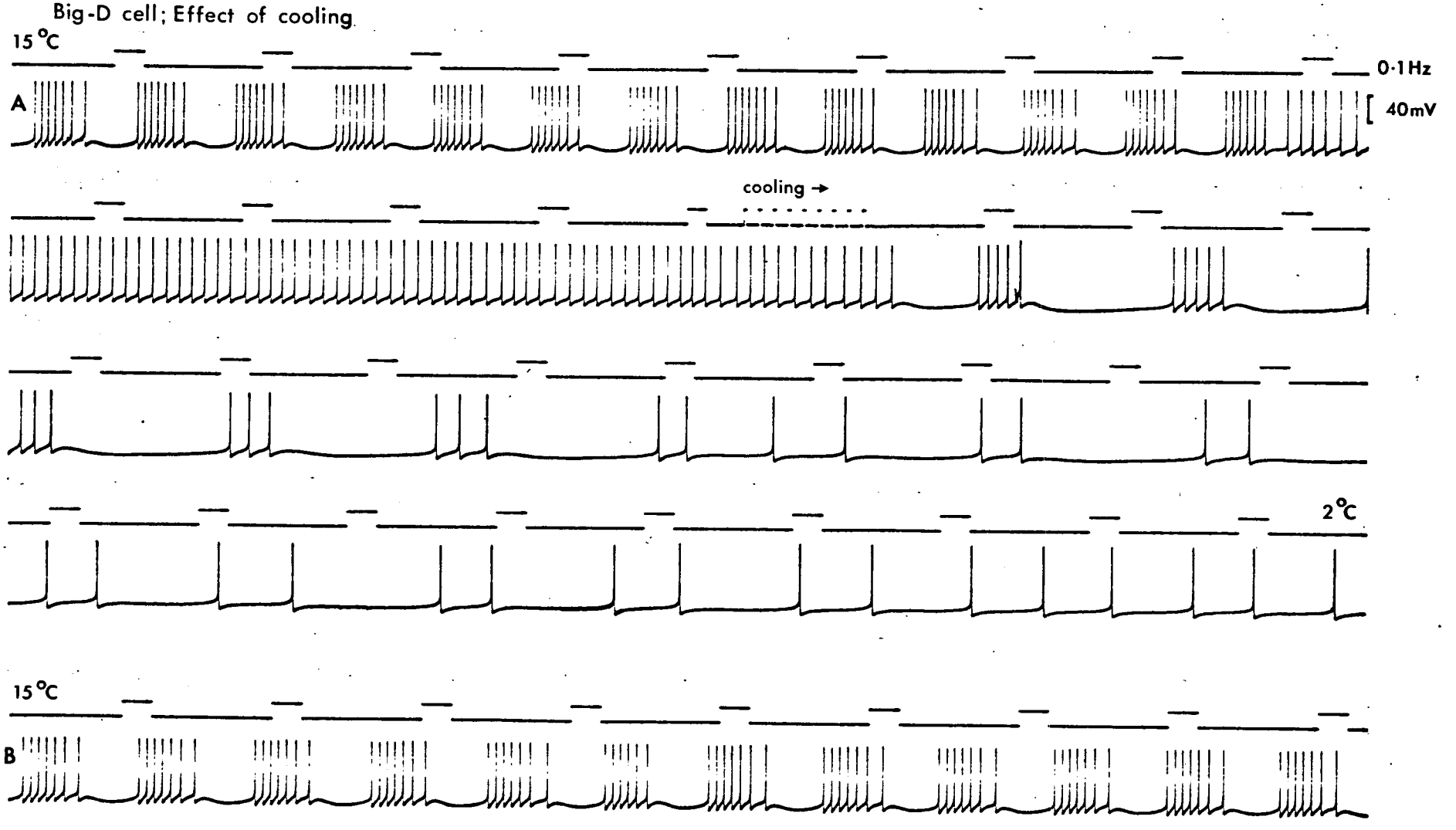

FIGURE 117; p 145

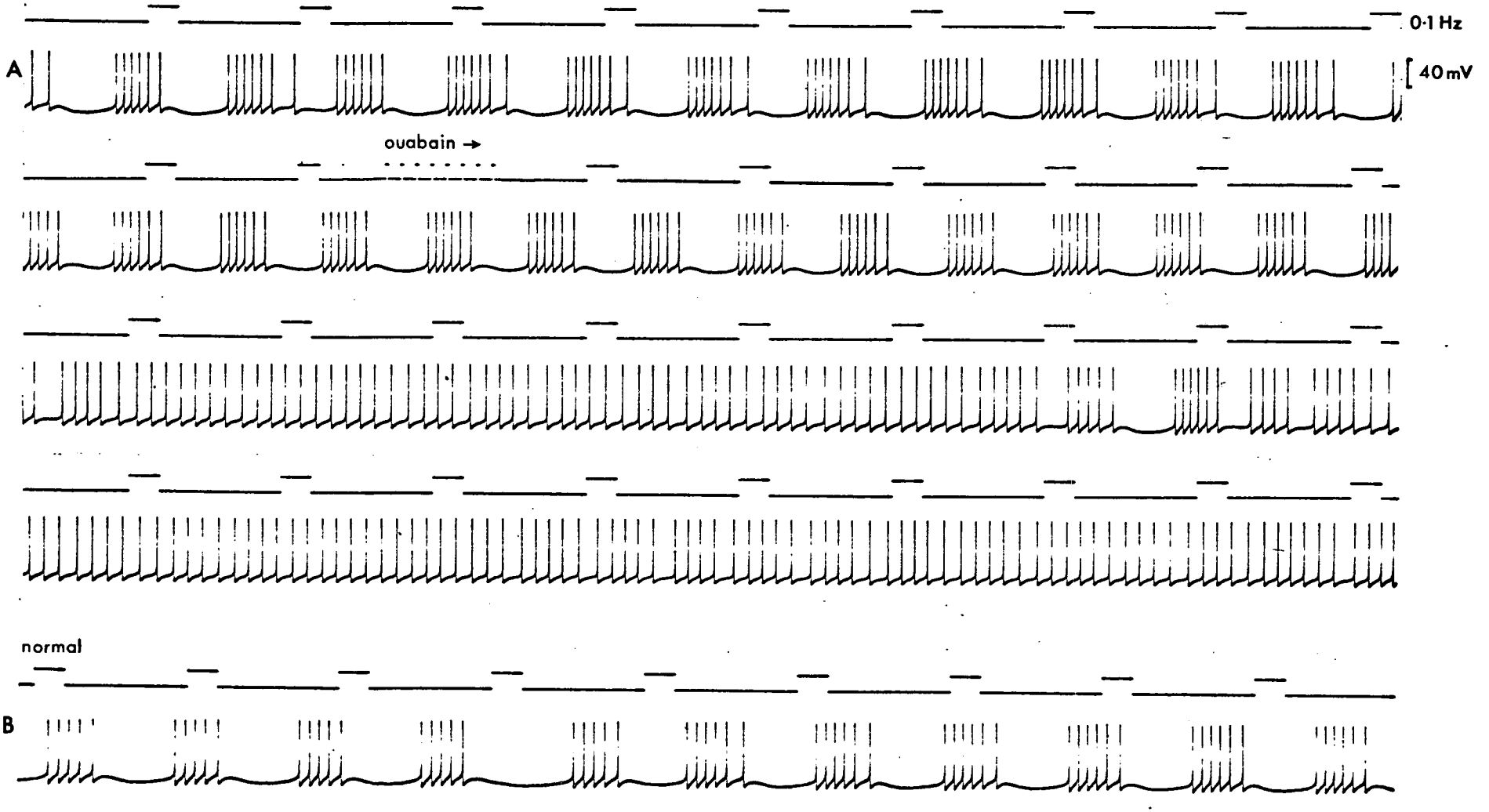

To determine the effect of cooling the reservoir of saline from which the preparation was perfused was replaced by one containing cold ($2^{o}C$) saline of identical composition. Big-D cell activity was recorded during the exchange of salines in the preparation chamber. A typical result is given in Figure 116. The initial temperature in this case was $15^{o}C$ and record (A) shows that as the temperature of saline bathing the preparation is reduced there is a definite increase in the period of the bursting rhythm. This is accompanied by a reduction both in the number and instantaneous frequency of action potentials in successive bursts. As cooling continues the bursting pattern of discharge is lost and the cell fires monotonically at a slow rate. The effect of cooling is reversible; record (B) shows the restoration of the initial activity pattern after a return to normal saline at $15^{o}C$. The abolition of bursting, but not of monotonic activity in the cooled preparation is consistent with the suggestion that the electrogenic sodium pump may contribute to interburst hyperpolarization under normal conditions. Similar results have been obtained for an identifiable bursting neuron in Helix pomatia (SALANKI, VADASZ & VERO, 1973).

Treatment with ouabain also suppresses the bursting rhythm of the Big-D cell as shown in Figure 117. Record (A) shows the time course of changes in spontaneous activity as normal saline containing ouabain (B.D.H. Strophanthin G) at a concentration of 10^{-4} M flowed into the preparation chamber. This concentration should be sufficient to block the sodium pump without altering other membrane properties (MORETON, 1969; GORMAN & MARMOR, 1970a). After a short delay, bursting is abolished and the cell fires monotonically at a relatively high frequency. The effect of ouabain is reversible if the

preparation is returned to normal saline after several minutes and record (B) shows the restoration of bursting similar to that observed initially. The spontaneous activity cycle of the R 15 cell of Aplysia is affected by ouabain in a similar manner (JUNGE & STEPHENS, 1973).

4) Effect of extracellular potassium concentration;

Extracellular potassium concentration is an important factor in determining the rate of sodium pump activity (MORETON, 1969; GORMAN & MARMOR, 1970a; KERKUT & YORK, 1971). The sodium pump is inhibited in potassium-free solutions and in the case of Helix aspersa neurons the hyperpolarization in resting potential which can be attributed to pump activity has been shown to rise steeply towards a plateau level as extracellular potassium concentration is increased (MORETON, 1969). The plateau level is reached at an extracellular concentration of about 3 mM but since membrane resistance will fall progressively with further increases in concentration it is clear that the current transferred by the pump must also continue to rise. It may well be that the relationship between pump current and extracellular potassium concentration resembles that demonstrated between the pump current and intracellular sodium concentration (THOMAS, 1969). Above a 'resting' level the latter relationship is approximately linear.

If the generation of the interburst hyperpolarization in bursting pacemakers is dependent on sodium pump activity some indication of this dependence would be expected when extracellular potassium concentration is altered. To investigate this possibility recordings were obtained of the spontaneous activity of Big-D cells

exposed to a series of salines of differing potassium concentration. The composition of the salines used has been given previously; the series was prepared simply by addition or omission of potassium chloride as appropriate since osmotic pressure differences were relatively small over the range of concentrations normally used. Typical results, recorded from a single cell, are given in Figure 118; extracellular potassium concentration is indicated to the right of each record. Ambient temperature was constant at 19°C throughout the series and, after a return to normal saline, full recovery to a normal pattern of activity was observed in each case.

Record (C) obtained during perfusion with normal (3 m$\bar{M}$ K^+) saline is a typical example of spontaneous activity and shows a clearly defined bursting pattern of action potential discharge. When the potassium concentration of the perfusing solution is reduced to 2 m$\bar{M}$ (record (B)) discharge becomes irregular and while hyperpolarizations of the interburst type are present these are less frequent and there is no definite bursting cycle. A further reduction in concentration (record (A), 1 m$\bar{M}$ K^+) leads to the abolition of such hyperpolarizations and the Big-D cell fires monotonically. Reducing the extracellular potassium concentration to 1 m$\bar{M}$ will significantly inhibit the sodium pump and these observations are therefore consistent with its involvement in the generation of the interburst hyperpolarization. However, it must be pointed out that inhibition of the sodium pump by this means may lead to a slight depolarization (MORETON, 1969; GORMAN & MARMOR, 1970a). This in turn could lead to the loss of a regular bursting cycle and eventually to monotonic firing as demonstrated by artificial depolarization in the R 15 cell of Aplysia (ARVANITAKI & CHALAZONITIS, 1968).

FIGURE 118; p147

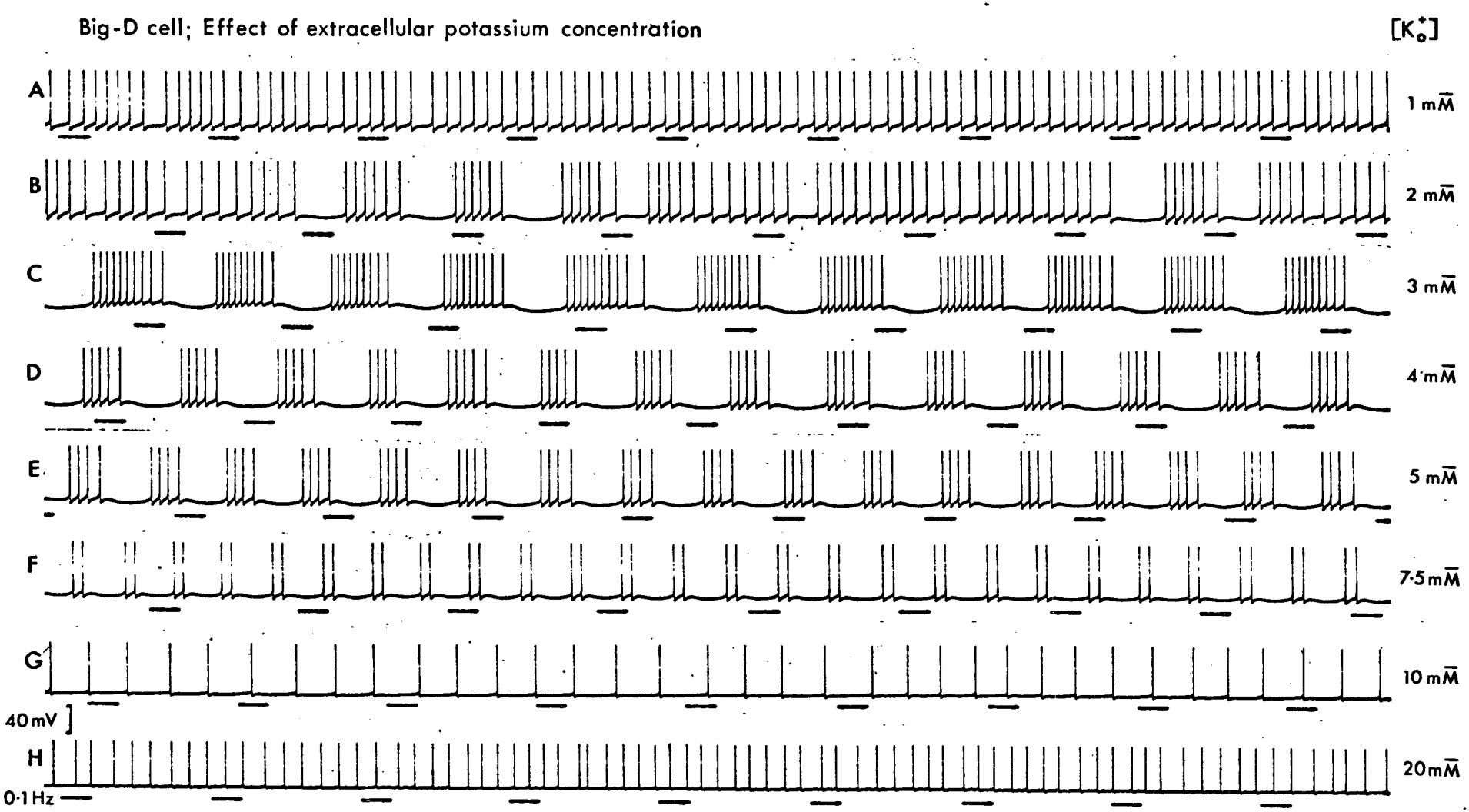

The effects of increasing extracellular potassium concentration above its normal level are illustrated in records (D) - (H). These show a progressive reduction in the period of the bursting cycle accompanied by a decrease in the number and frequency of action potentials within each burst. At extracellular potassium concentrations of 10 mM and 20 mM the cell fires monotonically. However, the frequency of action potentials in the 10 mM recording (record (G)) is comparable to the frequency of bursts observed in the 7.5 mM recording (record (F)). Each of these bursts contains only two action potentials; the second of these is apparently absent in the 10 mM recording and it may be that the mechanisms which underly the interburst hyperpolarization are still operative but that in this case the 'burst' consists of a single action potential. This interpretation can also be applied to the spontaneous activity observed with 20 mM K^+ saline (record (H)).

Depolarization is the normal result of increases in extracellular potassium concentration. Since membrane resistance will fall progressively as concentration is increased (KOSTYUK, 1968) it follows that this depolarization is affected by stimulation of the sodium pump only to a limited extent. In fact, above a concentration of 3 mM K^+, the electrogenic effect on membrane potential has been shown to be relatively constant (MORETON, 1969). Thus the depolarization produced by raising the extracellular potassium concentration to 7.5 mM or 10 mM is significant and characteristically exceeds that associated with inhibition of the sodium pump at a concentration of 1 mM (MORETON, 1969). On the other hand, the results of the present experiment clearly show that the frequency of spontaneous action potentials observed when the Big-D cell is exposed to 1 mM K^+ saline (Figure 118, record (A)) is much higher

than that observed with 7.5 mM or 10 mM K^+ saline (records (F) and (G)). Thus slight depolarization accompanied by inhibition of the sodium pump leads to a complete abolition of the bursting cycle while a greater depolarization accompanied by stimulation of the sodium pump either leads merely to a modification of the cycle (7.5 mM K^+) or to what can be considered as only a partial abolition (10 mM K^+). Only when the extracellular potassium concentration is raised to 20 mM and the depolarization produced is substantial (record (H)) does the frequency of spontaneous action potentials approach that observed with 1 mM K^+ saline. These results are inconsistent with the view that modifications in the bursting cycle associated with inhibition of the sodium pump are purely the result of the concomitant depolarization and that membrane potential alone is the primary factor in determining the activity pattern of bursting cells.

To amplify these conclusions and to illustrate more fully the changes in activity associated with variations in extracellular potassium concentration, the continuous photographic record from which the recordings of Figure 118 were taken has been analyzed in a manner similar to that used in quantifying the characteristics of burst generation. A regular bursting rhythm was maintained in four of the salines used (3 mM, 4 mM, 5 mM and 7.5 mM K^+). All the parameters of 20 consecutive bursts were measured in each case in order to derive the corresponding statistical bursting patterns. In the absence of a regular bursting cycle (1 mM, 2 mM, 10 mM and 20 mM K^+) the components of action potential amplitude were measured for each of 20 consecutive action potentials. For all the salines used the intervals preceding a total of 200 consecutive action potentials were measured. Table 9 gives the mean values calculated

for all these parameters with the range of observation (2 standard deviations) indicated where appropriate.

The statistical bursting patterns derived are given in Figure 119 and illustrate more clearly the characteristics of the reduction in the period of the bursting cycle associated with increases in extracellular potassium concentration. Thus it can be seen that the reduction in period is very largely the result of a marked decrease in burst duration while the duration of the interburst hyperpolarization decreases only slightly. It is also clear that the maximum hyperpolarization observed during the interburst interval occurs at a progressively more depolarized level. This is an indication of the depolarizing action of increases in extracellular potassium and could be related to the reduction in burst duration in a manner consistent with the effects of artificial hyperpolarization previously described. This suggestion is supported by the increase in overshoot and the decrease in action potential frequency which accompany reductions in burst duration.

To illustrate the relationships between extracellular potassium levels and action potential frequency the mean prespike interval values given in Table 9 were plotted as in Figure 120 and the corresponding frequency distribution of individual intervals were constructed as in Figure 121.

Figure 120 shows that the characteristic pattern of action potential frequency within the burst changes as extracellular potassium concentration is raised above its normal level. There is an overall increase in corresponding prespike intervals and the peak frequency occurs progressively earlier in the burst. The mean interburst intervals and the mean prespike intervals for concentrations

Table 9.

Big-D cell; Effect of extracellular potassium concentration on spontaneous activity.

(K_o^+)		Amplitude (mV)	Overshoot (mV)	Undershoot (mV)	Interval (msec)	Hz
1mM	1	80.44(0.82)	31.41(0.80)	49.03(1.02)	949 (266.8)	1.05
2mM	1	81.01(1.31)	31.08(1.31)	49.93(2.37)	1086(1518.4)	0.92
3mM	1	76.44(0.82)	25.97(0.80)	50.47(1.10)	3996 (723.9)	0.25
	2	75.68(0.80)	26.29(0.53)	49.39(0.96)	464 (48.0)	2.16
	3	74.92(0.77)	26.69(0.82)	48.23(1.08)	418 (40.8)	2.39
	4	74.28(0.77)	26.97(0.77)	47.31(1.17)	404 (35.8)	2.48
	5	73.68(1.02)	27.21(0.77)	46.47(1.33)	424 (36.8)	2.36
	6	73.36(0.75)	27.49(0.82)	45.87(1.23)	446 (46.6)	2.24
	7	73.08(0.77)	28.01(0.60)	45.07(0.98)	484 (51.2)	2.07
	8	73.08(0.77)	28.17(0.77)	44.91(1.17)	564 (89.4)	1.77
	9	73.24(0.82)	28.25(0.82)	44.99(1.15)	718 (169.1)	1.39
	10	73.20(1.13)	28.29(1.13)	44.91(2.26)	960 (565.7)	1.04
Total		74.18(2.46)	27.24(1.73)	46.95(4.00)		
4mM	1	79.20(0.74)	28.77(0.72)	50.43(1.02)	3882 (371.1)	0.26
	2	78.52(0.78)	28.89(0.49)	49.63(0.87)	538 (40.8)	1.86
	3	78.16(0.76)	29.21(0.75)	48.95(1.10)	504 (40.0)	1.98
	4	77.68(0.90)	29.61(0.66)	48.07(1.17)	618 (111.4)	1.62
	5	77.85(0.76)	29.62(0.63)	48.23(1.02)	708 (240.7)	1.41
Total		78.30(1.34)	29.20(0.96)	49.10(2.05)		
5mM	1	79.20(0.00)	28.93(0.69)	50.27(0.72)	3176 (263.9)	0.31
	2	78.52(0.60)	29.37(0.66)	49.15(0.94)	558 (54.8)	1.79
	3	78.36(0.35)	29.69(0.66)	48.67(0.72)	578 (48.7)	1.73
	4	78.28(0.77)	29.97(0.82)	48.31(1.28)	940 (368.4)	1.06
Total		78.59(0.87)	29.49(1.04)	49.10(1.75)		
7.5mM	1	77.04(0.75)	29.93(0.60)	47.11(1.08)	2692 (331.5)	0.37
	2	76.40(0.82)	30.21(0.82)	46.19(1.37)	650 (51.2)	1.54
Total		76.72(1.02)	30.07(0.77)	46.65(1.54)		
10mM	1	70.44(0.96)	27.14(0.77)	43.30(1.31)	2658(1249.2)	0.38
20mM	1	59.56(0.96)	21.68(0.77)	37.88(1.20)	1362 (755.8)	0.73

Big-D cell; Effect of extracellular potassium concentration on statistical bursting pattern;

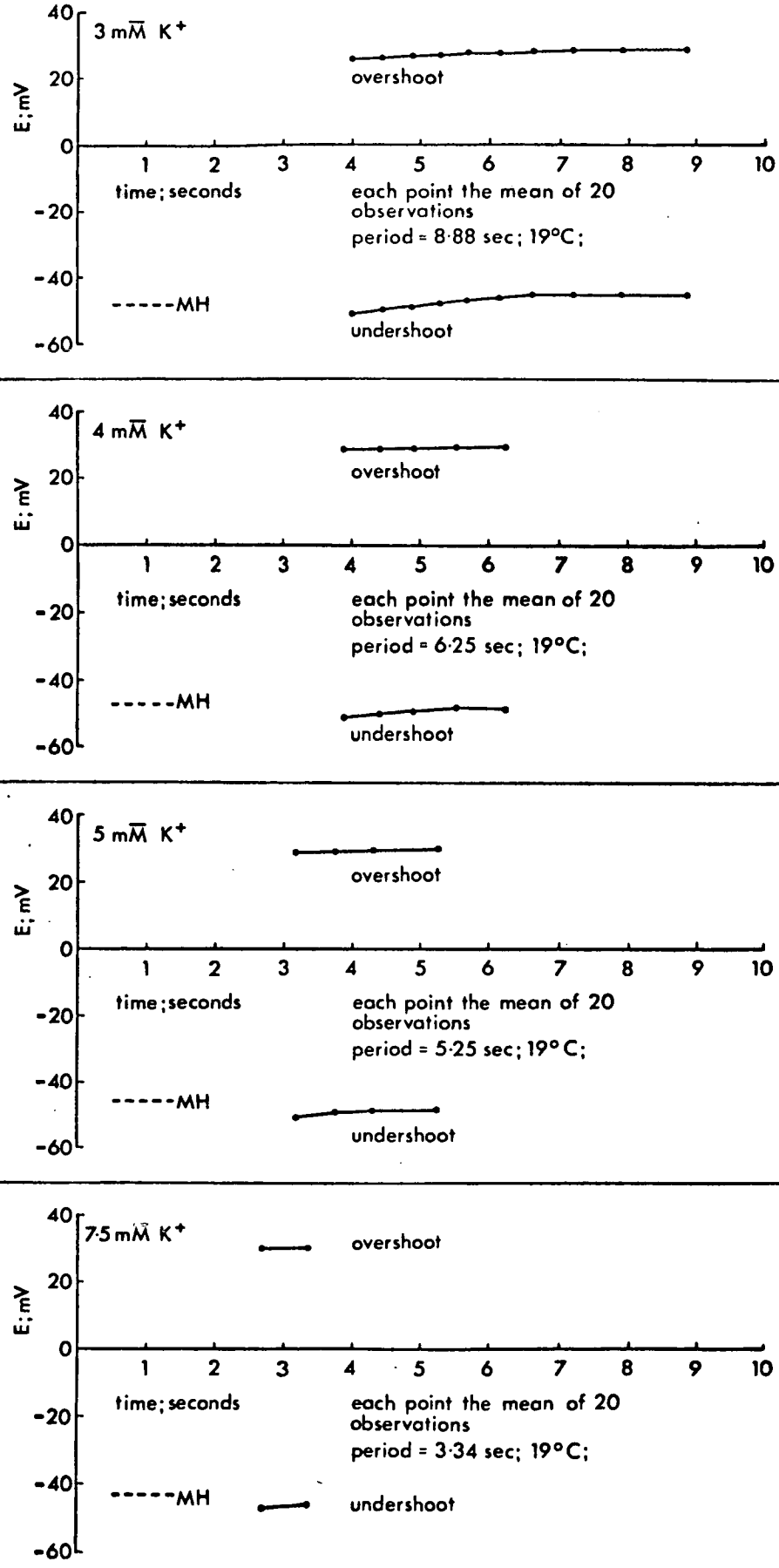

MH = maximum hyperpolarization

Big-D cell; Effect of extracellular potassium concentration on successive pre-spike intervals and on bursting behaviour;

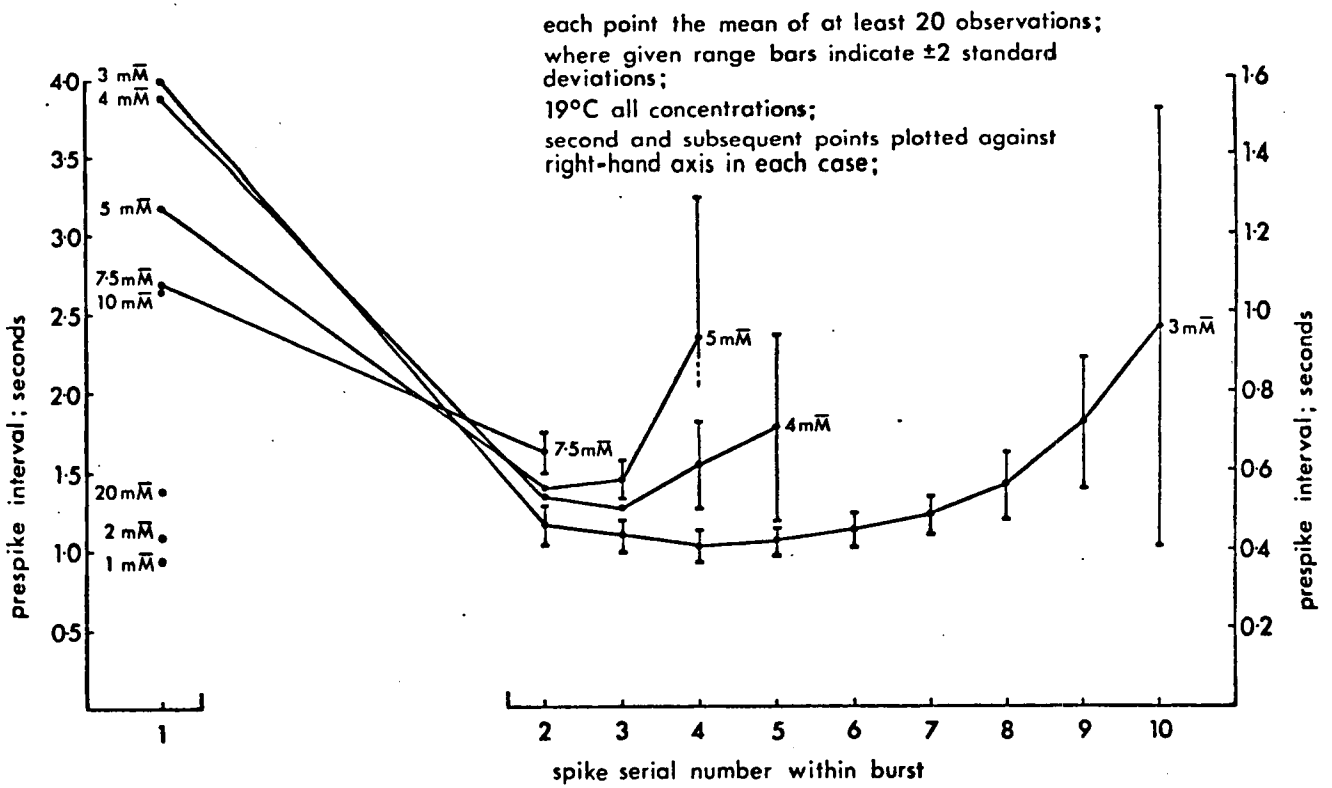

Big-D cell; Effect of extracellular potassium concentration on distribution of interspike intervals;

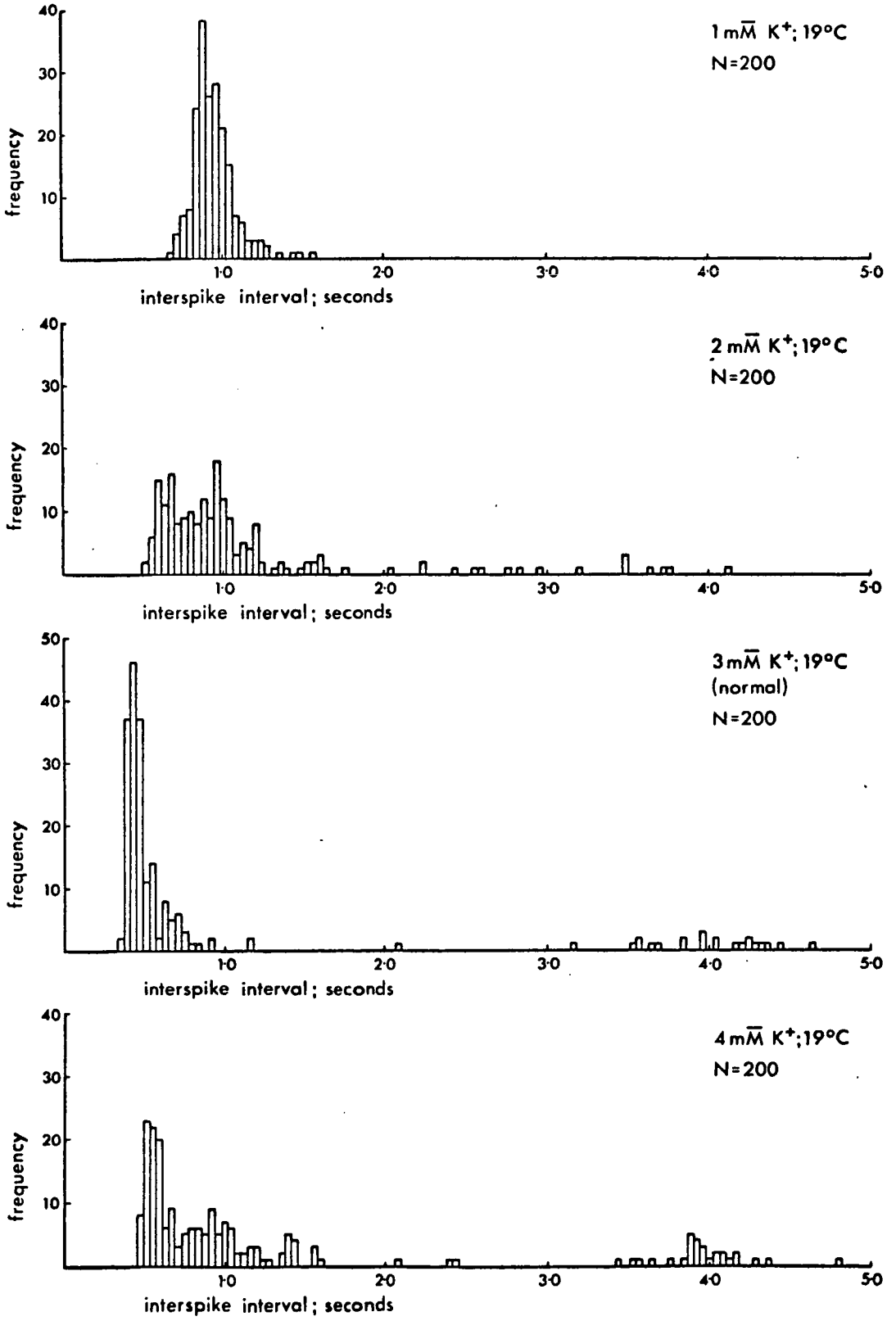

Big-D cell; Effect of extracellular potassium concentration on distribution of interspike intervals;

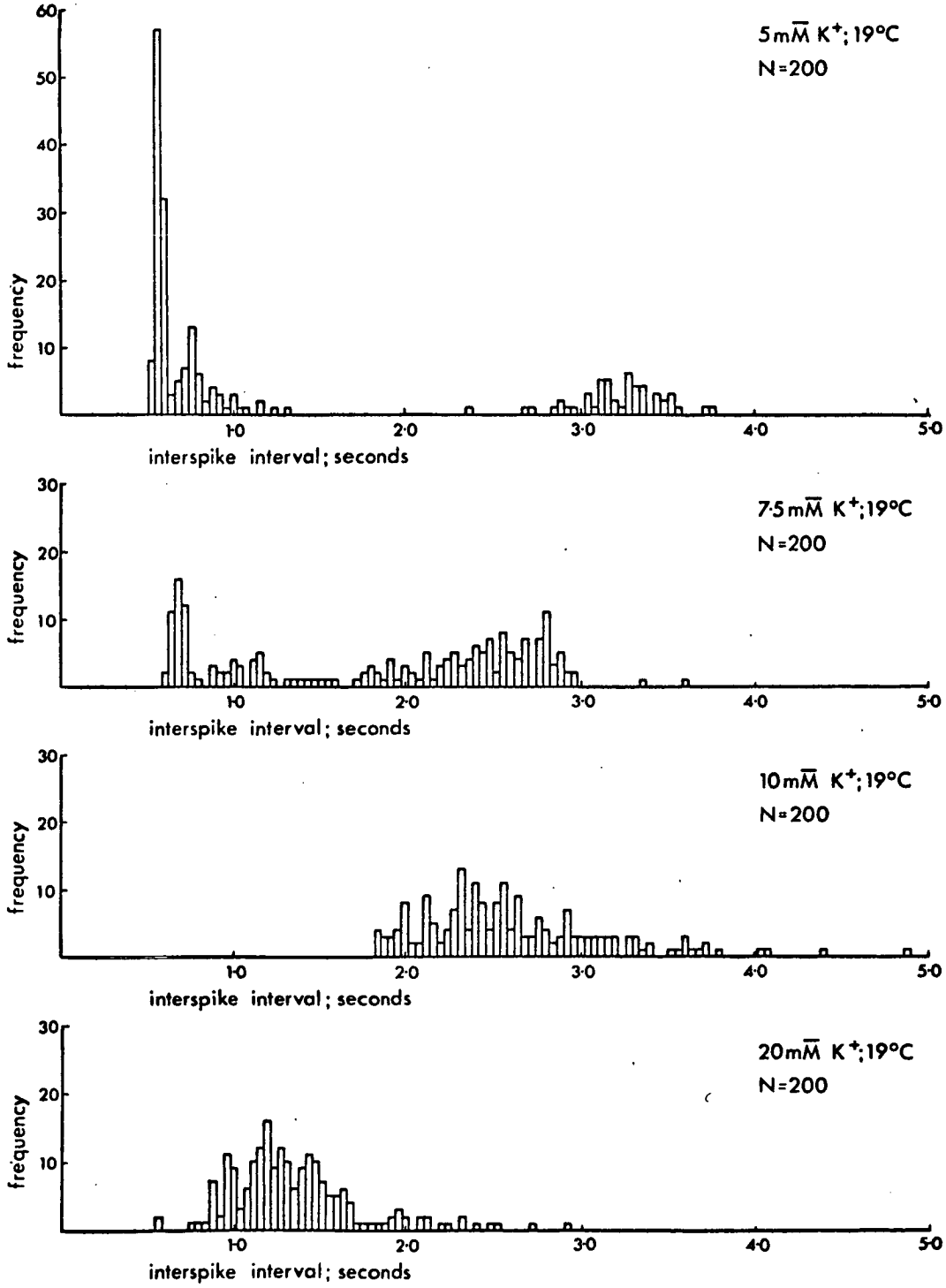

which support only monotonic or irregular firing have been plotted against the left hand axis to emphasize the discrepancy between the magnitudes of the interburst intervals and those of the interspike intervals observed with 1 mM and 2 mM K^+ salines; the latter cannot be regarded as reduced interburst intervals.

The frequency distribution corresponding to Big-D cell activity in 1 mM K^+ saline (Figure 121) is approximately normal in form and conforms to that expected for a monotonic pacemaker. When the potassium concentration is raised to 2 mM this pattern is lost and there is a clear tendency towards a bimodal distribution. This is an accurate reflection of the irregularity of action potential discharge in the corresponding intracellular recording (Figure 118, record (B)). With 3 mM K^+ saline the distribution is clearly bimodal and discontinuous indicating the development of a regular bursting cycle (see also Figure 112). With further increases in concentration this bimodality is at first preserved but the two peaks converge and the secondary peak is progressively augmented at the expense of the primary peak as the number of action potentials within each burst becomes reduced. Eventually the distribution becomes continuous (10 mM and 20 mM K^+). It is clear throughout that the secondary peak is largely composed of the interburst intervals while the primary peak consists of the prespike intervals for the second and subsequent action potentials in each burst. The restoration of a continuous distribution apparently coincides with the loss of the primary peak while the secondary peak remains. It is therefore probable, as already suggested, that the mechanisms of interburst hyperpolarization have not been lost. In addition, the distribution of intervals even for 20 mM K^+ saline is clearly not

identical to that for 1 mM K^+ saline and it follows that depolarization associated with reductions in extracellular potassium concentration is not equivalent to the depolarization associated with increases in concentration. Thus changes in the activity of the Big-D cell produced by variations in extracellular potassium concentration cannot be interpreted simply in terms of changes in membrane potential. It would seem at least probable that the electrogenic sodium pump is involved in the generation of the interburst hyperpolarization.

C) Discussion:

Bursting neurons have been shown to have other important properties in addition to those demonstrated above which must be considered in attempting to develop a theoretical model for burst generation.

In the R 15 cell of Aplysia intracellular pressure injection of potassium chloride causes an initial decrease in the magnitude and duration of the interburst hyperpolarization which may be followed by the suppression of bursting (STRUMWASSER, 1965). Intracellular injections of potassium sulphate have little effect on spontaneous activity and it can be concluded that these changes are the result of alterations in the intracellular concentration of chloride ions. When 200 picolitres of 2.7 M KCl are injected into a 210 μ diameter cell bursting stops and the cell remains silent for 30 minutes or more before the process of burst generation resumes spontaneously. The volume of a 250 μ diameter cell is approximately 8,200 picolitres and, while the volume of injected salt solution is only 2.5% of this amount, the intracellular chloride concentration should be increased by at least 60 mM. This increase might be expected to lead to a substantial membrane depolarization and to repetitive (monotonic) activity which is not in fact observed. (Monotonic rather than bursting activity can be produced by sustained artificial depolarization during the first half of the silent period induced by KCl injection.) A normal activity pattern is eventually restored in injected cells but the first spontaneous bursts which follow the silent period are of longer than normal duration and contain a higher number of action potentials. The interburst hyperpolarization is also of increased duration and its maximum occurs

at a far more hyperpolarized level than that observed during normal activity. These effects are consistent with a net membrane hyperpolarization rather than with depolarization.

As an explanation of this situation it has been suggested (STRUMWASSER, 1965) that excess intracellular chloride ions are extruded by the action of a metabolic pump and that when KCl is injected the pump 'overshoots' and reduces the intracellular chloride concentration to below its normal level. The interburst hyperpolarization can thus be regarded as dependent on a specific increase in the membrane conductance of chloride ions. To account for the suppression of bursting in the presence of ouabain this hypothesis has been modified (STRUMWASSER, 1968) and it is suggested that an electrogenic sodium pump (possibly coupled to a chloride ion pump) also contributes to the interburst hyperpolarization. In either form this interpretation seems improbable since the resumption of spontaneous bursting after KCl injection would be expected to coincide with or even precede the return of chloride concentration to its normal level and it is difficult to see why it should be delayed until the concentration is at a minimum. In addition, present knowledge of metabolic pumps does not suggest that a significant 'overshoot' in function is possible since the rate of ion transfer is directly dependent on the concentration of substrate available (KERKUT & YORK, 1971; THOMAS, 1969).

An alternative and more plausible explanation of the effects of intracellular KCl injection can be proposed. Thus it is probable that potassium ions and chloride ions are distributed across the nerve cell membrane according to a Donnan equilibrium, the membrane being permeable to both ions. A significant proportion

of organic anions to which the membrane is impermeable will be present intracellularly. To preserve overall electrical neutrality the electrical charge of some of the intracellular potassium ions must be balanced by that of the indiffusible anions while the remainder is balanced by chloride ions. It follows that the intracellular concentration of potassium ions is higher and that of chloride ions lower than the corresponding extracellular concentration. An equilibrium is passively established when the product of the intracellular concentrations of diffusible ions is equal to the product of the extracellular concentrations of diffusible ions (AIDLEY, 1971). When the intracellular concentration of potassium and chloride ions is artificially raised by KCl injection membrane potential will alter until both species of ion leave the cell passively at equal rates and eventually the same equilibrium point will be reached. This is true since, if the initial flow of chloride ions predominates, the membrane will depolarize and potassium conductance will increase until the flow of potassium ions balances that of chloride ions. Conversely if the initial flow of potassium ions predominates the membrane will hyperpolarize until the two rates of flow are equal. (The chloride conductance of the membrane can be regarded as effectively constant.)

The nerve membrane is impermeable to sulphate ions (KERKUT & THOMAS, 1964) and consequently when potassium sulphate is injected intracellularly the sulphate ion assumes the role of an indiffusible anion. It follows that a higher than normal intracellular potassium concentration can be maintained more or less indefinitely and that a new Donnan equilibrium will be established. An equal number of potassium and chloride ions will still leave the cell but the total flow of ions across the membrane will be very much

less than that expected when KCl is injected. Thus the principal difference between a KCl injection and a K_2SO_4 injection probably lies in the magnitude of the resultant (passive) flow of ions across the cell membrane; it may be that the transfer of potassium ions rather than that of chloride ions contributes to alterations in spontaneous activity.

Significant extracellular accumulation of potassium ions subsequent to the passage of outward current can be demonstrated for the R 15 cell of Aplysia (EATON, 1972) and since extracellular potassium concentration is an important factor in determining the rate of sodium pump activity (MORETON, 1969) it seems likely that stimulation of the sodium pump will be a direct result of the relatively massive KCl injection necessary to suppress bursting. The alterations in spontaneous activity produced by injection are entirely consistent with this suggestion and the interburst hyperpolarization could therefore be considered as due solely to the electrogenic component of sodium pump activity and there is no need to postulate a metabolic pump for chloride ions or indeed to suppose that chloride ions make any contribution to the process of burst generation which is other than incidental.

Further evidence supports the suggestion that generation of the interburst hyperpolarization is dependent on the activation of the sodium pump rather more directly. The membrane potential of the Big-D cell of Helix aspersa is sensitive to alterations in the partial pressure of oxygen (pO_2) in the perfusing solution (KERKUT & YORK, 1969). An increase in pO_2 leads to a hyperpolarization which can be blocked by ouabain or scillaren and it seems reasonable to conclude that the mechanism of the sodium pump involves a process

which requires oxygen and that the rate of pump activity will be limited by the concentration of oxygen available. The neurons of Aplysia contain a haemoprotein (pigment) which reacts reversibly with oxygen and permits limited intracellular storage. Changes in the saturation of the haemoprotein are accompanied by specific changes in its absorbency such that the proportion of saturated haemoprotein can be measured as a function of transmitted light. It is therefore possible to obtain simultaneous continuous recordings of intracellular pO_2 and membrane potential from individual cells in the isolated ganglia (CHALAZONITIS, GOLA & ARVANITAKI, 1965). This has been done for the R 15 cell; as pO_2 is reduced from its normal level the period of the bursting cycle is reduced as are the magnitude and duration of the interburst hyperpolarization. When the haemoprotein is completely desaturated action potential discharge becomes monotonic. Conversely when intracellular pO_2 is increased the period of the bursting cycle lengthens and the interburst hyperpolarization increases in magnitude and duration. When the haemoprotein is completely saturated the cell may become silent (CHALAZONITIS, GOLA & ARVANITAKI, 1965; ARVANITAKI & CHALAZONITIS, 1968). Clearly, these alterations in activity correlate closely with the expected effects of pO_2 on the behaviour of the sodium pump.

The possible involvement of the electrogenic sodium pump in the generation of the bursting cycle of the R 15 cell has more recently been studied in some detail (CARPENTER, 1973; JUNGE & STEPHENS, 1973). When the cell was perfused with saline containing ouabain (4×10^{-4} M) the interburst hyperpolarization was reduced in magnitude and duration and after about 1 minute the cell began to fire regularly. However, immediately after this, it was found possible to reinstate the bursting pattern of discharge and to

restore the interburst hyperpolarization to more or less its normal magnitude and duration by sustained artificial hyperpolarization. This effect could be demonstrated for about 15 minutes in the continued presence of ouabain. Subsequently, bursting could not be reinstated either by the application of inward current or by a return to normal saline (JUNGE & STEPHENS, 1973). Similar results have been obtained for other bursting neurons in Aplysia and the irreversibility of ouabain treatment can be regarded as characteristic (CARPENTER & ALVING, 1968). The interburst hyperpolarization can also be demonstrated with artificial inward current when the cell is perfused with potassium-free saline or saline in which sodium ions are replaced by lithium ions (JUNGE & STEPHENS, 1973). Lithium ions can substitute for sodium ions during action potential production but apparently cannot act as an effective substrate for the sodium pump (CARPENTER & ALVING, 1968); both treatments should therefore inhibit the sodium pump.

These results strongly suggest that the sodium pump does not contribute directly to the generation of the interburst hyperpolarization but merely serves to modulate bursting activity through its electrogenic effect on membrane potential. As an alternative mechanism it was proposed that cyclic variation of potassium conductance is the critical factor in determining burst generation (JUNGE & STEPHENS, 1973). The results of intracellular pressure injection of KCl and K_2SO_4 (STRUMWASSER, 1965; 1968) seem inconsistent with this proposal. A 200 picolitre injection of 2.7 M KCl which should increase intracellular potassium concentration by at least 60 mM and substantially alter the potassium equilibrium potential (E_K) leads to a suppression of bursting as might be expected but a comparable K_2SO_4 injection has little effect although

this is likely to lead to a more permanent increase in intracellular potassium concentration. The effects of variations in extracellular potassium concentration also fail to provide convincing support for this hypothesis. Some enhancement in the magnitude and duration of the interburst hyperpolarization would be expected in potassium-free solutions when inward current is applied to offset the depolarization caused by sodium pump inhibition. Such an enhancement is not in fact observed and artificial hyperpolarization fails to restore magnitude and duration even to their normal values (JUNGE & STEPHENS, 1973). For the Big-D cell of Helix aspersa the results of Figure 119 show that increases in extracellular potassium concentration have a differential effect on action potential undershoot and the maximum interburst hyperpolarization. It is difficult to see why this should be the case if both depend directly on the potassium equilibrium potential.

All this does not exclude the possibility that changes in potassium conductance contribute to the interburst hyperpolarization and indeed the evidence for such a contribution is convincing (JUNGE & STEPHENS, 1973). Nevertheless, it can be suggested that potassium conductance changes are secondary to some other process. The duration of action potentials increases progressively throughout the burst (STRUMWASSER, 1968; SALANKI, VADASZ & ELEKES, 1972) and this and the changes in action potential undershoot during a burst suggest that there is a significant extracellular accumulation of potassium ions and that the potassium equilibrium potential therefore becomes progressively more depolarized. This in turn should increase the resting level of potassium conductance and would be expected to prolong monotonic activity. However, if a burst were terminated by some other mechanism, potassium conductance would remain high and

decline only as extracellular potassium fell to its normal level. In this case the variation in potassium conductance during the interburst hyperpolarization can be regarded as an after effect of burst production and not as its primary cause.

The reinstatement of bursting in the presence of ouabain apparently excludes activation of the electrogenic sodium pump as the mechanism which terminates the burst but if an alternative explanation can be found for these observations this becomes an attractive possibility since potassium accumulation during the burst could stimulate sodium pump activity which in turn could lead to its termination. A plausible alternative explanation can in fact be proposed. This depends on the fact that the membrane of R 15 and other similar cells is very extensively infolded (COGGESHALL, 1967; BULLOCK & HORRIDGE, 1965). Indeed it seems likely from capacitance measurements that in some cells up to 90% of the membrane surface may be invaginated (COGGESHALL, 1967; CARPENTER, 1970; EATON, 1972). It seems possible that such pronounced invagination will affect extracellular diffusion to some extent.

The relationship between membrane invagination and potassium ion diffusion has been studied in some detail in the non-bursting giant cell (G-cell) of Anisodoris (MIROLLI & GORMAN, 1973). Glial cell processes penetrate the invaginations and the extraneuronal space is reduced to as little as 150-200 $\mathring{A}$ but remains large compared to the hydrated potassium ion which has a diameter of somewhat less than 4 $\mathring{A}$ (see KATZ, 1966). When the rate of diffusion of potassium ions is estimated from the rate of change of cell membrane potential following a change in the potassium concentration of the perfusing solution it becomes clear that invagination represents only a

relatively minor restriction to diffusion. It can be calculated that at equilibrium a concentration difference greater than 2 mM cannot be maintained between the immediate extracellular space and the perfusing solution (MIROLLI & GORMAN, 1973). These observations do not exclude the possibility of transient potassium ion accumulation in invaginations subsequent to the passage of outward current and it has been proposed that the extracellular accumulation of potassium ions demonstrated for the R 15 cell of Aplysia can be accounted for in this way (EATON, 1972).

On an anatomical basis it is not unreasonable to regard the membrane of cells which show significant invagination as being divided into two components, one of which is relatively accessible to perfusion and a second which is less accessible. For the diffusion of small ions or molecules the difference in accessibility may be relatively minor but clearly could become significant with larger molecules.

Ouabain ($C_{29}H_{44}O_{12}$) has a molecular weight of 584 and the structure illustrated in Figure 122 (BAKER, 1966). Ouabain is a glycoside and its molecule consists of a monosaccharide coupled to an aglucone. The length of a covalent bond between carbon atoms in a six-sided ring is 1.39 Å (STOKES, 1961) and the ring itself therefore has a diameter of about 3 Å. From this it can be estimated that the ouabain molecule will be at least 20-25 Å in length. In the ideal case, the rate of diffusion of a molecule is inversely proportional to the square root of its molecular weight (SIENKO & PLANE, 1961) and on this basis the diffusion of ouabain would be expected to be at least 15 times slower than that of potassium (atomic weight 39.1). This does not allow for the hydration of the

Molecular structure of ouabain;

MW = 584

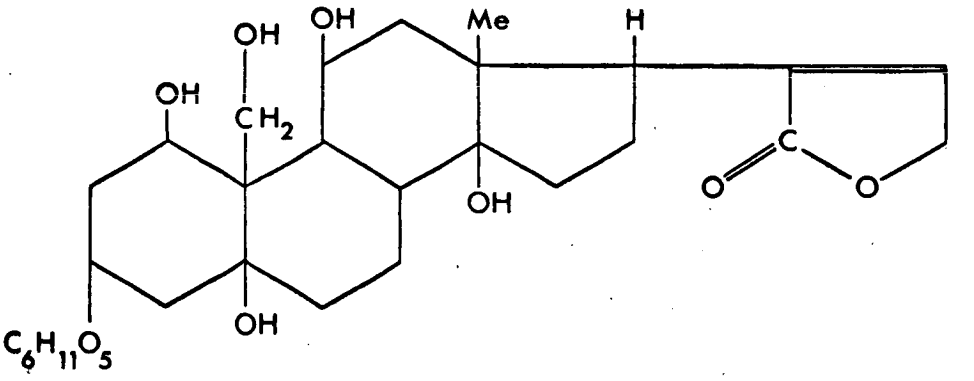

monosaccharide aglucone

After Baker (1966)

potassium ion but ouabain will also hydrate to a significant extent because its molecule is rich in OH groups and these tend to become hydrogen-bonded to surrounding water molecules slowing diffusion and increasing the effective molecular size (NYSTROM, 1973).

The slow diffusion and relatively large (hydrated) size of the ouabain molecule suggest that there will be an appreciable delay in its effect on membrane properties and it seems likely that the difference in accessibility between the two anatomical components of the cell membrane will now be significant. Thus the effects of ouabain treatment on the R 15 cell may be accounted for as follows; shortly after perfusion with saline containing ouabain has begun, the solution penetrates to the relatively accessible component of the cell membrane and inhibits the sodium pump causing an overall membrane depolarization which in turn leads to monotonic action potential discharge. However, it can be assumed that the sodium pump corresponding to the less accessible component of the membrane has not yet been inhibited and consequently, when artificial hyperpolarization is applied to offset the depolarizing effect of partial sodium pump inhibition, the bursting pattern of discharge can be reinstated. Eventually ouabain penetrates to the full extent of the membrane invaginations and sodium pump inhibition becomes complete. At this point bursting cannot be reinstated by inward current. When the cell is subsequently perfused with normal saline it may be that ouabain remains trapped to some extent in membrane invaginations and that the normal level of sodium pump activity is therefore difficult to restore. This could account for the characteristic irreversibility of ouabain treatment in bursting neurons (CARPENTER & ALVING, 1968; JUNGE & STEPHENS, 1973). In the context of this explanation for the effects of ouabain it may be

significant that pacemakers in general and bursting neurons in particular seem to show more pronounced membrane invaginations than do silent cells (COGGESHALL, 1967; FRAZIER et al, 1967; ALVING, 1969; EATON, 1972).

Under normal conditions the average loss of potassium ions across the cell membrane should be exactly balanced by active uptake such that the intracellular concentration of potassium is constant. On the other hand, when sodium pump inhibition is complete, a net loss of potassium ions would be expected. Depending on the rate of transfer, this could lead to a slight extracellular accumulation in the case of highly invaginated cells. Such an accumulation would cause a slight decrease in the potassium equilibrium potential leading to depolarization and a concomitant increase in potassium conductance, which in turn would be expected to accelerate the rate of potassium loss and thereby cause further extracellular accumulation. The process of depolarization and potassium conductance increase under these circumstances can be considered as regenerative. However, as extracellular accumulation increases, the rate of diffusion of potassium ions from the invaginations to the perfusing solution would also be expected to increase. This will limit any regenerative increase in potassium conductance since an equilibrium will be reached when the rate of potassium loss from invaginations is equal to the rate of loss across the cell membrane. Even if the maximum difference between the immediate extracellular concentration of potassium ions and the concentration in the perfusing solution is limited to 2 m$\bar{M}$ (MIROLLI & GORMAN, 1973) the change in potassium conductance could be appreciable (see Figure 68). It can be suggested that an increase in membrane conductance could be associated with inhibition of the sodium pump in highly-invaginated cells.

In the context of this speculation it is extremely interesting that a substantial increase in membrane conductance can be demonstrated in the R 15 cell of Aplysia during treatment with ouabain (CARPENTER, 1973). The conductance increase was not apparent immediately on application of ouabain but developed only after a relatively prolonged exposure. Once the membrane conductance had become high, it was not found possible to reinstate a bursting rhythm by artificial hyperpolarization. In some cases, after prolonged perfusion with normal saline, membrane conductance recovered more or less to its normal level and a bursting rhythm could then be reinstated by artificial hyperpolarization or might become apparent spontaneously. In explanation of these observations it was suggested that the potassium conductance of R 15 is 'ouabain-sensitive' and that an excessively high potassium conductance precludes burst generation although monotonic activity may still be apparent (CARPENTER, 1973). However, if the state of the membrane conductance is assumed to reflect the extent of sodium pump inhibition as suggested above, these observations clearly support the contention that the sodium pump contributes directly to burst generation. Thus, when the membrane conductance is high, the pump may be more or less completely inhibited and bursting cannot be reinstated; when membrane conductance is approximately normal the pump may be only partially inhibited and burst generation is possible.

The results of the other treatments used by Junge & Stephens (1973) to inhibit the sodium pump on closer examination also prove to be inconclusive regarding the involvement of the sodium pump in determining burst generation. When sodium ions were completely replaced by lithium ions in the perfusing solution the persistence of a bursting pattern of discharge in the R 15 cell was demonstrated

for periods of up to 20-25 minutes, sometimes even in the absence of artificial hyperpolarization. The effect of lithium is reversible and on a return to normal saline a relatively rapid restoration of the normal spontaneous activity pattern was observed. The diameter of the hydrated lithium ion is somewhat greater than that of the hydrated potassium ion but it cannot be supposed that membrane invagination represents a significant barrier to diffusion. Thus inhibition of the sodium pump should take place to more or less the same extent for both anatomical components of the cell membrane. However, there is some evidence that limited transport of lithium ions by the sodium pump is possible (CARPENTER, 1973) and in a normal (silent) cell, the period required for the apparently complete inhibition of the sodium pump by lithium ions may be up to 30 minutes (CARPENTER & ALVING, 1968). The persistence of bursting for up to 20-25 minutes therefore does not exclude the possibility of a sodium pump contribution to the interburst hyperpolarization. Depending on the rate of potassium loss and sodium uptake by the cell, the more or less indefinite persistence of bursting in sodium-free lithium saline would be expected if the sodium pump does not make such a contribution. Generally speaking, effective sodium pump inhibition should lead to a depolarization and to the establishment of monotonic action potential discharge as observed in the presence of ouabain. The persistence of a bursting rhythm in the absence of artificial hyperpolarization may in itself be an indication that inhibition is only partial.

For the Big-D cell of Helix aspersa, perfusion with 1 mM potassium saline leads to a prompt suppression of the bursting cycle and monotonic activity is established (Figure 118, record (A)). This is consistent with sodium pump inhibition and slight depolariz-

ation. On the other hand, the bursting cycle of the R 15 cell of Aplysia is not always lost even in potassium-free solutions and without artificial hyperpolarization (JUNGE & STEPHENS, 1973). The obvious inference is that sodium pump inhibition is incomplete in the latter case. For this to be true all that is required is a slight degree of potassium accumulation in membrane invaginations such that the absence of potassium in the perfusing solution is not fully reflected in the immediate extracellular solution. Such limited accumulation is not excluded by the findings of Mirolli & Gorman (1973) and seems likely in view of the substantial accumulation associated with outward current (EATON, 1972).

The Big-D cell shows a range of spontaneous activity (Figure 108) and is generally a less 'reliable' bursting neuron than R 15 which almost invariably shows a well developed bursting cycle (FRAZIER et al, 1967). If it is supposed that the nature of the bursting pattern depends in some way on the extent of membrane invagination it can be suggested that the Big-D cell will show less pronounced invagination than R 15. While there is no direct evidence for this, such a difference could conceivably account for the different effects of perfusion with low potassium salines on the two cells.

Finally, there is the question of sodium pump inhibition by cooling. Clearly, cooling should affect both anatomical components of the membrane equally and apparently offers the critical test of whether or not the sodium pump is involved in burst generation. The problem is not resolved by the observation that cooling to $10^{o}C$ does not suppress bursting in R 15 (JUNGE & STEPHENS, 1973); there is ample evidence that sodium pump inhibition

is only slight at 10°C (CARPENTER & ALVING, 1968; GORMAN & MARMOR, 1970a; 1970b; MARMOR & GORMAN, 1970; MARMOR, 1971b; KOSTYUK, KRISHTAL & PIDOPLICHKO, 1972). Cooling to temperatures below 10°C has been shown to suppress bursting in an identified bursting neuron of Helix pomatia (SALANKI, VADASZ & VERO, 1973) and also in the Big-D cell of Helix aspersa (Figure 117). However, the implications of these observations are not entirely clear since the ratio between the resting membrane sodium and potassium conductances has been shown to alter with temperature and it has been suggested that the Q_{10} for P_{Na^+} is greater than that for P_{K^+} (CARPENTER, 1970; GORMAN & MARMOR, 1970b). The current-voltage relation of the G-cell of Anisodoris shows pronounced anomalous rectification at 10-15°C; this is absent at 0-5°C but is unaffected by ouabain (MARMOR, 1971a; 1971b). Thus, reductions in temperature may have an effect on membrane properties which is independent of sodium pump inhibition. Consequently, observations obtained with cooling become difficult to interpret. The R 15 cell of Aplysia shows a steady-state negative resistance characteristic (N.R.C.) which is essentially similar to anomalous rectification and is also absent in the cooled preparation (WACHTEL & WILSON, 1973; WILSON & WACHTEL, 1974). It was suggested that this contributes to burst generation as opposed to monotonic activity. However, the absolute potential theory of intrinsic pacemakers developed above suggests that a steady-state negative resistance characteristic will be associated with purely monotonic pacemaker activity (see Figures 89-92) and it may be that the N.R.C. does not contribute directly to burst generation.

In summary it can be said that none of the currently available results obtained with treatments designed to inhibit the sodium pump in bursting neurons conclusivley exclude an

electrogenic contribution to the interburst hyperpolarization. Ouabain is probably the most effective method of inhibition but has a two-stage effect on bursting and membrane conductance which is consistent with an initial partial inhibition followed by a progressively more complete inhibition as ouabain penetrates to the full extent of membrane invaginations. Lithium saline inhibits the sodium pump in normal cells only slowly and the persistence of bursting has not so far been shown to exceed the period required for apparently complete inhibition. The alterations in activity observed with potassium-free saline perfusion of the R 15 cell of Aplysia suggest that pump inhibition is only partial. Cooling does not offer a critical test of sodium pump involvement since changes in temperature can lead to alterations in membrane properties which are independent of sodium pump activity. In the present analysis the view is adopted that the sodium pump does make an electrogenic contribution to the interburst hyperpolarization. This leads to a model for the process of burst generation which is much more satisfactory than any which can be proposed if the alternative assumption is made.

When the R 15 cell of Aplysia is perfused with saline containing tetrodotoxin (TTX) action potential production is blocked but spontaneous oscillations in membrane potential fairly similar in frequency, magnitude and time-course to the normal interburst hyperpolarization may persist (STRUMWASSER, 1968; JUNGE & STEPHENS, 1973). These 'endogenous waves' of membrane potential can be reliably observed in TTX saline which is also free of calcium ions. The waves in Ca^{++}-free TTX saline can be inhibited by ouabain treatment and can be reinstated by artificial hyperpolarization but only for a limited period as in the case of burst reinstatement

in normal saline containing ouabain (JUNGE & STEPHENS, 1973). It therefore seems probable that the mechanisms which underly normal burst generation also determine the production of endogenous waves of membrane potential in Ca^{++}-free TTX saline.

Tetrodotoxin selectively blocks the sodium channel in squid giant axon (MOORE et al, 1967). In some Aplysia neurons the inward current during action potential production appears to be carried by both sodium ions and calcium ions. Application of TTX to such neurons blocks the flow of sodium ions but inward current can still be carried by calcium ions and action potential production remains possible (GEDULDIG & GRUENER, 1970). Action potential blockage in R 15 therefore suggests that the inward current is carried almost exclusively by sodium ions. Thus, the observation that endogenous waves of membrane potential may persist in the presence of TTX apparently excludes the possibility that the interburst hyperpolarization is triggered by an intracellular accumulation of sodium ions. Nevertheless, a model based on this assumption has been proposed (STRUMWASSER & KIM, 1969) and such an accumulation might be possible in view of the relatively low conductivity of the intracellular solution in Aplysia neurons (CARPENTER, HOVEY & BAK, 1971).

It has also been suggested that intracellular accumulation of calcium ions triggers the interburst hyperpolarization (JUNGE & STEPHENS, 1973). This is extremely unlikely since under normal conditions calcium ions do not appear to contribute significantly to the inward current during action potential production in R 15. In addition, the calcium equilibrium potential will be reversed in Ca^{++}-free TTX saline such that there should be a net loss of calcium

ions across the cell membrane; this does not inhibit endogenous waves of membrane potential but leads instead to an apparent enhancement (JUNGE & STEPHENS, 1973).

In accounting for the presence of endogenous waves of membrane potential in Ca^{++}-free TTX solution two obvious possibilities remain; the question of chloride involvement in normal burst generation has already been discussed and it does not seem likely that chloride ions will contribute in any significant way (CARPENTER, 1973; JUNGE & STEPHENS, 1973). It can be concluded that the process underlying endogenous waves and normal burst generation is probably determined in some way by the movement of potassium ions across the cell membrane. The apparent enhancement of endogenous waves of membrane potential in Ca^{++}-free TTX saline is consistent with this suggestion since a primary effect of decalcification is an increase in potassium conductance (FRANKENHAEUSER & HODGKIN, 1957).

There is some suggestion that the endogenous waves of membrane potential which appear to underly burst generation arise primarily in a membrane region which is anatomically distinct from that which determines action potential production during the burst (CHALAZONITIS, 1968). Thus, in the R 15 cell of Aplysia, a constant depolarizing current applied intracellularly can sometimes alternately activate a somatic area giving rise to a burst of somatic spikes and, during the interburst hyperpolarization, a deeper, axonal area giving rise to small amplitude axon spikes. This 'bifocal' activation has been attributed to an increase in the conductance of the more remote axonal area which short-circuits some of the depolarizing current. While there is no doubt that the bursting rhythm of R 15 is determined intrinsically (STRUMWASSER,

1965; 1968; ARVANITAKI & CHALAZONITIS, 1968; CARPENTER, 1973; JUNGE & STEPHENS, 1973) a long-lasting hyperpolarization (L.L.H.) with the characteristics of the spontaneous interburst hyperpolarization can be initiated synaptically and it seems that this also could involve an increase in the conductance of an axonal region of the membrane (CHALAZONITIS, 1968).

The Big-D cell of Helix aspersa is also an intrinsic pacemaker (WALKER et al, 1970) in which synaptic initiation of L.L.H. (by stimulation of the left pallial nerve) can be demonstrated (KERKUT & HORN, 1968). The synaptically initiated L.L.H. can be mimicked by the iontophoretic application of dopamine and does not reverse even when membrane potential is markedly hyperpolarized (KERKUT, HORN & WALKER, 1969). The hyperpolarizing action of dopamine in identified Helix aspersa neurons is blocked by ouabain and is apparently due to stimulation of the electrogenic sodium pump (KERKUT, BROWN & WALKER, 1969a). Other identified neurons show a hyperpolarization in response to acetylcholine which can also be attributed to the electrogenic sodium pump (KERKUT, BROWN & WALKER, 1969b).

An axonal localization seems characteristic for synaptic potentials in molluscan neurons (BULLOCK & HORRIDGE, 1965; GORMAN & MIROLLI, 1970) and these observations regarding the synaptic initiation of L.L.H. can therefore be related to the characteristic pattern of membrane invaginations in pacemaker cells. The invaginations in the axonal region of the cell are normally somewhat less numerous but very much deeper than those which occur over the surface of the soma. Indeed, in larger cells, the axonal invaginations may be so extensive that the axon hillock region is broken up,

forming a 'trophospongium' (BULLOCK & HORRIDGE, 1965; COGGESHALL, 1967). This region of pronounced invagination coincides with the probable axonal localization of pre-synaptic terminals and it seems reasonable to suggest that, in the case of bursting neurons, the two anatomical components of the cell membrane may also be functionally distinct.

A model for the process of burst generation which takes into account all the properties of bursting neurons discussed above can now be proposed. It is assumed that a bursting neuron is fundamentally an intrinsic monotonic pacemaker and that its membrane is more or less homogeneous with respect to its excitable properties but can be divided into two anatomical components. One component corresponds to the non-invaginated surface of the cell and is assumed to be relatively accessible to perfusion; the other component corresponds to membrane invaginations and is assumed to be somewhat less accessible. The two components of the membrane are closely coupled electrically. During action potential discharge potassium ions accumulate extracellularly initially to the same extent for both components of the membrane but diffuse away from the non-invaginated surface rather more quickly than from invaginations. If the interval between successive action potentials is sufficiently small accumulation will become additive in the first instance for the invaginated component of the cell membrane. This will reduce the potassium equilibrium potential and lead to depolarization, an increase in potassium conductance and accelerated accumulation. At the same time the non-invaginated membrane surface will be slightly depolarized electrotonically and the frequency of action potential production will tend to increase; this too will facilitate potassium ion accumulation in invaginations. Thus, the

process of accumulation, once begun, can be regarded as essentially regenerative. As already pointed out, regenerative accumulation is likely to be limited by the loss of potassium ions from invaginations by diffusion into the perfusing solution but active transport by the sodium pump could also contribute appreciably if the extent of accumulation is sufficient to stimulate pump activity.

If it is supposed that the sodium pump does not respond instantaneously to changes in extracellular potassium concentration but does so only after some delay then burst generation can be seen as the natural result of an adequate extracellular accumulation of potassium ions. The sequence of events during the normal bursting cycle can be visualized as follows; on recovery from the interburst hyperpolarization an action potential is produced because of the intrinsic pacemaker characteristics of the membrane and there is a slight extracellular accumulation of potassium ions. The interval between the first and second action potentials is sufficiently short for accumulation to become additive and the associated depolarization causes a progressive increase in action potential frequency towards the middle of the burst. The electrogenic effect of sodium pump stimulation now becomes appreciable and there is a reduction in action potential frequency. This and the active uptake of potassium ions across the cell membrane reduce the rate of extracellular accumulation. The sodium pump does not respond immediately to any associated reduction in extracellular potassium concentration and at the end of the burst the electrogenic hyperpolarization is sufficient to suppress action potential production. Potassium conductance at this time may exceed its 'resting' level and the membrane is driven to a hyperpolarized potential partly determined by the magnitude of the electrogenic current and partly

by the potassium equilibrium potential. The flow of potassium ions during hyperpolarization will be considerably less than that during activity and the extracellular concentration will therefore decline to its normal level. With some delay, the electrogenic current will also decrease allowing the membrane to depolarize; when the threshold for action potential production is reached the cycle will begin anew.

The flow of ions through the electrically excitable sodium channel of the membrane is necessary for action potential production and will therefore contribute to the normal pattern of burst generation. However, if the sodium channel is blocked by TTX, the essential component relationships of the model described above should not be affected. It can therefore be suggested that the model provides a satisfactory explanation for the occurrence of endogenous waves of membrane potential during TTX treatment and, because of increased potassium conductance, also for their enhancement in Ca^{++}-free TTX saline. In addition, the model is consistent with the characteristics of normal burst generation and seems adequate to account for most if not all of the other known properties of bursting neurons. For example, if the membrane is depolarized, or if the extent of extracellular accumulation is less than adequate, the electrogenic current associated with sodium pump activity may never become sufficient to suppress action potential production and monotonic activity will be observed. In these circumstances sodium pump activity will tend to occur at a more or less constant rate and will not vary in a cyclic manner. In the same way, irregular or monotonic activity is likely to be the result of a partial sodium pump inhibition; the application of artificial hyperpolarization will tend to inhibit action potential

production and in this case the (reduced) electrogenic current may once more become sufficient to prevent prolonged discharge thereby causing a reinstatement of bursting.

Although plausible, explanations of this kind are satisfactory only in a rather limited way because the model proposed is rather complex and so far has been stated only in a qualitative manner. Thus, it is not entirely clear from the model system whether burst generation will depend on a highly specific combination of parameter values or whether it will occur for a wide range of values. In addition, it is not possible to infer which of the various parameters and interrelationships are especially critical in determining the pattern of activity and which are less important. Clearly a more precise statement of the proposed model is required; this can be provided either in terms of an electronic analogue for the model or in terms of an attempted simulation based on the absolute potential equations previously developed. In the two sections which follow these two methods of more precise statement are examined.

D) Proposed mechanism; an analogue model

The function of a satisfactory analogue model is twofold; firstly, it can give an indication of whether the particular system of interrelationships which forms the model is in fact sufficient to account for the observed activity pattern of the real system which the model is intended to represent. Secondly, it may be possible to determine which of the interrelationships is likely to be especially important in determining activity patterns in the real system and whether or not a particular activity pattern depends on a highly specific combination of parameter values. An analogue model is normally a considerably simplified representation of the real system and retains only those characteristics presumed to be essential for a tolerably accurate mimicry of the behaviour of the real system. Thus, an analogue model will often lack quantitative precision to some extent but its simplified nature facilitates a rapid test of a particular hypothesis. In addition, the model can easily be modified on a trial and error basis in an attempt to provide a better representantion of the real system. On the other hand, an inherently more complex representation such as a mathematical model although precise may be tedious to construct and difficult to modify.

The circuit of the electronic analogue model constructed for the proposed mechanism of spontaneous burst generation is illustrated in Figure 123. From a functional point of view the circuit consists of five interconnected units; these have been termed the spike generator, summing amplifier, undershoot control, K^+ accumulation control and sodium pump control. The spike generator consists of two operational amplifiers; the first of these

Bursting neuron simulator;

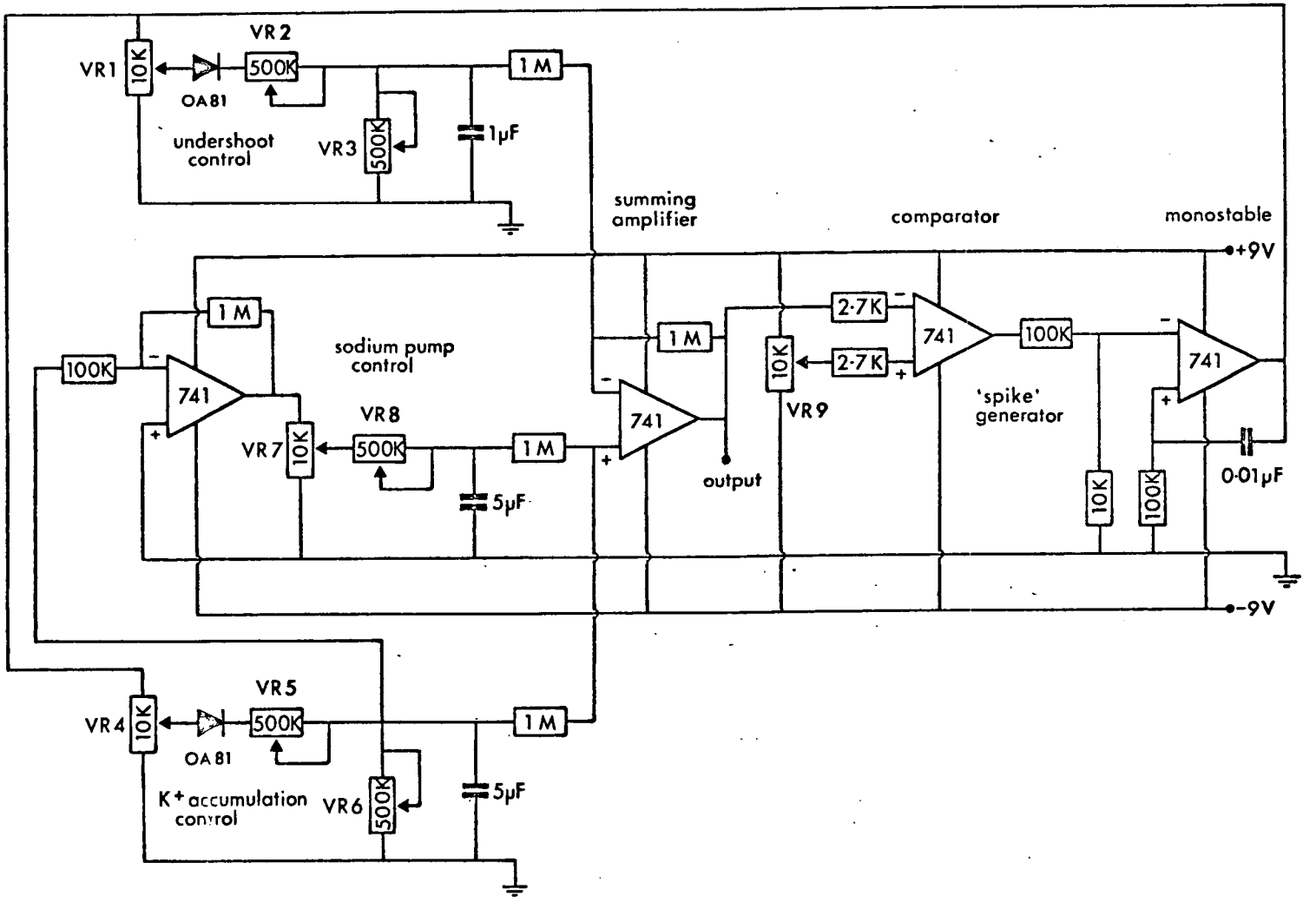

is connected to form a comparator such that its output is either fully positive (+9 V) if the voltage at the non-inverting (+) input exceeds that at the inverting (-) input or fully negative (-9 V) if the reverse is true. The 'threshold' of the comparator and of the spike generator as a whole is set at the non-inverting input by adjustment of VR 9.

Suppose that the (threshold) voltage at the non-inverting input does not exceed that at the inverting input and that the output of the comparator is therefore -9 V. If now a negative pulse is applied at the inverting input and reverses this situation, the output of the comparator will rise (almost instantaneously) to +9 V and will remain high for the duration of the negative pulse. At the end of the negative pulse the output of the comparator will fall (almost instantaneously) to -9 V. This latter voltage change is the input required to trigger the second operational amplifier (monostable) of the spike generator. The monostable produces a positive going rectangular pulse of 1 msec duration.

This monostable pulse is passed to the undershoot control circuit and charges up the corresponding (1 μF) capacitor to a potential which is determined partly by the setting of VR 1 and partly by the potential divider formed by VR 2 and VR 3. At the end of the monostable pulse the capacitor cannot discharge through VR 2 and VR 1 because of the reverse-biased diode in series, but discharges instead through VR 3 which therefore determines the time constant of the voltage decline. Thus, the output of the undershoot control circuit is a positive going pulse which rises with an almost square leading edge to an adjustable amplitude level and declines exponentially with an adjustable time constant.

This output is inverted by the unity gain summing amplifier and transferred to the inverting input of the comparator stage of the spike generator causing its output to go fully positive. Thus, a negative going change in comparator output causes a monostable pulse which, modified by the undershoot control and inverted by the summing amplifier, almost immediatley causes a second (positive going) change in comparator output. The comparator output remains high as the negative potential at the inverting input declines exponentially towards zero (earth) potential until it once more exceeds the threshold potential at the non-inverting input. The resultant change in comparator output initiates a second monostable pulse and the cycle is repeated. Together, the spike generator, undershoot control and summing amplifier form a simple, but for the present purpose adequate, analogue representation of an intrinsic monotonic pacemaker neuron. The frequency of monotonic activity can be modified by changing the amplitude or time constant of the undershoot pulse, by altering threshold or by applying 'depolarization' or 'hyperpolarization' at the inverting input of the comparator stage of the spike generator.

The potassium (K^+) accumulation circuit is identical to that for undershoot control except that the associated capacitor is larger (5 μF) to allow longer time constants of output pulse decline. The K^+ accumulation circuit is driven directly by spike generator pulses and its output is transferred by the unity gain summing amplifier to the inverting input of the comparator without inversion such that K^+ accumulation has an acceleratory ('depolarizing') effect on the frequency of spike generator pulses. VR 5 is intented to control the amplitude of individual 'accumulation' pulses. If the frequency of spike generator pulses is sufficient, these accumulation

pulses may summate. This summation process is limited by the setting of VR 4 which attenuates spike generator pulses. Thus, the potential representing K^+ accumulation may reach (but cannot exceed) a plateau level corresponding to the attenuated amplitude of the spike generator pulses.

The sodium pump control circuit is not driven directly by spike generator pulses but instead derives its input from the K^+ accumulation control circuit. The potential representing accumulation is amplified (10x) and inverted before charging the sodium pump capacitor (5 μF). The direction of discharge of this capacitor is not diode-limited and in effect the potential representing electrogenic sodium pump activity will follow K^+ accumulation with a time constant largely determined by VR 8; VR 7 determines the multiplicative relationship between accumulation and the electrogenic sodium pump potential. Transferred to the spike generator the output of the sodium pump control circuit has an inhibitory effect on 'spike' production.

The analogue membrane potential is measured at the output of the summing amplifier and represents the sum of all the factors other than threshold which affect 'spike' production by the spike generator. The spike generator pulses do not appear directly at this point and positive transients representing action potential overshoots are absent from the analogue membrane potential. This simplification is justified provided that the after effects of action potential production are appropriately modelled; the occurrence of spike generator pulses is indicated by negative transients representing action potential undershoots.

The behaviour of the analogue model as a whole was found to be rather sensitive to the threshold potential set by adjustment of VR 9. Provided satisfactory adjustment of threshold was obtained, the analogue membrane potential showed a bursting pattern of activity for a wide range of adjustment of other parameters. Bursting can in fact be regarded as the normal output of the analogue model and the proposed mechanism for the process of burst generation therefore seems sufficient to account for a bursting pattern of action potential discharge in the real situation.

The effect on the output of the analogue model of increasing the amplitude of individual undershoot pulses by adjustment of VR 2 from its minimum to its maximum, while other parameters were constant at intermediate values, is illustrated in Figure 124(A). The period of the bursting rhythm shows a maximum when the undershoot amplitude is least and, at the same time, maximum values of interburst 'spike' frequency, K^+ accumulation and electrogenic sodium pump 'activity' are observed. As the undershoot amplitude increases, the intraburst spike frequency declines and there is an associated reduction in accumulation, pump activity and also in the period of the bursting cycle. For higher values of undershoot amplitude the bursting cycle is lost and spike discharge becomes monotonic. The effect of increasing the time constant of undershoot decline (by adjustment of VR 3 from its minimum to its maximum) is shown in Figure 124(B). The results obtained illustrate a similar dependence of the bursting pattern of analogue output on an adequate frequency of spike discharge. Since the time constants of real membrane conductance changes are very sensitive to alterations in temperature (GUTTMAN & BARNHILL, 1970) it may be significant that the temperature dependent changes

FIGURE 124; p 180

Analogue model;

A; Undershoot amplitude (VR 2)

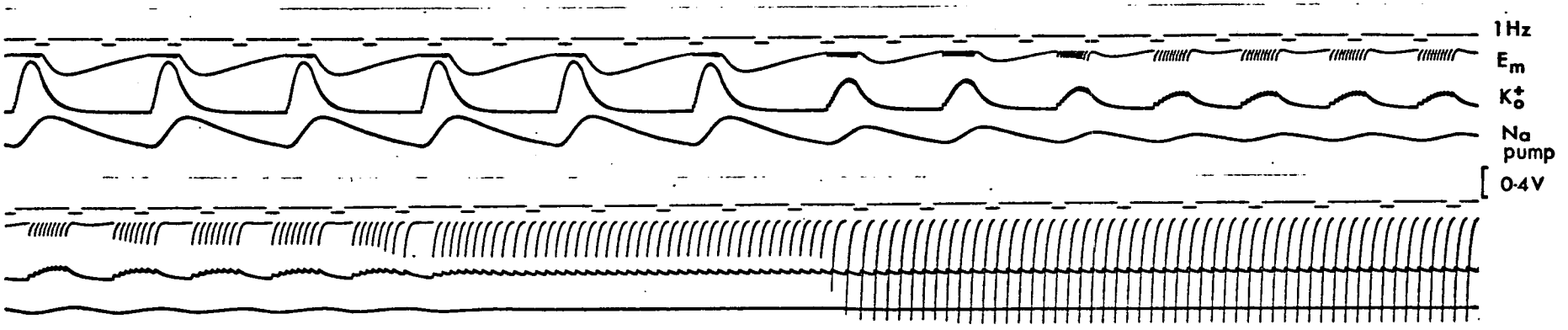

B; Undershoot time constant (VR 3)

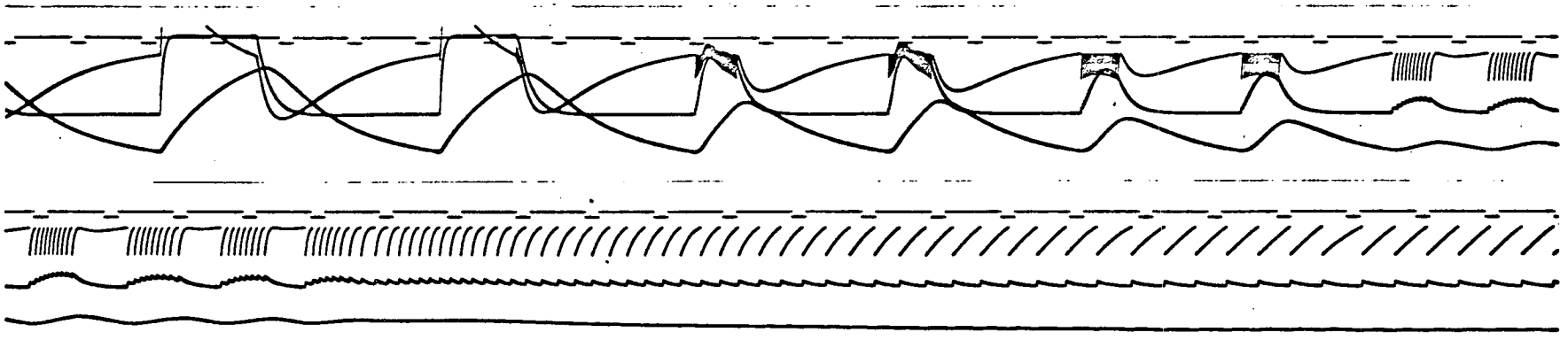

FIGURE 125; p181

Analogue model;

A; K^+ accumulation amplitude (VR5)

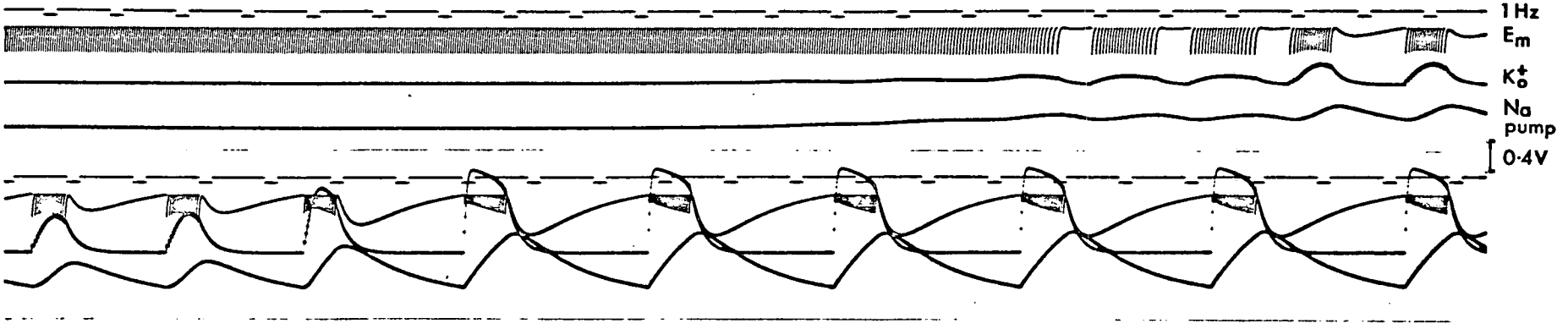

B; K^+ accumulation time constant (VR6)

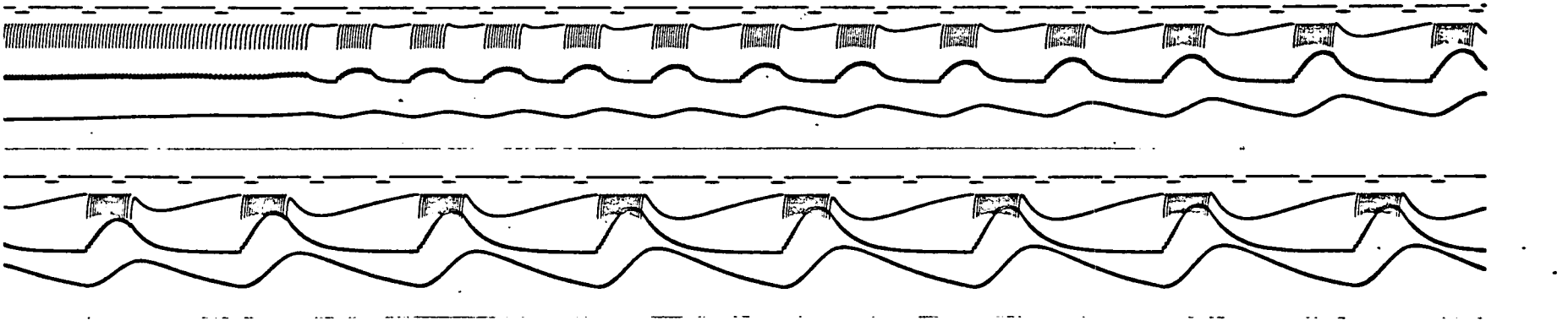

in bursting rhythm observed in the real situation (SALANKI, VADASZ & VERO, 1973; JUNGE & STEPHENS, 1973; WACHTEL & WILSON, 1973) resemble those obtained by altering the analogue undershoot time constant.

Figure 125(A) shows the alteration obtained in analogue output by increasing the amplitude of individual accumulation pulses (VR 5). Spike discharge is monotonic for low amplitude values and the development of a bursting pattern of discharge only becomes apparent when amplitude is sufficient for accumulation to become additive. The period of the bursting rhythm lengthens while intraburst spike frequency and the interburst 'hyperpolarization' are progressively enhanced with further increases in amplitude. Figure 125(B) shows the effect of increasing the decay time constant of accumulation (VR 6) for an intermediate amplitude value. Changes in time constant have a similar effect on the period of the bursting cycle but do not lead to such a pronounced enhancement of intraburst spike frequency. In the real situation, membrane invaginations would be expected to increase the decay time constant of accumulation rather than the amount of accumulation per action potential. Provided that accumulation per action potential can be considered adequate, the behaviour of the analogue model suggests that a bursting pattern of discharge will occur when the decay time constant of potassium ion accumulation is sufficiently increased by membrane invagination.

Increasing the magnitude of the potential representing electrogenic sodium pump activity (VR 7) for intermediate values of other parameters changes the behaviour of the analogue model in the manner illustrated in Figure 126. When there is only a small

FIGURE 126; p 181

Analogue model;

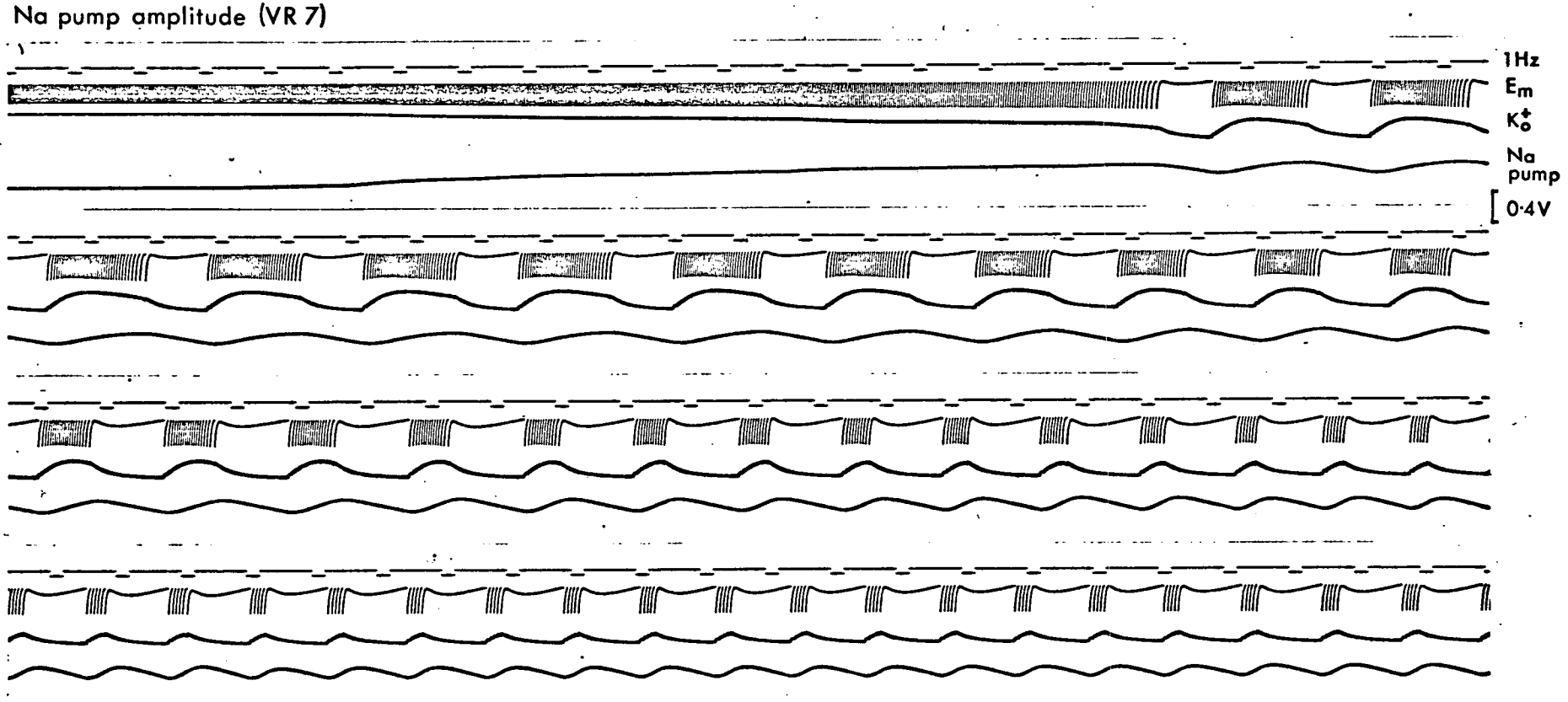

FIGURE 127; p 183

Analogue model;

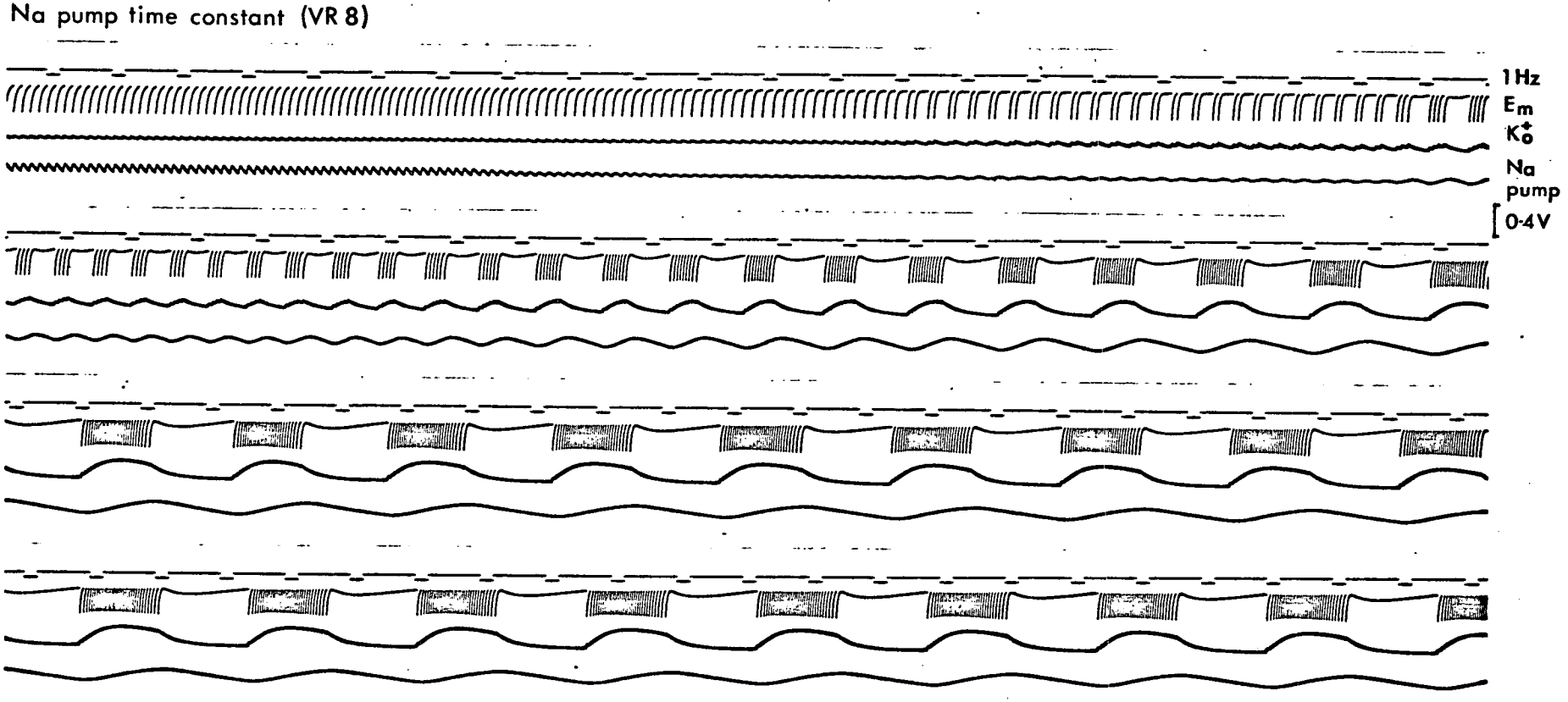

'electrogenic' contribution to the analogue membrane potential spike discharge is monotonic. The frequency of discharge is reduced as this contribution increases and when bursting first becomes apparent the period of the bursting cycle has a maximum value. Further increases in sodium pump 'activity' cause a reduction in the number and frequency of spikes within each burst while the duration of the interburst interval is comparatively little affected. These alterations are closely similar to those observed with increased extracellular potassium concentration in the case of the Big-D cell of Helix aspersa (Figure 118) and it can therefore be suggested that changes in sodium pump activity determine the pattern of activity in the real situation in the same way as in the analogue model.

It is reasonable to suppose that an increase in electrogenic sodium pump activity should reduce burst duration and spike content since a lesser degree of accumulation should produce the electrogenic pump potential necessary for burst termination. This conclusion seems inconsistent with the observation that increases in intracellular pO_2, which should lead to sodium pump stimulation (KERKUT & YORK, 1969), cause an increase rather than a decrease in the period of the bursting rhythm and also in burst duration and spike content (ARVANITAKI & CHALAZONITIS, 1968). However, in the real situation, enhanced sodium pump activity causes a significant overall hyperpolarization (KERKUT & YORK, 1971). In the case of bursting neurons in Helix pomatia, hyperpolarization has been shown to cause a significant increase in the transmembrane flow of potassium ions during action potential production (LUX & ECKERT, 1974) such that the duration of individual action potentials will be reduced and the amount of potassium accumulation per action

potential increased. Neither of these effects is represented in the analogue model; the period of the bursting rhythm and the number of analogue spikes per burst rapidly increase with the amplitude of accumulation pulses (Figure 125(A)). While its analogue representation is not entirely adequate, it seems that the proposed mechanism for the process of burst generation could account for an increase in the period of the real bursting cycle when the sodium pump is stimulated by increases in intracellular pO_2. In the case of increases in extracellular potassium concentration, the hyperpolarization caused by sodium pump stimulation is offset by the depolarizing effect of reductions in E_K. Clearly, this could account for the difference in effect between the two methods of pump stimulation.

The effect of increasing the time constant (VR 8) with which the analogue electrogenic sodium pump potential follows K^+ accumulation is illustrated in Figure 127. Increases in time constant increase the period of the bursting cycle and bursting occurs over a wide range of time constants. It can be suggested that, in the real situation, bursting may occur provided that the time constant of changes in sodium pump activity exceeds a certain minimum value. Real sodium pump activity is a relatively complex process (KERKUT & YORK, 1971) and it seems reasonable to suppose that the time constant of changes in activity will in fact be adequate to account for the development of a bursting pattern of action potential discharge.

In summary it can be said that the behaviour of the analogue model suggests that the proposed mechanism for the process of burst generation is sufficient to account for the occurrence of bursting in the real case and for at least some of its modifications

under different experimental conditions. In addition, with the possible exception of threshold, none of the parameters or interrelationships involved appear to be especially critical in determining whether or not bursting will occur but instead tend to modify the bursting pattern over a reasonable range and exclude it only at relatively extreme values. The precise nature of the bursting pattern at least in the analogue case is determined by the mutual interrelationship of several factors rather than having a single primary cause. Such a complex dependence is plausible in view of the diversity of experimental results obtained with bursting neurons.

E) Attempts at computer simulation;

1) Additional assumptions required;

The results obtained with the electronic analogue model for the proposed mechanism of burst generation are sufficiently encouraging to justify an attempt at a full computer simulation of the proposed mechanism incorporating the system of absolute potential equations previously developed. Before this can be done it is necessary (in the absence of suitable experimental data) to make a number of arbitrary assumptions regarding the characteristics of potassium accumulation and the relationship between extracellular potassium concentration and sodium pump activity.

The problem of potassium accumulation is relatively easily overcome. For normal action potential simulation the transmembrane potassium current (denoted by IK in the computer programmes of Appendices 1-6) is calculated at each time step in the integration process. The charge transferred during each time step is directly related to the number of potassium ions transferred and can be found simply by multiplying the calculated current (IK) by the size of the time increment for integration (DT). If it is assumed that the potassium ions transferred diffuse rapidly into a small, totally restricted (closed) extracellular space then the alteration in extracellular potassium concentration for a given time step can be found by multiplying the charge transferred by an appropriate constant quantity. This constant has been termed the scale constant (SC). With a closed extracellular space and in the absence of active uptake of K^+ ions across the membrane, the change in extracellular potassium concentration for any given time step can be written in computer programme notation as IK*DT*SC.

Relatively recent experiments with ion-sensitive electrodes show that during action potential production there is a measurable change in extracellular potassium concentration near the exposed surface of Helix pomatia neurons (NEHER & LUX, 1973; LUX & ECKERT, 1974). The peak increase in extracellular concentration measured during a single action potential was 0.5 mM; this could be a slight underestimate of the immediate extracellular change depending on the proximity of the ion-sensitive electrode. Progressive extracellular potassium ion accumulation could be demonstrated during a brief volley of action potentials (NEHER & LUX, 1973). These observations suggest that the scale constant used in simulation should provide changes in extracellular potassium concentration per action potential within the range 0.5-2 mM. By trial and error, scale constant values between 0.0001 and 0.0004 were found to be appropriate.

The assumption of a closed extracellular space does not necessarily lead to significant inaccuracies in calculating the change in extracellular potassium concentration associated with transmembrane current during a given time step provided that the duration of the time step is sufficiently short. In the real situation, the extracellular space is not closed and potassium ions will diffuse away from the membrane surface. If the immediate extracellular concentration (denoted by K_EXT) exceeds that in the perfusing solution (K_EXTREST) at any time $t = t_o$ such that $K\_EXT = K\_EXT_o$, then, in the absence of any transmembrane potassium current, the immediate extracellular concentration will decline exponentially towards the concentration in the perfusing solution. Thus the process of diffusion has a time constant; if the time

increment for integration used in simulation is small compared to the time constant of diffusion, there will be little error in assuming a closed extracellular space for the purpose of calculating the change in extracellular concentration associated with transmembrane K^+ current during any individual time step. However, in the longer term, it is clearly essential to consider the reduction in extracellular concentration due to diffusion. In the absence of transmembrane K^+ current, the immediate extracellular potassium concentration at any time can be written as;

$$K\_EXT_t = (K\_EXT_o - K\_EXTREST).e^{-\frac{t}{\tau}} + K\_EXTREST \quad (88)$$

where τ is the time constant of diffusion. Differentiation of this expression provides;

$$\frac{d(K\_EXT)}{dt} = -\frac{(K\_EXT_o - K\_EXTREST).e^{-\frac{t}{\tau}}}{\tau} \quad (89)$$

The change in extracellular potassium concentration $\Delta(K\_EXT)$ for a small time increment, Δt, is given by;

$$\Delta(K\_EXT)_{t \rightarrow (t+\Delta t)} = -\frac{\Delta t(K\_EXT_t - K\_EXTREST).e^{-\frac{\Delta t}{\tau}}}{\tau} \quad (90)$$

After collecting the constant terms equation (90) can be written as;

$$\Delta(K\_EXT)_{t \rightarrow (t+\Delta t)} = \Delta t(K\_EXT_t - K\_EXTREST).DC \quad (91)$$

where;

$$DC = \frac{-\Delta t.e^{-\frac{\Delta t}{\tau}}}{\tau} \quad (92)$$

The expressions describing extracellular potassium accumulation and diffusion loss can be grouped to form a composite

expression such that, in computer notation;

$$K\_EXT1 = K\_EXT + (K\_EXT - K\_EXTREST)*DC + IK*DT*SC \qquad (93)$$

where K_EXT1 is the extracellular concentration at the end of any time step and K_EXT is the concentration at the end of the immediately preceding time step. Equation (93) was used in simulation of the proposed mechanism of burst generation and is included in the Algol W programmes of Appendices 5 and 6. Because changes in extracellular potassium concentration alter the potassium equilibrium potential (E_K), the mathematical representation of the effects of potassium accumulation is incomplete unless the simulation process involves the recalculation of E_K, according to the Nernst equation, for each time step in the integration. The simulation programmes developed incorporate this modification.

It is less easy to derive a satisfactory mathematical description of sodium pump activity because so little is known of its mechanism. However, the results obtained with the electronic analogue model suggest that the precise relationship between extracellular K^+ accumulation and pump activity is less than critical in determining whether or not burst generation is possible provided that the time constant of changes in pump activity exceeds a certain minimum value. In this case, simulation using an essentially arbitrary mathematical description of the sodium pump can be justified and still seems likely to offer a more useful statement of the proposed mechanism of burst generation than that afforded either by the corresponding 'word model' or its electronic analogue.

The characteristics of sodium pump activity presumed to

be necessary for reasonable simulation of the process of burst generation were as follows; 1) Sodium pump activity associated with normal extracellular potassium concentration (3 mM in the case of Helix aspersa neurons) should be relatively slight but should rise steeply in an approximately linear manner with increases in concentration, possibly reaching a (saturated) plateau level for relatively high extracellular concentrations. This pattern of variation seems consistent with the experimentally demonstrated effects of extracellular potassium concentration on the magnitude of the electrogenic contribution of sodium pump activity to the resting potential of Helix aspersa neurons (MORETON, 1969). 2) The ratio between the number of sodium ions and potassium ions transferred by the pump was assumed to be constant at 3:2 (see KERKUT & YORK, 1971). 3) Changes in the level of pump activity in response to changes in extracellular potassium concentration were assumed to take place with an appreciable time constant.

The control of sodium pump activity by intracellular sodium concentration (THOMAS, 1969) is not a necessary assumption for simulation of the proposed mechanism of burst generation; it has previously been argued that intracellular accumulation of sodium ions is unlikely to contribute significantly to burst termination. However, if any stimulation of pump activity does occur through intracellular sodium accumulation, it can be assumed that its time course will be nearly identical to that of the stimulation associated with extracellular potassium accumulation. Thus, the relationship between a given change in extracellular potassium concentration and the magnitude of the corresponding change in sodium pump activity can be adjusted (by trial and error) during preliminary simulations to provide an appropriate change in

simulated membrane potential. If there is any stimulation of the sodium pump by intracellular accumulation in the real situation this should be included in the empirically derived multiplicative relationship between extracellular potassium concentration and sodium pump current (which in this instance will be an overestimate of that probable in the real situation).

The approach adopted in developing a mathematical description of sodium pump activity was to consider the rate of ion transfer by the sodium pump as being controlled by the state of a unitless variable in exactly the same manner as unitless variables control sodium and potassium conductance in the Hodgkin-Huxley system of equations. In the Hodgkin-Huxley system the rate constants of conductance change are assumed to be instantaneous functions of membrane potential; in developing equations for the sodium pump it was assumed that the rate constants of activity change were instantaneous functions of extracellular potassium concentration. The sodium pump 'activation variable' has been denoted by P and the sodium pump 'reaction' can be written as;

$$(1 - P) \underset{\beta_P}{\overset{\alpha_P}{\rightleftharpoons}} P \qquad (94)$$

The reaction is assumed to obey first order kinetics such that;

$$\frac{dP}{dt} = \alpha_P(1 - P) - \beta_P.P \qquad (95)$$

where α_P and β_P are the rate constants of the forward and reverse reactions. When a step function change in extracellular potassium concentration is applied to the system, α_P and β_P instantaneously take up new values and P approaches its steady state value P_∞ along

a simple exponential time course. At equilibrium;

$$P_\infty = \frac{\alpha_p}{(\alpha_p+\beta_p)} \tag{96}$$

The time constant τ_p of the reaction is given by;

$$\tau_p = \frac{1}{(\alpha_p+\beta_p)} \tag{97}$$

For $P = P_o$ when $t = 0$ equation (95) has the solution;

$$P = P_\infty - (P_\infty - P_o).\exp(-\frac{t}{\tau_p}) \tag{98}$$

Description of sodium pump activity by this means leaves the problem of deriving suitable equations relating the rate constants α_p and β_p to extracellular potassium concentration. By trial and error it was found that rate constant equations appropriate for simulation could be expressed in the form;

$$\alpha_p = \frac{Q.(K\_EXT - 5)}{1 - \exp(\frac{(K\_EXT - 5)}{X})} \tag{99}$$

$$\beta_p = \frac{Q.(K\_EXT - 5)}{\exp(\frac{(K\_EXT - 5)}{X}) - 1} \tag{100}$$

where Q and X are arbitrary constants. The magnitude of Q controls the time constant of the sodium pump reaction; the magnitude of X affects the range of extracellular potassium concentration over which pronounced changes in the value of P_∞ are observed. The effect of X on the relationship between P_∞ and K_EXT is illustrated in Figure 128; the relationship becomes steeper such that a given alteration in the value of P_∞ occurs over a progressively more restricted range of extracellular potassium concentrations as the value of X is reduced.

Relationships between hypothetical sodium pump activation variable and extracellular potassium concentration;

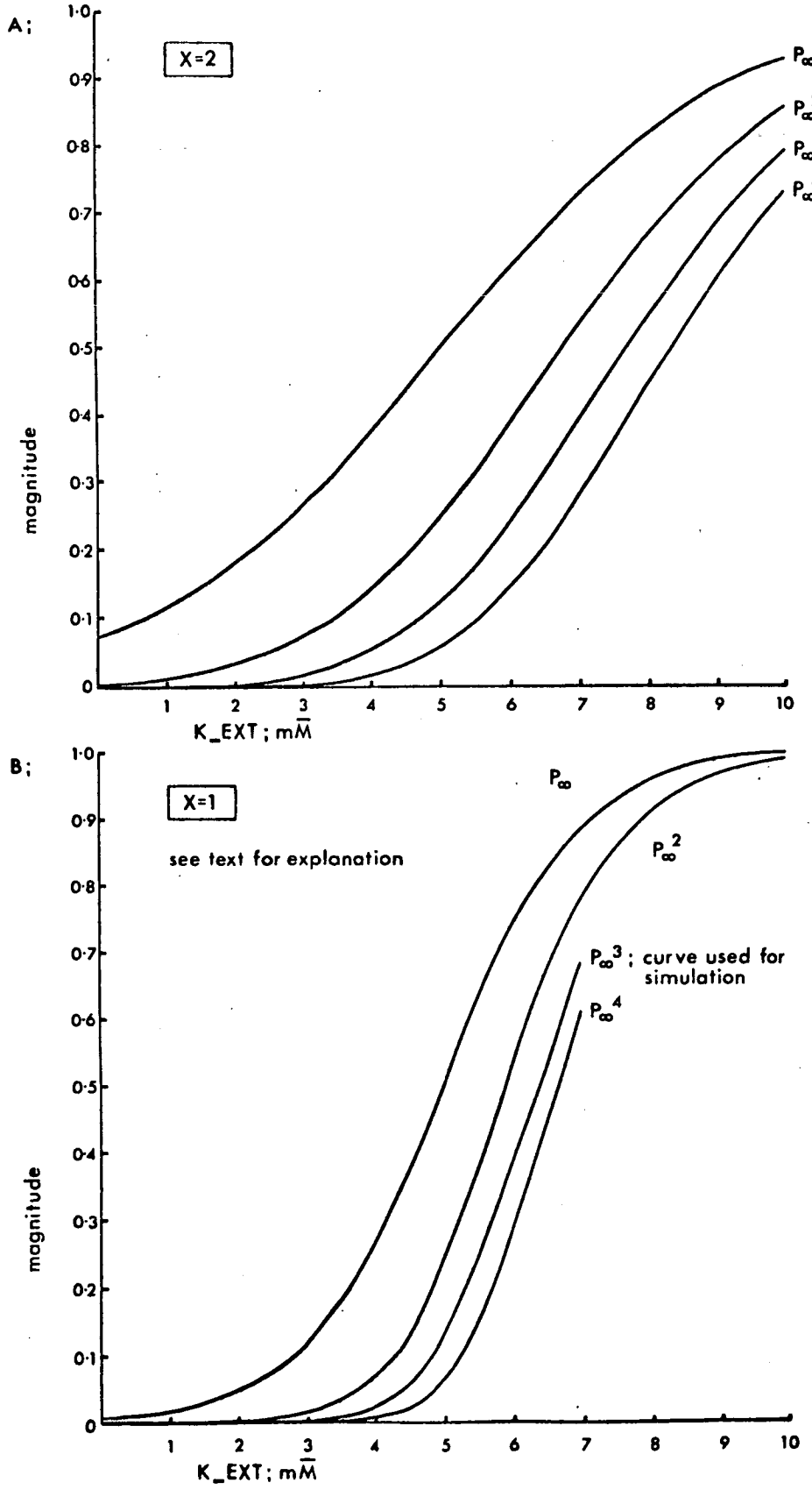

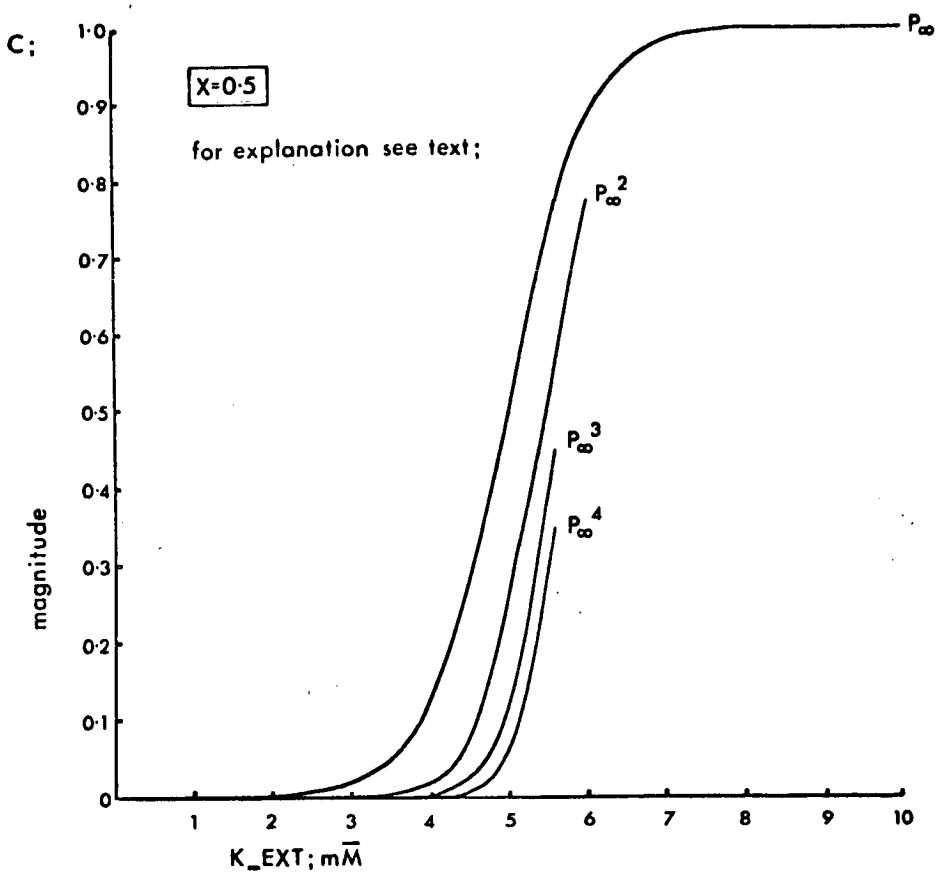
C;
X=0·5
for explanation see text;
magnitude
K_EXT; mM
1·0
0·9
0·8
0·7
0·6
0·5
0·4
0·3
0·2
0·1
0
1
2
3
4
5
6
7
8
9
10
P_∞
P_∞^2
P_∞^3
P_∞^4

Figure 128 also shows the relationships between K_EXT and P_∞^2, P_∞^3 and P_∞^4 for the different values of X. For simulation purposes it is necessary to select a particular value of X and a particular power, y, of P_∞ such that the relationship between P_∞^y and K_EXT has the same shape as the presumed relationship between the current transferred by the sodium pump and extracellular potassium concentration. There is as yet no experimental data which permits the selection of the individual curve which best describes the real relationship. However, it has already been suggested that the precise form of the relationship will be less than critical in determining whether or not bursting will occur. It follows that selection of any one of a number of tolerably appropriate curves should permit a reasonable simulation of the proposed mechanism of burst generation. The relationship between P_∞^3 and K_EXT when X = 1 seems appropriate and was used in all the simulations described below. (A limited number of simulations carried out with other relationships suggested that, as in the case of the electronic analogue model, the precise nature of the relationship was in fact less than critical.)

While derived in an arbitrary way, the equations developed above offer a plausible description of sodium pump activity and it is at least conceivable than when sufficient experimental data become available it will be possible to describe pump activity in terms of a fairly similar system of equations. A more complete description of pump activity would include the known effect of intracellular sodium concentration; this problem could be approached by assuming a second unitless pump activation variable or by making the rate constants of a single variable simultaneously functions of

intracellular sodium concentration and extracellular potassium concentration.

In applying the present, arbitrary, system of equations to simulation of the proposed mechanism of burst generation a number of further modifications to the normal simulation procedure are necessary. In the Algol W programmes Of Appendices 5 and 6, the sodium pump activation variable (P) is denoted by PUMP_CON and the current of sodium ions transferred by the sodium pump (I_PUMP_NA) has been assumed to take values such than, in programme notation;

$$\text{I\_PUMP\_NA} := \text{I\_PUMP\_NA\_MAX}*(\text{PUMP\_CON}**3); \qquad (101)$$

where I_PUMP_NA_MAX is the maximum possible sodium ion current which the pump can transfer.

Assuming a constant 3:2 ratio of ion transport, the potassium ion current transferred by the pump at any time step in the integration process is given by;

$$\text{I\_PUMP\_K} := -(2*\text{I\_PUMP\_NA})/3; \qquad (102)$$

The ion currents transferred by the pump alter the charge on the membrane capacitance in exactly the same way as the ion currents which flow through the normal conductance channels and it follows that the appropriate descriptions of net transmembrane sodium and potassium ion currents can be written as;

$$\text{INA} := \text{GNA}*(\text{E}-\text{ENA}) + \text{I\_PUMP\_NA}; \qquad (103)$$

$$\text{IK} := \text{GK}*(\text{E}-\text{EK}) + \text{I\_PUMP\_K}; \qquad (104)$$

Together with the necessary equations describing potassium accumulation and the associated variation in the pump activation variable, these modifications, incorporated into a programme for

action potential simulation with an appropriate system of absolute potential equations, provide a programme for simulation of the proposed mechanism of burst generation.

Recent results (LUX & ECKERT, 1974) indicate that bursting may occur in Helix pomatia neurons which lack the transient outward current channel included in the expanded model previously developed. For this reason, in attempting to produce a satisfactory simulation of bursting activity, attention was restricted to simulations incorporating only the absolute potential equivalents of the Hodgkin-Huxley equations.

2) One compartment simulation;

Appendix 5 gives the Algol W programme used for simulation of the proposed mechanism of burst generation for a single membrane region with a relatively long time constant for diffusion of extracellular potassium ions. Table 10 lists all the parameters necessary for simulation and the values normally assigned to them. With the exception of a brief (20 msec) stimulus at the beginning of simulation to ensure the occurrence of a single action potential, simulated activity was unstimulated and therefore 'intrinsic'. Because of restrictions in C.P.U. time available for running a single programme, simulations corresponding to more than 1500 msec of activity were carried out by transferring parameter values into one or more continuation programmes.

Figure 129 shows the results obtained when simulation was carried out with the values listed in Table 10 and with the scale constant for extracellular potassium accumulation, SC = 0.0001; Figure 130 shows the simulation with SC = 0.0002.

Table 10.

Input parameters for one compartment simulation of proposed mechanism of burst generation (see Appendix 5);

Parameter	Explanation	Normal value
I_STIM	stimulus current	5 $\mu A/cm^2$
T_STIM	stimulus duration	20.00 msec
T_MAX	total stimulation time	1500.00 msec
DT	time increment for integration	0.05 msec
K_EXTREST	normal extracellular potassium concentration	3 m$\bar{M}$
K_INT	intracellular potassium concentration (corresponding to EK $\simeq$ -62 mV)	35 m$\bar{M}$
ENA	sodium equilibrium potential	+55 mV
EL	leakage equilibrium potential	-40 mV
G_K	maximum potassium conductance, $\bar{g}_K$	36.0 m.mho/cm^2
G_NA	maximum sodium conductance, $\bar{g}_{Na}$	120.0 m.mho/cm^2
GL	leakage conductance, g_l	0.3 m.mho/cm^2
E_REST	membrane potential at beginning of simulation	-56 mV
I_PUMP_NA_MAX	maximum sodium pump current (extrusion of Na^+ ions)	200 $\mu A/cm^2$
SC	scale constant for extracellular potassium accumulation	0.0001 - 0.0003
TAU	diffusion time constant for extracellular K^+ ions	500.00 msec
Q	factor controlling sodium pump time constant (corresponding to τ_p = 500 msec)	0.001

Proposed mechanism of burst generation; One compartment simulation;

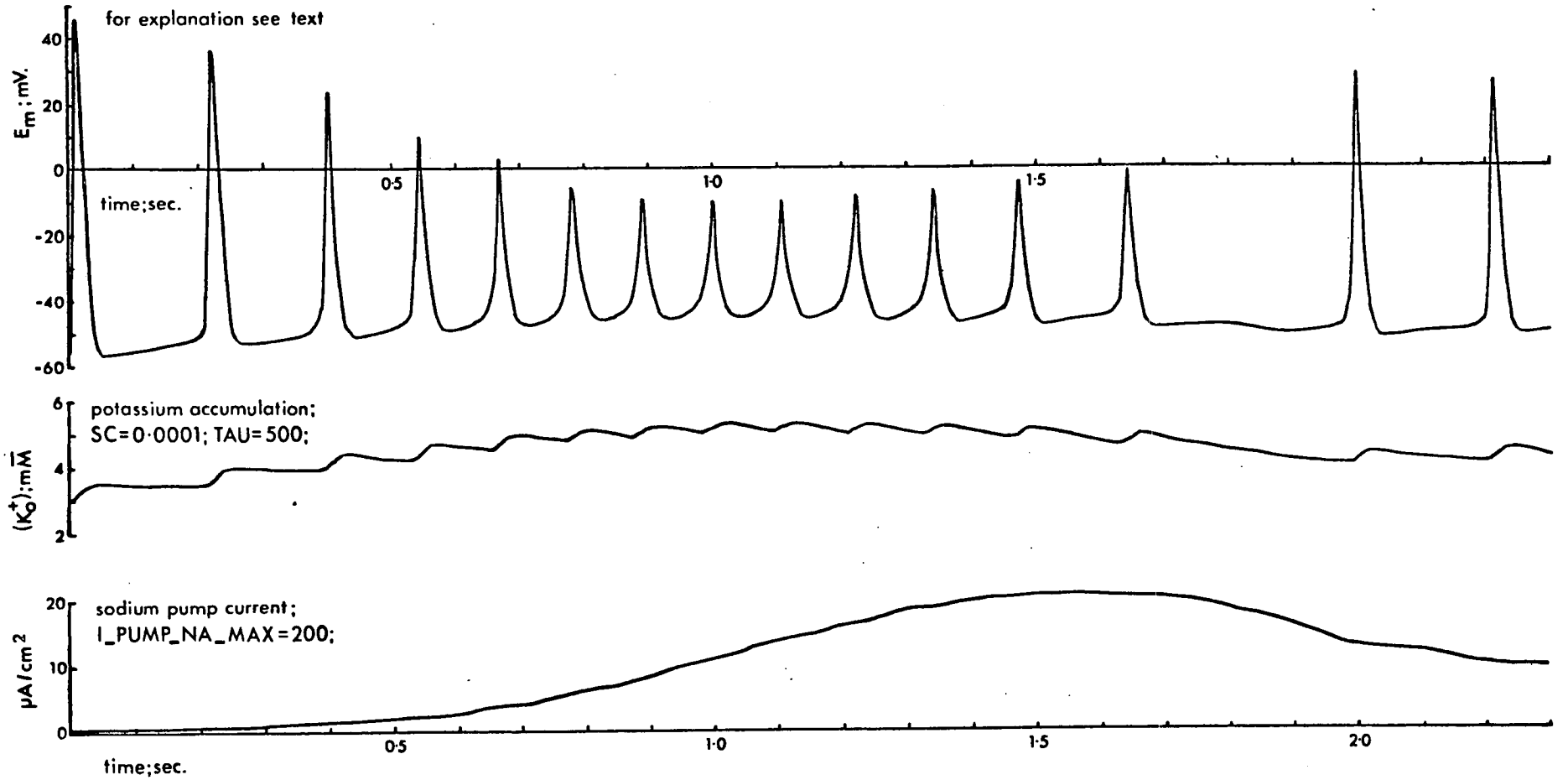

Proposed mechanism of burst generation; One compartment simulation;
for explanation see text

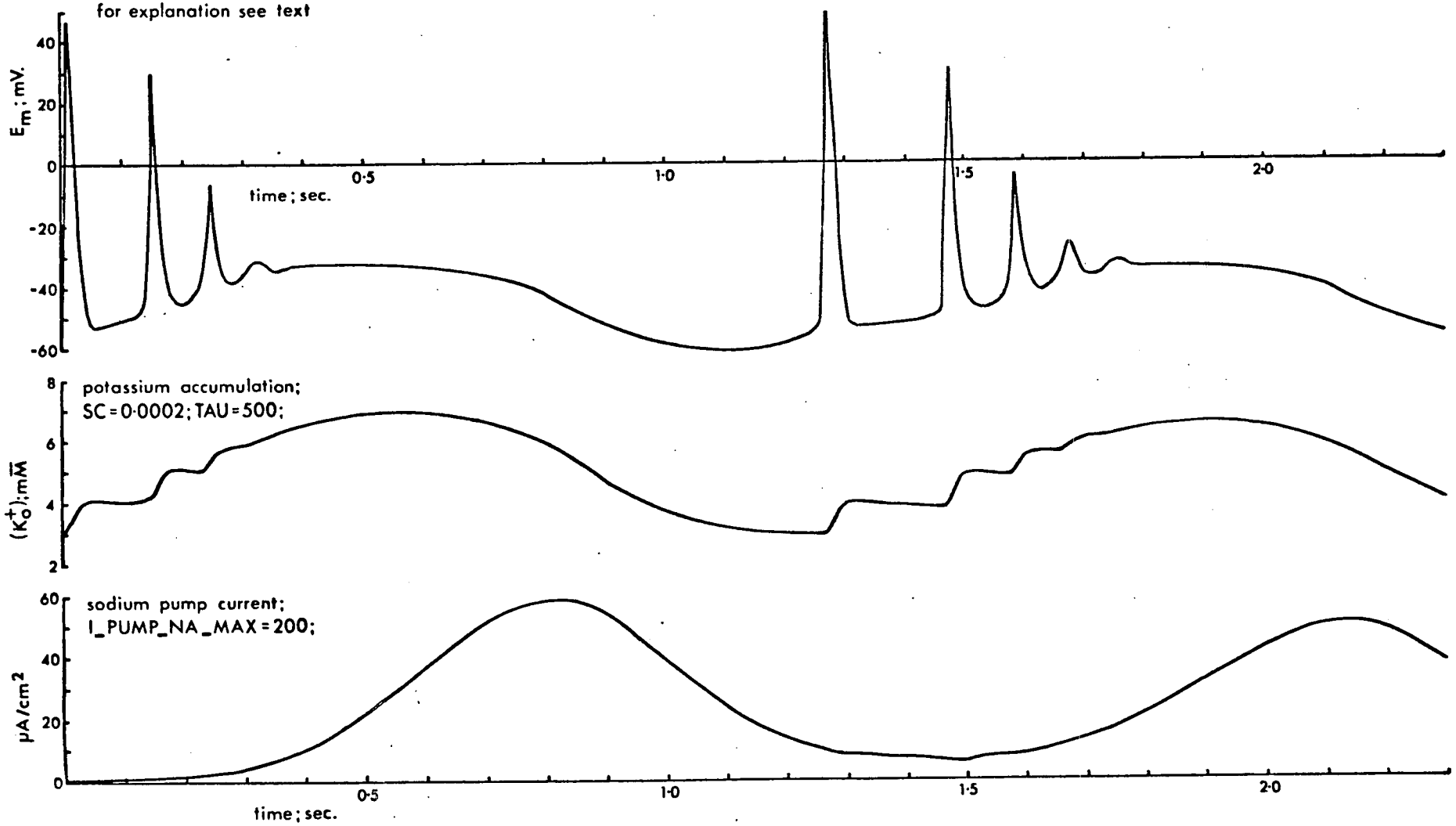

In general, a cyclic pattern of activity can easily be obtained with the simulation procedure described and the period of the cycle can be modified by changes in parameter values in the manner expected from the behaviour of the analogue model. Where action potentials occur during the depolarized phase of the cycle (Figure 129), their frequency is increased towards the middle of the 'burst'. However, most simulations which show a well developed cycle of activity (Figure 130) fail to produce action potentials during most of the depolarized phase. As depolarization develops, there is a clear tendency for action potential overshoot to decline; this is in sharp contrast to the change which occurs during the depolarizing phase of the cycle in real bursting neurons. In the real situation, action potential overshoot increases during depolarization. The decrease during the simulated cycle is a direct result of extracellular potassium accumulation and it follows that satisfactory mimicry of the real bursting cycle cannot be obtained in the case of a one compartment simulation of the proposed mechanism of burst generation.

The one compartment simulation can be assumed to correspond to the invaginated component of the membrane surface in real bursting neurons and its behaviour could conceivably account for the occurrence of endogenous waves of membrane potential when action potential production is suppressed. Thus, the possibility remains that a more satisfactory approximation might be obtained with a two compartment simulation where the compartment corresponding to invaginated membrane surface controls action potential production in a second compartment corresponding to non-invaginated membrane.

3) Two compartment simulation;

Appendix 6 gives the Algol W programme used for two compartment simulation. The individual simulations for the two membrane regions depend on an identical system of equations and were carried out simultaneously. Input parameters were also identical except in the case of the diffusion time constant for extracellular potassium ions. For the invaginated membrane surface the diffusion time constant, denoted by TAU_V, was 500 msec, as in the case of the one compartment simulations described above. For the non-invaginated (soma) membrane surface the diffusion time constant, denoted by TAU_S, was 10 msec; this value is rather lower than that probable in the real situation but was chosen deliberately so that extracellular potassium accumulation for the non-invaginated membrane surface would be negligible.

Interaction was achieved by interposing a resistance (R) between the two compartments and by supposing the flow of lateral currents proportional to the corresponding difference in potential. Lateral current through the invaginated membrane surface is denoted by I_LAT_V and can be written as;

$$I\_LAT\_V := (E\_S - E\_V)/R; \qquad (105)$$

where E_V is the potential across the invaginated membrane surface and E_S the potential across the non-invaginated membrane surface.

Similarly, the lateral current through the non-invaginated membrane surface is given by;

$$I\_LAT\_S := (E\_V - E\_S)/R; \qquad (106)$$

These lateral currents are added to the normal ionic currents and any stimulus current in determining the change in

membrane potential at each time step in integration such that;

$$E\_V1 := E\_V + ((I\_LAT\_V + I\_STIM + I\_V)*DT)/C; \quad (107)$$

$$E\_S1 := E\_S + ((I\_LAT\_S + I\_STIM + I\_S)*DT)/C; \quad (108)$$

These few modifications provide a suitable programme for two compartment simulation. However, the final programme is rather unwieldy and involves such a complex integration procedure that the possible timespan of simulation is severely restricted; it is necessary to run several continuation programmes to obtain simulations of reasonable duration.

An example of the results which can be obtained with two compartment simulation is given in Figure 131. This simulation was carried out with the parameter values listed in Table 10 but with the following alterations; SC = 0.0003, I_PUMP_NA_MAX = 400; TAU was replaced by TAU_V = 500 and TAU_S = 10; the coupling resistance between the two compartments, R, was arbitrarily given the value 1.0 K. The increases in the scale constant for potassium accumulation and sodium pump current were found to be necessary because the invaginated compartment now drives the non-invaginated compartment in addition to the cyclic changes in potential across its own membrane.

4) Discussion;

The simulated 'bursting' pattern of action potential production for the non-invaginated membrane compartment during two-compartment simulation represents a much closer approximation to the real bursting cycle than any which is possible with one compartment simulation. However, even with two compartments, the

Proposed mechanism of burst generation; Two compartment simulation;

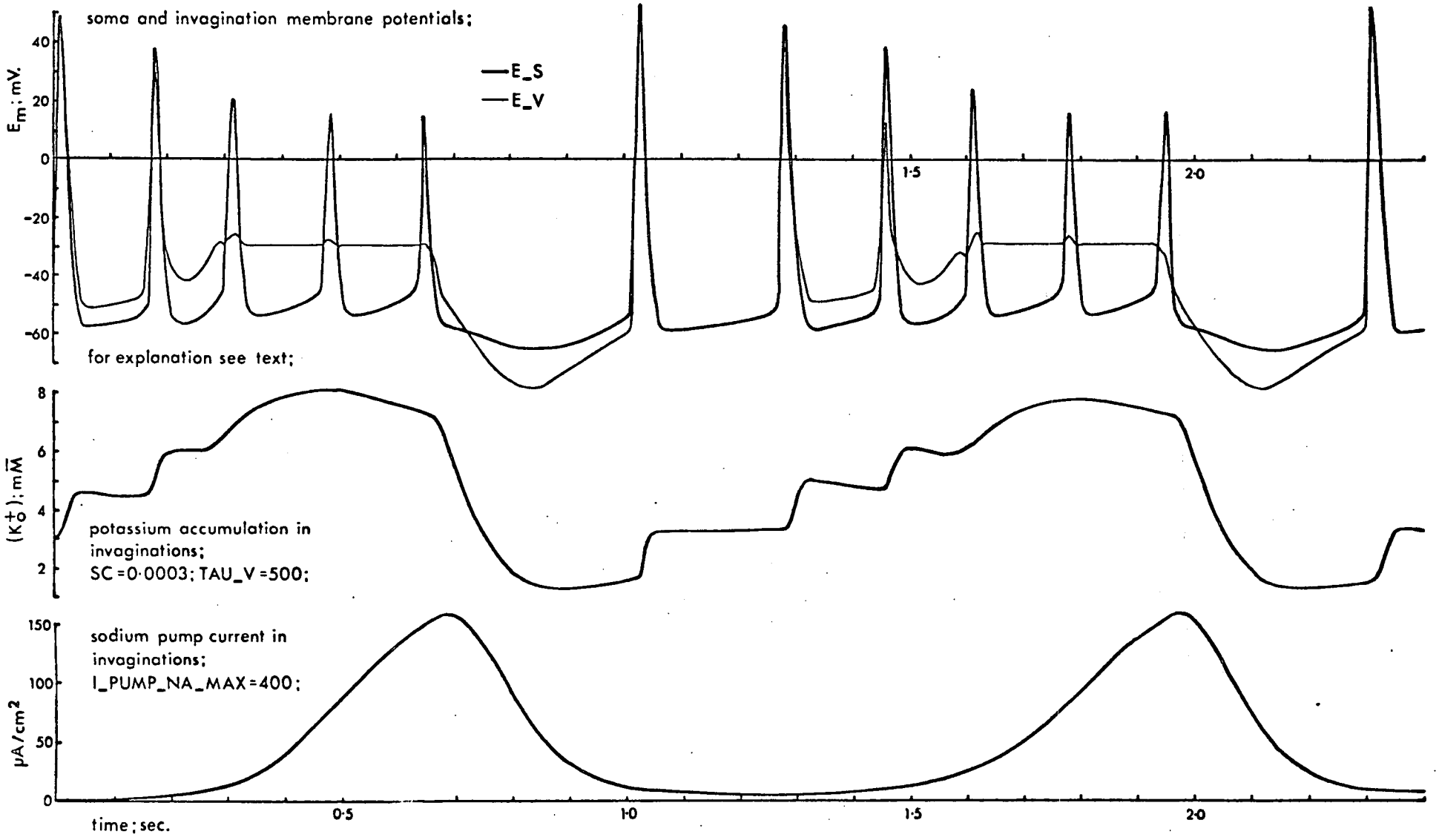

simulation available clearly does not mimic real activity with sufficient accuracy. The results of Figure 131 were obtained for negligible potassium accumulation near the non-invaginated membrane surface and represent a best case approximation to real bursting activity. It follows that the system of equations on which simulation is based is, in some respect, insufficient to account for the characteristics of burst generation in the real situation.

The major discrepancy between the simulated and the real bursting cycle lies in the change in action potential characteristics during the burst. The simulated action potentials show a progressive decline in overshoot. This is much less pronounced than that apparent with one compartment simulation but is nevertheless inconsistent with the increase in overshoot in real bursting neurons.

Within the system of absolute potential equations equivalent to the Hodgkin-Huxley equations, action potential overshoot is determined partially by the product m^3h and partially by n^4. Hyperpolarization increases the magnitude of the sodium activation variable h, and reduces potassium activation, n^4; both these changes tend to increase action potential overshoot. On the other hand, depolarization reduces the magnitude of h and increases n^4 and should result in a reduction in overshoot. Thus, the changes in action potential overshoot during the simulated burst are in fact those predicted by the Hodgkin-Huxley equations. It is therefore probable that at least some of the discrepancy in burst simulation is associated with the system of equations which describe the characteristics of normal action potential production. The changes in action potential overshoot which follow artificial hyperpolarization in the Big-D cell of Helix aspersa (Figure 114) also suggest

that the Hodgkin-Huxley equations may be a less than adequate description of membrane properties in the case of bursting neurons. Thus, moderate hyperpolarization clearly depresses rather than enhances overshoot.

There are essentially only two ways in which hyperpolarization could lead to a depression of action potential overshoot; either hyperpolarization reduces the maximum inward current possible during action potential production or increases the possible outward current. A reduction in the possible inward current could follow a reduction in the availability of inward current sites (equivalent to a reduction in the magnitude of h), an increase in the time constant of sodium activation (τ_m) or a decrease in the time constant of inactivation (τ_h). An increase in the possible outward current could follow an increase in the availability of outward current sites (equivalent to an increase in n^4) or a decrease in the time constant of potassium activation (τ_n). Alternatively, inward current could be reduced or outward current increased respectively through inactivation or activation of a type not included in the Hodgkin-Huxley formulation.

Long-lasting depression of delayed outward potassium currents can be demonstrated in a number of molluscan preparations (CONNOR & STEVENS, 1971a; ADELMAN, PALTI & SENFT, 1973; ADAM, 1973; LUX & ECKERT, 1974). While some of this 'inactivation' can be accounted for by extracellular K^+ accumulation, at least in the case of bursting neurons in Helix pomatia, it appears that there must also be a true inactivation of potassium gates. Hyperpolarization removes some of this inactivation and subsequent outward currents are enhanced (LUX & ECKERT, 1974). By comparing the

extent of extracellular potassium accumulation (measured with an ion-sensitive electrode) near the membrane of Helix pomatia bursting neurons with the magnitude of outward currents recorded during two consecutive voltage clamp pulses it has also been possible to infer the existence of a slow inward current. This inward current component appears to be more or less inactivated at normal resting potential but becomes appreciable during depolarization (LUX & ECKERT, 1974). Neither true potassium inactivation nor this slow inward current, both of which predict depression of action potential overshoot following hyperpolarization, are represented in the absolute potential Hodgkin-Huxley equations.

It seems more than probable that if suitable equations describing these effects could be developed, their inclusion in the simulation developed for the proposed mechanism of burst generation would provide a close approximation to real bursting activity. While potassium inactivation could possibly be included, the origin and detailed properties of slow inward current are at present obscure and even arbitrary equations cannot be derived. Nevertheless, it can be suggested that the proposed mechanism of burst generation probably does provide a reasonably valid description of real events and, in this case, the shortcomings in simulation can be wholly attributed to inadequacies in the system of equations which describes normal action potential production.

Chapter 7

CONCLUSIONS

It is generally accepted that the Hodgkin-Huxley equations provide an extremely good description of nerve membrane properties and indeed their significance in the development of the present understanding of nerve membrane function can hardly be underestimated. Nevertheless, it is remarkable that the equations have survived in their original form for more than 20 years. During the same period, the literature dealing with the properties of excitable membranes has become immense and there is now a clear need for a more modern and more comprehensive statement of the mathematical model. The absolute potential approach developed above represents only a small step towards restatement but it can be suggested that such an approach may prove useful because an absolute potential system of equations can be simply and directly modified or expanded to include additional mechanisms, thereby providing a more accurate representation of real events. The expansion of the absolute potential system proposed for bursting neurons, while not entirely satisfactory, does give some indication of what might be achieved; expressions describing extracellular potassium ion accumulation and sodium pump activity could not be successfully incorporated in simulations based on the original Hodgkin-Huxley equations.

A certain amount is now known regarding the probable nature of the physical membrane mechanisms which underly potential-dependent alterations in conductance. For example, artificial bimolecular lipid membranes can become electrically excitable when treated with 'excita-

bility-incucing material' (EIM), a proteinaceous extract obtained from bacterial culture (MUELLER & RUDIN, 1968). When sufficiently small amounts of EIM are added, the conductance of the membrane is limited to a few discrete levels and changes abruptly from one level to another. From the characteristics of these fluctuations it can be inferred that the EIM doped bilayer contains ion-conducting elements capable of undergoing a transition between two states of conductance. The difference in current between the 'open' and 'closed' states is directly proportional to the applied membrane potential and corresponds to a conductance of 3×10^{-10}.ohm^{-1}. The fraction of the total number of elements in the open state varies from zero to unity as a function of potential (EHRENSTEIN, LECAR & NOSSAL, 1970). These observations strongly support the contention that electrical excitability is determined at a number of discrete 'sites' and is not a homogeneous or labile membrane property. In real nerve membrane, the number of presumed 'sodium sites' can be estimated from the amount of tetrodotoxin (TTX) which must be absorbed in order to block the sodium conductance; apparently there are fewer than 13 sodium sites per square micron of membrane (MOORE, NARAHASHI & SHAW, 1967). Recently, a molecular structure has been proposed for the sodium site which is stereochemically compatible with the action of TTX and other inhibitors (SMYTHIES et al, 1974).

A number of important inferences follow from the assumption that nerve membrane conductance is determined at discrete sites which can exist in either an open or a closed configuration. Firstly it is reasonable to suppose that the absolute potential system of equations which adequately describes the sodium conductance (for example) will in fact be equivalent to a system which describes the probability of an individual sodium site being open or closed. This

implies that the equations should be modified to permit a certain amount of random variation in conductance; when the number of sites involved is relatively large, this variation will be of limited importance but when the number of sites is small, random variation could be a significant factor in determining the pattern of electrical activity. The Hodgkin-Huxley equations are normally solved in terms of specific membrane conductance and capacitance, that is for a membrane one square centimetre in area. No attempt has been made to produce a system of equations specifically appropriate for the very much smaller areas of membrane present in real neurons. In the absence of such a system, it is uncertain whether the variation in interspike interval observed in individual monotonic pacemaker neurons is dependent on random variations in conductance or whether other factors, such as occasional synaptic input, must also contribute.

Secondly, the assumption that membrane conductance is determined at fixed sites suggests a limit to the number of ways in which membrane properties can be altered. Thus, it seems probable that the membranes of neurons in a given preparation will contain only a few distinct types of site and that individual sites of a particular type will have fixed characteristics. It follows that differences in the properties of individual neurons are likely to depend either on differences in the numbers and distribution of sites over the membrane surface or on factors, such as ionic equilibrium potentials and diffusion time constants, which affect the rate of ion transfer through open sites. The theoretical explanation of intrinsic activity developed above is consistent with this interpretation; explanations which require alterations in the absolute potential dependency of membrane conductance clearly imply changes in

site characteristics and are therefore less probable.

Significant extracellular accumulation of potassium ions has been demonstrated in recent studies of the squid giant axon. The time course and magnitude of changes in potassium conductance differs markedly from that predicted from the Hodgkin-Huxley equations (ADAM, 1973) but can be adequately described using the equations in a quantitatively modified form (ADELMAN, PALTI & SENFT, 1973). While attention has so far been largely restricted to extracellular potassium ion accumulation, there seems to be no particular reason for supposing that the extracellular and intracellular accumulation or depletion of other ions does not significantly alter the transmembrane flow of ionic currents. In this case, the actual changes in membrane conductance will differ from those predicted by the Hodgkin-Huxley equations. It may well become necessary to modify the mathematical model to take account of several local alterations in ion concentration.

It is also clear that a more adequate mathematical model of membrane properties should incorporate equations describing the activity of metabolic ion pumps. While other metabolic pumps are known to exist (e.g. KEYNES, 1963), only in the case of the sodium (sodium-potassium exchange) pump is sufficient information available for there to be any immediate possibility of deriving suitable equations. In snail neurons it is possible to measure the electrogenic current transferred by the pump using the voltage-clamp technique and, after an intracellular injection of sodium ions, the relationship between pump activity and intracellular sodium concentration can be determined (THOMAS, 1968; 1969). Rather less is known regarding the relationship between pump activity and extra-

cellular potassium concentration (see MORETON, 1969); presumably this could be estimated more accurately by comparing the currents required to clamp membrane potential at a constant level for a neuron exposed to a number of different extracellular potassium concentrations, in the presence and absence of ouabain.

By comparison, any estimation of the time constant of changes in sodium pump activity is likely to be extremely difficult. Clearly, it is impossible to apply a step function change in sodium or potassium concentration to the system and, unless the pump time constant is relatively long compared to the time required for a concentration change, it will be impossible to obtain convincing results in this way. The possible involvement of the sodium pump in determining the activity of bursting neurons could conceivably provide at least a partial solution to this problem. Thus, changes in extracellular potassium concentration associated with action potential production in bursting neurons are likely to be fairly rapid and, if sufficient were known regarding the anatomy and membrane properties of bursting neurons and the characteristics of extracellular potassium accumulation, it might be possible to estimate the sodium pump time constant through computer simulations based on a more accurate and less arbitrary model of bursting neurons than that developed above.

In addition to emphasising the need for a general restatement of the mathematical model, the theoretical arguments presented in the thesis suggest a number of specific experimental studies which might usefully be carried out. Clearly, the predicted relationship between intracellular potassium concentration and the frequency of action potential discharge in monotonic pacemakers

should be tested directly using ion-sensitive electrodes. With suitable equipment this should be relatively easy to accomplish. There is some evidence that electrogenic sodium pump activity can affect pacemaker frequency (AYRAPETYAN, 1973) and it may be that the best estimate of the predicted relationship will be obtained when the pump is inhibited by treatment with ouabain. Any study using ion-sensitive electrodes could conveniently include a test of the relationship both in the presence and absence of ouabain and the relative importance of intracellular potassium concentration and electrogenic pump activity in determining action potential frequency could therefore be estimated.

The simple experiments, which are described in Chapter 3 and demonstrate a negative relationship between action potential amplitude and spontaneous frequency, could usefully be repeated using a larger number of cells. The simulations of intrinsic activity described in Chapter 5 suggest that action potential duration should be positively related to spontaneous frequency. A more thorough statistical study of spontaneous activity in the suboesophageal ganglia of Helix aspersa could test this prediction.

Another feature of the theoretical explanation of intrinsic activity which merits experimental study is the predicted relationship between intrinsic activity and a steady-state negative resistance characteristic ('anomalous rectification'). Recent results (SMITH, BARKER & GAINER, 1975) indicate that the negative resistance characteristic of bursting neurons changes with extracellular ion concentrations essentially in accordance with the predictions of the absolute potential approach but the problem has yet to be examined systematically. Internally perfused squid giant

axons (BAKER, HODGKIN & SHAW, 1962a) would probably be a favourable preparation for such a study. Because of their large size and relatively low resistance, the voltage-clamp technique can be more easily and more accurately applied to giant axons than to most individual neurons. Lateral current flow can be reduced to a minimum by clamping a large area of membrane and it follows that reliable measurements of the small currents which determine membrane behaviour in the threshold region should be relatively easy to obtain. On the other hand, voltage-clamping of neuron somata is seldom effective over a large area and it may be difficult to obtain recordings which are unaffected by current flow in unclamped regions of the cell.

Although experiments of the type suggested above are clearly necessary in establishing the validity or otherwise of the absolute potential equations and the proposed explanation of intrinsic activity, it can be suggested that the theoretical analysis presented leads to a reasonably general explanation of intrinsic activity which seems acceptable in relation to available experimental evidence. The thesis as a whole represents an attempt to produce a model for intrinsic pacemaker activity which to some extent has utility in the following terms;

'Any model has utility only insofar as it raises questions, suggests new relationships, and serves to focus one's thoughts. This is accomplished by using it to test hypotheses, to compute, to extrapolate and predict, and to suggest useful experiments. In this way models accelerate the process of learning about the real world.' (HARMON, 1964).

APPENDICES

1) Algol W programme for theoretical current-voltage curve production using an absolute potential system of Hodgkin-Huxley equations.

2) Algol W programme for action potential simulation using an absolute potential system of Hodgkin-Huxley equations.

3) Algol W programme for expanded model theoretical current-voltage curve production.

4) Algol W programme for expanded model action potential simulation.

5) Algol W programme for simulation of proposed mechansim of burst generation : One compartment simulation.

6) Algol W programme for simulation of proposed mechanism of burst generation : Two compartment simulation.

Appendix 1.

Algol W programme for theoretical current-voltage curve production using an absolute potential system of Hodgkin-Huxley equations;

```
1) BEGIN
    PROCEDURE CURRENT_VOLTAGE(REAL VALUE EMIN,EMAX,EINC,EK,ENA,
                                          EL,G_K,G_NA,GL);
2)  BEGIN
     LOGICAL STEADY_STATE,EARLY;
     REAL E,I,EINCMIN,I_LAST,AN,BN,N,AM,BM,M,AH,BH,H,X,Y,NREST,
          HREST,IK,INA,IL;
     REAL ARRAY E_INTERSECT(1::3);
     INTEGER INTERSECT;

     PROCEDURE ESTIMATE_POTENTIAL(REAL VALUE EMIN,EMAX,EINC;
         INTEGER VALUE INTERSECTION;LOGICAL VALUE PRINTOUT);
3)   BEGIN
      WRITE("E RUNS FROM",EMIN,"TO",EMAX);
      E:=EMIN; INTERSECT:=1;
      EINCMIN:=0.09;

      START: IF EARLY THEN
4)    BEGIN
       N:=NREST; H:=HREST;
4)    END;

      IF STEADY_STATE THEN
4)    BEGIN
       X:=EXP((-(E+60)+10)/10)-1;
       COMMENT WHEN X=0 THE VALUE OF AN IS INDETERMINATE;
       IF X=0 THEN
5)     BEGIN
        IF PRINTOUT THEN WRITE("NEXT VALUE");
        GO TO NEXT_VALUE;
5)     END;
       AN:=(0.01*(-(E+60)+10))/X;
       BN:=0.125*EXP((-(E+60))/80);
       N:=AN/(AN+BN);

       AH:=0.07*EXP((-(E+60))/20);
       BH:=1/(EXP((-(E+60)+30)/10)+1);
       H:=AH/(AH+BH);
4)    END;

      Y:=EXP((-(E+60)+25)/10)-1;
      COMMENT WHEN Y=0 THE VALUE OF AM IS INDETERMINATE;
      IF Y=0 THEN
4)    BEGIN
       IF PRINTOUT THEN WRITE("NEXT VALUE");
       GO TO NEXT_VALUE;
4)    END;
      AM:=(0.1*(-(E+60)+25))/Y;
      BM:=4*EXP((-(E+60))/18);
      M:=AM/(AM+BM);
```

```
      IK:=N**4*G_K*(E-EK);
      INA:=M**3*H*G_NA*(E-ENA);
      IL:=GL*(E-EL);

      I_LAST:=I;
      I:=IK+INA+IL;
      IF E=EMIN THEN I_LAST:=I;

      IF PRINTOUT THEN
4)    BEGIN
       WRITE(" ");
       WRITE("  E=",E,"  I=",I);
       WRITE("IK=",IK,"  INA=",INA,"  IL=",IL);
4)    END;

      IF((I_LAST<=0)AND(I>=0))OR((I_LAST>=0)AND(I<=0))THEN
4)    BEGIN
       E_INTERSECT(INTERSECT):=E;
       IF INTERSECT=1 THEN WRITE("FIRST INTERSECTION");
       IF INTERSECT=2 THEN WRITE("SECOND INTERSECTION");
       IF INTERSECT=3 THEN WRITE("THIRD INTERSECTION");
       IF PRINTOUT THEN WRITEON(" BETWEEN PRECEDING TWO VALUES");
       INTERSECT:=INTERSECT+1;

       IF EINC<=EINCMIN THEN
5)     BEGIN
        IF STEADY_STATE THEN
6)      BEGIN
         NREST:=N; HREST:=H;
6)      END;
        GO TO LOOP_EXIT;
5)     END;
4)    END;

      NEXT_VALUE: E:=E+EINC;
      IF E<=EMAX THEN GO TO START;

      IF INTERSECT>INTERSECTION THEN
      ESTIMATE_POTENTIAL(E_INTERSECT(INTERSECTION)-EINC,
         E_INTERSECT(INTERSECTION)+EINC,EINC/10,1,FALSE);

      LOOP_EXIT: IF EINC<=EINCMIN THEN WRITE("LOOP EXIT");

3)  END ESTIMATE_POTENTIAL;

      WRITE(" ");
      WRITE("CURRENT-VOLTAGE RELATIONSHIPS");
      WRITE("HODGKIN-HUXLEY MODEL");
      WRITE(" ");

      STEADY_STATE:=TRUE; EARLY:=FALSE;

      WRITE(" EK=",EK,"  G_K=",G_K);
      WRITE("ENA=",ENA," G_NA=",G_NA);
      WRITE(" EL=",EL,"   GL=",GL);
      WRITE(" ");
      WRITE("STEADY-STATE CURRENT-VOLTAGE RELATIONSHIP");
      WRITE(" ");
```

```
      ESTIMATE_POTENTIAL(EMIN,EMAX,EINC,1,TRUE);
      WRITE(" ");
      WRITE("ESTIMATED RESTING POTENTIAL=",E_INTERSECT(1));

      STEADY_STATE:=FALSE; EARLY:=TRUE;

      WRITE(" ");
      WRITE("EARLY CURRENT-VOLTAGE RELATIONSHIP");
      WRITE("N=",NREST,"  H=",HREST);
      WRITE(" ");

      ESTIMATE_POTENTIAL(EMIN,EMAX,EINC,1,TRUE);
      WRITE(" ");
      WRITE("ESTIMATED RESTING POTENTIAL=",E_INTERSECT(1));
      WRITE(" ");

      ESTIMATE_POTENTIAL(EMIN,EMAX,EINC,2,FALSE);
      WRITE(" ");
      WRITE("ESTIMATED UNIFORM THRESHOLD=",E_INTERSECT(1));
      WRITE(" ");

      ESTIMATE_POTENTIAL(EMIN,EMAX,EINC,3,FALSE);
      WRITE(" ");
      WRITE("ESTIMATED ACTION POTENTIAL PEAK=",E_INTERSECT(1));
      WRITE(" ");

2)  END CURRENT_VOLTAGE;

    REAL EMIN,EMAX,EINC,EK,ENA,EL,G_K,G_NA,GL;
    INTEGER NTIMES,OPERATIONS;
    READ(OPERATIONS);
    READ(EMIN,EMAX,EINC);
    NTIMES:=1;
    REPEAT: READ(EK,ENA,EL,G_K,G_NA,GL);

    CURRENT_VOLTAGE(EMIN,EMAX,EINC,EK,ENA,EL,G_K,G_NA,GL);

    NTIMES:=NTIMES+1;
    IF NTIMES<=OPERATIONS THEN GO TO REPEAT;

1) END.
```

Note that the numbers in the left hand margin do not form part of the programme but have been added to indicate its block structure.

Appendix 2.

Algol W programme for action potential simulation using an absolute potential system of Hodgkin-Huxley equations;

```
1) BEGIN
    PROCEDURE SIMULATION(REAL VALUE I_STIM,T_STIM,T_MAX,DT,EREST,
                                    EK,ENA,EL,G_K,G_NA,GL);
2)  BEGIN
     COMMENT PLOTTING PROCEDURES;
     PROCEDURE CALL_CILPLT(INTEGER VALUE A);
      FORTRAN "CILPLT";
     PROCEDURE CALL_GARGS(INTEGER VALUE A);
      FORTRAN "GARGS";
     PROCEDURE CALL_CMS;
      FORTRAN "CMS";
     PROCEDURE CALL_PSPACE(REAL VALUE A,B,C,D);
      FORTRAN "PSPACE";
     PROCEDURE CALL_LIMITS(REAL VALUE A,B,C,D);
      FORTRAN "LIMITS";
     PROCEDURE CALL_CTRSET(INTEGER VALUE A);
      FORTRAN "CTRSET";
     PROCEDURE CALL_CRSIZE(REAL VALUE X);
      FORTRAN "CRSIZE";
     PROCEDURE CALL_MSPACE(REAL VALUE A,B,C,D);
      FORTRAN "MSPACE";
     PROCEDURE CALL_AXES;
      FORTRAN "AXES";
     PROCEDURE CALL_POINT(REAL VALUE X,Y);
      FORTRAN "POINT";
     PROCEDURE CALL_JOIN(REAL VALUE X,Y);
      FORTRAN "JOIN";
     PROCEDURE CALL_FRAME;
      FORTRAN "FRAME";

     PROCEDURE ACTION_POTENTIAL(REAL VALUE I_STIM,T_STIM);
3)   BEGIN
      REAL E,E1,T,C,AN,BN,N,N1,AM,BM,M,M1,AH,BH,H,H1,IK,INA,IL;
      INTEGER PLOTTING_INTERVAL,PRINTOUT_INTERVAL;

      WRITE(" ");
      WRITE(" STIMULUS CURRENT=",I_STIM);
      WRITE("STIMULUS DURATION=",T_STIM);
      WRITE(" ");

      T:=0; C:=1;
      PLOTTING_INTERVAL:=0; PRINTOUT_INTERVAL:=0;

      START: IF T=0 THEN E:=EREST;
      IF T>0 THEN
4)    BEGIN
       N:=N1; M:=M1; H:=H1;
       E:=E1;
4)    END;
```

```
      AN:=(0.01*(-(E+60)+10))/(EXP((-(E+60)+10)/10)-1);
      BN:=0.125*EXP((-(E+60))/80);
      IF T=0 THEN N:=AN/(AN+BN);

      AM:=(0.1*(-(E+60)+25))/(EXP((-(E+60)+25)/10)-1);
      BM:=4*EXP((-(E+60))/18);
      IF T=0 THEN M:=AM/(AM+BM);

      AH:=0.07*EXP((-(E+60))/20);
      BH:=1/(EXP((-(E+60)+30)/10)+1);
      IF T=0 THEN H:=AH/(AH+BH);

      IK:=N**4*G_K*(E-EK);
      INA:=M**3*H*G_NA*(E-ENA);
      IL:=GL*(E-EL);

      I:=IK+INA+IL;

      IF T>=T_STIM THEN I_STIM:=0;
      E1:=E+((I_STIM-I)*DT)/C;

      N1:=(AN*(1-N)-BN*N)*DT+N;
      M1:=(AM*(1-M)-BM*M)*DT+M;
      H1:=(AH*(1-H)-BH*H)*DT+H;

      IF PLOTTING_INTERVAL=0 OR PLOTTING_INTERVAL=10 THEN
4)    BEGIN
       CALL_JOIN(T,E);
       PLOTTING_INTERVAL:=0;
4)    END;

      IF PRINTOUT_INTERVAL=0 OR PRINTOUT_INTERVAL=50 THEN
4)    BEGIN
       WRITE("T=",  T,"  E=",E);
       PRINTOUT_INTERVAL:=0;
4)    END;

      NEXT_VALUE: T:=T+DT;
      PLOTTING_INTERVAL:=PLOTTING_INTERVAL+1;
      PRINTOUT_INTERVAL:=PRINTOUT_INTERVAL+1;
      IF T<=T_MAX THEN GO TO START;
      WRITE(" "); WRITE(" ");
      WRITE("FINAL VALUES");
      WRITE("E=",E1);
      WRITE("N=",N1,"  M=",M1,"  H=",H1);
      WRITE(" "); WRITE(" ");

3)    END ACTION_POTENTIAL;

      WRITE(" ");
      WRITE("ACTION POTENTIAL SIMULATION");
      WRITE("HODGKIN-HUXLEY MODEL");
      WRITE(" ");
      WRITE("T_STIM=",T_STIM,"  T_MAX=",T_MAX,"  DT=",DT);
      WRITE("EREST=",EREST);
      WRITE(" ");
      WRITE(" EK=",EK,"  G_K=",G_K);
```

```
      WRITE("ENA=",ENA," G_NA=",G_NA);
      WRITE(" EL=",EL,"   GL=",GL);
      WRITE(" "); WRITE(" ");

      COMMENT DEFINING PLOTTING SPACE;
      CALL_CILPLT(1);
      CALL_GARGS(1);
      CALL_CMS;
      CALL_PSPACE(0.,T_MAX/10.,10.,20.);
      CALL_LIMITS(0.,T_MAX/10.+2.,8.,22.);
      CALL_CTRSET(1);
      CALL_CRSIZE(0.3);
      CALL_MSPACE(0.,T_MAX,-100.,100.);
      CALL_AXES;
      CALL_POINT(0.,EREST);

      ACTION_POTENTIAL(I_STIM,T_STIM);

      CALL_FRAME;

2)  END SIMULATION;

    REAL I_STIM,T_STIM,T_MAX,DT,EREST,EK,ENA,EL,G_K,G_NA,GL;
    PROCEDURE INIT;
     FORTRAN "IBCINT";
    INIT;

    READ(I_STIM);
    READ(T_STIM,T_MAX,DT);
    READ(EREST);
    READ(EK,ENA,EL,G_K,G_NA,GL);

    SIMULATION(I_STIM,T_STIM,T_MAX,DT,EREST,EK,ENA,EL,G_K,G_NA,GL);

1) END.
```

Note that the numbers in the left hand margin do not form part of the programme but have been added to indicate its block structure.

Appendix 3.

Algol W programme for expanded model theoretical current-voltage curve production;

```
1) BEGIN
    PROCEDURE CURRENT_VOLTAGE(REAL VALUE EMIN,EMAX,EINC,EK,ENA,EA,
                                          EL,G_K,G_NA,G_A,GL);
2)  BEGIN
     LOGICAL STEADY_STATE,EARLY;
     REAL E,I,EINCMIN,I_LAST,AN,BN,N,AM,BM,M,AH,BH,H,AA,BA,A,AB,BB,B,
          X,Y,XA,YA,XB,YB,NREST,HREST,BREST,IK,INA,IA,IL;
     REAL ARRAY E_INTERSECT(1::3);
     INTEGER INTERSECT;

     PROCEDURE ESTIMATE_POTENTIAL(REAL VALUE EMIN,EMAX,EINC;
         INTEGER VALUE INTERSECTION;LOGICAL VALUE PRINTOUT);
3)   BEGIN
      WRITE("E RUNS FROM",EMIN,"TO",EMAX);
      E:=EMIN; INTERSECT:=1;
      EINCMIN:=0.09;

      START: IF EARLY THEN
4)    BEGIN
       N:=NREST; H:=HREST; B:=BREST;
4)    END;

      IF STEADY_STATE THEN
4)    BEGIN
       X:=EXP((-(E+60)+10)/10)-1;
       COMMENT WHEN X=0 THE VALUE OF AN IS INDETERMINATE;
       IF X=0 THEN
5)     BEGIN
        IF PRINTOUT THEN WRITE("NEXT VALUE");
        GO TO NEXT_VALUE;
5)     END;
       AN:=(0.01*(-(E+60)+10))/X;
       BN:=0.125*EXP((-(E+60))/80);
       N:=AN/(AN+BN);

       AH:=0.07*EXP((-(E+60))/20);
       BH:=1/(EXP((-(E+60)+30)/10)+1);
       H:=AH/(AH+BH);

       XB:=1-EXP(-(-(E+60)-10)/10);
       COMMENT WHEN XB=0 THE VALUE OF AB IS INDETERMINATE;
       IF XB=0 THEN
5)     BEGIN
        IF PRINTOUT THEN WRITE("NEXT VALUE");
        GO TO NEXT_VALUE;
5)     END;

       YB:=EXP((-(E+60)-10)/10)-1;
       COMMENT WHEN YB=0 THE VALUE OF BB IS INDETERMINATE;
```

```
        IF YB=0 THEN
5)      BEGIN
         IF PRINTOUT THEN WRITE("NEXT VALUE");
         GO TO NEXT_VALUE;
5)      END;

        AB:=(0.0002128*(-(E+60)-10))/XB;
        BB:=(0.0002128*(-(E+60)-10))/YB;
        B:=AB/(AB+BB);

4)    END;

      Y:=EXP((-(E+60)+25)/10)-1;
      COMMENT WHEN Y=0 THE VALUE OF AM IS INDETERMINATE;
      IF Y=0 THEN
4)    BEGIN
       IF PRINTOUT THEN WRITE("NEXT VALUE");
       GO TO NEXT_VALUE;
4)    END;
      AM:=(0.1*(-(E+60)+25))/Y;
      BM:=4*EXP((-(E+60))/18);
      M:=AM/(AM+BM);

      XA:=EXP((-(E+60)+10)/10)-1;
      COMMENT WHEN XA=0 THE VALUE OF AA IS INDETERMINATE;
      IF XA=0 THEN
4)    BEGIN
       IF PRINTOUT THEN WRITE("NEXT VALUE");
       GO TO NEXT_VALUE;
4)    END;

      YA:=1-EXP(-(-(E+60)+10)/10);
      COMMENT WHEN YA=0 THE VALUE OF BA IS INDETERMINATE;
      IF YA=0 THEN
4)    BEGIN
       IF PRINTOUT THEN WRITE("NEXT VALUE");
       GO TO NEXT_VALUE;
4)    END;

      AA:=(0.004167*(-(E+60)+10))/XA;
      BA:=(0.004167*(-(E+60)+10))/YA;
      A:=AA/(AA+BA);

      IK:=N**4*G_K*(E-EK);
      INA:=M**3*H*G_NA*(E-ENA);
      IA:=A**4*B*G_A*(E-EA);
      IL:=GL*(E-EL);

      I_LAST:=I;
      I:=IK+INA+IA+IL;
      IF E=EMIN THEN I_LAST:=I;

      IF PRINTOUT THEN
4)    BEGIN
       WRITE(" ");
       WRITE("  E=",E,"  I=",I);
       WRITE("IK=",IK,"  INA=",INA,"    IA=",IA,"  IL=",IL);
4)    END;
```

```
        IF((I_LAST<=0)AND(I>=0))OR((I_LAST>=0)AND(I<=0))THEN
4)      BEGIN
         E_INTERSECT(INTERSECT):=E;
         IF INTERSECT=1 THEN WRITE("FIRST INTERSECTION");
         IF INTERSECT=2 THEN WRITE("SECOND INTERSECTION");
         IF INTERSECT=3 THEN WRITE("THIRD INTERSECTION");
         IF PRINTOUT THEN WRITEON(" BETWEEN PRECEDING TWO VALUES");
         INTERSECT:=INTERSECT+1;

         IF EINC<=EINCMIN THEN
5)       BEGIN
          IF STEADY_STATE THEN
6)        BEGIN
           NREST:=N; HREST:=H; BREST:=B;
6)        END;
          GO TO LOOP_EXIT;
5)       END;
4)      END;

        NEXT_VALUE: E:=E+EINC;
        IF E<=EMAX THEN GO TO START;

        IF INTERSECT>INTERSECTION THEN
        ESTIMATE_POTENTIAL(E_INTERSECT(INTERSECTION)-EINC,
           E_INTERSECT(INTERSECTION)+EINC,EINC/10,1,FALSE);

        LOOP_EXIT: IF EINC<=EINCMIN THEN WRITE("LOOP EXIT");

3)    END ESTIMATE_POTENTIAL;

      WRITE(" ");
      WRITE("CURRENT-VOLTAGE RELATIONSHIPS");
      WRITE("EXPANDED MODEL");
      WRITE(" ");

      STEADY_STATE:=TRUE; EARLY:=FALSE;

      WRITE(" EK=",EK,"  G_K=",G_K);
      WRITE("ENA=",ENA," G_NA=",G_NA);
      WRITE(" EA=",EA,"  G_A=",G_A);
      WRITE(" EL=",EL,"   GL=",GL);
      WRITE(" ");
      WRITE("STEADY-STATE CURRENT-VOLTAGE RELATIONSHIP");
      WRITE(" ");

      ESTIMATE_POTENTIAL(EMIN,EMAX,EINC,1,TRUE);
      WRITE(" ");
      WRITE("ESTIMATED RESTING POTENTIAL=",E_INTERSECT(1));

      STEADY_STATE:=FALSE; EARLY:=TRUE;

      WRITE(" ");
      WRITE("EARLY CURRENT-VOLTAGE RELATIONSHIP");
      WRITE("N=",NREST,"  H=",HREST);
      WRITE("B=",BREST);
      WRITE(" ");
```

```
      ESTIMATE_POTENTIAL(EMIN,EMAX,EINC,1,TRUE);
      WRITE(" ");
      WRITE("ESTIMATED RESTING POTENTIAL=",E_INTERSECT(1));
      WRITE(" ");

      ESTIMATE_POTENTIAL(EMIN,EMAX,EINC,2,FALSE);
      WRITE(" ");
      WRITE("ESTIMATED UNIFORM THRESHOLD=",E_INTERSECT(1));
      WRITE(" ");

      ESTIMATE_POTENTIAL(EMIN,EMAX,EINC,3,FALSE);
      WRITE(" ");
      WRITE("ESTIMATED ACTION POTENTIAL PEAK=",E_INTERSECT(1));
      WRITE(" ");

2)  END CURRENT_VOLTAGE;

    REAL EMIN,EMAX,EINC,EK,ENA,EA,EL,G_K,G_NA,G_A,GL;
    INTEGER NTIMES,OPERATIONS;
    READ(OPERATIONS);
    READ(EMIN,EMAX,EINC);
    NTIMES:=1;
    REPEAT: READ(EK,ENA,EA,EL,G_K,G_NA,G_A,GL);

    CURRENT_VOLTAGE(EMIN,EMAX,EINC,EK,ENA,EA,EL,G_K,G_NA,G_A,GL);

    NTIMES:=NTIMES+1;
    IF NTIMES<=OPERATIONS THEN GO TO REPEAT;

1) END.
```

Note that the numbers in the left hand margin do not form part of the programme but have been added to indicate its block structure.

Appendix 4.

Algol W programme for expanded model action potential simulation;

```
1) BEGIN
    PROCEDURE SIMULATION(REAL VALUE I_STIM,T_STIM,T_MAX,DT,EREST,
                                    EK,ENA,EA,EL,G_K,G_NA,G_A,GL);
2)  BEGIN
     COMMENT PLOTTING PROCEDURES;
     PROCEDURE CALL_CILPLT(INTEGER VALUE A);
      FORTRAN "CILPLT";
     PROCEDURE CALL_GARGS(INTEGER VALUE A);
      FORTRAN "GARGS";
     PROCEDURE CALL_CMS;
      FORTRAN "CMS";
     PROCEDURE CALL_PSPACE(REAL VALUE A,B,C,D);
      FORTRAN "PSPACE";
     PROCEDURE CALL_LIMITS(REAL VALUE A,B,C,D);
      FORTRAN "LIMITS";
     PROCEDURE CALL_CTRSET(INTEGER VALUE A);
      FORTRAN "CTRSET";
     PROCEDURE CALL_CRSIZE(REAL VALUE X);
      FORTRAN "CRSIZE";
     PROCEDURE CALL_MSPACE(REAL VALUE A,B,C,D);
      FORTRAN "MSPACE";
     PROCEDURE CALL_AXES;
      FORTRAN "AXES";
     PROCEDURE CALL_POINT(REAL VALUE X,Y);
      FORTRAN "POINT";
     PROCEDURE CALL_JOIN(REAL VALUE X,Y);
      FORTRAN "JOIN";
     PROCEDURE CALL_FRAME;
      FORTRAN "FRAME";

     PROCEDURE ACTION POTENTIAL(REAL VALUE I_STIM,T_STIM);
3)   BEGIN
      REAL E,E1,T,C,AN,BN,N,N1,AM,BM,M,M1,AH,BH,H,H1,AA,BA,A,A1,
           AB,BB,B,B1,IK,INA,IA,IL;
      INTEGER VALUE PLOTTING_INTERVAL,PRINTOUT_INTERVAL;

      WRITE(" ");
      WRITE(" STIMULUS CURRENT=",I_STIM);
      WRITE("STIMULUS DURATION=",T_STIM);
      WRITE(" ");

      T:=0; C:=1;
      PLOTTING_INTERVAL:=0; PRINTOUT_INTERVAL:=0;

      START: IF T=0 THEN E:=EREST;
      IF T>0 THEN
4)    BEGIN
       N:=N1; M:=M1; H:=H1; A:=A1; B:=B1;
       E:=E1;
4)    END;
```

```
      AN:=(0.01*(-(E+60)+10))/(EXP((-(E+60)+10)/10)-1);
      BN:=0.125*EXP((-(E+60))/80);
      IF T=0 THEN N:=AN/(AN+BN);

      AM:=(0.1*(-(E+60)+25))/(EXP((-(E+60)+25)/10)-1);
      BM:=4*EXP((-(E+60))/18);
      IF T=0 THEN M:=AM/(AM+BM);

      AH:=0.07*EXP((-(E+60))/20);
      BH:=1/(EXP((-(E+60)+30)/10)+1);
      IF T=0 THEN H:=AH/(AH+BH);

      AA:=(0.004167*(-(E+60)+10))/(EXP((-(E+60)+10)/10)-1);
      BA:=(0.004167*(-(E+60)+10))/(1-EXP(-(-(E+60)+10)/10));
      IF T=0 THEN A:=AA/(AA+BA);

      AB:=(0.0002128*(-(E+60)-10))/(1-EXP(-(-(E+60)-10)/10));
      BB:=(0.0002128*(-(E+60)-10))/(EXP((-(E+60)-10)/10)-1);
      IF T=0 THEN B:=AB/(AB+BB);

      IK:=N**4*G_K*(E-EK);
      INA:=M**3*H*G_NA*(E-ENA);
      IA:=A**4*B*G_A*(E-EA);
      IL:=GL*(E-EL);

      I:=IK+INA+IA+IL;

      IF T>=T_STIM THEN I_STIM:=0;
      E1:=E+((I_STIM-I)*DT)/C;

      N1:=(AN*(1-N)-BN*N)*DT+N;
      M1:=(AM*(1-M)-BM*M)*DT+M;
      H1:=(AH*(1-H)-BH*H)*DT+H;
      A1:=(AA*(1-A)-BA*A)*DT+A;
      B1:=(AB*(1-B)-BB*B)*DT+B;

      IF PLOTTING_INTERVAL=0 OR PLOTTING_INTERVAL=10 THEN
4)    BEGIN
       CALL_JOIN(T,E);
       PLOTTING_INTERVAL:=0;
4)    END;

      IF PRINTOUT_INTERVAL=0 OR PRINTOUT_INTERVAL=50 THEN
4)    BEGIN
       WRITE("T=",T,"  E=",E,"  IA=",IA);
       PRINTOUT_INTERVAL:=0;
4)    END;

      NEXT_VALUE: T:=T+DT;
      PLOTTING_INTERVAL:=PLOTTING_INTERVAL+1;
      PRINTOUT_INTERVAL:=PRINTOUT_INTERVAL+1;
      IF T<=T_MAX THEN GO TO START;
      WRITE(" "); WRITE(" ");
      WRITE("FINAL VALUES");
      WRITE("E=",E1);
      WRITE("N=",N1,"  M=",M1,"  H=",H1);
      WRITE("A=",A1,"  B=",B1);
```

```
      WRITE(" "); WRITE(" ");

3)    END ACTION_POTENTIAL;

      WRITE(" ");
      WRITE("ACTION POTENTIAL SIMULATION");
      WRITE("EXPANDED MODEL");
      WRITE(" ");
      WRITE("T_STIM=",T_STIM,"  T_MAX=",T_MAX,"  DT=",DT);
      WRITE("EREST=",EREST);
      WRITE(" ");
      WRITE(" EK=",EK,"  G_K=",G_K);
      WRITE("ENA=",ENA," G_NA=",G_NA);
      WRITE(" EA=",EA,"  G_A=",G_A);
      WRITE(" EL=",EL,"   GL=",GL);
      WRITE(" "); WRITE(" ");

      COMMENT DEFINING PLOTTING SPACE;
      CALL_CILPLT(1);
      CALL_GARGS(1);
      CALL_CMS;
      CALL_PSPACE(0.,T_MAX/10.,10.,20.);
      CALL_LIMITS(0.,T_MAX/10.+2.,8.,22.);
      CALL_CTRSET(1);
      CALL_CRSIZE(0.3);
      CALL_MSPACE(0.,T_MAX,-100.,100.);
      CALL_AXES;
      CALL_POINT(0.,EREST);

      ACTION_POTENTIAL(I_STIM,T_STIM);

      CALL_FRAME;

2)  END SIMULATION;

    REAL I_STIM,T_STIM,T_MAX,DT,EREST,EK,ENA,EA,EL,G_K,G_NA,G_A,GL;
    PROCEDURE INIT;
     FORTRAN "IBCINT";
    INIT;

    READ(I_STIM);
    READ(T_STIM,T_MAX,DT);
    READ(EREST);
    READ(EK,ENA,EA,EL,G_K,G_NA,G_A,GL);

    SIMULATION(I_STIM,T_STIM,T_MAX,DT,EREST,EK,ENA,EA,EL,G_K,G_NA,
               G_A,GL);

1) END.
```

Note that the numbers in the left hand margin do not form part of the programme but have been added to indicate its block structure.

Appendix 5.

Algol W programme for simulation of proposed mechanism of burst generation : One compartment simulation;

```
1) BEGIN
    PROCEDURE SIMULATION(REAL VALUE I_STIM,T_STIM,T_MAX,DT,K_EXTREST,
                                    K_INT,ENA,EL,G_K,G_NA,GL);

2)  BEGIN
     COMMENT PLOTTING PROCEDURES;
     PROCEDURE CALL_CILPLT(INTEGER VALUE A);
      FORTRAN "CILPLT";
     PROCEDURE CALL_GARGS(INTEGER VALUE A);
      FORTRAN "GARGS";
     PROCEDURE CALL_CMS;
      FORTRAN "CMS";
     PROCEDURE CALL_PSPACE(REAL VALUE A,B,C,D);
      FORTRAN "PSPACE";
     PROCEDURE CALL_LIMITS(REAL VALUE A,B,C,D);
      FORTRAN "LIMITS";
     PROCEDURE CALL_CTRSET(INTEGER VALUE A);
      FORTRAN "CTRSET";
     PROCEDURE CALL_CRSIZE(REAL VALUE X);
      FORTRAN "CRSIZE";
     PROCEDURE CALL_MSPACE(REAL VALUE A,B,C,D);
      FORTRAN "MSPACE";
     PROCEDURE CALL_AXES;
      FORTRAN "AXES";
     PROCEDURE CALL_POINT(REAL VALUE X,Y);
      FORTRAN "POINT";
     PROCEDURE CALL_JOIN(REAL VALUE X,Y);
      FORTRAN "JOIN";
     PROCEDURE CALL_FRAME;
      FORTRAN "FRAME";

     PROCEDURE ACTION_POTENTIAL(REAL VALUE I_STIM,T_STIM);
3)   BEGIN
      REAL E,E1,T,C,AN,BN,N,N1,AM,BM,M,M1,AH,BH,H,H1,GK,GNA,IK,INA,IL,
           I,K_EXT,K_EXT1,PUMP_CON,PUMP_CON1,I_PUMP_NA,I_PUMP_K,AP,BP,
           EK;
      INTEGER PLOTTING_INTERVAL,PRINTOUT_INTERVAL;

      WRITE(" ");
      WRITE(" STIMULUS CURRENT=",I_STIM);
      WRITE("STIMULUS DURATION=",T_STIM);
      WRITE(" ");

      T:=0; C:=1;
      PLOTTING_INTERVAL:=0; PRINTOUT_INTERVAL:=0;

      START: IF T=0 THEN
4)    BEGIN
       E:=EREST; K_EXT:=K_EXTREST;
4)    END;
```

```
      IF T>0 THEN
4)    BEGIN
       N:=N1; M:=M1; H:=H1;
       E:=E1; K_EXT:=K_EXT1;
       PUMP_CON:=PUMP_CON1;
4)    END;

      AN:=(0.00025*(-(E+60)+10))/(EXP((-(E+60)+10)/10)-1);
      BN:=0.003125*EXP((-(E+60))/80);
      IF T=0 THEN N:=AN/(AN+BN);

      AM:=(0.01*(-(E+60)+25))/(EXP((-(E+60)+25)/10)-1);
      BM:=0.4*EXP((-(E+60))/18);
      IF T=0 THEN M:=AM/(AM+BM);

      AH:=0.01*EXP((-(E+60))/20);
      BH:=0.143/(EXP((-(E+60)+30)/10)+1);
      IF T=0 THEN H:=AH/(AH+BH);

      AP:=(Q*(K_EXT-5))/(1-(EXP(-(K_EXT-5)/1)));
      BP:=(Q*(K_EXT-5))/(EXP((K_EXT-5)/1)-1);
      IF T=0 THEN PUMP_CON:=AP/(AP+BP);

      GK:=G_K*N**4;
      GNA:=G_NA*M**3*H;

      I_PUMP_NA:=I_PUMP_NA_MAX*(PUMP_CON**3);

      I_PUMP_K:= -(2*I_PUMP_NA)/3;

      EK:=58*LOG(K_EXT/K_INT);

      IK:=GK*(E-EK)+I_PUMP_K;
      INA:=GNA*(E-ENA)+I_PUMP_NA;
      IL:=GL*(E-EL);

      I:=IK+INA+IL;

      IF T>=T_STIM THEN I_STIM:=0;
      E1:=E+((I_STIM-I)*DT)/C;
      K_EXT1:=K_EXT+(K_EXT-K_EXTREST)*DC+IK*DT*SC;

      N1:=(AN*(1-N)-BN*N)*DT+N;
      M1:=(AM*(1-M)-BM*M)*DT+M;
      H1:=(AH*(1-H)-BH*H)*DT+H;
      PUMP_CON1:=(AP*(1-PUMP_CON)-BP*PUMP_CON)*DT+PUMP_CON;

      IF PLOTTING_INTERVAL=0 OR PLOTTING_INTERVAL=10 THEN
4)    BEGIN
       CALL_JOIN(T,E);
       PLOTTING_INTERVAL=0;
4)    END;

      IF PRINTOUT_INTERVAL=0 OR PRINTOUT_INTERVAL=200 THEN
4)    BEGIN
       WRITE("T=",T,"   E=",E);
       WRITE("IK=",IK,"  INA=",INA);
```

```
        WRITE("K_EXT=",K_EXT,"   EK=",EK);
        WRITE("I_PUMP_NA=",I_PUMP_NA,"  I_PUMP_K=",I_PUMP_K);
        WRITE(" ");
4)    END;

      NEXT_VALUE: T:=T+DT;
      PLOTTING_INTERVAL:=PLOTTING_INTERVAL+1;
      PRINTOUT_INTERVAL:=PRINTOUT_INTERVAL+1;
      IF T<=(T_MAX+2) THEN GO TO START;

      WRITE("FINAL VALUES"); WRITE(" ");
      WRITE("E=",E1);
      WRITE("N=",N1,"  M=",M1,"  H=",H1);
      WRITE("K_EXT=",K_EXT1,"  EK=",EK);
      WRITE("I_PUMP_NA=",I_PUMP_NA,"  I_PUMP_K=",I_PUMP_K);
      WRITE(" "); WRITE(" ");

3)    END ACTION_POTENTIAL;

      WRITE(" ");
      WRITE("HH ACTION POTENTIAL SIMULATION");
      WRITE("POTASSIUM ACCUMULATION MODEL");
      WRITE(" ");
      WRITE("T_STIM=",T_STIM,"  T_MAX=",T_MAX,"  DT=",DT);
      WRITE("E_REST=",E_REST,"  K_EXTREST=",K_EXTREST);
      WRITE("K_INT=",K_INT,"  G_K=",G_K);
      WRITE("ENA=",ENA,"  G_NA=",G_NA);
      WRITE("EL=",EL,"  GL=",GL);
      WRITE("SC=",SC);
      WRITE("TAU=",TAU);
      WRITE("Q=",Q);
      WRITE("I_PUMP_NA_MAX=",I_PUMP_NA_MAX);
      WRITE(" "); WRITE(" ");

      COMMENT DEFINING PLOTTING SPACE;
      CALL_CILPLT(1);
      CALL_GARGS(1);
      CALL_CMS;
      CALL_PSPACE(0.,T_MAX/50.,10.,20.);
      CALL_LIMITS(0.,T_MAX/50.+5.,8.,22.);
      CALL_CTRSET(1);
      CALL_CRSIZE(0.5);
      CALL_MSPACE(0.,T_MAX,-100.,100.);
      CALL_AXES;
      CALL_POINT(0.,E_REST);

      ACTION_POTENTIAL(I_STIM,T_STIM);

      CALL_FRAME;

2)  END SIMULATION;

    REAL I_STIM,T_STIM,T_MAX,DT,K_EXTREST,K_INT,ENA,EL,G_K,G_NA,GL,
         E_REST,I_PUMP_NA_MAX,DC,SC,TAU,Q;
    PROCEDURE INIT;
     FORTRAN "IBCINT";
    INIT;
```

```
    READ(I_STIM,T_STIM,T_MAX,DT);
    READ(K_EXTREST,K_INT);
    READ(ENA,EL);
    READ(G_K,G_NA,GL);
    READ(E_REST);
    READ(I_PUMP_NA_MAX);
    READ(SC);
    READ(TAU);
    READ(Q);
    DC:=-(EXP(-DT/TAU)/TAU)*DT;

    SIMULATION(I_STIM,T_STIM,T_MAX,DT,K_EXTREST,K_INT,ENA,EL,
               G_K,G_NA,GL);

1) END.
```

Note that the numbers in the left hand margin do not form part of the programme but have been added to indicate its block structure.

Appendix 6.

Algol W programme for simulation of proposed mechanism of burst generation : Two compartment simulation;

```
1) BEGIN
    PROCEDURE SIMULATION(REAL VALUE I_STIM,T_STIM,T_MAX,DT,K_EXTREST,
                                    K_INT,ENA,EL,G_K,G_NA,GL);

2)  BEGIN
     COMMENT PLOTTING PROCEDURES;
     PROCEDURE CALL_CILPLT(INTEGER VALUE A);
      FORTRAN "CILPLT";
     PROCEDURE CALL_GARGS(INTEGER VALUE A);
      FORTRAN "GARGS";
     PROCEDURE CALL_CMS;
      FORTRAN "CMS";
     PROCEDURE CALL_PSPACE(REAL VALUE A,B,C,D);
      FORTRAN "PSPACE";
     PROCEDURE CALL_LIMITS(REAL VALUE A,B,C,D);
      FORTRAN "LIMITS";
     PROCEDURE CALL_CTRSET(INTEGER VALUE A);
      FORTRAN "CTRSET";
     PROCEDURE CALL_CRSIZE(REAL VALUE X);
      FORTRAN "CRSIZE";
     PROCEDURE CALL_MSPACE(REAL VALUE A,B,C,D);
      FORTRAN "MSPACE";
     PROCEDURE CALL_AXES;
      FORTRAN "AXES";
     PROCEDURE CALL_POINT(REAL VALUE X,Y);
      FORTRAN "POINT";
     PROCEDURE CALL_JOIN(REAL VALUE X,Y);
      FORTRAN "JOIN";
     PROCEDURE CALL_FRAME;
      FORTRAN "FRAME";

     PROCEDURE ACTION_POTENTIAL(REAL VALUE I_STIM,T_STIM);
3)   BEGIN
      REAL E_V,E_V1,AN_V,BN_V,N_V,N_V1,AM_V,BM_V,M_V,M_V1,AH_V,BH_V,H_V,
           H_V1,IK_V,INA_V,IL_V,I_V,K_EXT_V,K_EXT_V1,PUMP_CON_V,I_LAT_V,
           PUMP_CON_V1,I_PUMP_NA_V,I_PUMP_K_V,AP_V,BP_V,EK_V,GK_V,GNA_V,

           E_S,E_S1,AN_S,BN_S,N_S,N_S1,AM_S,BM_S,M_S,M_S1,AH_S,BH_S,H_S,
           H_S1,IK_S,INA_S,IL_S,I_S,K_EXT_S,K_EXT_S1,PUMP_CON_S,I_LAT_S,
           PUMP_CON_S1,I_PUMP_NA_S,I_PUMP_K_S,AP_S,BP_S,EK_S,GK_S,GNA_S,

           T,C;

      INTEGER PLOTTING_INTERVAL,PRINTOUT_INTERVAL;

      WRITE(" ");
      WRITE(" STIMULUS CURRENT=",I_STIM);
      WRITE("STIMULUS DURATION=",T_STIM);
      WRITE(" ");
```

```
      T:=0; C:=1;
      PLOTTING_INTERVAL:=0; PRINTOUT_INTERVAL:=0;

      START: IF T=0 THEN
4)    BEGIN
       E_V:=E_REST; K_EXT_V:=K_EXTREST;
       E_S:=E_REST; K_EXT_S:=K_EXTREST;
4)    END;

      IT T>0 THEN
4)    BEGIN
       N_V:=N_V1; M_V:=M_V1; H_V:=H_V1;
       E_V:=E_V1; K_EXT_V:=K_EXT_V1; PUMP_CON_V:=PUMP_CON_V1;
       N_S:=N_S1; M_S:=M_S1; H_S:=H_S1;
       E_S:=E_S1; K_EXT_S:=K_EXT_S1; PUMP_CON_S:=PUMP_CON_S1;
4)    END;

      AN_V:= IF (E_V>-51) AND (E_V<-49) THEN 0.0025
      ELSE   (0.00025*(-(E_V+60)+10))/(EXP((-(E_V+60)+10)/10)-1);
      BN_V:= IF (E_V>-61) AND (E_V<-59) THEN 0.003135
      ELSE   0.003125*EXP((-(E_V+60))/80);
      IF T=0 THEN N_V:=AN_V/(AN_V+BN_V);

      AM_V:= IF (E_V>-36) AND (E_V<-34) THEN 0.1
      ELSE   (0.01*(-(E_V+60)+25))/(EXP((-(E_V+60)+25)/10)-1);
      BM_V:= IF (E_V>-61) AND (E_V<-59) THEN 0.4
      ELSE   0.4*EXP((-(E_V+60))/18);
      IF T=0 THEN M_V:=AM_V/(AM_V+BM_V);

      AH_V:= IF (E_V>-61) AND (E_V<-59) THEN 0.01
      ELSE   0.01*EXP((-(E_V+60))/20);
      BH_V:= IF (E_V>-31) AND (E_V<-29) THEN 0.0143
      ELSE   0.143/(EXP((-(E_V+60)+30)/10)+1);
      IF T=0 THEN H_V:=AH_V/(AH_V+BH_V);

      AP_V:= IF (K_EXT_V>4.9) AND (K_EXT_V<5.1) THEN Q
      ELSE   (Q*(K_EXT_V-5))/(1-(EXP(-(K_EXT_V-5))));
      BP_V:= IF (K_EXT_V>4.9) AND (K_EXT_V<5.1) THEN Q
      ELSE   (Q*(K_EXT_V-5))/(EXP(K_EXT_V-5)-1);
      IF T=0 THEN PUMP_CON_V:=AP_V/(AP_V+BP_V);

      GK_V:=G_K*N_V**4;
      GNA_V:=G_NA*M_V**3*H_V;

      I_PUMP_NA_V:=I_PUMP_NA_MAX*(PUMP_CON_V**3);

      I_PUMP_K_V:= -(2*I_PUMP_NA_V)/3;

      EK_V:=58*LOG(K_EXT_V/K_INT);

      IK_V:=GK_V*(E_V-EK_V)+I_PUMP_K_V;
      INA_V:=GNA_V*(E_V-ENA)+I_PUMP_NA_V;
      IL_V:=GL*(E_V-EL);

      I_V:=IK_V+INA_V+IL_V;

      IF T>=T_STIM THEN I_STIM:=0;
```

```
I_LAT_V:=(E_S-E_V)/R;

E_V1:=E_V+((I_STIM+I_LAT_V-I_V)*DT)/C;

K_EXT_V1:=K_EXT_V+(K_EXT_V-K_EXTREST)*DC_V+IK_V*DT*SC;

N_V1:=(AN_V*(1-N_V)-BN_V*N_V)*DT+N_V;
M_V1:=(AM_V*(1-M_V)-BM_V*M_V)*DT+M_V;
H_V1:=(AH_V*(1-H_V)-BH_V*H_V)*DT+H_V;
PUMP_CON_V1:=(AP_V*(1-PUMP_CON_V)-BP_V*PUMP_CON_V)*DT+PUMP_CON_V;


AN_S:= IF (E_S>-51) AND (E_S<-49) THEN 0.0025
ELSE   (0.00025*(-(E_S+60)+10))/(EXP((-(E_S+60)+10)/10)-1);
BN_S:= IF (E_S>-61) AND (E_S<-59) THEN 0.003125
ELSE   0.003125*EXP((-(E_S+60))/80);
IF T=0 THEN N_S:=AN_S/(AN_S+BN_S);

AM_S:= IF (E_S>-36) AND (E_S<-34) THEN 0.1
ELSE   (0.01*(-(E_S+60)+25))/(EXP((-(E_S+60)+25)/10)-1);
BM_S:= IF (E_S>-61) AND (E_S<-59) THEN 0.4
ELSE   0.4*EXP((-(E_S+60))/18);
IF T=0 THEN M_S:=AM_S/(AM_S+BM_S);

AH_S:= IF (E_S>-61) AND (E_S<-59) THEN 0.01
ELSE   0.01*EXP((-(E_S+60))/20);
BH_S:= IF (E_S>-31) AND (E_S<-29) THEN 0.0143
ELSE   0.143/(EXP((-(E_S+60)+30)/10)+1);
IF T=0 THEN H_S:=AH_S/(AH_S+BH_S);

AP_S:= IF (K_EXT_S>4.9) AND (K_EXT_S<5.1) THEN Q
ELSE   (Q*(K_EXT_S-5))/(1-(EXP(-(K_EXT_S-5))));
BP_S:= IF (K_EXT_S>4.9) AND (K_EXT_S<5.1) THEN Q
ELSE   (Q*(K_EXT_S-5))/(EXP(K_EXT_S-5)-1);
IF T=0 THEN PUMP_CON_S:=AP_S/(AP_S+BP_S);

GK_S:=G_K*N_S**4;
GNA_S:=G_NA*M_S**3*H_S;

I_PUMP_NA_S:=I_PUMP_NA_MAX*(PUMP_CON_S**3);

I_PUMP_K_S:= -(2*I_PUMP_NA_S)/3;

EK_S:=58*LOG(K_EXT_S/K_INT);

IK_S:=GK_S*(E_S-EK_S)+I_PUMP_K_S;
INA_S:=GNA_S*(E_S-ENA)+I_PUMP_NA_S;
IL_S:=GL*(E_S-EL);

I_S:=IK_S+INA_S+IL_S;

I_LAT_S:=(E_V-E_S)/R;

E_S1:=E_S+((I_STIM+I_LAT_S-I_S)*DT)/C;

K_EXT_S1:=K_EXT_S+(K_EXT_S-K_EXTREST)*DC_S+IK_S*DT*SC;
```

```
      N_S1:=(AN_S*(1-N_S)-BN_S*N_S)*DT+N_S;
      M_S1:=(AM_S*(1-M_S)-BM_S*M_S)*DT+M_S;
      H_S1:=(AH_S*(1-H_S)-BH_S*H_S)*DT+H_S;
      PUMP_CON_S1:=(AP_S*(1-PUMP_CON_S)-BP_S*PUMP_CON_S)*DT+PUMP_CON_S;

      IF PLOTTING_INTERVAL=0 OR PLOTTING_INTERVAL=10 THEN
4)    BEGIN
       CALL_JOIN(T,E_S);
       PLOTTING_INTERVAL:=0;
4)    END;

      IF PRINTOUT_INTERVAL=0 OR PRINTOUT_INTERVAL=200 THEN
4)    BEGIN
       WRITE("T=",T);
       WRITE("E_S=",E_S,"   E_V=",E_V);
       WRITE("IK_S=",IK_S,"  INA_S=",INA_S,"  IK_V=",IK_V,"  INA_V=",
             INA_V);
       WRITE("K_EXT_S=",K_EXT_S,"  EK_S=",EK_S,"  K_EXT_V=",K_EXT_V,
             "  EK_V=",EK_V);
       WRITE("I_PUMP_NA_S=",I_PUMP_NA_S,"  I_PUMP_K_S=",I_PUMP_K_S);
       WRITE("I_PUMP_NA_V=",I_PUMP_NA_V,"  I_PUMP_K_V=",I_PUMP_K_V);
       WRITE("PUMP_CON_S=",PUMP_CON_S,"  PUMP_CON_V=",PUMP_CON_V);
       WRITE("I_LAT_S=",I_LAT_S); WRITE(" ");
       PRINTOUT_INTERVAL:=0;
4)    END;

      NEXT_VALUE: T:=T+DT;
      PLOTTING_INTERVAL:=PLOTTING_INTERVAL+1;
      PRINTOUT_INTERVAL:=PRINTOUT_INTERVAL+1;
      IF T<=(T_MAX+2) THEN GO TO START;

      WRITE("FINAL VALUES"); WRITE(" ");
      WRITE("E_S=",E_S1);
      WRITE("N_S=",N_S1,"  M_S=",M_S1,"  H_S=",H_S1);
      WRITE("K_EXT_S=",K_EXT_S1,"  EK_S=",EK_S);
      WRITE("PUMP_CON_S=",PUMP_CON_S1);
      WRITE(" ");
      WRITE("E_V=",E_V1);
      WRITE("N_V=",N_V1,"  M_V=",M_V1,"  H_V=",H_V1);
      WRITE("K_EXT_V=",K_EXT_V1,"  EK_V=",EK_V);
      WRITE("PUMP_CON_V=",PUMP_CON_V1);
      WRITE(" "); WRITE(" ");

3)    END ACTION_POTENTIAL;

      WRITE(" ");
      WRITE("HH ACTION POTENTIAL SIMULATION");
      WRITE("POTASSIUM ACCUMULATION MODEL");
      WRITE(" ");
      WRITE("INVAGINATIONS INTERACT WITH SOMA");
      WRITE(" ");
      WRITE("T_STIM=",T_STIM,"  T_MAX=",T_MAX,"  DT=",DT);
      WRITE("E_REST=",E_REST,"  K_EXTREST=",K_EXTREST);
      WRITE("K_INT=",K_INT,"  G_K=",G_K);
      WRITE("ENA=",ENA,"  G_NA=",G_NA);
      WRITE("EL=",EL,"  GL=",GL);
      WRITE("SC=",SC);
```

```
      WRITE("Q=",Q);
      WRITE("R=",R);
      WRITE("TAU_S=",TAU_S,"  TAU_V=",TAU_V);
      WRITE("I_PUMP_NA_MAX=",I_PUMP_NA_MAX);
      WRITE(" "); WRITE(" ");

      COMMENT DEFINING PLOTTING SPACE;
      CALL_CILPLT(1);
      CALL_GARGS(1);
      CALL_CMS;
      CALL_PSPACE(0.,T_MAX/100.,10.,20.);
      CALL_LIMITS(0.,T_MAX/100.+5.,8.,22.);
      CALL_CTRSET(1);
      CALL_CRSIZE(0.5);
      CALL_MSPACE(0.,T_MAX,-100.,100.);
      CALL_AXES;
      CALL_POINT(0.,E_REST);

      ACTION_POTENTIAL(I_STIM,T_STIM);

      CALL_FRAME;

2)    END SIMULATION;

      REAL I_STIM,T_STIM,T_MAX,DT,K_EXTREST,K_INT,ENA,EL,G_K,G_NA,GL,
           E_REST,I_PUMP_NA_MAX,DC_V,DC_S,TAU_V,TAU_S,SC,Q,R;
      PROCEDURE INIT;
       FORTRAN "IBCINT";
      INIT;

      READ(I_STIM,T_STIM,T_MAX,DT);
      READ(K_EXTREST,K_INT);
      READ(ENA,EL);
      READ(G_K,G_NA,GL);
      READ(E_REST);
      READ(I_PUMP_NA_MAX);
      READ(SC);
      READ(Q);
      READ(TAU_V,TAU_S);
      READ(R);
      DC_V:= -(EXP(-DT/TAU_V)/TAU_V)*DT;
      DC_S:= -(EXP(-DT/TAU_S)/TAU_S)*DT;

      SIMULATION(I_STIM,T_STIM,T_MAX,DT,K_EXTREST,K_INT,ENA,EL,
                 G_K,G_NA,GL);

1) END.
```

Note that the numbers in the left hand margin do not form part of the programme but have been added to indicate its block structure.

REFERENCES

ADAM, G. (1973). 'The effect of potassium diffusion through the Schwann cell layer on potassium conductance of the squid axon.' J. Membrane Biol. 13; 353-386.

ADELMAN, W.J. & PALTI, Y. (1969a). 'The influence of external potassium on the inactivation of sodium currents in the giant axon of the squid, Loligo pealei.' J. gen. Physiol. 53; 685-703.

ADELMAN, W.J. & PALTI,Y. (1969b). 'Effects of external potassium and long duration voltage conditioning on the amplitude of sodium currents in the giant axon of the squid, Loligo pealei.' J. gen. Physiol. 54; 589-606.

ADELMAN, W.J., PALTI, Y. & SENFT, J.P. (1973). 'Potassium ion accumulation in a periaxonal space and its effect on the measurement of membrane potassium ion conductance.' J. Membrane Biol. 13; 387-410.

AIDLEY, D.J. (1971). 'The Physiology of Excitable Cells.' Cambridge University Press.

ALVING, B.O. (1968). 'Spontaneous activity in isolated somata of Aplysia pacemaker neurons.' J. gen. Physiol. 51; 29-45.

ALVING, B.O. (1969). 'Differences between pacemaker and nonpacemaker neurons of Aplysia on voltage clamping.' J. gen. Physiol. 54; 512-531.

ARVANITAKI, A. & CHALAZONITIS, N. (1968). 'Electrical properties and temporal organization in oscillatory neurons (Aplysia).' in 'Neurobiology of Invertebrates' ed. SALANKI, J.; 169-199. New York: Plenum Press.

AYRAPETYAN, S.N. (1973). 'On the regulation of the mechanism of rhythmic activity of Helix neurones.' in 'Neurobiology of Invertebrates' 2nd Int. Symposium ed. SALANKI, J.; 81-92. Budapest: Akademiai Kiado.

BAKER, P.F. (1966). 'The sodium pump.' Endeavour 25; 166-172.

BAKER, P.F., HODGKIN, A.L. & SHAW, T.I. (1962a). 'Replacement of the axoplasm of giant nerve fibres with artificial solutions.' J. Physiol. Lond. 164; 330-354.

BAKER, P.F., HODGKIN, A.L. & SHAW, T.I. (1962b). 'The effects of changes in internal ionic concentrations on the electrical properties of perfused giant axons.' J. Physiol. Lond. 164; 355-374.

BANNISTER, W.J. (1963). 'A transistor delay and pulse generator.' Electronic Eng. 35; No. 429, p. 746-747.

BANNISTER, W.J. & KAY, R.H. (1965). 'A versatile transistor stimulator.' Electronic Eng. 37; No. 454, p. 793-795.

BULLOCK, T.H. & HORRIDGE, G.A. (1965). 'Structure and Function in the Nervous Systems of Invertebrates.' San Francisco: W.H. Freeman & Co.

BURES, J., PETRAN, M. & ZACHAR, J. (1962). 'Electrophysiological Methods in Biological Research.' Prague: Publishing House of the Czechoslovak Academy of Sciences.

BURTON, R.F. (1967). 'Ionic regulation in the snail, Helix aspersa.' Comp. Biochem Physiol. 25; 501-508.

CARPENTER, D.O. (1970). 'Membrane potential produced directly by the Na^+ pump in Aplysia neurons.' Comp. Biochem. Physiol. 35; 371-385.

CARPENTER, D.O. (1973). 'Ionic mechanisms and models of endogenous discharge of Aplysia neurones.' in 'Neurobioloby of Invertebrates' 2nd Int. Symposium ed. SALANKI, J.; 35-58. Budapest: Akademiai Kiado.

CARPENTER, D.O. & ALVING, B.O. (1968). 'A contribution of an electrogenic Na^+ pump to membrane potential in Aplysia neurons.' J. gen. Physiol. 52; 1-21.

CARPENTER, D.O., HOVEY, M. & BAK, A.F. (1971). 'Intracellular conductance of Aplysia neurons and squid axon as determined by a new technique.' Int. J. Neurosci. 2; 35-48.

CHALAZONITIS, N. (1968). 'Synaptic properties of oscillatory neurons (Aplysia and Helix).' in 'Neurobioloby of Invertebrates' ed. SALANKI, J.; 201-226. New York: Plenum Press.

CHALAZONITIS, N., GOLA, M. & ARVANITAKI, A. (1965). 'Oscillations lentes du potentiel de membrane neuronique, fonction de la pO_2 intracellulaire (Neurones autoactifs d'Aplysia depilans).' C. r. Seanc. Soc. Biol. 159; 2451-2455.

CHAMBERLAIN, S.G. & KERKUT, G.A. (1969). 'Voltage clamp analysis of the sodium and calcium inward currents in snail neurones.' Comp. Biochem. Physiol. 28; 787-801.

CHANDLER, W.K., HODGKIN, A.L. & MEVES, H. (1965). 'The effect of changing the internal solution on sodium inactivation and related phenomena in giant axons.' J. Physiol. Lond. 180; 821-836.

CHEN, C.F. VON BAUMGARTEN, R. & TAKEDA, R. (1971). 'Pacemaker properties of completely isolated neurones in Aplysia californica.' Nature New Biology 233; 27-29.

CHRISTOFFERSEN, G.R.J. (1973). 'Chloride conductance and the effect of extracellular calcium concentration on resting neurons in the snail, Helix pomatia.' Comp. Biochem. Physiol. 46A; 371-389.

CLAYTON, G.B. (1972). 'Experiments with operational amplifiers. 2. Measurement of input bias currents and offset voltage.' Wireless World 78; No. 1441, p. 324.

COGGESHALL, R.E. (1967). 'A light and electron microscope study of the abdominal ganglion of Aplysia californica.' J. Neurophysiol. 30; 1263-1287.

COLE, K.S. & CURTIS, H.J. (1939). 'Electric impedance of the squid giant axon during activity.' J. gen. Physiol. 22; 649-670.

CONNOR, J.A. & STEVENS, C.F. (1971a). 'Inward and delayed outward membrane currents in isolated neural somata under voltage clamp.' J. Physiol. Lond. 213; 1-19.

CONNOR, J.A. & STEVENS, C.F. (1971b). 'Voltage clamp studies of a transient outward membrane current in gastropod neural somata.' J. Physiol. Lond. 213; 21-30.

CONNOR, J.A. & STEVENS, C.F. (1971c). 'Prediction of repetitive firing behaviour from voltage clamp data on an isolated neurone soma.' J. Physiol. Lond. 213; 31-53.

CUERVO, L.A. & ADELMAN, W.J. (1970). 'Equilibrium and kinetic properties of the interaction between Tetrodotoxin and the excitable membrane of the squid giant axon.' J. gen. Physiol. 55; 309-335.

EATON, D.C. (1972). 'Potassium ion accumulation near a pace-making cell of Aplysia.' J. Physiol. Lond. 224; 421-440.

EHRENSTEIN, G., LECAR, H. & NOSSAL, R. (1970). 'The nature of the negative resistance in bimolecular lipid membranes containing excitability-inducing material.' J. gen. Physiol. 55; 119-133.

FRANKENHAEUSER, B. & HODGKIN, A.L. (1957). 'The action of calcium on the electrical properties of squid axons.' J. Physiol. Lond. 137; 218-244.

FRAZIER, W.T., KANDEL, E.R., KUPFERMANN, I., WAZIRI, R. & COGGESHALL, R.E. (1967). 'Morphological and functional properties of identified neurons in the abdominal ganglion of Aplysia californica.' J. Neurophysiol. 30; 1288-1351.

GEDULDIG, D. & GRUENER, R. (1970). 'Voltage clamp on Aplysia giant neurone: Early sodium and calcium currents.' J. Physiol. Lond. 211; 217-244.

GOLA, M. (1974). 'Evolution de la forme des potentiels d'action par stimulations répétitives: Analyse per la méthode du voltage imposé (Neurones d'Helix pomatia).' Pfluegers Arch. Ges. Physiol. 346; 121-140.

GORMAN, A.L.F. & MARMOR, M.F. (1970a). 'Contributions of the sodium pump and ionic gradients to the membrane potential of a molluscan neurone.' J. Physiol. Lond. 210; 897-917.

GORMAN, A.L.F. & MARMOR, M.F. (1970b). 'Temperature dependence of the sodium-potassium permeability ratio of a molluscan neurone.' J. Physiol. Lond. 210; 919-931.

GORMAN, A.L.F. & MIROLLI, M. (1970). 'Axonal localization of an excitatory post-synaptic potential in a molluscan neurone.' J. exp. Biol. 53; 727-736.

GULD, C. (1959). 'Use of screened power transformers and output transformers to reduce stimulus artefacts.' Proc. Int. Conf. Med. Electronics, 2nd, Paris, June 1959 (London: Iliffe, 1960).

GUTTMAN, R. & BARNHILL, R. (1970). 'Oscillation and repetitive firing in squid axons. Comparison of experiments with computations.' J. gen. Physiol. 55; 104-118.

HARMON, L.D. (1964). 'Problems in neural modelling.' in 'Neural Theory and Modeling' ed. REISS, R.F.; 9-30. Stanford University Press.

HILLE, B. (1967). 'The selective inhibition of delayed potassium currents in nerve by Tetraethlyammonium ion.' J. gen. Physiol. 50; 1287-1302.

HODGKIN, A.L. (1958). 'Ionic movements and electrical activity in giant nerve fibres.' Proc. R. Soc. B 148; 1-37.

HODGKIN, A.L. & HOROWICZ, P. (1959). 'The influence of potassium and chloride ions on the membrane potential of single muscle fibres.' J. Physiol. Lond. 148; 127-160.

HODGKIN, A.L. & HUXLEY, A.F. (1952a). 'Currents carried by sodium and potassium ions through the membrane of the giant axon of Loligo.' J. Physiol. Lond. 116; 449-472.

HODGKIN, A.L. & HUXLEY, A.F. (1952b). 'The components of membrane conductance in the giant axon of Loligo.' J. Physiol. Lond. 116; 473-496.

HODGKIN, A.L. & HUXLEY, A.F. (1952c). 'The dual effect of membrane potential on sodium conductance in the giant axon of Loligo.' J. Physiol. Lond. 116; 497-506.

HODGKIN, A.L. & HUXLEY, A.F. (1952d). 'A quantitative description of membrane current and its application to conduction and excitation in nerve.' J. Physiol. Lond. 117; 500-544.

HODGKIN, A.L., HUXLEY, A.F. & KATZ, B. (1952). 'Measurement of current-voltage relations in the membrane of the giant axon of Loligo.' J. Physiol. Lond. 116; 424-448.

HODGKIN, A.L. & KATZ, B. (1949). 'The effect of sodium ions on the electrical activity of the giant axon of the squid.' J. Physiol. Lond. 108; 37-77.

HUXLEY, A.F. (1959). 'Ion movements during nerve activity.' Ann. N.Y. Acad. Sci. 81; 221-246.

JERELOVA, O.M., KRASTS, I.V. & VEPRINTSEV, B.N. (1971). 'The effect of sodium, calcium and magnesium on the amplitude of the action potentials from giant neurons of Limnaea stagnalis.' Comp. Biochem. Physiol. 40A; 281-293.

JUNGE, D. & STEPEHENS, C.L. (1973). 'Cyclic variation of potassium conductance in a burst-generating neurone in Aplysia.' J. Physiol. Lond. 235; 155-181.

KATZ, B. (1966). 'Nerve, Muscle and Synapse.' New York: McGraw-Hill.

KERKUT, G.A., BROWN, L.C. & WALKER, R.J. (1969a). 'Post-synaptic stimulation of the electrogenic sodium pump.' Life Sci. 8(1); 297-300.

KERKUT, G.A., BROWN, L.C. & WALKER, R.J. (1969b). 'Cholinergic IPSP by stimulation of the electrogenic sodium pump.' Nature Lond. 223; 864-865.

KERKUT, G.A., FRENCH, M.C. & WALKER, R.J. (1970). 'The location of axonal pathways of identifiable neurones of Helix aspersa using the dye Procion yellow M-4R.' Comp. Biochem. Physiol. 32; 681-690.

KERKUT, G.A. & GARDNER, D.R. (1967). 'The role of calcium ions in the action potentials of Helix aspersa neurones.' Comp. Biochem. Physiol. 20; 147-162.

KERKUT, G.A. & HORN, N. (1968). 'Dopamine and long lasting inhibition of snail neurones.' Life Sci. 7; 567-569.

KERKUT, G.A., HORN, N. & WALKER, R.J. (1969). 'Long-lasting synaptic inhibition and its transmitter in the snail, Helix aspersa.' Comp. Biochem. Physiol. 30; 1061-1074.

KERKUT, G.A. & MEECH, R.W. (1966). 'The internal chloride concentration of H and D cells in the snail brain.' Comp. Biochem. Physiol. 19; 819-832.

KERKUT, G.A. & MEECH, R.W. (1967). 'The effect of ions on the membrane properties of snail neurones,' Comp. Biochem. Physiol. 20; 411-429.

KERKUT, G.A. & THOMAS, R.C. (1964). 'The effect of anion injection and changes in the external potassium and chloride concentration on the reversal potentials of the IPSP and acetylcholine.' Comp. Biochem. Physiol. 11; 199-213.

KERKUT, G.A. & WALKER, R.J. (1961). 'The resting potential and potassium levels of cells from active and inactive cells.' Comp. Biochem. Physiol. 2; 76-79.

KERKUT, G.A. & WALKER, R.J. (1962). 'The specific chemical sensitivity of Helix nerve cells. Comp. Biochem. Physiol. 7; 277-288.

KERKUT, G.A. & YORK, B. (1969). 'The oxygen sensitivity of the electrogenic sodium pump in snail neurones.' Comp. Biochem. Physiol. 28; 1125-1134.

KERKUT, G.A. & YORK, B. (1971). 'The Electrogenic Sodium Pump.' Bristol: Scientechnica (Publishers) Ltd.

KEYNES, R.D. (1963). 'Chloride in the squid giant axon.' J. Physiol. Lond. 169; 690-705.

KISS, I. (1973). 'Statistical analysis of rhythmic discharges and chemical sensitivity of central neurones in Lymneaa stagnalis L.' in 'Neurobiology of Invertebrates' 2nd Int. Symposium ed. SALANKI, J.; 99-108. Budapest: Akademiai Kiado.

KOSTYUK, P.G. (1968). 'Ionic background of activity in giant neurons of molluscs.' in 'Neurobiology of Invertebrates' ed. SALANKI, J. 145-167. New York: Plenum Press.

KOSTYUK, P.G., KRISHTAL, O.A. & PIDOPLICHKO, V.I. (1972). 'Potential-dependent membrane current during the active transport of ions in snail neurones.' J. Physiol. Lond. 226; 373-392.

KRULL, H. (1934). 'Die aufhebung der chiastoneurie bei den Pulmonaten.' Zool. Anz. 105; 173-182.

LUX, H.D. & ECKERT, R. (1974). 'Inferred slow inward current in snail neurones.' Nature, Lond. 250; 574-576.

MARMOR, M.F. (1971a). 'The effects of temperature and ions on the current-voltage relation and electrical characteristics of a molluscan neurone.' J. Physiol. Lond. 218; 573-598.

MARMOR, M.F. (1971b). 'The independence of electrogenic sodium transport and membrane potential in a molluscan neurone.' J. Physiol. Lond. 218; 599-608.

MARMOR, M.F. & GORMAN, A.L.F. (1970). 'Membrane potential as the sum of ionic and metabolic components.' Science, N.Y. 167; 65-67.

MIROLLI, M. & GORMAN, A.L.F. (1973). 'The extracellular space of a simple molluscan nervous system and its permeability to potassium.' J. exp. Biol. 58; 423-435.

MOORE, J.W., BLAUSTEIN, M.P., ANDERSON, N.C. & NARAHASHI, T. (1967). 'Basis of Tetrodotoxin's selectivity in blockage of squid axons.' J. gen. Physiol. 50; 1401-1411.

MOORE, J.W., NARAHASHI, T. & SHAW, T.I. (1967). 'An upper limit to the number of sodium channels in nerve membrane?' J. Physiol. Lond. 188; 99-105.

MORETON, R.B. (1968). 'An application of the constant field theory to the behaviour of giant neurones of the snail, Helix aspersa.' J. exp. Biol. 48; 611-623.

MORETON, R.B. (1969). 'An investigation of the electrogenic sodium pump in snail neurones, using the constant-field theory.' J. exp Biol. 51; 181-201.

MORETON, R.B. (1972). 'Electrophysiology and ionic movements in the central nervous system of the snail, Helix aspersa.' J. exp. Biol. 57; 513-541.

MUELLER, P. & RUDIN, D.O. (1968). 'Resting and action potentials in bimolecular lipid membranes.' J. Theor. Biol. 18; 222-258.

MURRAY, R.W. (1966). 'The effect of temperature on the membrane properties of neurons in the visceral ganglion of Aplysia.' Comp. Biochem. Physiol. 18; 291-303.

NATIONAL SEMICONDUCTOR CORPORATION (1971). 'Linear Integrated Circuits.' Data Handbook; January, 1971.

NEHER, E. (1971). 'Two fast transient current components during voltage clamp on snail neurons.' J. gen. Physiol. 58; 36-53.

NEHER, E. & LUX, H.D. (1969). 'Voltage clamp on Helix pomatia neuronal membrane; current measurement over a limited area of the soma surface.' Pfluegers Arch. Ges. Physiol. 311; 272-277.

NEHER, E. & LUX, H.D. (1971). 'Properties of somatic membrane patches of snail neurons under voltage clamp.' Pfluegers Arch. Ges. Physiol. 322; 35-38.

NEHER, E. & LUX, H.D. (1973). 'Rapid changes of potassium concentration at the outer surface of exposed single neurons during membrane current flow.' J. gen. Physiol. 61; 385-399.

NOBLE, D. (1962). 'A modification of the Hodgkin-Huxley equations applicable to Purkinje fibre action and pace-maker potentials.' J. Physiol. Lond. 160; 317-352.

NOBLE, D. (1966). 'Applications of Hodgkin-Huxley equations to excitable tissues.' Physiol. Rev. 46; 1-50.

NYSTROM, R.A. (1973). 'Membrane Physiology.' New Jersey: Prentice-Hall Inc.

SALANKI, J., VADASZ, I. & ELEKES, K. (1972). 'Physiological and morphological characteristics of Br-type neuron in the central nervous system of the snail, Helix pomatia L.' Acta. Physiol. Acad. Sci. Hung. 42; 243-254.

SALANKI, J., VADASZ, I. & VERO, M. (1973). 'Temperature dependence of the activity pattern in the Br-type cell of the snail Helix pomatia L.' Acta. Physiol. Acad. Sci. Hung. 43; 115-124.

SCHLOTE, R. (1957). 'Submikroskopiche morphologie von Gastropoden-nerven.' Z. Zellforsch 45; 543-568.

SIENKO, M. & PLANE, P. (1961). 'Chemistry.' New York: McGraw-Hill.

SMITH, T.G., BARKER, J.L. & GAINER, H. (1975). 'Requirements for bursting pacemaker potential activity in molluscan neurones.' Nature, Lond. 253; 450-452.

SMYTHIES, J.R., BENINGTON, F., BRADLEY, R.J., BRIDGERS, W.F. & MORIN, R.D. (1974). 'The molecular structure of the sodium channel.' J. Theor. Biol. 43; 29-42.

STEIN, R.B. (1967). 'The frequency of nerve action potentials generated by applied currents.' Proc. R. Soc. B 167; 64-86.

STOKES, B.J. (1961). 'Organic Chemistry.' London: Arnold.

STRUMWASSER, F. (1965). 'The demonstration and manipulation of a circadian clock in a single neuron,' in 'Circadian Clocks' ed. ASCHOFF, J.; 442-462. Amsterdam: N. Holland Publishing Co.

STRUMWASSER, F. (1968). 'Membrane and intracellular mechansim governing endogenous activity in neurons.' in 'Physiological and Biochemical Aspects of Nervous Integration' ed. CARLSON, F.D.; 329-341. New Jersey: Prentice-Hall Inc.

STRUMWASSER, F. & KIM, M. (1969). 'Experimental studies of a neuron with an endogenous oscillator and a quantitative model of its mechanism.' Physiologist 12; 367.

TAKATA, M., MOORE, J.W., KAO, C.Y. & FUHRMAN, F.A. (1966). 'Blockage of sodium conductance increase in lobster giant axon by Tarichatoxin (Tetrodotoxin).' J. gen. Physiol. 49; 977-988.

TAUC, L. (1966). 'Physiology of the nervous system.' in 'Physiology of Mollusca' ed. WILBUR, K.M. & YONGE, C.M. Vol. 2; 387-454. New York: Academic Press.

THOMAS, R.C. (1968). 'Measurement of current produced by the sodium pump in snail neurone.' J. Physiol. Lond. 195; 23-24P.

THOMAS, R.C. (1969). 'Membrane current and intracellular sodium changes in a snail neurone during extrusion of injected sodium.' J. Physiol. Lond. 201; 495-514.

TOWERS, T.D. (1968). 'High input-impedance amplifier circuits.' Wireless World 74; No. 1393, p. 197-201.

TRAUTWEIN, W. & KASSEBAUM, D.G. (1961). 'On the mechanism of spontaneous impulse generation in the pacemaker of the heart.' J. gen. Physiol. 45; 317-330.

WACHTEL, H. & WILSON, W.A. (1973). 'Voltage clamp analysis of rhythmic slow wave generation in bursting neurones.' in 'Neurobiology of Invertebrates' 2nd Int. Symposium ed. SALANKI, J.; 59-80. Budapest: Akademiai Kiado.

WALKER, R.J. (1968). 'B. Intracellular microelectrode recording from the brain of Helix.' in 'Experiments in Physiology and Biochemistry' ed. KERKUT, G.A. Vol. 1; 342-345. London: Academic Press.

WALKER, R.J., LAMBERT, J.D.C., WOODRUFF, G.N. & KERKUT, G.A. (1970). 'Action potential shape and frequency as criteria for neuron identification in the snail, Helix aspersa.' Comp. gen. Pharmac. 1; 409-425.

WEBB, R.E. (1965). 'Field effect transistors for biological amplifiers.' Electronic Eng. 37; No. 454, p. 803-805.

WHITFIELD, I.C. (1960). 'An Introduction to Electronics for Physiological Workers.' London: MacMillan.

WILSON, W.A. & WACHTEL, H. (1974). 'Negative resistance characteristic essential for the maintenance of slow oscillations in bursting neurons.' Science N.Y. 186; 932-934.